# Elucidation of DNA repair activity of *PfBLM* and potentiation of artemisinin action by small molecule inhibitor of RecQ helicase

#### **A** Thesis

Submitted to the University of Hyderabad in partial fulfilment of the award of a Ph.D. degree in the Department of Biochemistry, School of Life Sciences

 $\mathbf{B}\mathbf{y}$ 

# S.NIRANJAN 14LBPH04



Department of Biochemistry

**School of Life Sciences** 

University of Hyderabad

Hyderabad-500046

Telangana, India

November-2020



#### University of Hyderabad

#### Hyderabad-500046, India

#### CERTIFICATE

This is to certify that this thesis entitled "Elucidation of DNA repair activity of PBLM and potentiation of artemisinin action by small molecule inhibitor of RecQ helicase" submitted by Mr. S.Niranjan bearing registration number 14LBPH04 in partial fulfilment of the requirements for award of Doctor of Philosophy in the Department of Biochemistry, School of Life Sciences, is a bonafide work carried out by him under my supervision and guidance.

This thesis is free from plagiarism and has not been submitted previously in part or in full to this or any other University or Institution for award of any degree or diploma.

Parts of this thesis have been:

#### A. Published in the following journal:

- **Niranjan Suthram**, Siladitya Padhi, Payal Jha, Sunanda Bhattacharyya, Gopalakrishnan Bulusu, Arijit Roy, and Mrinal Kanti Bhattacharyya. Elucidation of DNA repair function of *PfBLM* and potentiation of artemisinin action by a small molecule inhibitor of RecQ helicase. **mSphere** (Accepted).
- Pratap Vydyam, Dibyendu Dutta, Niranjan Suthram, Sunanda Bhattacharyya, and Mrinal Kanti Bhattacharyya. A Small molecule inhibitor of the DNA recombinase Rad51 from *Plasmodium falciparum* synergizes with the antimalarial drugs artemisinin and chloroquine. J Biol Chem 2019 doi: 10.1074/jbc.RA118.005009.

#### B. Presented in the following conferences:

- Niranjan Suthram, Wahida Tabassum and Mrinal Kanti Bhattacharyya. Characterization of RecQ and RecG helicases of Plasmodium falciparum. National conference on Malaria parasite biology: Drug designing and vaccine development. 2016. Abstract No. 11, held at Nirma University, Ahmedabad, India.
- Niranjan Suthram, Sunanda Bhattacharyya and Mrinal Kanti Bhattacharyya. Role of RecQ helicases in *Plasmodium* biology. International Symposium on Malaria Biology & 29th National Congress of Parasitology on Basic and Applied Aspects (ISMBNCP-2018). 2018. Abstract No. M13, held at University of Hyderabad, Hyderabad, India.
- 3. **Niranjan Suthram**, Sunanda Bhattacharyya and Mrinal Kanti Bhattacharyya. Deciphering the functional role of RecQ helicases in *Plasmodium* DNA repair. National seminar on Biomolecular interactions in development and disease. 2019. Abstract No. 23, held at University of Hyderabad, Hyderabad, India.

Further, the student has passed the following courses towards fulfilment of coursework requirement for Ph.D.

Course code	Name	Credits	Pass/Fail
BC 801	Analytical Techniques	4	Passed
BC 802	Research ethics, Data analysis and Biostatistics	3	Passed
BC 803	Lab seminar and Record	5	Passed

Dr. MRINA Supervisor HATTACHARYYA PhD Head, Dept. of Biochemistry

PROFESSOR
DEPARTMENT OF BIOCHEMISTRY
SCHOOL OF LIFE SCIENCES
UNIVERSITY OF HYDERABAD
HYDERABAD-500046, INDIA.

Dept. of Biochemistry
SCHOOL OF LIFE SCIENCES
UNIVERSITY OF HYDERABAD
HYDERABAD-500 046.

Dean, School of Life Sciences

School of Life Sciences University of Hyderabad Hyderabad - 500 046.



# University of Hyderabad Hyderabad-500046, India

#### **DECLARATION**

I, S.Niranjan, hereby declare that this thesis entitled "Elucidation of DNA repair activity of *PfBLM* and potentiation of artemisinin action by small molecule inhibitor of RecQ helicase" submitted by me under the guidance and supervision of Prof. Mrinal Kanti Bhattacharyya, is an original and independent research work. I also declare that it has not been submitted previously in part or in full to this University or any other University or Institution for the award of any degree or diploma.

Date 19.11.2020

Signature of the student

Signature of the Supervisor

(Prof. Mrinal Kanti Bhattacharyya)

Dr. MRINAL KANTI BHATTACHARYYA PhD
PROFESSOR
DEPARTMENT OF BIOCHEMISTRY
SCHOOL OF LIFE SCIENCES
UNIVERSITY OF HYDERABAD
HYDERABAD-500046, INDIA.

## Acknowledgements

I would like to take this opportunity to thank all those people who made this thesis possible.

First and foremost, I would like to gracefully acknowledge my thesis advisor, **Prof. Mrinal Kanti Bhattacharyya**, for giving me the chance to work with him. I thank him sincerely for his excellent scientific guidance and valuable suggestions during this work.

I'm grateful to **Dr. Sunanda Bhattacharyya** for data interpretation in research work and extending her lab facilities. I am also thankful for her critical inputs and providing very useful suggestions during lab meetings

I wish to express my sincere thanks to my doctoral committee members, **Prof. Naresh Babu Sepuri,** and **Dr. Sudipta Saraswati** for their valuable suggestion during my project presentations.

I thank the Head of Biochemistry department, **Prof. Krishnaveni Mishra**, and the former heads, **Prof. Mrinal Kanti Bhattacharyya** and **Prof. N Shiva Kumar** for allowing to use all the research facilities.

I thank the Dean of School of Life Sciences, **Prof. S Dayananda**, and the former Deans **Prof R.P. Sharma**, **Prof. P Reddanna**, and **Prof. KVA Ramaiah** for providing all the research facilities.

I thank **Prof. H.A.Nagarajaram**, Department of Systems and Computational biology, for helping me with *in silico* analysis.

I thank **Dr. Siladitya Padhi**, **Dr. Gopalakrishnan Bulusu**, **Dr. Arijit Roy**, TCS innovation labs for helping me with *in silico* analysis.

I thank all the teaching and non-teaching staff members of the School of Life Sciences for their help and support.

I thank **UGC** for all its financial support for five years of my research.

I thank funding agencies **DBT**, **DST-SERB**, **CSIR**, **DST-FIST**, and **UGC-SAP** for the financial assistance to the lab.

I thank **DST-FIST**, **DBT-CREBB**, **UGC-SAP**, **DST-PURSE** for funding to school and department towards common facilities that aided my research work.

I thank my lab mates **Dr. Sugith**, **Dr. Shalu**, **Dr. Shyamasree**, **Dr. Suresh**, **Dr. Nidhi**, **Dr. Tanvi**, **Dr. Nabi**, **Dr. Swati Chakrabarty**, **Dr. Vydyam Pratap**, **Dr. Purna Chandra**, **Wahida**, **Payal**, **Abhilasha**, **Tanishka**, **Shephali**, **Nupur**, **Priyanka**, and **Khushboo** for their timely help, support, and I thank them for keeping lively environment in the lab.

I thank all the previous and present **M.Sc. Project students** from the lab of Prof. Mrinal Kanti Bhattacharyya and Dr. Sunanda Bhattacharyya for their help and co-operation.

I thank our lab attender Mr. Ramesh for his help in the lab.

I'm really grateful to all my **SLS friends** (juniors & seniors) for scientific discussions,

suggestions and fun chats in the corridors.

I thank staff of Health Centre, University of Hyderabad for helping me whenever needed.

And at last, I'm immensely grateful to my family for their invaluable support and encouragement without which I could not have completed my PhD. My parents have been a great source of constant motivation during my PhD.

Finally, I would like to thank **God Almighty** for giving me the strength, knowledge, ability and opportunity to undertake this research study and to persevere and complete it satisfactorily.

S.Niranjan

## **CONTENTS**

List of figures	X
List of Tables	Xi
Abbreviations	X11
Chapter I	1
1. Introduction	2
1.1 Malaria	2
1.1.1 Life cycle of <i>Plasmodium</i>	2
1.1.2 Drug treatment for malaria	4
1.2 DNA DSB repair pathway as reliable drug	
Target	5
1.2.1 DNA DSB repair pathways	5
1.2.1a Non-homologous end joining (NHEJ)	5
1.2.1b Homologous recombination (HR)	6
1.3 DNA DSB repair in <i>Plasmodium</i>	10
1.3.1a NHEJ in <i>Plasmodium</i>	10
1.3.1b HR in <i>Plasmodium</i>	10
1.4 RecQ helicases in DNA metabolism	11
1.4.1 Biochemical functions of RecQ helicases	12
1.5 RecQ helicases: Implications in DNA repair	14
1.5.1a RecQ helicases in NHEJ	14
1.5.1b RecQ helicases in HR	14
1.5.2 RecQ helicases in <i>Plasmodium</i>	16
1.6 Artemisinin as DNA DSB inducer in the <i>Plasmodium</i>	
genome	18
1.6.1 Artemisinin-based combination therapies (ACTs)	18
1.7 Significance of the study	20

1.8 Objectives of the study	21
1.9 Aims of the study	22
Chapter II: Materials and Methodology	
2.1 Recombinant DNA Methods	24
2.1.1 Bacterial competent cell preparation	24
2.1.2 Bacterial transformation	24
2.1.3 Plasmid DNA isolation by alkaline lysis method	25
2.1.4 Site-directed mutagenesis by splice overlap PCR	
method	26
2.2 Yeast methods	26
2.2.1 Yeast Competent Cell Preparation	26
2.2.2 Yeast transformation	26
2.2.3 RNA isolation from yeast strains	27
2.2.4 Yeast-two hybrid analysis	28
2.2.5 DNA damage experiments in yeast	28
2.3 Recombinant protein expression	29
2.4 Methods in <i>Plasmodium falciparum</i> culture	29
2.4.1 Washing of red blood cells (RBCs)	29
2.4.2 Thawing of parasites from liquid nitrogen	30
2.4.3 Freezing of <i>Plasmodium</i> parasites	30
2.4.4 Maintenance of <i>Plasmodium in vitro</i> culture	31
2.4.5 Synchronization of <i>Plasmodium</i> parasites by sorbitol method	31
2.4.6 Genomic DNA isolation from Plasmodium falciparum	31
2.4.7 Protein preparation from parasite	32
2.4.8 RNA isolation from parasite	32
2.4.9 Transfection in <i>Plasmodium falciparum</i>	33

2.5 DNA damage experiments in parasite	34
2.6 Drug studies in <i>Plasmodium</i>	34
2.6.1 Inhibitory concentration determination assay in <i>Plasmodium</i>	
2.6.2 In vivo growth inhibition with ML216	35
2.6.3 Effect of ML216 on DNA damaged cells	35
2.6.4 Fixed ratio method to determine interaction between ML216	
and DHA/CQ/ATQ	36
2.7 Co-purification assay	36
2.8 Western blot analysis	37
2.9 Bioinformatics analysis	38
Chapter III: Implications of PfBLM in Plasmodium DNA repair	
3. Introduction	42
3.1 Results	44
3.1.1 Expression of <i>PfBLM</i> and antibody generation	44
3.1.2 PfBLM expression is maximum at mitotically active schizont stage	44
3.1.3 DNA damage induced up-regulation of PfBLM during IDC stages	47
3.1.4 PfBlm interacts with key DNA repair proteins PfRad51 and PfalMre11	52
3.1.5 Interaction points between PfBlm and PfRad51	55
3.1.6 PfBLM functionally complements MMS sensitivity of Δsgs1 mutant of	
S. cerevisiae	55
3.1.7 Over-expression of <i>PfBLM</i> provides survival advantage to the parasites	
under DNA damaging conditions	58
3.2 Summary of the results	64

Chapter IV: Studying the effect of small molecule inhibitor of RecQ helicase on <i>Plasmodium</i> g	rowth
4 Introduction	66
4.1 Results	67
4.1.1 <i>In silico</i> analysis of the binding poses and binding	
affinities of the inhibitors against PfBlm	67
4.1.2 Compared to MIRA-1, ML216 is a more potent inhibitor of	
the intra erythrocytic stages of P. falciparum	67
4.1.3 ML216 inhibits In vivo growth of Plasmodium	74
4.1.4 Parasites treated with ML216 becomes hypersensitive to DNA damaging	
Agent	77
4.2 Summary of the results	
Chapter V: Studying the interaction of RecQ helicase inhibitor with current anti-malarial drug	(s
5. Introduction	81
5.1 Results	82
5.1.1 ML216 interacts synergistically with ART and CQ	82
5.1.2 ML216 lowers the IC <sub>50</sub> of anti-malarial drugs and vice versa	82
5.2 Summary of the results	88
Chapter VI: Discussion	89
References	94
Appendix	
Synopsis	104

## List of figures:

Figure 1: Depiction of the <i>Plasmodium falciparum</i> life cycle	3
Figure 2: Sources of DNA damage	8
Figure 3: Models of distinct DNA repair pathways in eukaryotes	9
Figure 4: Schematic diagram of domain analysis of well-studied RecQ helicases	13
Figure 5: Functions of RecQ helicases in different DNA repair pathways	17
Figure 6: Expression of recombinant protein PfBlm in different bacterial expression vectors	45
Figure 7: PfBLM expression is maximum at mitotically active schizont stage	48
Figure 8: DNA damage induced up-regulation of <i>PfBLM</i> during intra-erythrocytic developmental stages	50
Figure 9: PfBlm interacts with key DNA repair proteins PfRad51 and PfalMre11	53
Figure 10: Interaction points between PfRad51 and PfBlm	56
Figure 11: $PfBLM$ functionally complements MMS sensitivity of $\Delta sgs1$ mutant of $S.$ cerevisiae	59
Figure 12: Over-expression of <i>PfBLM</i> provides survival advantage under DNA damaging conditions	62
Figure 13: <i>In silico</i> analysis of the binding poses and binding affinities of inhibitors against PfBlm	68
Figure 14: Compared to MIRA-1, ML216 is a potent inhibitor of <i>Plasmodium</i> in vitro growth	72
Figure 15: ML216 inhibits in vivo growth of Plasmodium berghei	75
Figure 16: ML216 interacts synergistically with DHA and CQ	84

## List of tables:

Table 1: List of primers used in this study	39
Table 2: List of yeast strains used in this study	40
Table 3: Free energies of binding of inhibitors bound to PfBlm	69
Table 4: IC <sub>50</sub> values of ML216 with or without MMS treated cultures at different IDC stages in 3D7 and Dd2 strains	78
Table 5: FIC values of drug combinations	83
Table 6: IC <sub>50</sub> of ML216 in combination with ART/CQ and vice versa	87

#### **Abbreviations:**

ACT Artemisinin-based Combination Therapy

Alt-NHEJ Alternative Non-Homologous End Joining

Ade Adenine

DHA Dihydroartemisinin

BIR Break Induced Repair

bp Base pair

BRCA2 Breast Cancer type2

°C Degree Celsius

c-NHEJ Canonical Non-Homologous End Joining

CQ Chloroquine

DEPC Diethyl-pyro carbonate

DMSO Dimethyl sulfoxide

DNase Deoxy ribonuclease

DSB Double Strand Break

dsDNA Double stranded DNA

DTT Dithiothreitol

gDNA Genomic DNA

EDTA Ethylene diamine tetra acetic acid

FIC Fractional Inhibitory Concentration

HR Homologous Recombination

His Histidine

IC50 Half maximal inhibitory concentration

IgG Immunoglobulin G

IPTG IsoPropyl-β-D-1-Thio Galacto-pyranoside

iRBC Infected Red blood cell

kDa Kilo Dalton

Leu Leucine

MMS Methyl Methane Sulphate

Mg Milligram

mM Millimolar

min Minutes

ml Milliliter

mV Milli Volt

NHEJ Non-Homologous End Joining

nM Nanomolar

OD Optical Density

PAGE Poly-acrylamide gel electrophoresis

PCIA Phenol chloroform isoamyl alcohol

PEG Polyethylene glycol

PMSF Phenyl-methane-sulfonyl-fluoride

PY Pyrimethamine

RNA Ribonucleic acid

RNase Ribonuclease

ROS Reactive Oxygen Species

RPA Replication Protein A

Rpm Rotations per minute

RPMI Roswell park memorial institute medium

SC Synthetic complete

SDS Sodium Dodecyl Sulfate

SDSA Synthesis Dependent Strand Annealing

SSA Single Strand Annealing

ssDNA Salmon sperm DNA

WHO World health organization

WT Wild Type

XRCC4 X-Ray Cross complementing factor 4

YNB Yeast nitrogen base

YPD Yeast extract, peptone, dextrose

μF Micro Faraday

μg Microgram

μl Microliter

μm Micrometer

 $\mu M$  Micromolar

Ura Uracil

# **CHAPTER-I**

# **INTRODUCTION**

#### 1.1 Malaria:

Malaria is a vector-borne disease that occurs mainly in tropical and sub-tropical regions of the world. The disease is manifested in humans and other animals by the protozoan parasite *Plasmodium*. Human beings are infected by five species of *Plasmodium*, namely *P. falciparum*, *P. vivax*, *P. malariae*, *P. ovale*, and *P. knowlesi*. The infection caused by *P. falciparum* is dreadful because it impacts the central nervous system (cerebral malaria). In addition to cerebral malaria, it also accounts for renal failure and severe anemia. As per the WHO (World Health Organization) report 2019, there were 228 million cases and 40 5000 deaths recorded due to malaria worldwide in 2018. About nineteen countries in sub-Saharan Africa and India account for almost 85% of the global malaria burden. Out of 40 5000 deaths, 67% (27 2000) are children under the age group of 5 years [1].

#### 1.1.1 Life cycle of *Plasmodium falciparum*:

Plasmodium shuttles between mosquito and human to complete its life cycle. It enters as sporozoite form in humans when an infected female anopheles' mosquito bites. Initially, these sporozoites are transported to the liver from circulation and undergo exo-erythrocytic schizogony in hepatocytes to produce multiple merozoites. These merozoites enter the blood stream to infect red blood cells (RBC) and reproduce asexually (erythrocytic schizogony). These parasites develop into ring, trophozoite, and schizont stages, which also ruptures to produce merozoites. Few of the parasites differentiate into male and female gametocytes in the erythrocytic stage taken up by the mosquito during its blood meal to perpetuate the life cycle. In the mosquito, sexual reproduction takes place to produce a diploid zygote. The zygote becomes motile and elongated (ookinete), invading the midgut wall of the mosquito. In the mosquito midgut, it develops into an oocyst and undergoes sporogony to release sporozoites. These sporozoites reach salivary glands for further inoculation in human beings.

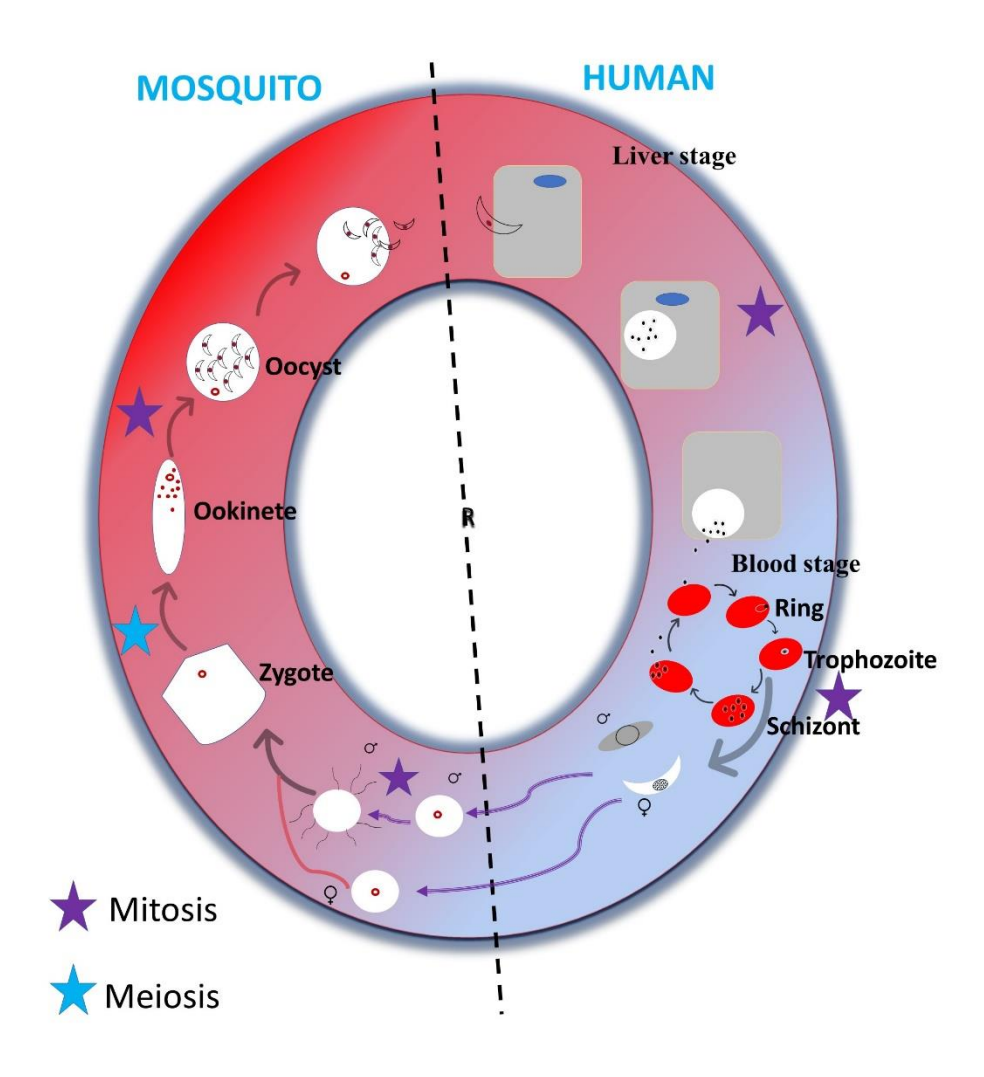


Figure 1: The life cycle of *Plasmodium falciparum* depicting the stages where mitosis and meiosis takes place.

#### 1.1.2 Drug treatment for malaria:

Chloroquine (CQ) was introduced as an anti-malarial drug in 1934 and was used on a large scale from 1955 during the global malaria eradication program conducted by WHO. However, chloroquine resistance was observed in various parts of the world at different time points beginning from 1957. The resistance was spread rapidly throughout the world by the end of 1980 [2]. Although, other drugs like atovaquone, mefloquine, pyrimethamine, sulfadoxine, and proguanil were introduced but their cost-effectiveness and toxicity limited the usage. Later, artemisinin was used as an anti-malarial drug in the year 1972. Artemisinin was also given in combination with other anti-malarial drugs called as Artemisinin-based combination therapy (ACT). ACT is an effective strategy because combining two drugs with a different mode of action ensures the immediate and complete elimination of parasites. However, artemisinin resistance was first reported in Pailin, western Cambodia, in 2009 [3]. Interestingly, resistance to chloroquine has also emerged from the same region [2]. On the other hand, antigenic variation in parasites makes vaccine development an inefficient process. Because drug resistance is emerging at alarming rates in *Plasmodium,* there is always a need for identifying new drug targets. To identify new drug target, understanding Plasmodium biology is a pre-requisite. The cellular pathways which are crucial for the survival of parasites at all the stages might serve the purpose. Every cell frequently encounters damage to DNA from multiple sources and DNA double strand break repair pathway (DSBR) is pivotal to repair such damages. Plasmodium being a unicellular organism cannot afford to skip the repair process or else it will become detrimental to the cell. DSB repair is essential during liver, blood and mosquito stages of parasite as it involves replication of DNA. DSB repair pathway fulfils the major criteria of potential essentiality for a drug target. Exploring key players of DSB repair pathway will guide us towards achieving the goal.

#### 1.2 DNA DSB repair pathway as a reliable drug target:

Every cell experience multiple genomic assaults (DSB) during its life cycle. The sources for such assaults might be exogenic, endogenic, or physiological stress. The exogenic sources include radiomimetic drugs, radiation, and the endogenic sources comprise reactive oxygen species (ROS) produced during metabolic activity of cell. The physiological assault mainly due to replication errors. In addition to random sources, some cells facilitate programmed DNA damage during V(D)J recombination, meiotic crossover, mating-type switching in yeast. Each of those DSB needs to be appropriately mended to ensure proper genome stability. Mutations in DSB repair genes accounts for genomic instability, ultimately resulting in human diseases associated with developmental disorders, cancer predisposition, and premature aging.

#### 1.2.1 DNA DSB repair pathways:

Repair of DNA DSB carried in two pathways

- a) Non-homologous end joining (NHEJ)
- **b)** Homologous recombination (HR)

#### 1.2.1a Non-homologous end joining (NHEJ):

NHEJ is considered an "error-prone" method because it does not utilize the homologous DNA sequence of sister chromatid or homologous chromosome. Initially, DSB is recognized by the MRN (Mre11-Rad51-Nbs1) complex, and in the case of yeast, it is MRX (Mre11-Rad51-Xrs2) complex. MRN complex recruits Ku70-Ku80 heterodimer complex, which helps in the protection of DNA ends from degradation. Ku complex further recruits and activates DNA-PKcs, which exists in a tight complex with the nuclease, artemis. The endonuclease, artemis chops the broken ends. Further, poly X family polymerases (Pol  $\mu$  and Pol  $\lambda$ ) add nucleotides to broken ends. Finally, the DSB end's ligation is carried out by DNA ligase IV

complex along with XRCC4, XLF, and PAXX protein [4]. In addition to canonical NHEJ, there is one more end-joining pathway called microhomology-mediated end joining (MMEJ) or alternative end-joining (A-EJ). The A-EJ pathway is independent of Ku-or ligase IV and may or may not require microhomology (generally  $\geq$  4bp) to perform the repair function. The core proteins are MRN complex, Pol  $\theta$ , PARP1, ligase III, XRCC1, and PNK [5].

#### 1.2.1b Homologous recombination (HR):

As the name suggests, HR involves using a DNA template from a sister chromatid or homologous chromosome to repair the broken DNA. HR is involved in the repair of DSB, during meiosis, and it is necessary for the exchange of genetic material. HR is initiated when MRN complex sense and binds to the DSB. Resection of DSB ends to produce 3' ssDNA overhangs happens in two steps. In the first step, initial resection or short-range resection (about 200bp) is performed by nuclease activity of Mre11 protein, activated by CtIP (Sae2 in yeast). In the second step, long-range resection (1000bp) could happen in two different independent pathways carried out by either Exo1 or Blm-Dna2-Rpa protein complex. The 3' ssDNA overhangs generated after long-range resection are bound by ssDNA binding protein RPA. The binding of RPA to ssDNA ends helps in protection from nucleases and in removing secondary structures. The critical player of HR, Rad51, displaces RPA protein and forms Rad51 nucleo-protein filament, also called a presynaptic complex. The loading of Rad51 to ssDNA is mediated by BRCA2 in humans, whereas Rad52 in yeast. Further, Rad51 performs a homology search and invades the strand onto the donor template to form a loop-like structure called displacement loop (D-loop). In the post synapsis phase, Rad51 dissociates from dsDNA when DNA synthesis is initiated using the invading 3'-end as a primer. After the DNA synthesis, the DNA repair intermediate can be resolved in three pathways: a) Double-strand break repair (DSBR). b) Synthesis dependent strand annealing (SDSA). c) Break induce

replication (BIR). DSBR involves forming a double-Holliday junction (dHJ) by capturing the second end of the DSB. dHJ can be either dissolved by BTR complex (Blm-TopoIII-RmiI) to produce exclusively non-crossover products or resolved by dHJ resolvases GEN1, MUS81/EME1 (YEN1, Mus81-Mms4 in yeast) to make both cross over and non-crossover products. In SDSA, the invading strand anneals with complementary strand associated with another end of DSB. SDSA results in the formation of only non-crossover products. BIR occurs mainly during replication fork collapse or during telomere lengthening, which repairs one ended double-stranded break. In addition to the above pathways, there is a Rad51 independent pathway to repair DSB called single-strand annealing (SSA). SSA involves the annealing and ligation of homologous sequences present in both sides of DSB. SSA is often associated with the deletion of the intervening DNA sequence [6-9].

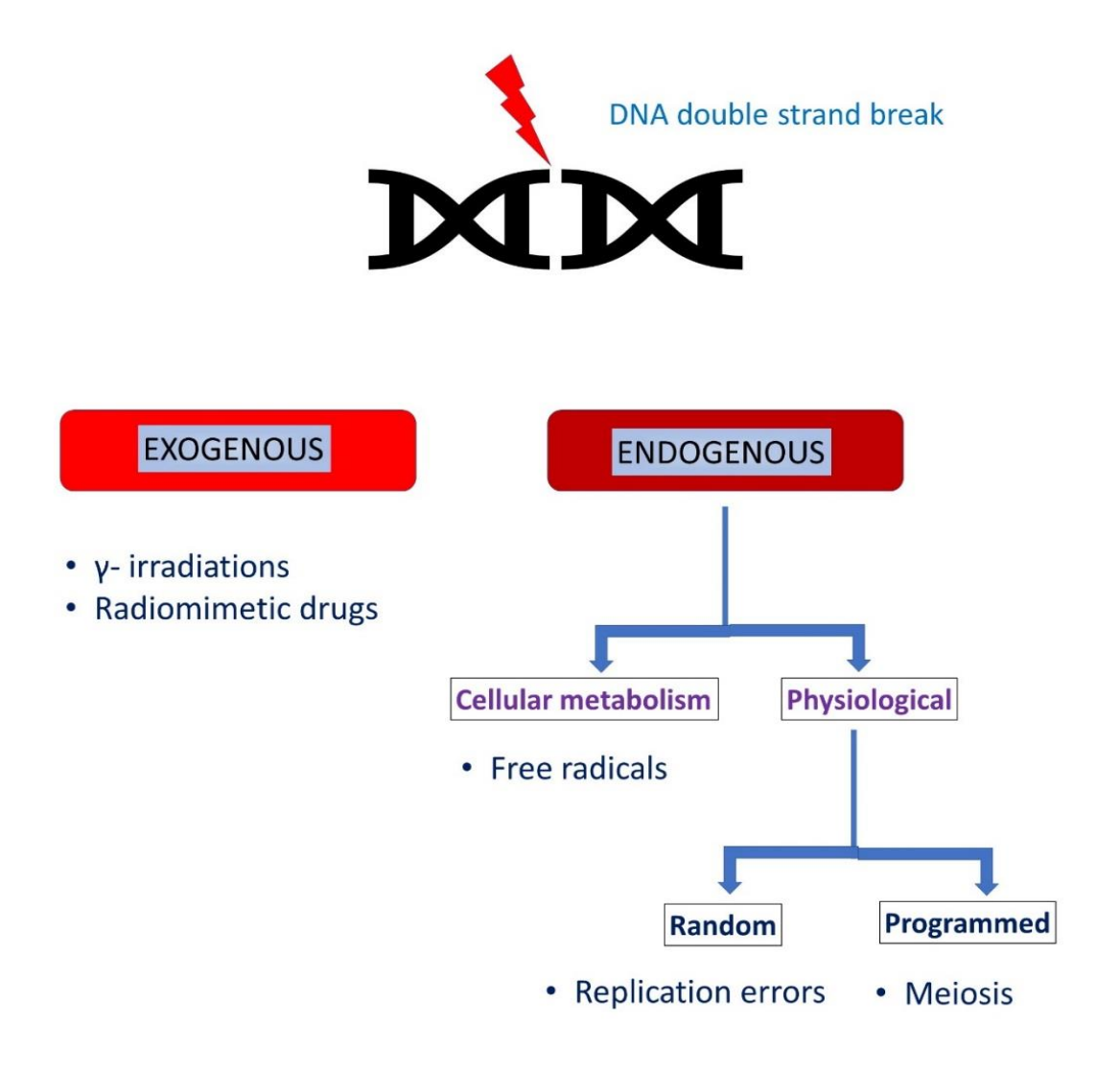


Figure 2: Multiple sources of DNA damage in a cellular environment.

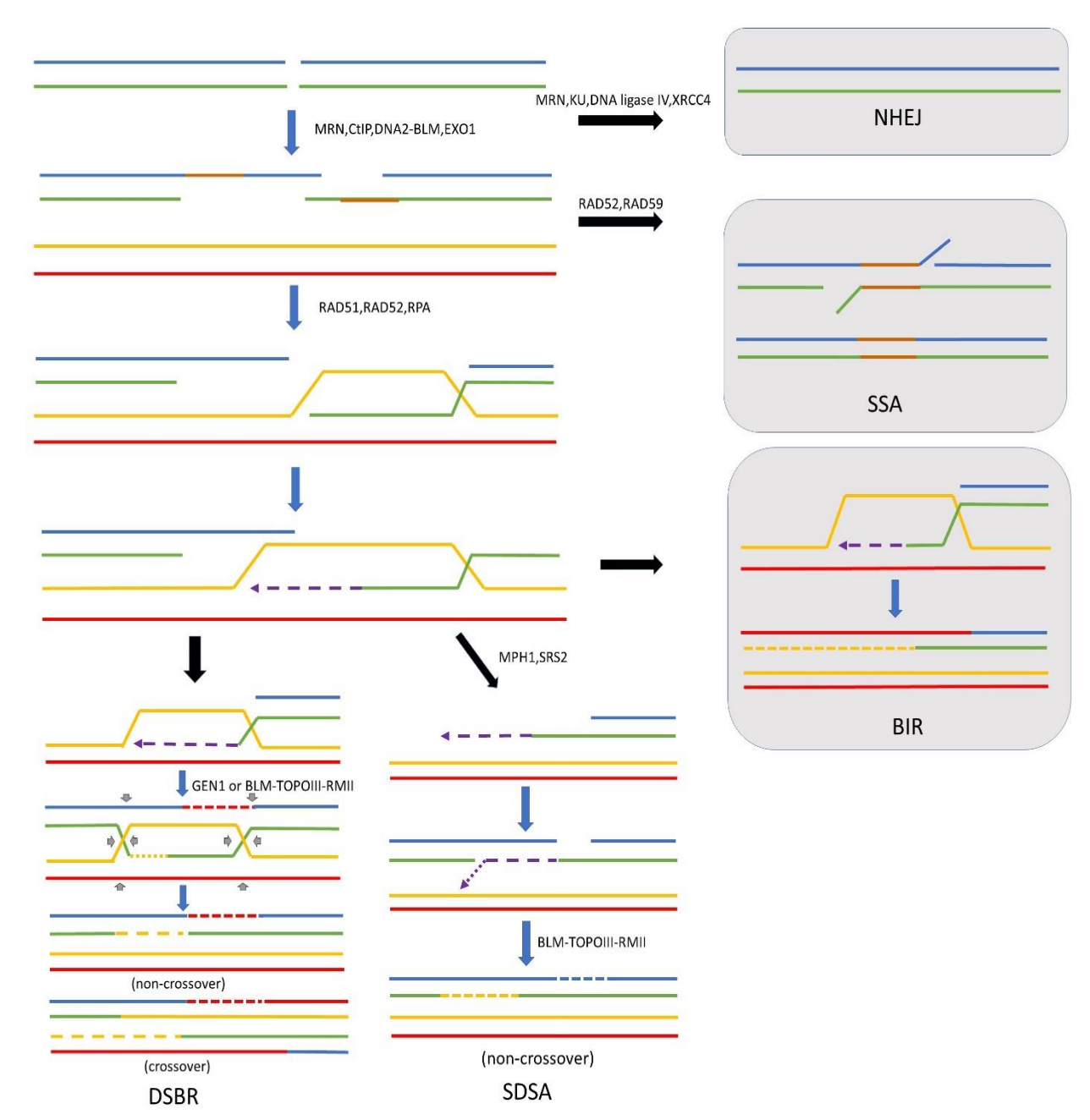


Figure 3: Models for distinct DNA DSB repair pathways in eukaryotes and the important proteins involved in it. NHEJ takes place by joining of the broken ends without the involvement of donor template but HR mediated repair requires sister chromatid or homologous chromosome sequence as template. SSA is a Rad51 independent DSB repair pathway.

#### 1.3 DNA DSB repair in *Plasmodium*:

#### 1.3a NHEJ in *Plasmodium*:

So far, there are no reports available for the canonical NHEJ pathway in *Plasmodium*. Moreover, the genome sequence did not reveal the presence of NHEJ genes [10]. This is in contrast with another apicomplexan parasite *Toxoplasma gondii* [11]. It was reported that *Plasmodium* utilizes an alternative end-joining pathway to a minor extent to repair DSB [12]. However, the dominant repair pathway in *Plasmodium* is found to be homologous recombination [13].

#### 1.3b HR in Plasmodium:

HR was established as a significant pathway to repair DSB, followed by A-EJ. PfalMre11 was identified, and its nuclease activity was found to be conserved in Plasmodium [14]. The key recombinase of HR, PfRad51, was characterized biochemically and functionally [13, 15, 16]. Recent studies have shown that chemical knockout of PfRad51 with small molecular inhibitor B02 abrogates repair in Plasmodium [17]. PfRpa1 variants were identified and established as single-stranded binding proteins (SSB) [18]. Rad52 protein, essential for Rad51 nucleofilament formation, was not identified in *Plasmodium*. However, BRCA2, which performs similar functions in mammals, has been annotated [10]. The motor protein, Rad54, which enhances the strand exchange activity of Rad51, has been identified, and biochemical studies confirm its strand exchange activity [18]. PfDmc1, a meiotic recombinase, has been identified, and its knockout negatively impacts oocyst formation in Plasmodium berghei [19]. Finally, two RecQ helicases PfBlm and PfWrn, have been identified and biochemically characterized [20, 21]. The essential functions of RecQ helicases in replication, transcription and clonal expression of var gene has been characterized but not during the DNA repair [22, 23].

#### 1.4 RecQ helicases in DNA metabolism:

The RecQ helicases of humans belong to the SF2 family of helicases. RecQ helicases' functions cover different DNA metabolic pathways, including DNA transcription, replication, repair, and recombination [24]. In humans, there are five RecQ helicases, whereas, in bacteria (RecQ) and yeast (SGS1), only one RecQ helicase is present. Germline mutations in human RecQ helicases (BLM, WRN, and RECQL4) are connected with genetic disorders, namely Bloom's syndrome (BS), Werner's syndrome (WS), and Rothmund-Thomson syndrome (RTS) [25]. Out of five RecQ helicases in humans, functions of BLM and WRN are well characterized. There are multiple functions for RecQ helicases in DNA metabolism; few of them are discussed here. Some of the replication functions include: both BLM and WRN, which are known to rescue stalled replication fork, whereas RECQL4 and RECQL1 help in the initiation of replication [26]. RECQL4 assist in loading DNA polymerase α onto the replication origin [27]. BLM and WRN rescue replication fork by resolving different structures such as hairpins and G-quadruplexes, which hinder the fork movement [28-30]. In addition to this, BLM, along with TOPO3, dissolve duplex structures for efficient termination of replication [31]. RECQL5 inhibits transcription by binding to the initiation and elongation form of RNA polymerase II. Such inhibition is to prevent collision of replication machinery with transcription [32-34]. Both BLM and WRN stimulate ribosomal transcription by interacting with Topo I [35, 36]. It was reported that BLM and WRN regulate transcription by targeting G-quadruplexes at the transcription start site (TSS) [37, 38]. BLM, WRN, and RECQL4 play a major role in telomere replication and repair by unwinding telomeric forks and D-loops. This unwinding activity is stimulated by shelterin proteins (TRF1, TRF2 and POT1 [39-42]. WRN and RECQL4 participates in the base excision repair (BER) pathway in which WRN stimulates NEIL1 glycosylase whereas RECQL4 stimulates APE1 enzyme [43, 44]. RecQ helicases have no direct role in nucleotide excision repair (NER) however XPG protein (NER protein) stimulates WRN helicase activity [45].

#### 1.4.1 Biochemical functions of RecQ helicases:

Members of the RecQ family are 3'-5' helicases. They have three domains in common key helicase domain, RecQ C-terminal (RQC) domain, helicase, and RNase D-like C-terminal (HRDC) domain. All the domains have a unique function in DNA metabolism. Helicase domain derives energy from ATP hydrolysis and participates in the unwinding of different dsDNA substrates. RQC domain helps stabilize the protein, dsDNA binding, and in some cases, protein-protein interactions. RQC domain mediates binding to G-quadruplexes [46]. HRDC has a supporting role in DNA binding, and this domain is also present in some RNases [47]. Interestingly, in humans the HRDC domain is least conserved since it is present only in RECQL2 and RECQL3 [48]. WRN is unique among other helicases in having an exonuclease domain. RecQ helicases unwind a broad variety of DNA substrates depending upon the pathway they are involved. Some substrates include D-loops, Holliday junctions, G-quadruplexes, fork duplexes, 3'tailed duplexes, bubble structures, and heteroduplexes [49-53]. BLM and WRN have strong activity for unwinding Gquadruplexes and Holliday junctions [49, 51, 53]. Bacterial RecQ helicase (RecQ) unwinds blunt-end DNA duplexes, whereas eukaryotic RecQ helicases cannot perform this function [54, 55]. In addition to their biochemical activity, RecQ helicases interact with different proteins. This interaction can either stimulate or inhibit the activity of partner proteins [56].

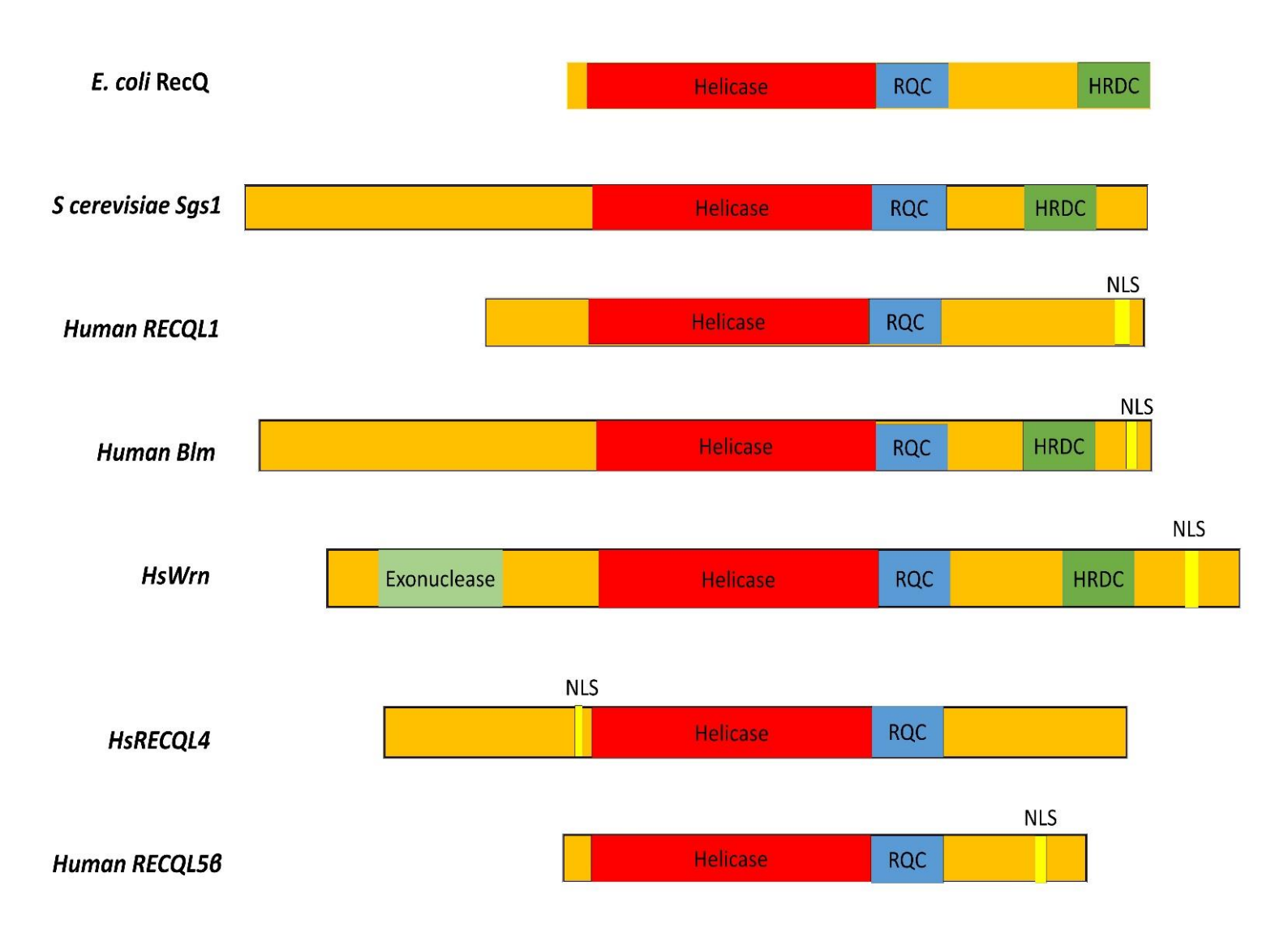


Figure 4: Schematic diagram showing domain analysis of well-studied RecQ helicases from different organisms. RQC: RecQ C-terminal domain; HRDC: Helicase, and RNase D-like C-terminal domain; NLS: Nuclear localization signal.

#### 1.5 RecQ helicases: implications in DNA repair:

RecQ helicases have major functions in DNA DSB repair, specifically in the HR pathway. Most of the DNA substrates unwound by RecQ helicases mirror DNA repair intermediates. RecQ helicases also have helicase independent regulatory functions in DSB repair. Here, we discuss the role of RecQ helicases in two DNA DSB repair pathways.

#### 1.5.1a RecQ helicases in NHEJ:

The functions of RecQ helicases in NHEJ are not established thoroughly. However, Reports have shown that Ku and XRCC4/LIG IV proteins augment exonuclease activity of WRN but not helicase activity [57, 58]. Inversely, exonuclease activity of WRN but not helicase activity stimulated by DNA-PKcs [59]. RECQL1 binds to Ku70/80 complex and unwind partial duplex DNA substrate. In addition to this, reduced end-joining activity was displayed by RECQL1 depleted cell extract [60]. There is no compelling evidence for the participation of RecQ helicases in the NHEJ pathway. WRN seems to influence the A-EJ pathway by forming a complex with DNA ligase IIIa [61]. However, the functions of RecQ helicases in the A-EJ pathway are dispensable.

#### 1.5.1b RecQ helicases in HR:

RecQ helicases, more specifically BLM, have significant functions in the HR pathway. BLM functions at various steps of the HR pathway. HR process starts with nucleolytic degradation of DNA DSB ends to produce ssDNA tails, and this process is called resection. The process of resection happens in two steps, short-range resection, and long-range resection. The short-range resection is carried out by MRN complex (MRX in yeast), which is stimulated by CtIP (Sae2 in yeast) [62-64]. CtIP stimulates the cryptic endonuclease activity of Mre11 to create nick around 200bp away from DSB. Further, 3'-5' exonuclease activity of Mre11 performs the short-

range resection [65, 66]. To the site of nick, long-range resection machinery is recruited [66]. The process of long-range resection happens in two independent pathways involving Exo1 and Dna2-Blm-Rpa complexes [67]. Although Dna2 has helicase and nuclease activity, its helicase activity is weak, relying on Blm for DNA unwinding. On the other hand, Exo1 can perform the nucleolytic function on dsDNA with no requirement of DNA unwinding [68]. In the Dna2-Blm-Rpa (Dna2-Sgs1-Rpa in yeast) resection pathway, Blm unwinds the DNA, and Dna2 performs the nucleolytic degradation [69]. Rpa stimulates helicase activity of the Blm and exonuclease activity of Dna2 [67]. Rpa also promotes 5'-3' resection polarity of Dna2 by inhibiting degradation of 3'-terminated ssDNA [70]. TopoIII-Rmi1-Rmi2 and MRN complex stimulates helicase activity of Blm and helps in recruiting Blm to DSB site. This stimulatory effect of TopoIII is independent of its catalytic activity [67, 71, 72]. The primary function of TopoIII-RMI1-RMI2 is to form a complex with Blm (BTR complex) and assist in dissolving dHJ junctions. The second resection pathway is carried out alone by Exo1 protein. However, Rpa, Blm, and MRN (MRX in yeast) stimulate the resection activity of Exo1 [73-75], but their activities are dispensable. Blm alone has a stimulatory effect on Exo1 mediated resection compared to other RecQ helicases [73]. During the presynaptic step of HR, Blm and RECQL5 exhibit anti-recombinogenic activity by disrupting Rad51 nucleofilament [76, 77]. However, this effect is reversed in two cases. First, when Blm gets SUMOylated, it facilitates the recruitment of Rad51 at the site of DSB [78]. Second, Blm stimulates strand exchange activity when Rad51 is in ATP-bound form in place of ADP-bound form [79]. Conversely, WRN, and RECQL1 unable to disrupt filaments of Rad51 [76, 77]. Displacement loop (D-loop) formed after strand invasion can further proceed in three different pathways: a) double Holliday junction formation (dHJ) b) Synthesis dependent single-strand annealing (SDSA) c) Break induced replication (BIR). Double Holliday junctions (dHJ) are resolved by either resolvase GEN1, MUS81/EME1 (YEN1, Mus81-Mms4 in yeast) to generate

crossover and non-crossover products or by dissolvosome complex (Blm-TopoIII-Rmi1/BLAP75) to generate exclusively non-crossover products [80-82]. RECQL1 and WRN are also able to perform processing of Holliday junctions [83, 84]. BLM has a definite role in SDSA, which results in the formation of non-crossover products [85].

#### 1.5.2 RecQ helicases in *Plasmodium*:

Two members of RecQ helicases (*PfBLM* and *PfWRN*) have been identified in *Plasmodium*. Biochemical experiments confirmed the conservation of helicase activity in 3'-5' direction. Immunofluorescence data highlights the expression of both the proteins in all intra-erythrocytic stages [20, 21]. Both the RecQ helicases affect the replication and transcription of genes. The rate of structural variant (SV), microindel, and SNP increased near *var* locus in case of *PfWRN* knockdown parasites in contrast to  $\Delta Pfblm$  strain emphasizing anti-recombinogenic activity of *PfWRN* but not *PfBLM* [22]. Most importantly, *PfBLM* was found to be having a significant effect on the clonal expression of *var* genes but not *PfWRN* [23]. However, there are no reports highlighting the DNA repair activity of either *PfBLM* or *PfWRN*.

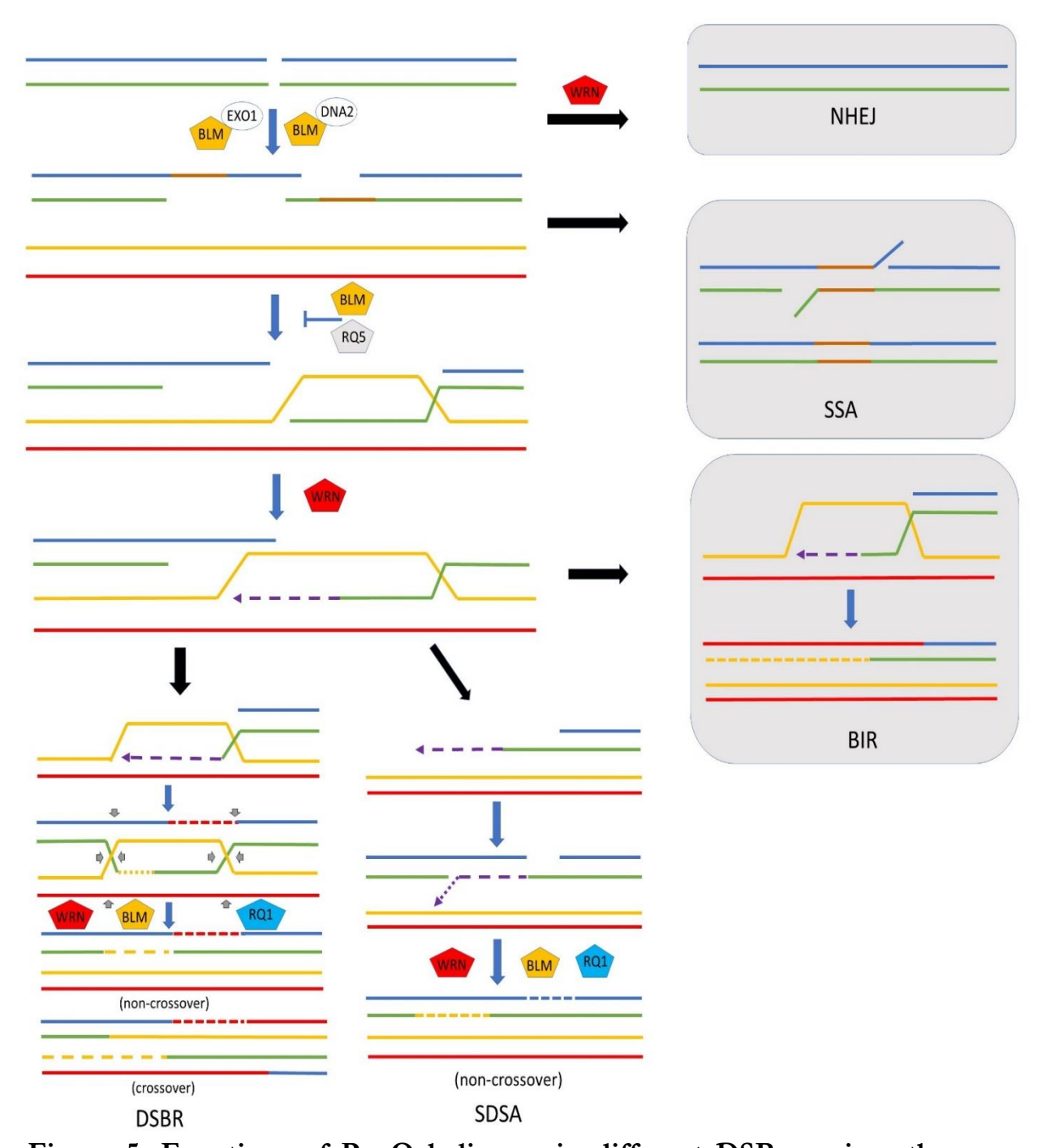


Figure 5: Functions of RecQ helicases in different DSB repair pathways. BLM has predominant functions in multiple steps of HR pathway compared to other RecQ helicases. The functions of other RecQ helicases RECQL1, RECQL5, and WRN in HR and NHEJ pathway are dispensable.

#### 1.6 Artemisinin as a DNA DSB inducer in the *Plasmodium* genome:

The profound efficacy of artemisinin lies in its interference with multiple cellular targets in parasite. Artemisinin alkylates parasite proteins and heme [86-88], Inhibits PfATP6 [89], abrogates functions of mitochondria, and generates ROS to depolarize parasite membranes [90]. Recent reports have shown that artemisinin also creates ROS mediated DNA DSB in the *Plasmodium* genome [91]. Drug resistance for ART is considerably increasing, so there is a need for a novel strategy to curb the disease [92]. The generation of DSB may not be the primary mode of action for ART, but it may affect parasite survival as it is a unicellular organism. Since WHO is currently recommending Artemisinin-combination therapy (ACT), a combination of ART with a DNA repair inhibitor may give promising results.

#### 1.6.1 Artemisinin-based combination therapies (ACTs):

Artemisinin-based combination therapy is the widely accepted anti-malarial regimen by WHO. The half-life of artemisinin and its derivatives (artesunate, artemether, and dihydro-artemisinin) is short when used as monotherapy. Therefore, artemisinin derivatives are given in combination with another drug with different mode of action and long-acting [93]. The biochemical target of the partner drug should be different from the artemisinin derivative. The idea behind the ACT is that the synergistic effect of two drugs will enhance the therapeutic efficiency, and the emergence of drug resistance to each compound will be delayed. Currently, five WHO-approved ACTs are used for the treatment of malaria: artesunate-amodiaquine (ASAQ), artesunate-sulfadoxine-pyrimethamine (ASSP), artemether-lumefantrine (A.L.), dihydro-artemisinin—piperaquine (D.P.), artesunate-mefloquine (ASMQ) [94]. Earlier reports have shown that the ART-mefloquine combination stopped the mefloquine resistance progression. In addition to this, ACT also reduces malaria's transmissibility by reducing gametocyte formation, which ultimately leads to less carriage of gametocytes to peripheral blood [95, 96]. ACT even has an impact on

malaria caused by *P. vivax* along with *P.falciparum*. However, recent reports have shown the emergence of resistance to the available ACTs in different regions of the world [97]. As there are no immediate alternatives for ACTs, it is necessary to develop new partner drugs for artemisinin, which interact synergistically.

#### 1.7 Significance of the study:

Genome integrity determines the fate of cells, and to maintain genomic integrity, cells must be equipped with repair machinery. DNA DSB is one such damage that leads to lethal consequences if ignored. Since Plasmodium is a unicellular organism, unrepaired DSB will have a significant impact on cell survival. Earlier, it was reported that the functional knockdown of essential repair protein of *Plasmodium* (PfRad51) compromised parasites' survivability [13]. However, DNA repair genes that are characterized so far in *Plasmodium* share high sequence similarity with human orthologues. This high similarity might be a barrier for aiming as a drug target. Keeping this in mind, we selected RecQ helicase (PfBlm) for our study since it shares less homology with human counterparts. Here, we reported the importance of PfBlm in Plasmodium DNA repair. We observed the expression of PfBLM induced upon DNA damage and its ability to interact with well-known DNA repair proteins of Plasmodium. Using the yeast surrogate system, we deciphered the DNA repair activity of PfBLM and further confirmed it in parasite by performing overexpression studies. We tested the effect of small molecule inhibitors of PfBlm (ML216 and MIRA-1) on parasite growth and evaluated the impact of inhibitors on *Plasmodium's* DNA repair. Finally, our studies have shown synergistic interaction of RecQ helicase inhibitor with clinically used anti-malarial drugs.

Our study enlightens the use of DNA repair inhibitors, more specifically, RecQ helicase inhibitors as anti-malarial drugs. Since RecQ helicases have an essential role in most of the DNA metabolic activities, it will be beneficial to target them. Our study also provided insights on the synergistic effect of artemisinin and RecQ helicase inhibitor combination. This combination study sheds light on the possibility of using RecQ helicase inhibitors as partner drugs for artemisinin since ACTs are currently in application to treat malaria.

#### 1.8 Objectives of the study:

Parasite poses a threat to the complete elimination of malaria with the rapid evolution of drug resistance. To avoid major crises, it is necessary to figure out new drug targets and inhibitors for immediate use. DNA repair genes of *Plasmodium* are entitled to targeting because earlier reports have shown that defective DSB repair pathway culminates in parasite's death. In this work, we have asked two main questions. Firstly, we wanted to check whether the RecQ helicase of *Plasmodium* has any role in DNA repair. To that end, we utilized the yeast surrogate system and *in vitro* parasite culture to establish the DNA repair functions of *PfBLM*. Secondly, we wanted to try a chemical knockout approach for PfBlm to address the essentiality of protein functions in parasite survival. To that end, we tested the effect of two known RecQ helicase inhibitors on parasite and tried to establish its DNA repair inhibitory activity when used in combination with artemisinin.

#### 1.9 Aims of Ph.D. work:

#### 1. Implications of *PfBLM* in *Plasmodium* DNA response:

- i) Stage specific expression of *PfBLM*
- ii) DNA damage specific expression of PfBLM
- iii) Interaction of PfBlm with key DNA repair proteins
- iv) Complementation of DNA damage sensitivity of  $\Delta sgs1$  mutant by PfBLM
- v) Validation of DNA repair activity of PfBLM in parasite

# 2. Testing the effect of small molecule inhibitor of PfBlm on *Plasmodium* growth:

- i) In silico analysis of RecQ helicase inhibitors
- ii) Inhibition of in vitro and in vivo growth of parasite with RecQ helicase inhibitors
- iii) Effect of ML216 on DNA damaged cells

# 3. Checking the interaction of PfBlm inhibitor with current anti-malarial drugs:

- i) Interaction between ML216 and artemisinin
- ii) Interaction between ML216 and chloroquine

## **CHAPTER-II**

### **MATERIALS AND METHODOLOGY**

#### 2.1 Recombinant DNA Methods:

#### 2.1.1 Bacterial competent cell preparation :

For primary inoculum, 5 ml of LB medium with proper antibiotics were inoculated with bacterial cells from a single colony and allowed it to grow overnight at 37°C, 200 rpm. From the primary inoculum, 1ml was taken and added into 50 ml LB media with proper antibiotics and allowed to grow in the same conditions as the primary inoculum until OD<sub>600</sub> reaches 0.5-0.7. The harvesting of cells was done by centrifuging cells for 8 minutes at 8000 rpm, 4°C. The obtained pellet was then resuspended in 25ml of 0.1M ice-cold CaCl<sub>2</sub>. After re-suspension, centrifugation was done for 8 minutes at 8000 rpm, 4°C. Again, the pellet was re-suspended in 0.1M ice-cold CaCl<sub>2</sub> solution (12.5 ml) and incubated for 4-8 hours. After the incubation, cells were then centrifuged for 8 minutes at 8000 rpm, 4°C. Finally, the pellet was re-suspended in 0.1M ice-cold CaCl<sub>2</sub> solution (1.07ml), and 170µl 100% glycerol was added. Pre-chilled microfuge tubes were aliquoted with 100µl of suspension and frozen in liquid nitrogen. After freezing, cells were shifted to -80°C for long term storage.

#### 2.1.2 Bacterial transformation:

The competent cell was taken from -80°C and thawed on ice before starting the experiment. The plasmid DNA of interest (25-50ng) was added on the top of cells and incubated on ice for 30 minutes. After incubation, the cells were given heat shock for 30sec (TOP 10 cells) or 90sec (expression strains) and immediately shifted the tube on ice for 2 minutes. LB medium (900µl) was added in the tube and incubated in a shaker incubator at 37°C, 200 rpm, to allow cells to grow for 1 hour. The cells were then pelleted down by spinning at 10000 rpm, 2 minutes, and most of the supernatant was discarded. The pellet was re-suspended in the leftover supernatant and spread on the LB-agar plate containing appropriate antibiotic. The plate was incubated at 37°C till the appearance of colonies for 16 hours.

#### 2.1.3 Plasmid DNA isolation by alkaline lysis method:

The primary inoculum was given from the bacterial colony, harboring the desired plasmid in 5 ml of LB medium with the proper antibiotic. The culture was grown overnight at 37°C, 200 rpm. The harvesting of cells was done by centrifuging for 5 minutes at 4000 rpm, 4°C. The pellet was re-suspended in 200µl of pre-chilled solution 1 (25 mM Tris pH 8.0, 10 mM EDTA pH 8.0) and transferred to a microfuge tube. To this, 200µl of solution 2 (0.2 M NaOH, 1% SDS) was added and inverted several times. The suspension was incubated at RT for 5 minutes. Then, 150µl of solution 3 (3 M NaOAc pH 5.2) was added and incubated on ice for 5 minutes with intermittent mixing. The centrifugation of the sample was done at 12000 rpm, 15 minutes, and the supernatant was collected. To this, 100% alcohol was added in 2.2 volumes and incubated at -20°C for 90 minutes. The spinning of the samples was done for 30 minutes at 12000 rpm, 4°C. This spinning precipitates the DNA. Washing of the pellet was done with 70% alcohol and spun for 5 minutes at 12000 rpm, 4°C. The air-dried pellet was re-suspended in 30µl of 1X TE (10 mM Tris pH 8.0, 1 mM EDTA pH 8.0), and 5µl of RNase (10 mg/ml) was added and incubated for 30 minutes at 37°C. The sample volume was made up to 400µl by adding 1X TE, and 400µl of PCIA (Phenol: Chloroform: Isoamyl alcohol) solution was added to it. The sample was vortexed for 3 minutes and spun at 12000 rpm for 15 minutes, RT. Out of three layers formed after centrifugation, the aqueous layer was taken in a new tube, and 1/10th volume of solution 3, 2.2 volume of 100% alcohol was added to precipitate DNA. The sample was incubated at -80°C for 4 hours. Final precipitation of plasmid DNA was done by centrifuging samples for thirty minutes at 12000 rpm, 4°C. Pellet was washed by adding 70% alcohol (500 µl) and spun at 12000 rpm, 4°C for 5 minutes. The pellet was air-dried and was resuspended in 30µl of 1X TE buffer. The integrity of plasmid DNA was checked by agarose gel electrophoresis.

#### 2.1.4 Site-directed mutagenesis by splice overlap PCR method:

PfblmK83R mutant was generated by a splice overlap PCR method. ORF of PfbLM was PCR amplified in two fragments bearing the desired mutation in each fragment. The internal overlap sequence between two fragments allows them to anneal and act as a template to amplify full-length ORF. Full-length ORF harboring desired point mutation was amplified by employing the fusion PCR technique. The list of primers used for the generation of PfblmK83R mutant is listed in Table 1. The amplified PCR fragment was cloned in InsTA vector pTZ57R/T (Thermo Scientific) and sent for sequencing to confirm the point mutation. After sequence confirmation, the insert was subcloned into pBFM and pARL vectors, respectively.

#### 2.2 Yeast methods

#### 2.2.1 Yeast competent cell preparation:

The primary inoculum was given by inoculating the desired yeast strain in 5 ml of yeast growth medium and growing overnight at 30°C, 200 rpm. Next day, a certain volume was taken from the primary inoculum and added in a 40 ml growth medium. The volume of primary culture to be added in the secondary inoculum was calculated using the formula:

Volume required = (Volume of secondary culture x 0.5 OD<sub>600</sub>)/ (Overnight OD<sub>600</sub> of primary culture x 2<sup>n</sup>, n= no. of generations, generally 2 generations). The secondary culture was allowed to grow until OD<sub>600</sub> reaches 0.6 to 0.8. The centrifugation of cells was done at 3500 rpm, 4°C, and the pellet was washed with 10ml autoclaved Milli-Q water to remove culture media remnants. Finally, cells were re-suspended in 300µl Lithium acetate solution (1X Tris-EDTA, 1X Lithium Acetate) to attain the competency.

#### 2.2.2 Yeast transformation:

To the 200µl of competent yeast cells prepared, about 0.5-1µg of desired sample DNA mixed with 10µg of carrier DNA (salmon sperm DNA) was added. PEG solution [10X LiOAc (Sigma), 10X TE, 50% PEG 2000 (Sigma)] of about 1.2ml was added, and it was incubated for 30 minutes, 200 rpm, 30°C. After incubation, heat

shock was given at 42°C and placed on ice immediately for 2 minutes. The cells were spun at 5000 rpm for 1 minute, and the supernatant was discarded completely. The obtained pellet was re-suspended in 200µl 1X Tris-EDTA buffer and then spread on the proper plate. The plates were kept in a 30°C incubator till the appearance of colonies.

#### 2.2.3 RNA isolation from yeast strains:

Yeast cells grown in 10ml of suitable media were taken at mid-log (OD<sub>600</sub> 1) for RNA isolation. Cells were harvested by spinning them for 5 minutes at 3500 rpm. The obtained pellet was re-suspended in 500µl of DEPC water. After re-suspension, cells were given a short spin, and the supernatant was discarded. To the pellet, 400µl of TES (10 mM Tris-Cl pH 7.5, 10 mM EDTA, and 0.5% SDS) solution, 400µl of phenol (H<sub>2</sub>O buffered) was added and vortexed for 10 seconds. Then samples were incubated for 60 minutes on a dry bath with temperature 65°C and vortexed in between every 15 minutes. After that, samples were kept on ice for five minutes and centrifuged for ten minutes at 14000 rpm, 4°C. The acquired aqueous layer was aliquoted to a new tube, and to this, 400µl of chloroform was added. After chloroform addition, samples were vortexed for ten seconds and spun for 10 minutes at 14000 rpm, 4°C. The acquired aqueous layer was transferred to a new microfuge tube. Precipitation of RNA was done by adding 2.2 volume of pre-chilled 100% ethanol and 1/10th volume of 3M NaOAc pH 5.2. The samples were kept at -80°C for 1 hour. After incubation, samples were centrifuged at 14000 rpm for ten minutes, 4°C, and washed the pellet with 500µl of 70% alcohol (prepared with DEPC water). After washing, cells were spun for 10 minutes at 14000 rpm, 4°C. The air-dried pellet was re-suspended in 50µl of DEPC water. The RNA sample's integrity was checked by FA gel electrophoresis, and the concentration by measuring  $OD_{260}$  ( $OD_{260}$  of 1 is equal to a concentration of 40 µg/ml).

#### 2.2.4 Yeast two-hybrid analyses:

For yeast two-hybrid analysis, the PJ69-4A strain was used. pGBDUC1 plasmid with gene of interest was fused to the binding domain, and the second gene was fused to the activation domain in pGADC1 plasmid. The presence of both the plasmid was confirmed by transforming them in PJ69-4A strain and selecting the colonies on double dropout plates Sc-Ura-Leu. The interaction was determined by patching the cells from double dropout plate to triple drop out plates SC-Ura-Leu-Ade/ SC-Ura-Leu-His plates. The weak interaction was scored on SC-Ura-Leu-His plate, whereas strong interaction was scored on the SC-Ura-Leu-Ade plate. Self-activation of the gene was checked by transforming either empty bait or prey vectors and respective plasmids containing the gene of interest. All bait fusion constructs were transformed in the PJ694A strain to generate SNY10, SNY14. In PJ69-4A, as a control, empty pGADC1 and empty pGBDUC1 were transformed to generate SNY16, SNY17. Next, we transformed empty pGADC1 in SNY10, SNY16, SNY14 to generate SNY11 SNY12, and SNY15. Also, prey fusion was transformed in PJ69-4A to generate SNY7. To SNY7, empty pGBDUC1 and BD-RAD51 were transformed to create SNY9 and SNY8. Finally, to SNY14, prey fusion was transformed to generate SNY13. Yeast strains are listed in the **Table 2**.

#### 2.2.5 DNA damage experiments in yeast:

To perform MMS sensitivity assay evaluated by spotting assay, the primary inoculum was given with yeast strains SNY2-SNY6 in media lacking histidine. Next day, secondary inoculum was given and grown till OD<sub>600</sub> reaches 0.5. The cells were normalized, and 10-fold serial diluted and spotted on the SC-HIS plate containing 0.01% MMS. As a control, spotting was also done on the SC-HIS plate without MMS. The plates were shifted to incubator (30°C), and comparison of the growth was done. Return to growth assay was performed to check the efficiency of *PfBLM* to complement MMS sensitivity. Yeast strains (SNY2-SNY6) were grown till they reach the log phase and then divided into two equal portions. One portion was exposed to 0.03% MMS for 2 hrs, whereas the other portion was incubated without

any treatment. After washing MMS, equal numbers of cells from both the parts for each strain were spread on the SC-HIS plate and incubated for 48 hrs. at 30°C. The percent survival was determined by calculating the number of colonies formed between treated versus untreated cultures. Each assay was repeated three times (n=3), and the The graph was plotted using GraphPad Prism software. Two tailed t-test was used to calculate the p value (\* represents P value <0.05; \*\* represents P value < 0.01; \*\*\* represents P value < 0.001; N.S. indicates not significant).

#### 2.3 Recombinant protein expression:

*PfBLM* was cloned in bacterial expression vectors pET22b, pGEX6p2. These constructs were individually transformed into bacterial expression strains, BL21 (DE3\*), Codon plus, and Rosetta. The primary inoculum was given from transformed samples directly and incubated at 37°C incubator, 200 rpm overnight. From the overnight culture, the secondary inoculum was given and grown until OD<sub>600</sub> reaches 0.6-0.8. Induction was given with 1mM isopropyl thiogalactoside (IPTG, Sigma) incubating at different temperatures individually. Induction at 37°C was kept for 4 hrs. incubation, whereas at 25°C was kept for overnight. After OD<sub>600</sub> was measured, induced and un-induced samples were normalized, and the cell pellet was collected. Finally, the pellet was dissolved in 1x laemmlli buffer. The recombinant protein was visualized by SDS-PAGE.

#### 2.4 Methods in *Plasmodium falciparum* culture:

#### 2.4.1 Washing of red blood cells (RBCs):

From a healthy volunteer, 10 ml of blood was collected in a tube containing 1.5ml of CPDA (2.63% Trisodium citrate, 0.32% citric acid, 3.19% dextrose, 0.22% NaH2PO4.H2O, and 0.02% adenine) and stored at 4°C till washing started. The blood washing should be done within 6 hours of collection. Initially, the blood was centrifuged at 1,500 rpm for 15 minutes at 4°C. The supernatant (serum) and the white buffy layer at the junction were aspirated carefully with a Pasteur pipette. After spinning, volume of the RBC layer obtained was evaluated, and to that an equal volume of chilled incomplete medium was added and mixed them gently with

pipette. Centrifugation of the sample was done at 2,500 rpm for 10 minutes at 4<sup>o</sup>C. The supernatant was aspirated and rewashed with a pre-chilled incomplete medium. The washing step was repeated once again, and the washed RBC was mixed with an equal volume of incomplete medium to make hematocrit (hct) 50%. The washed blood was stored at 4<sup>o</sup>C.

#### 2.4.2 Thawing of *Plasmodium* parasites from liquid nitrogen:

Frozen parasite vial was taken out from the liquid nitrogen tank and kept for warming in a water bath at 37°C for 3 minutes. Proper care was taken to avoid contamination of the vial. The content of the vial was transferred into a new 50ml falcon tube, and 0.2ml of the solution 1 (12% NaCl) was added dropwise (approximately one drop/second) by shaking gently. After adding solution 1, the sample was left undisturbed for 3-4 minutes. To this, 10ml of solution 2 (1.6% NaCl) was added dropwise with intermittent gentle shaking. The sample was centrifuged at room temperature for ten minutes at 2000 rpm. The supernatant was aspirated, and to the pellet, 10ml of solution 3 (0.9% NaCl, 0.2% Glucose) was added dropwise by gentle shaking. The sample was spun for 10 minutes at 2000 rpm. The supernatant was discarded, and to the pellet 0.2ml of fresh RBCs (50% hct), 3 ml of complete medium was added. Finally, the contents in the tube were transferred into a sterile 6 well culture plate and kept in a candle jar which was kept in a 37°C incubator. The volumes of solutions added are calculated according to 1 ml of the sample.

#### 2.4.3 Freezing of *Plasmodium* parasites:

The early ring-stage parasites with a parasitemia of about 2-4% were transferred into a 15 ml falcon tube, centrifuged at 2500 rpm for 10 minutes. The supernatant was aspirated, to the estimated PCV (packed cell volume), equal volume of freezing solution (5% Glycerol, 1.6% sodium lactate, 0.03% KCl, 25mM Sodium phosphate) was added dropwise (1 drop/second). The contents were mixed gently and left undisturbed for 5 minutes. To the tube, 1.3 volumes of the freezing solution were added dropwise. Finally, 1ml of the sample was transferred into each cryo-vial. These cryo-vials were transferred to a frozen container having iso-proponal for gradual

freezing. The freezing container was stored at -20°C overnight. Next day, for long-term storage, the vials were shifted into a liquid nitrogen tank.

#### 2.4.4 Maintenance of *Plasmodium in vitro* culture:

The candle jar method was followed to maintain strains of *P. falciparum in vitro*. The culture was maintained in RPMI-1640 complete media containing Albumax-II (5mg/ml), Hypoxanthine (0.5mg/ml). The hematocrit of RBC was maintained at 5%, and subculture was done once the parasitemia reaches 2.5%. During subculture, parasitemia was diluted to 0.5% by adding fresh media and blood. The volume of the culture was adjusted to 5ml accordingly. Parasitemia was estimated by counting the Giemsa stained blood smears.

#### 2.4.5 Synchronization of *Plasmodium* parasites by sorbitol method:

The culture with early ring-stage parasites of 5 ml was transferred into a 15ml falcon tube and centrifuged for 10 minutes at 2000 rpm, RT. The supernatant was aspirated, and 0.5ml of pre-warmed 5% sorbitol solution was added to the pellet. The pellet was incubated at 37°C in a water bath for 20 minutes with intermittent mixing for 5 minutes. After incubation, a pre-warmed incomplete medium was added to make up the volume to 5 ml and centrifuged for ten minutes at 2500 rpm, RT. Supernatant was aspirated, and washing was repeated thrice. Finally, the pellet was re-suspended in complete medium, transferred into a new well in 6 well culture plate, and kept in candle jar which was in a 37°C incubator.

#### 2.4.6 Genomic DNA isolation from *Plasmodium*:

The parasite culture of 10ml having 6-8 % parasitemia was harvested and centrifuged for ten minutes at 3000 rpm, RT. To the pellet obtained, two PCV volumes of 0.15% saponin was added and incubated for 30 minutes in a 37°C water bath with intermittent vortexing. After that, five volumes of pre-warmed incomplete medium were added and centrifuged for 10 minutes at 6000 rpm at 4°C. The obtained pellet was washed with a 1x PBS (phosphate buffer saline) solution to remove saponin remnants. To this pellet, 75 µl of Milli-Q water and 25 µl of lysis buffer (10mM Tris-HCl pH-8, 20mM EDTA pH-8, 0.5% SDS, and 0.1mg proteinase K) was added and

incubated at 37°C for 3 hrs. with intermittent mixing at every 30 minutes. After incubation, Milli-Q water was added to make the volume to 400µl, and to this, an equal volume of PCIA (phenol, chloroform, isoamyl alcohol) solution was added. The sample was spun at 12000 rpm for 15 minutes at room temperature. The aqueous layer was collected into a new microfuge tube and treated with RNase for 30 minutes at 37°C. After RNase treatment, the PCIA step was repeated. To the aqueous layer obtained, 2.2 volumes of 100% ethanol and Solution 3 (1/10 volume) was added. The sample was incubated for overnight precipitation at -80°C. The next day, the sample was centrifuged at 12000 rpm for 30 minutes, 4°C. Finally, 1xTE buffer the pellet was dissolved, and the integrity of genomic DNA was checked by running agarose gel electrophoresis.

#### 2.4.7 Protein preparation from *Plasmodium*:

Parasite cultures of about 5-10ml were collected and centrifuged for 10 minutes at 3000 rpm, RT. Two PCV of 0.15% saponin was added to the pellet and was incubated at 37°C water bath for twenty minutes with intermittent mixing. The sample was mixed with 5 volumes of pre-warmed incomplete medium and spun at 4000 rpm for ten minutes at 4°C. The obtained parasite pellet was washed with 1x PBS 3-4 times to remove the remnants of saponin. Finally, the parasite pellet was resuspended in 1X Laemmli buffer(Tris-HCl, 63 mM (pH 6.8), 10% Glycerol, 0.0005% Bromophenol blue, 0.1% 2-Mercaptoethanol). The quality and integrity of protein preparation were checked by running SDS-PAGE.

#### 2.4.8 RNA isolation from *Plasmodium*:

The parasite culture of about 10ml was harvested and spun for 10 minutes at 3000 rpm. The supernatant was discarded, and the cell pellet was loosened by tapping. To the pellet, pre-warmed TRIzol (10 pellet volumes for the ring and 20 pellet volumes for trophozoite and schizont) was added. The pellet was shaken thoroughly to avoid clumping. The sample was incubated at 37°C for 5 minutes. After incubation, 0.2 TRIzol volumes of chloroform were added, and the sample was shaken vigorously. The sample was allowed to settle for 2-3 minutes and centrifuged at 4°C for 30 minutes.

minutes at high speed. In a new microfuge tube, the obtained aqueous layer was shifted, and 2-proponal (1ml) was added. At 4°C, the sample was kept for incubation overnight. The samples were centrifuged next day at 14000 rpm, 4°C for 30 minutes. The pellet was washed with 75% ethanol (prepared with DEPC waster) and spun at 14000 rpm for thirty minutes, 4°C. At last, air-dried pellet was re-suspended in 50µl of DEPC water. The integrity of RNA was checked by running FA agarose gel electrophoresis, and the concentration was determined by measuring OD<sub>260</sub>.

#### 2.4.9 Transfection in *Plasmodium falciparum*:

Synchronized early ring-stage parasites having parasitemia around 6-8% were taken for transfection. The desired plasmid (80-100µg) was resuspended in 50µl of cytomix solution (10mM K<sub>2</sub>HPO<sub>4</sub> pH-7.6, 120mM KCl, 0.15mM CaCl<sub>2</sub>, 25mM HEPES pH-7.6, 2mM EGTA pH-7.6, and 5mM MgCl<sub>2</sub>) and kept in 4°C for overnight before the day of transfection. On the day of transfection, 10 ml of the parasite culture was centrifuged at 3000 rpm for 5 minutes at room temperature and, the supernatant was aspirated. The pellet was added with 5ml of pre-warmed cytomix solution and spun for 5 minutes at 3000 rpm. Washing with cytomix was repeated once again. To the pellet, 1250µl of pre-warmed cytomix was added and pipetted gently. From the re-suspension, 350µl was taken and added to a microfuge tube containing 50µl of cytomix re-suspended DNA. The contents from the microfuge tube were transferred to the electroporator cuvette without generating any air bubbles. Then, the cuvette was placed in the Bio-Rad Gene Pulsar, and pulse was given by selecting the program having 0.31kV, 950μF, α resistance. After the pulse, the sample in the cuvette was mixed with cold complete media and transferred to 6 well culture plate. Pre-warmed complete media of about 3ml and 100µl of fresh RBC was added to the 6 well plate. The plate was kept in an incubator containing a candle jar at 37°C. The complete medium was changed daily until the parasitemia reaches up to 4-8 %. After the parasitemia was reached, pyrimethamine containing complete media was added to eliminate non-transfectants and allow only transfectants to grow.

#### 2.5 DNA damage experiments in parasites:

For the stage-specific DNA damage experiments the cells were treated with 0.05% MMS for 6 hrs. and untreated cells were also grown simultaneously. Semi-quantitative PCR and western blotting was performed after isolating RNA/protein from both the group of cells.

Return to growth assay was performed with 3D7 cells harboring pARL-PfBLM and pARL-PfblmK83R overexpression plasmids. Synchronized parasites of three IDC stages were taken with parasitemia around 1% and treated with 0.002% or 0.005% MMS for 2 hrs. After the treatment, cells were washed twice and allowed to grow in complete media for 48 hrs. 3D7(wild type) parasites were also given MMS treatment, as mentioned above, which acted as a control. Percentage survival was obtained by taking the ratio of percentage survival between treated and untreated cultures. The experiment was repeated thrice (n=3), and the graph was plotted using GraphPad Prism software. Two tailed t-test was used to calculate the p value (\* represents P value <0.05; \*\* represents P value < 0.01; \*\*\* represents P value < 0.001; N.S. indicates not significant).

#### 2.6 Drug studies in *Plasmodium*:

#### 2.6.1 Inhibitory concentration determination assay in *Plasmodium*:

Synchronized trophozoite stage parasites (3D7 & Dd2) having parasitemia 1% were used for the assays. The assay was performed with 1ml culture in 1.5ml microfuge tubes. The culture was spun at 2500 rpm for five minutes, and the obtained supernatant was discarded. To the cells in pellet, 1ml complete media containing varying concentrations of drugs was added and transferred to 24 well culture plates. The plate was incubated for 48 hrs. in a 37°C incubator containing a candle jar. The concentrations of ML216 and MIRA-1 taken for assay ranged from 0.001μM to 1000μM. DMSO treated culture was taken as vehicle control. Cell survivability was evaluated by both Giemsa staining method as well as SYBR Green-I based assay like previously described [98]. Dose-response curves were plotted using Graph Pad

Prism to obtain  $IC_{50}$  values. Each assay was reproduced thrice for reproducibility (n=3).

#### 2.6.2 *In vivo* growth inhibition assay with ML216:

The *in vivo* antimalarial activity of ML216 was evaluated by performing Peters 4-day suppressive test [99]. Two random group of mice were made with 4 individuals in each group, and an equal number of pRBCs (*P. berghei* ANKA) was injected intraperitoneally in mice. The animals in the test group were injected with 25mg/Kg ML216 intraperitoneally after three hours of infection. The animals in negative-control group were injected with 200µl of the vehicle (0.1% DMSO in water). The drug treatment was given for 4 days beginning from day 0 of infection. Blood smears were prepared from all the groups of mice from day 0, and Giemsa stained to assess the parasitemia levels. The host survivability in all groups was monitored daily for a period of 40 days following inoculation. The parasitemia of mice each group was plotted against the days post infection and kaplan-meier survival curve was plotted for the mice used in the experiment.

#### 2.6.3 Effect of ML216 on DNA damaged cells:

The synchronized parasites from three blood stages, having parasitemia 1% was taken for assay. The assay was performed with 1ml culture in a 24 well plate. The cultures were split into 2 equal parts; to one half 0.005% MMS treatment was done for 2 hrs. and MMS was washed after treatment. Complete medium containing different concentrations of ML216 (0.1 nM to 1000 µM) was added to the cells and allowed it to grow for 48 hours. The second part of the culture was grown in ML216 without MMS treatment. Two controls were kept in this experiment, one in which MMS treatment was done without the addition of M216 and the other in which both MMS and ML216 was added. Cell survivability was evaluated by Giemsa staining method. Dose-response curves were plotted using Graph Pad Prism to obtain IC50 values. Each assay was reproduced thrice for reproducibility (n=3).

# 2.6.4 Fixed ratio method to determine the interaction between ML216 and DHA/CQ/ATQ:

Trophozoite stage parasites were used to determine the interactions between ML216 and DHA/CQ/ATQ. IC<sub>50</sub> of DHA/CQ/ATQ was determined similarly like ML216. For each drug, 8-fold of their IC<sub>50</sub> concentration was taken as 100% and 6 fixed ratios were prepared (5:0, 4:1, 3:2, 2:3, 1:4, and 0:5) based on that. Each combination was 2-fold serial diluted six times so that in the 3<sup>rd</sup> and 4<sup>th</sup> of a serial dilution the IC<sub>50</sub> value falls. The inhibitory effect of 2-fold serial dilutions of each drug combination on the parasite was determined in a 96-well plate in triplicates. Each well contained 200µl culture, 1% parasitemia, and 2.5% hematocrit. Incubation of the plate was done at 37 °C after drug treatment for 48hrs. After the incubation period, smears were prepared for Giemsa staining based determination of parasitemia. For each combination, semi-log graph was plotted to determine IC<sub>50</sub> value using GraphPad Prism software. The fractional inhibitory concentration (FIC) for each compound was determined using the equation: FIC=IC<sub>50</sub> of the drug in combination/IC<sub>50</sub> of individual drug. The FIC values of both drugs were used to determine the interaction between ML216 and DHA by using the equation.

 $\Sigma$ FIC= (IC<sub>50</sub> of DHA in combination /IC<sub>50</sub> of DHA) + (IC<sub>50</sub> of ML216 in combination/IC<sub>50</sub> of ML216). GraphPad Prism software was used to plot isobologram.  $\Sigma$ FIC <1 represents synergism;  $\Sigma$ FIC $\geq$ 1 and 2 represent additive interaction, and  $\Sigma$ FIC $\geq$ 2 represents antagonism. A similar equation was used for CQ/ATQ and ML216 combination.

#### 2.7 Co-purification assay:

Rosetta (DE3) bacterial expression cells harboring pGEX6P2: *PfBLM* was induced with 1mM Isopropyl thiogalactosidase (IPTG) at 16°C overnight, whereas the same cells harboring pET101D: *PfRAD51* was induced with IPTG (1mM) at 37°C for 4 hours. All the pellets were lysed using the standard laboratory protocol. Briefly, 0.5 gm of cell pellets were suspended in 2 ml lysis buffer (50% Glycerol, 50 mM NaH<sub>2</sub>PO<sub>4</sub>, 20 mM imidazole, 20 mM β-mercaptoethanol, 200 mM NaCl and 2%

Tween 20) containing 1 mg/ml lysozyme and protease inhibitor (PMSF). For each pellet, sonication was done on ice separately to attain proper lysis. After sonication, the pellets were spun at 10000g for 40 minutes at 4°C and supernatant was collected. The supernatant of PfRad51 and PfBlm were mixed in equal volumes and incubated for 1 hour in the rocking condition. The supernatant mixture was then added with 50% Ni-NTA slurry and incubated for 1 hour in a rocking position and 1 hour in the column in a standing position. Initially, loading flow-through was collected, after that the column was washed with the wash buffers I and II containing varied concentrations of imidazole (20mM and 50mM). Elution was done with buffer containing imidazole concentration 400mM. Co-purification was also performed with supernatants of PfRad51 and an empty GST tag mixture, which acted as a control. The eluted samples were further analyzed by western blotting technique.

#### 2.8 Western blot analysis:

The protein samples of interest were separated on SDS-PAGE and transferred onto the Poly Vinylidene di Fluoride (PVDF) membrane. Before the transfer, the membrane was treated with methanol for 20 seconds, water for 2 minutes, with 1x transfer buffer (5.86 gm glycine, 11.64 gm Tris base, and 0.75 gm SDS) for 5 minutes. Semi-dry transfer method was used, and the transfer conditions were 240mA of current for 80 minutes. After the transfer, blocking of the membrane was done by 5% blocking buffer (5 gm skimmed milk powder, 100ml 1x TBS) for 2 hrs. RT. The blot was added with the primary antibody and kept at 4°C overnight in a rocking position. Next day, washing of the blot was done with 1xTBST (0.2 M Tris base, 9% sodium chloride pH 7.6, and 0.1% Tween 20) three times. HRP conjugated antibodies were used for secondary antibody treatment for 2 hrs. and washed as previously described. The blot was developed by the chemiluminescence system (Pierce) substrate and visualized in a Bio-Rad chemidoc system. Quantification of blot intensities was done by using the Image J software. For probing PfBlm peptide, the antibody was generated for a unique sequence at the C-terminus of PfBlm protein (KELEKREEELNEKTKNDQE). The peptide antibody was generated in

rabbits. Anti-Blm antibody, anti-actin antibody, and anti-HIS antibody was used at 1:5,000 dilution. HRP-conjugated anti-rabbit secondary antibody (Calbiochem) was used at 1:10,000 dilution for PfBlm protein, whereas anti-mouse secondary antibody which was HRP-conjugated (Calbiochem) was used at 1:10,000 dilutions for actin and histidine-tagged proteins.

#### 2.9 Methods for bioinformatics analyses:

#### 2.9.1 Docking and molecular dynamics simulations:

The PfBlm protein was modeled using the I-TASSER server [100, 101]. A quality check of the predicted structural models was performed using the PROCHECK program [102]. The model closest to HsBLM structure (PDB ID: 4CGZ) [103] in terms of root mean square deviation (RMSD) was chosen for further studies. A 10 ns equilibration of the model was carried out using the GROMACS program with the CHARMM36 force field [104, 105]. In order to choose a representative structure from the simulation trajectory, a clustering of structures from the last 5 ns of the trajectory was performed using the GROMACS program. The structure at the center of the largest cluster was chosen as a representative structure for docking studies. The inhibitors ML216 and MIRA-1 were docked on to PfBlm model using the AutoDock Vina program [106]. Two independent docking runs were performed for both the inhibitors: one with the ATP-binding site as the docking search space, and one with the DNA-binding region as the docking search space. For each run, the docking pose with the highest number of protein-inhibitor hydrogen bonds was selected for molecular dynamics simulations. The protein-inhibitor complex was simulated for 50 ns using the GROMACS program with the CHARMM36 force field [104, 105]. Force field parameters for the inhibitor molecules were obtained using the Paramchem server [107, 108]. The binding free energy for the proteininhibitor complex was calculated using the molecular mechanics Poisson-Boltzmann surface area (MM-PBSA) method [109, 110].

## CHAPTER II Materials and methodology

Table. 1 List of primers used in this study

Primer	Primer Sequence	Purpose	
OMKB332	ATTCGAGATAAAGGAATTATTGAAG	F.P. to amplify <i>PfBLM</i> for Semi quantitative PCR	
OMKB333	ATGCTTCCTCTTTACATTCATAG	R.P. to amplify <i>PfBLM</i> for Semi quantitative PCR	
OSB94	CTGTAACACATAATAGATCCGAC	F.P. to amplify <i>PfARP</i> for Semi quantitative PCR and short-range PCR product	
OSB95	TTAACCATCGTTATCATCATTATTTC	F.P. to amplify <i>PfARP</i> for Semi quantitative PCR and long-range PCR product	
OMKB394	TCAGGATCCATGGTGACGAAGCCGTCAC	F.P. to amplify <i>ScSGS1</i> for cloning in pBFM vector	
OMKB395	TCAGTCGACCTTTCTTCCTCTGTAGTGAC	R.P. to amplify <i>ScSGS1</i> for cloning in pBFM vector	
OMKB372	TCAGGATCCATGAATGAAGATGCTATGAAAATTTTG	F.P. to amplify <i>PfBLM</i> for cloning in pBFM, pGEX-6P2 and pGADC1 vectors	
OMKB373	TCAGTCGACAATTTTCCTTGGAATTTTAAATGAAG	R.P. to amplify <i>PfBLM</i> for cloning in pBFM vector	
OMBK382	CTAGTCGACTCAAATTTTCCTTGGAATTTTAAATG	R.P. to amplify <i>PfBLM</i> for cloning in pGEX-6P2 and pGADC1 vectors	
OMKB19	ATCGGATCCATGAAACAAGCAAATACAAAAG	F.P. to amplify <i>PfRAD51</i> for cloning in pGBDUC-1 vector	
OMKB17	ATCGTCGACTTTATTTTTCCTCATAATCTGC	R.P. to amplify <i>PfRAD51</i> for cloning in pGBDUC-1 vector	
OMKB610	ATCGGTACCATGAATGAAGATGCTATGAAAATTTTG	F.P. to amplify <i>PfBLM</i> for cloning in pARL vector	
OMKB611	ATCCCTAGGAATTTTCCTTGGAATTTTAAATGAAG	R.P. to amplify <i>PfBLM</i> for cloning in pARL vector	
OMKB666	AAATTAAGGATCTCCCACCACCTG	Overlapping primer to create <i>PfblmK83R</i> mutation	
OMKB667	CAACAGGTGGTGGGAGATCC	Overlapping primer to create <i>PfblmK83R</i> mutation	
OMKB276	AAGAATTGGGACAACTCC	R.P. to amplify GFP for confirming Transfection	
OMKB463	TCAGTCGACATGTTGAATGATATGAATGATAAAAAAG	F.P. to amplify long-range PCR product	
OMKB464	TCAGTCGACTCAACCTATGTAACCTTTACACTTC	R.P. to amplify long-range PCR product	

F.P: Forward Primer: R.P: Reverse Primer

**Table 2.**List of yeast strains used in this study

Strain name	Genotype	Source
	MATa trpl-901 leu2-3,112 ura3-52 his3-200 ga14Δ ga180Δ	
PJ69-4A	LYS2::GALl-HIS3 GAL2-ADE2 met2::GAL7-lacZ	[14]
SNY1	<i>MAT</i> $\alpha$ <i>leu2-3,112 trp1-1 can1-100 ura3-1 ade2-1 his3-11,15,</i> $sgs1\Delta$ :: $KAN^r$	This study
SNY2	$MATα$ leu2-3,112 trp1-1 can1-100 ura3-1 ade2-1 his3-11,15, sgs1 $Δ$ :: $KAN^r$ pBFM / ScSGS1	This study
	<i>MATα leu2-3,112 trp1-1 can1-100 ura3-1 ade2-1 his3-11,15</i> ,	
SNY3	$sgs1\Delta::KAN^rpBFM/PfBLM$	This study
SNY4	MATα leu2-3,112 trp1-1 can1-100 ura3-1 ade2-1 his3-11,15, sgs1 $\Delta$ ::KAN <sup>r</sup> pBFM / PfblmK83R	This study
SNY5	MAT $\alpha$ leu2-3,112 trp1-1 can1-100 ura3-1 ade2-1 his3-11,15, sgs1 $\Delta$ ::KAN $^r$ pBFM / PfWRN	This study
51113	<i>MATα leu2-3,112 trp1-1 can1-100 ura3-1 ade2-1 his3-11,15</i> ,	This study
SNY6	$sgs1\Delta::KAN^rpBFM$	This study
	MATa trpl-901 leu2-3,112 ura3-52 his3-200 ga14∆ ga180∆	
SNY7	LYS2::GALl-HIS3 GAL2-ADE2 met2::GAL7-lacZ	This study
	pGADC1/PfBLM	
	MATa trpl-901 leu2-3,112 ura3-52 his3-200 ga14∆ ga180∆	
SNY8	LYS2::GALl-HIS3 GAL2-ADE2 met2::GAL7-lacZ	This study
	pGADC1/PfBLM pGBDUC1/PfRAD51	
CNINO	MATa trpl-901 leu2-3,112 ura3-52 his3-200 ga14∆ ga180∆	TD1-141
SNY9	LYS2::GALl-HIS3 GAL2-ADE2 met2::GAL7-lacZ	This study
	pGADC1/PfBLM pGBDUC1  MATa trpl-901 leu2-3,112 ura3-52 his3-200 ga14∆ ga180∆	
SNY10	LYS2::GALl-HIS3 GAL2-ADE2 met2::GAL7-lacZ	This study
511110	pGBDUC1/PfRAD51	Tims study
	MATa trpl-901 leu2-3,112 ura3-52 his3-200 ga14Δ ga180Δ	
SNY11	LYS2::GALl-HIS3 GAL2-ADE2 met2::GAL7-lacZ	This study
	pGBDUC1/PfRAD51 pGADC1	
	MATa trpl-901 leu2-3,112 ura3-52 his3-200 ga14∆ ga180∆	
SNY12	LYS2::GALl-HIS3 GAL2-ADE2 met2::GAL7-lacZ pGBDUC1	This study
	pGADC1	
	MATa trpl-901 leu2-3,112 ura3-52 his3-200 ga14∆ ga180∆	
SNY13	LYS2::GAL1-HIS3 GAL2-ADE2 met2::GAL7-lacZ	This study
	pGBDUC1/PfalMRE11 pGADC1/PfBLM	
CNIX71 4	MATa trpl-901 leu2-3,112 ura3-52 his3-200 ga14Δ ga180Δ	
SNY14	LYS2::GALl-HIS3 GAL2-ADE2 met2::GAL7-lacZ	This study
	pGBDUC1/PfalMRE11  MATa trpl-901 leu2-3,112 ura3-52 his3-200 ga14∆ ga180∆	
SNY15	LYS2::GALl-HIS3 GAL2-ADE2 met2::GAL7-lacZ	This study
511113	pGBDUC1/PfalMRE11 pGADC1	Tins study
	MATa trpl-901 leu2-3,112 ura3-52 his3-200 ga14Δ ga180Δ	
SNY16	LYS2::GALl-HIS3 GAL2-ADE2 met2::GAL7-lacZ pGBDUC1	This study
	MATa trpl-901 leu2-3,112 ura3-52 his3-200 ga14∆ ga180∆	
SNY17	LYS2::GAL1-HIS3 GAL2-ADE2 met2::GAL7-lacZ pAGDC1	This study

## **CHAPTER-III**

Implications of *PfBLM* in *Plasmodium* **DNA** repair

#### 3. Introduction:

Resistance to the available drugs obstructs the process of malaria treatment. It is necessary to be equipped with new drug molecules that target indispensable pathways in the parasite. Earlier reports have shown that *Plasmodium* relies on the homologous recombination (HR) pathway to repair DNA damage incurred during cellular processes [13]. To regard HR as a drug target, we need to study molecules of the pathway. RecQ helicases take part in different DNA metabolic pathways and are very crucial for maintaining genome stability. However, RecQ helicases have a critical role in homologous recombination since most of its substrates resemble repair intermediates of the pathway [111]. Out of five RecQ helicases in humans, Bloom's syndrome helicase (BLM) and Werner's syndrome helicase (WRN) have a crucial role in the HR pathway. BLM and WRN function at different steps to ensure the proper repair of damaged DNA. BLM particularly has a significant role at critical stages of the pathway. Extended resection of the broken ends prompts the cells to undergo homologous template mediated repair instead of NHEJ. BLM functions during this long-range resection stage carried out by two independent proteins DNA2 and EXO1. BLM's role in the DNA2 mediated pathway indispensable but not in EXO1 mediated pathway [67]. During the pre-synaptic and synaptic HR phase, BLM displays both pro and anti-recombinogenic activity depending upon its post-translational modifications [112]. BLM enriches key recombinase protein Rad51 to DSB ends when it is in SUMOylated state [78] and promotes strand exchange activity when Rad51 is in active ATP-bound form [79]. Termination of HR requires the resolution of the unusual DNA structures formed during the process. Double Holliday junction (dHJ) is one such repair intermediates whose resolution results in different end-product formation. Dissolution of dHJ by Blm along TopoIII-RmiI produces complete non-crossover products, an essential process during mitotic HR. Earlier reports have shown that *Plasmodium* RecQ helicases are required for normal replication and transcription, but none of them

demonstrated their DNA repair activity. Keeping in mind, the critical functions of *BLM* in DSB repair, we chose to study the DNA repair activity of *Plasmodium BLM*. To this end, we investigated the expression of *PfBLM* under DNA damaging conditions and its interaction with essential DNA repair proteins of *Plasmodium*. Next, we checked the DNA repair activity of *PfBLM* using a yeast surrogate system. Finally, we confirmed the DNA repair activity of *PfBLM* by performing overexpression studies in the parasite.

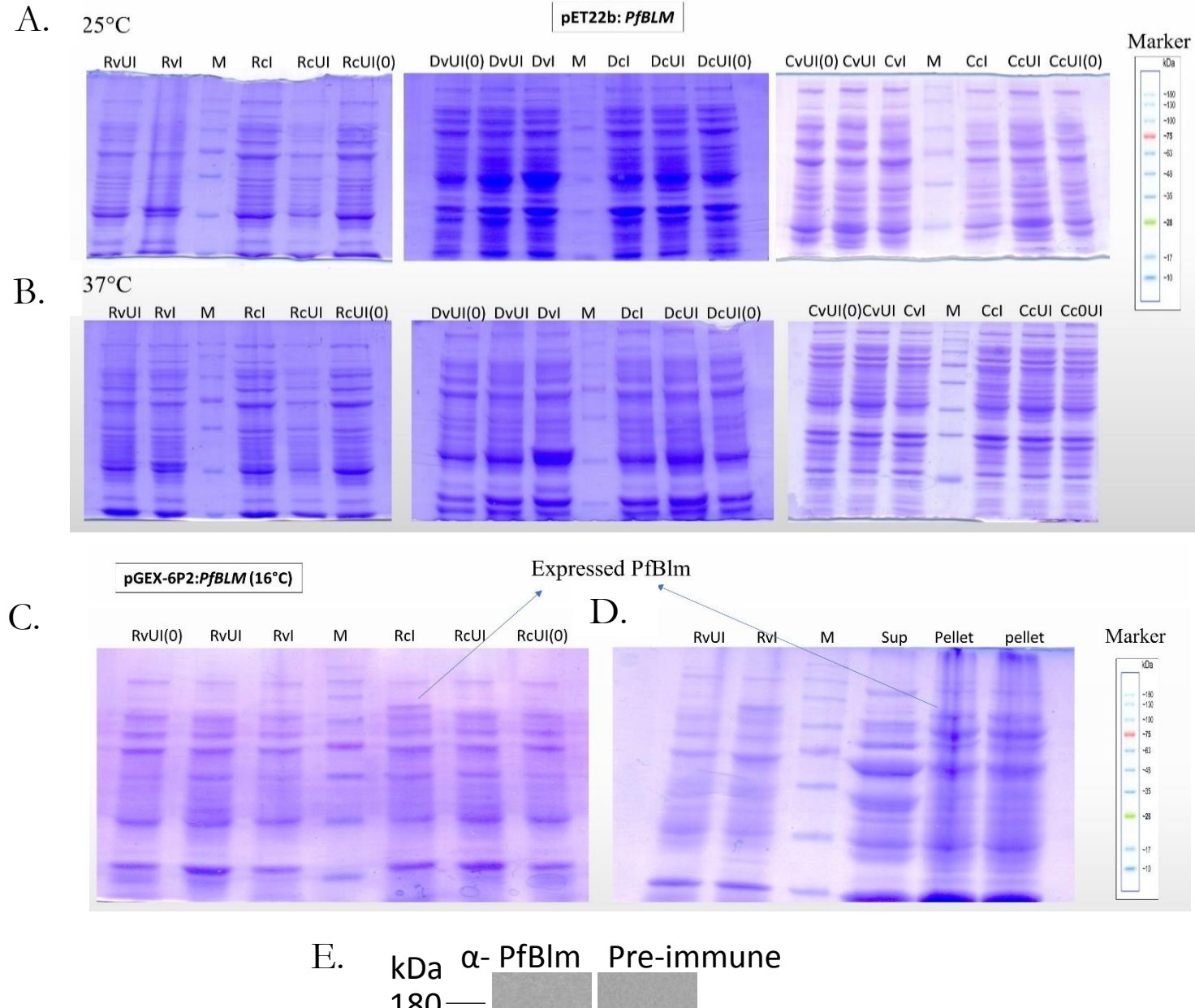
#### 3.1 Results:

#### 3.1.1 Expression of *PfBLM* and antibody generation:

To generate an antibody against PfBlm protein, we attempted to express and purify the full-length protein. To this end, we cloned the *PfBLM* gene in pET22b and pGEX-6P2 bacterial expression vectors. We transformed the constructs in different bacterial expression strains rosetta, BL21 DE3\*, and codon plus, and subjected to IPTG mediated induction at various conditions. Protein induction was not observed with the pET22b:*PfBLM* construct (Fig. 6A & 6B), but with the pGEX-6P2:*PfBLM* construct minimal expression was observed (Fig. 6C). However, protein induction was too low to proceed for purification, and remained in insoluble pellet fraction after sonication (Fig. 6D). We opted for peptide antibody generation and raised an antibody against the unique C-terminal region of the protein (Fig. 6E).

# 3.1.2 *PfBLM* expression is maximum at the mitotically active schizont stage of *P.falciparum*:

To check the expression of *PfBLM* during blood stages of *P. falciparum*, we performed real-time RT-PCR, semi-quantitative RT-PCR and western blotting. Previous reports have shown that *HsBLM* and *ScSGS1* expression levels are at peak during S-phase of cell cycle [113, 114]. Since intra-erythrocytic developmental stages of *Plasmodium* follow the pattern of regular cell cycle we sought to investigate its expression level during different blood stages. For this purpose, from synchronous parasites, we isolated RNA and protein at the ring, trophozoite and schizont stages to perform quantitative RT-PCR, and western blotting. At the RNA level, expression of *PfBLM* was found to be high during schizont and trophozoite stage compared to the ring stage. As a loading control, *PfARP* (Asparagine rich protein) was used. In quantitative RT-PCR, we observed five and eleven-fold up regulation of *PfBLM* in trophozoite and schizont stages in contrast to ring stage (Fig. 7A). Similar pattern of upregulation was observed with semi-quantitative RT-PCR as well (Fig. 7B).



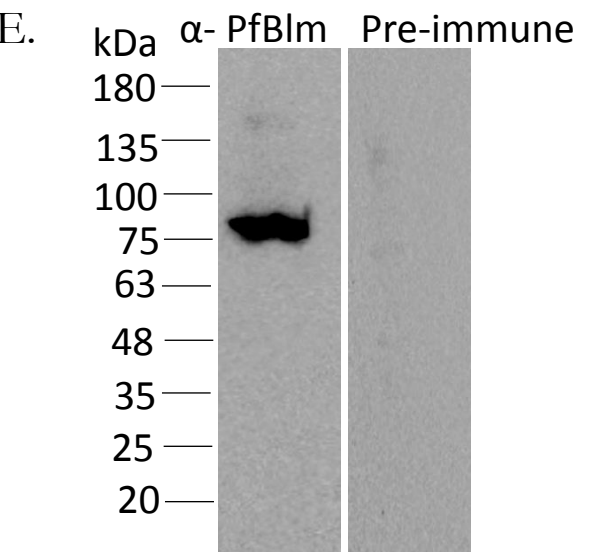


Fig. 6

Fig. 6: Expression of recombinant protein PfBlm in bacterial expression vectors pET22b and pGEX-6P2: (A) SDS-PAGE shows no expression of PfBlm as histidine tagged protein in Rosetta (R), BL21 DE3\* (D) and codon plus (C) strains at 25°C. (B) SDS-PAGE shows no expression of PfBlm as histidine tagged protein in Rosetta (R), BL21 DE3\* (D) and codon plus (C) strains at 37°C. C) SDS-PAGE shows the expression of *PfBLM* in pGEX-6P2 vector in Rosetta at 16°C. (D) SDS-PAGE shows the expressed pGEX-6P2:*PfBLM* clone after sonication where the majority of the induced protein is seen in pellet fraction. (E) Specificity of anti-PfBlm antibody that recognized a specific band of 80 kDa corresponding to PfBlm protein versus the pre-immune sera.

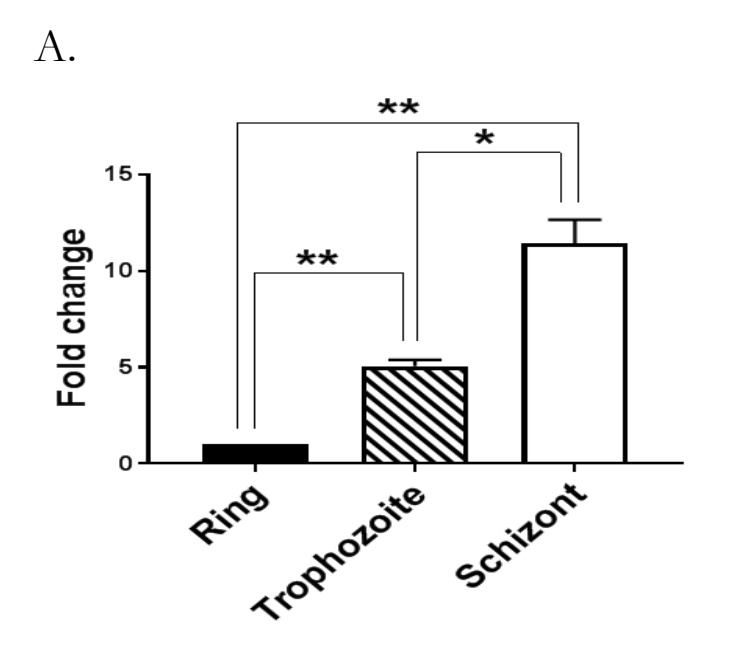
The abbreviation of the tags used in A, B, C, and D are presented below:

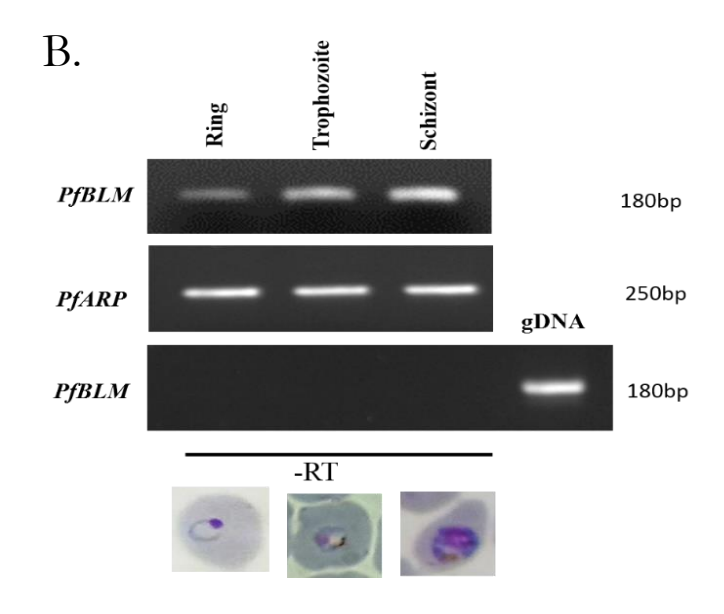
**RvUI** : Rosetta vector uninduced RcUI : Rosetta clone uninduced RvI: Rosetta vector induced RcUI(0) : Rosetta clone uninduced 0 hr. DvUI(0): BL21 DE3\* vector uninduced 0hr. : Rosetta clone induced RcI : BL21 DE3\* vector uninduced DcUI(0) : BL21 DE3\* clone uninduced 0hr. **DvUI** DvI : BL21 DE3\* vector induced **DcUI** : BL21 DE3\* clone uninduced : BL21 DE3\* clone induced CvUI(0) : Codon plus vector uninduced 0hr. DcI CvUI : Codon plus vector uninduced CcUI(0) : Codon plus clone uninduced 0hr. CvI : Codon plus vector induced CcUI : Codon plus clone uninduced CcI : Codon plus clone induced

These findings are in good agreement with several high-throughput transcriptome data available in the database [115, 116]. The schizont stage specific abundant expression of PfBlm protein corroborated well with the mRNA expression data (Fig. 7C & 7D). PfActin was used as loading control for the western blotting experiments. As the schizont stage is associated with replication and HR activities our results suggest the likely involvement of PfBlm in these two conserved processes.

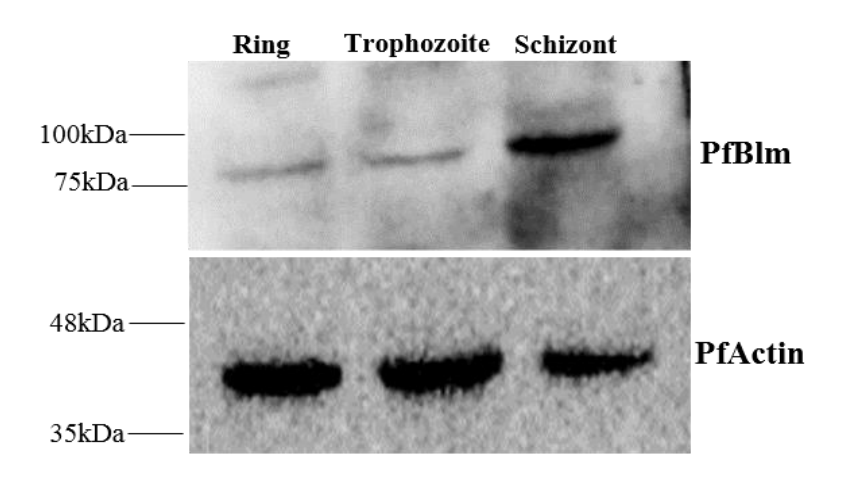
#### 3.1.3 DNA damage induced up-regulation of *PfBLM* during IDC stages:

We investigated whether *PfBLM* is over-expressed in response to DNA damage. Earlier reports have shown that *Plasmodium* proteins involved in DSB repair are overproduced upon DNA damage [14, 15]. Hence, we sought to investigate stage specific induction of PfBLM under DNA damaging conditions. For this purpose, we treated tightly synchronous parasites of the ring, trophozoite and schizont stages with known DNA damaging agent methyl methane sulfonate (MMS) for 6 hrs. After the treatment, total RNA/proteins were isolated from both the cultures (untreated and treated). We performed quantitative RT-PCR to check the expression of PfBLM in both treated and untreated cultures. As a loading control, PfARP was used. At the ring stage, we observed fourteen-fold up regulation of PfBLM under DNA damaging conditions and at the trophozoite stage five-fold up-regulation, but its level remained unchanged during the schizont stage (Fig. 8A). We examined induction of PfBlm protein with western blotting in the three blood stages of the parasite. The expression of PfBlm was increased almost three-fold under DNA damaging condition in the ring and the trophozoite stage whereas no significant induction was observed at the schizont stage (Fig. 8B & 8C) which correlates with the transcript level. It could be possible that the steady-state level of PfBLM mRNA or protein is already so high at the schizont stage that any further induction was not quantifiable. Nonetheless, the over production of *PfBLM* in response to DNA damage suggests its likely involvement in DSB repair.





C. D.



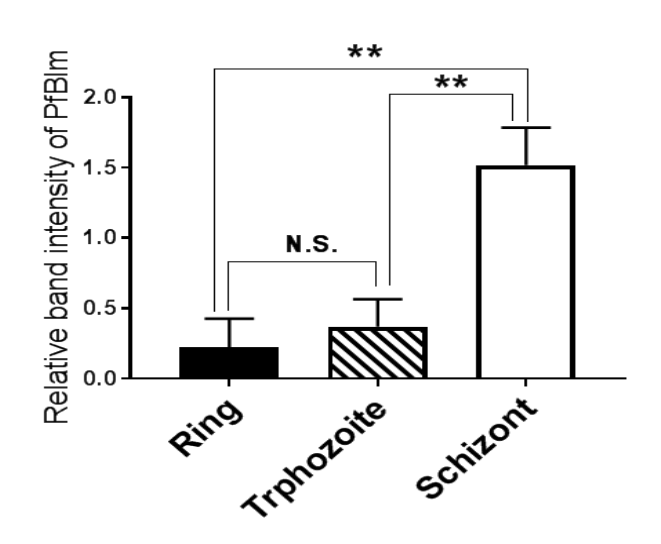
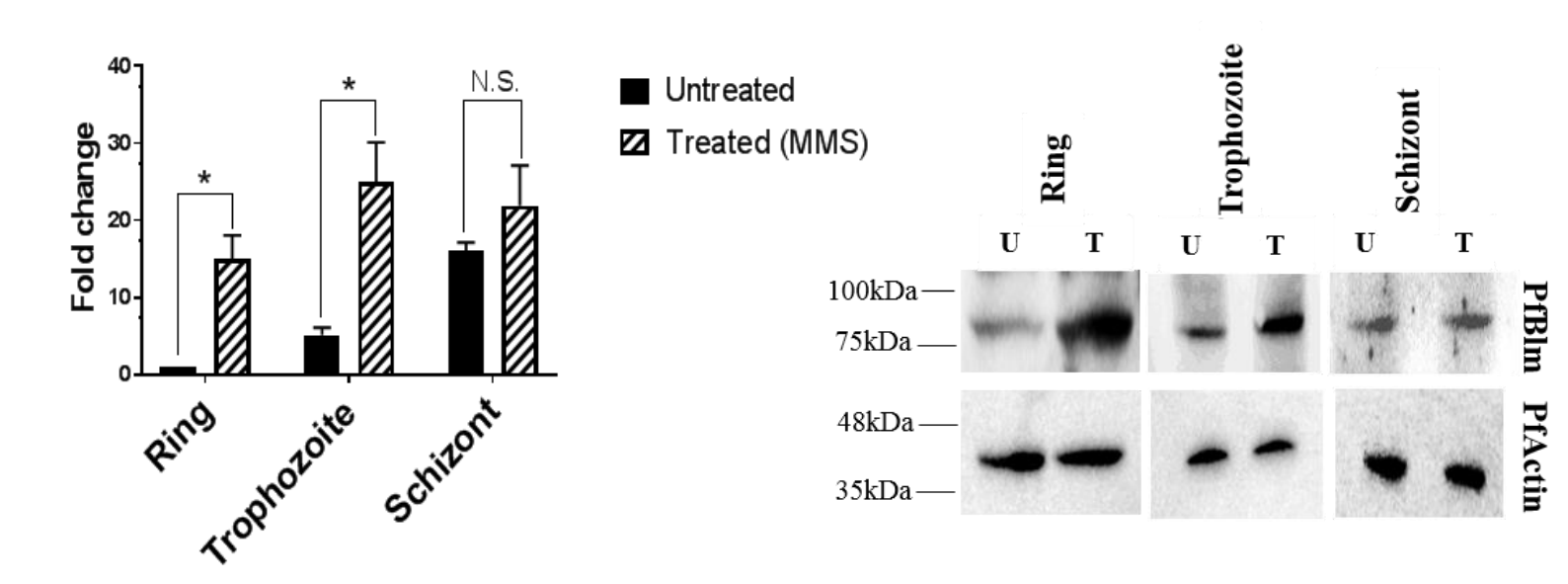


Fig. 7

FIG. 7: *PfBLM* expression is maximum at the mitotically active schizont stage. (A) Relative abundance of *PfBLM* transcript during ring (12 hpi), trophozoite (24 hpi) and schizont (38 hpi) stages quantified by Real-time RT-PCR analysis. Data was normalized against *PfARP*. The mean values  $\pm$  SD from three independent experiments are plotted. (B) Semiquantitative RT-PCR showing expression of *PfBLM* mRNA at the ring, trophozoite and schizont stages. *PfARP* was used as loading control. PCR without reverse transcription (-RT) shows no amplification of *PfBLM*. Representative microscopic images of different blood stages are shown below the blot. (C) Stage specific expression of PfBlm protein. PfActin was used as the loading control. The position of molecular markers is indicated on the left. (D) The quantification of western blotting from three independent experiments. Data was normalized against loading control PfActin. Each bar represents mean density  $\pm$ SD (n=3). Two tailed t-test was used to calculate the p value (\* indicates *P* value < 0.05; \*\* indicates *P* value < 0.01; N.S. indicates not significant). hpi: hours postinyasion.

A. B.



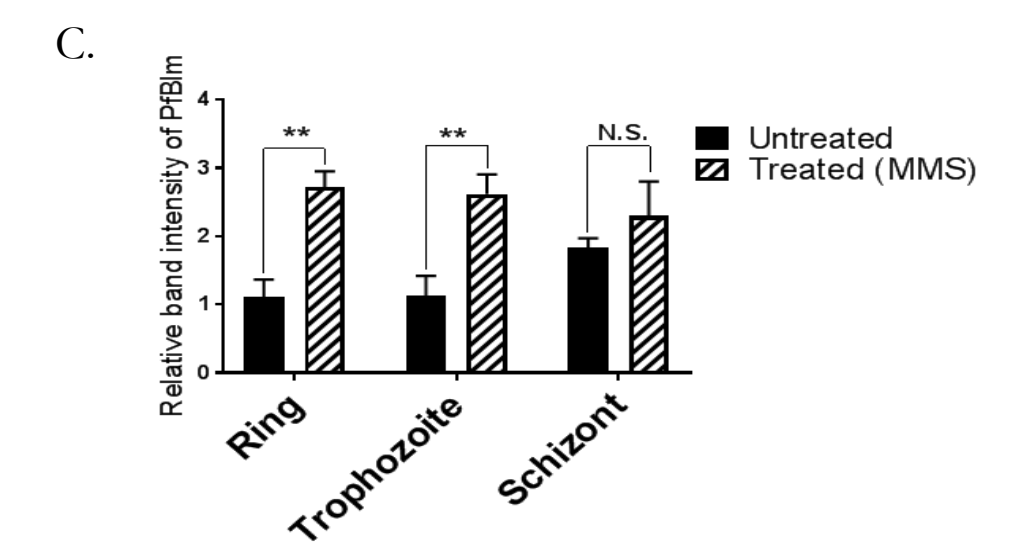


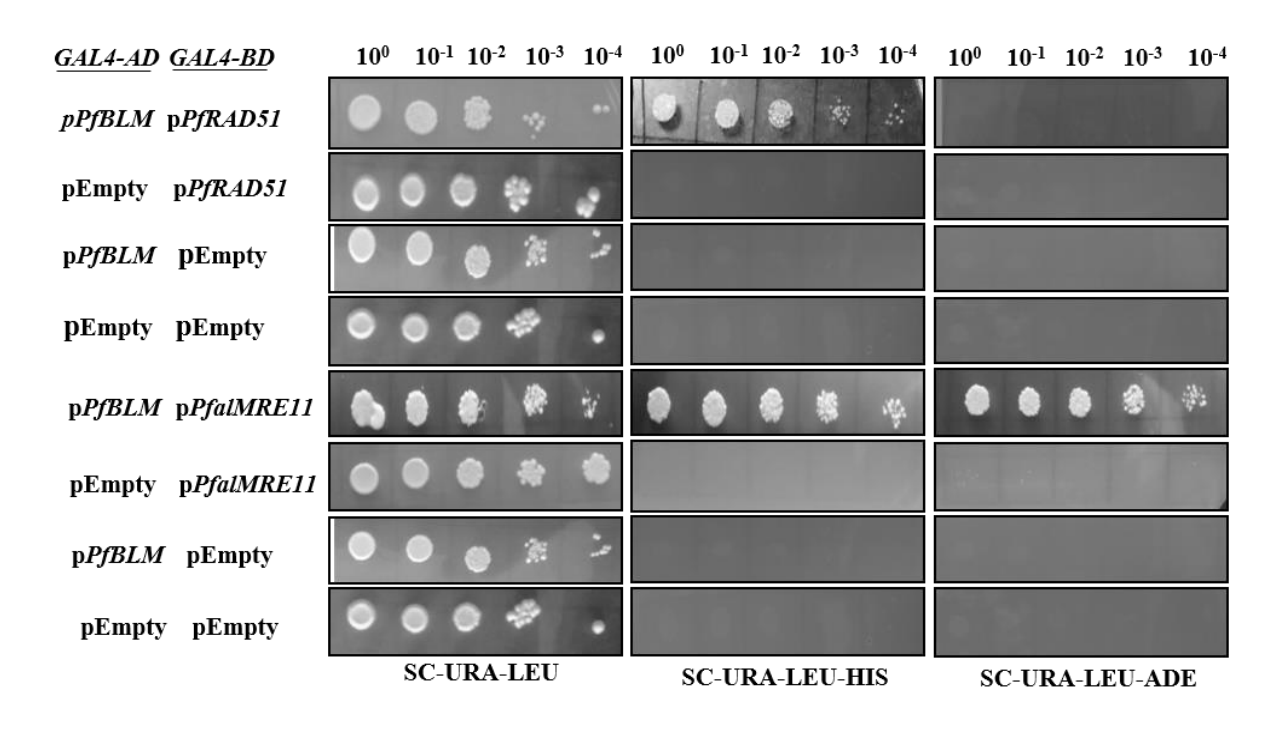
Fig. 8

FIG. 8: DNA damage induced up-regulation of *PfBLM* during intra erythrocytic developmental stages. (A) Synchronized *P. falciparum invitro* cultures at ring, trophozoite and schizont stages were either untreated (U) or treated (T) with 0.05% MMS for 6 hrs. Realtime RT-PCR from extracted RNA revealed up-regulation of *PfBLM* mRNA during ring and trophozoite stages upon DNA damage but its level was not changed during schizont stage. *PfARP* transcripts was used as loading control. Each bar represents mean value ±SD (n=3). (B) Western blots showing MMS induced expression of PfBlm protein at the ring and trophozoite stages but in case of schizont stage it remains unchanged. U: untreated; T: treated with MMS. PfActin acted as loading control. The position of molecular markers is indicated on the left. (C) The quantification of western blotting from three independent experiments. Data was normalized against PfActin. Each bar represents mean band intensity ±SD (n=3). Two tailed t-test was used to calculate the p value (\* indicates *P* value < 0.01; N.S. indicates not significant).

#### 3.1.4 PfBlm interacts with key DNA repair proteins PfRad51 and PfalMre11:

We investigated whether PfBlm physically interacts with other bona fide DSB repair proteins of *P. falciparum*. In order to function in the DSB repair pathway, PfBlm must interact with proteins of the HR pathway. Previous studies have shown that HsBLM interacts with both HsRad51 and HsMre11 [117, 118]. We investigated whether PfBlm interacts with PfRad51 and PfalMre11 which were previously implicated as DNA repair proteins in *Plasmodium*. For this purpose, we carried out yeast two hybrid analysis. In the prey vector harboring GAL4 activation domain and LEU2 selectable marker PfBLM was cloned. In the bait vector having GAL4 DNA binding domain and URA3 as selectable marker PfRAD51 or PfalMRE11 were cloned. Doubly transformed yeast cells were scored for the HIS3 or ADE2 reporter genes expression. Growth was seen on SC-Leu-Ura-His triple dropout plate indicating the interaction between PfBlm and PfRad51. The interaction between PfBlm and PfalMre11 was found to be much stronger as growth was detected not only on SC-Leu-Ura-His plates but also on SC-Ura-Leu-Ade triple dropout plates (Fig. 9A). To further confirm the interaction between PfBlm and PfRad51, co-purification assay was performed. To this end, we expressed recombinant PfRad51 with histidine tag and PfBlm with GST tag in E. coli. Both the cell lysates were mixed and passed through Ni-NTA column and eluted. We detected both PfBlm and PfRad51 signal in western blot of the elute suggesting their interaction whereas no signal was detected when only PfBlm-GST lysate was passed through Ni-NTA column or empty GST tag lysate was mixed with histidine tagged PfRad51 and passed through Ni-NTA column (Fig. 9B). As full length PfalMRE11 could not be expressed in bacterial systems [14], such co-purification experiment could not be performed for these pair of proteins. These observations that PfBlm associates itself with two well established DSB repair proteins of *P. falciparum* strongly suggests for a role of PfBlm in the DSB repair pathway in this parasite.

Α.



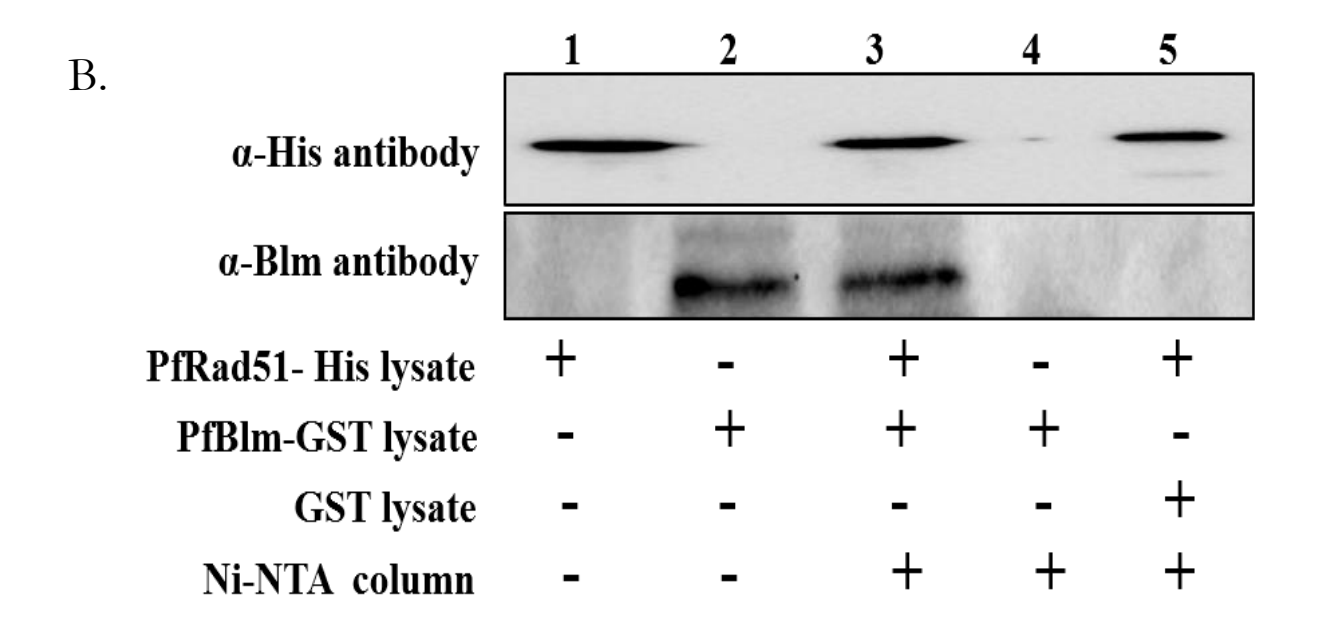


Fig. 9

#### FIG. 9: PfBlm interacts with key DNA repair proteins PfRad51 and PfalMre11.

(A) Full length *PfBLM* was fused to *GALA* activation domain of pGADC1. Similarly, full length *PfalMRE11* and *PfRAD51* were fused to *GALA* binding domain of pGBDUC1. Interaction was tested in yeast strain PJ69-4A which bears *ADE2* and *HIS* as reporter genes. Starting with same OD (1 OD/ml) ten-fold serial diluted cells were spotted on plates lacking leucine and uracil for checking the presence of bait and prey plasmids. Simultaneously cells were spotted on plates lacking histidine and adenine to check the interaction. (B) Western blotting shows the interaction between PfRad51 and PfBlm in Ni-NTA pull down (lane 3). The cell lysate of histidine tagged PfRad51 mixed with empty GST cell lysate (lane 5) did not show signal with anti-Blm antibody. The description of each lane is written at the bottom. The position of molecular markers is indicated on the right.

#### 3.1.5 Interaction points between PfRad51 and PfBlm:

Since the interaction between PfRad51 and PfBlm is essential for functional HR pathway. We reasoned that disruption of this interaction between these two proteins might affect the HR pathway. To this end, we did an in-silico analysis to predict contact points in PfRad51 protein. This was a collaborative work with a bioinformatics lab in our school and the data is not included in this thesis. Nonetheless, the *in-silico* protein-protein docking studies predicted two contact points in PfRad51 protein at 260th and 325th positions necessary for interaction with PfBlm protein. We generated two single mutants and a double mutant of PfRAD51 at those contact sites namely: Pfrad51R260A, *Pfrad51Y325A*, Pfrad51R260A&Y325A. We cloned these mutants in bait vector pGBDUC1 and performed a yeast two-hybrid assay to test their interaction with PfBLM. Simultaneously, we also expressed these mutants in E. coli and performed a copurification assay. To our surprise, both the single and double mutants interacted with PfBlm in both yeast two-hybrid assay and co-purification assay (Fig. 10A, 10B, 10C & 10D). Hence, we did not proceed further with this project. It might be possible that there are multiple contact points in PfRad51 protein, which are essential for interaction with PfBlm protein.

## 3.1.6 *PfBLM* functionally complements MMS sensitivity of $\triangle sgs1$ mutant of *S. cerevisiae*:

We investigated whether PfBLM can functionally rescue the DNA repair defect of the RecQ mutant of budding yeast. S. verevisiae possesses a single RecQ gene, namely SGS1. The DSB repair properties of Sgs1 are well established. Previous studies have shown that  $\Delta sgs1$  mutant strain is sensitive to genotoxic agent MMS [119] and the full length HsBLM was able to complement the MMS sensitivity [120]. The complementation was dependent on the helicase activity of HsBLM protein since helicase dead mutant HsblmK695R was not able to perform the DNA repair function [120]. In our study, we investigated whether full length PfBLM and helicase dead mutant of PfBLM

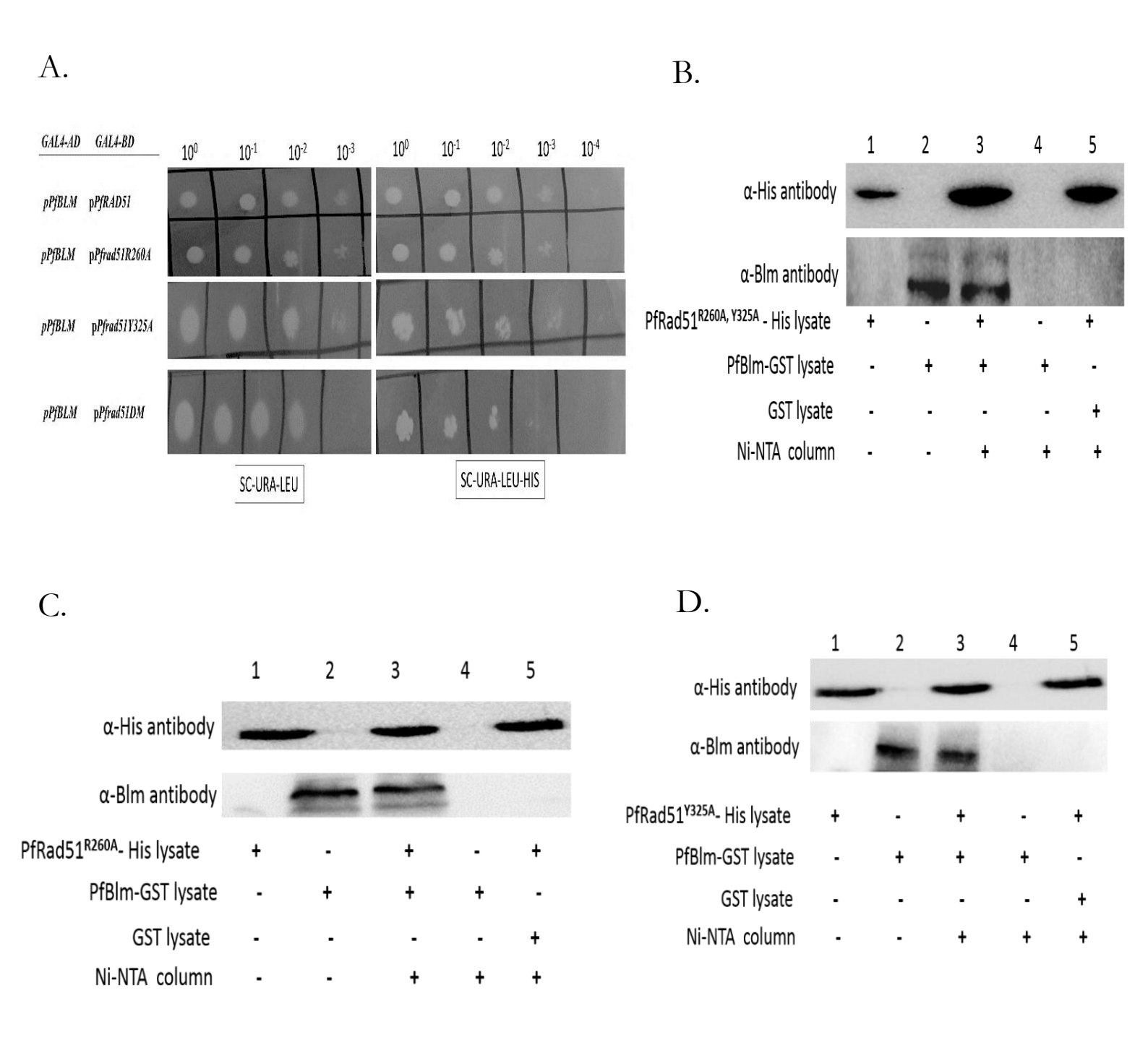


Fig. 10

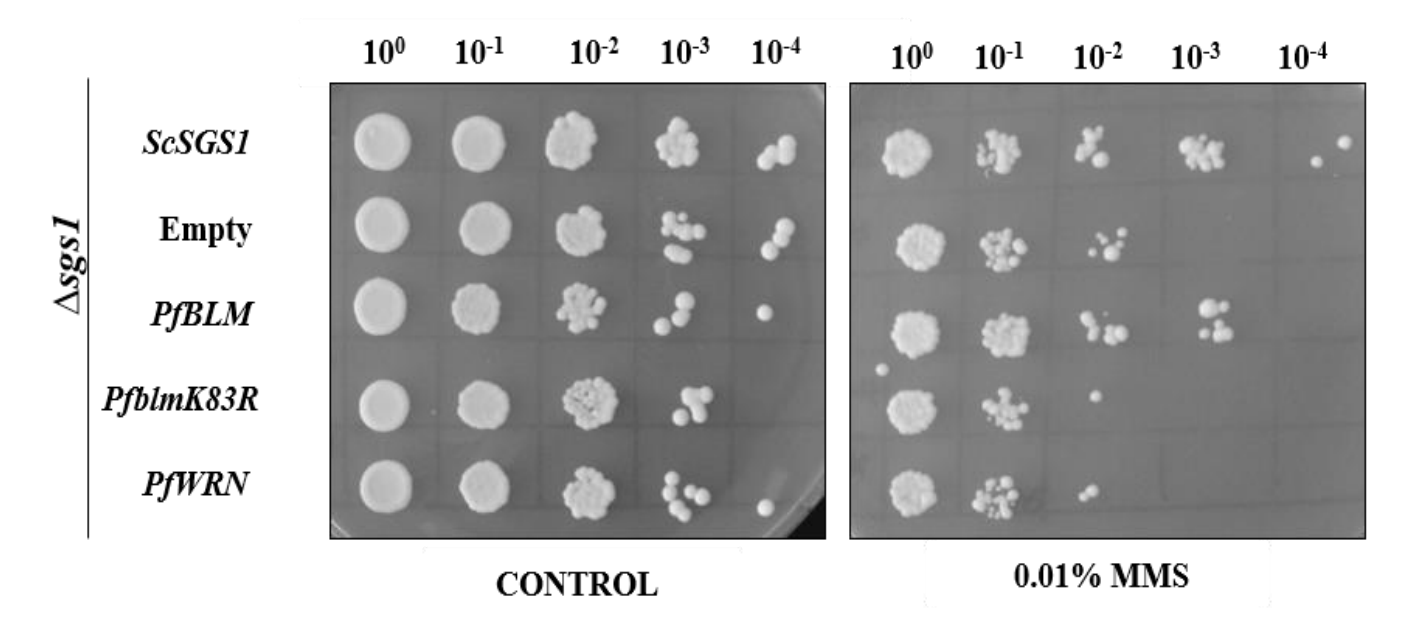
FIG. 10: Interaction points between PfRad51 and PfBlm: (A) Full length *PfBLM* was fused to *GALA* activation domain of pGADC1. Similarly, mutants of *PfRAD51*: *Pfrad51R260A*, *Pfrad51Y325A* and double mutant were fused to *GALA* binding domain of pGBDUC1. Interaction was tested in yeast strain PJ694A which bears ADE2 and HIS as reporter genes. Starting with same OD (1 OD/ml) ten-fold serial diluted cells were spotted on plates lacking leucine and uracil for checking the presence of bait and prey plasmids. Simultaneously cells were spotted on plates lacking histidine and adenine to check the interaction. (B),(C) and (D) Western blotting shows the interaction between mutants of PfRad51 and PfBlm in Ni-NTA pull down. The description of each lane is written at the bottom.

(*PfblmK83*R) can complement the DNA damage sensitivity of  $\Delta sgs1$  mutant strain. Along with PfBLM another identified RecQ helicase of Plasmodium PfWRN was also tested. To this end, we knocked out SGS1 gene from S. cerevisiae to generate SNY1 strain. PfBLM, PfblmK83R and PfWRN cloned in pBFM vector were transformed in SNY1 to generate SNY3, SNY4 and SNY5. We also transformed ScSGS1 cloned in pBFM vector and empty pBFM vector to generate SNY2 and SNY6 which acted as the positive and negative controls, respectively. Complementation studies were done using return to growth assay and by growing strains on plate containing MMS. In both the assays we observed that PfBLM could partially complement the DNA damage sensitivity of Δsgs1 mutant whereas PfblmK83R or PfWRN were inefficient to overcome the sensitivity (Fig. 11A & 11B). In return to growth assay the helicase dead mutant behaved similar to the negative control indicating the importance of helicase activity of PfBlm protein in performing DNA repair function. The expression levels of PfBLM, PfblmK83R and PfWRN were determined by semiquantitative RT-PCR method and the expression levels were found to be comparable to that of ScSGS1 (Fig. 11C). We used pBFM plasmid as it would enable us to detect the protein expression of the cloned genes using anti-Myc antibody. However, we failed to detect the expression of any Myc tagged proteins. These results strongly suggest that the DSB repair function of RecQ helicase is also conserved in PfBlm.

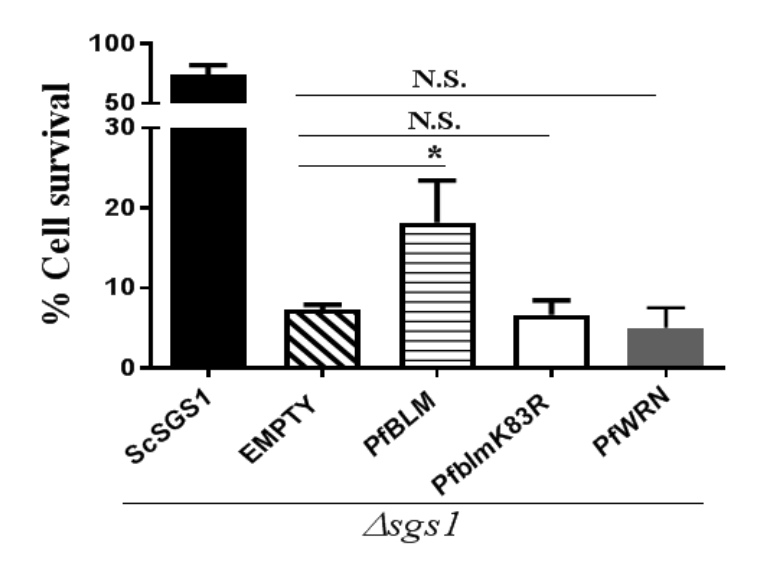
# 3.1.7 Over-expression of *PfBLM* provides survival advantage to the parasites under DNA damaging conditions:

In order to amplify the function of PfBlm in HR mediated DSB repair (if any) we performed over-expression studies. The idea behind such experiment was that if PfBlm is involved in the repair of DSB, over-expression of *PfBLM* would confer a better repair efficiency than the normal level of the protein. To this end, *P. falciparum* 3D7 cells were transfected separately with both wild type *PfBLM* and *PfblmK83R* mutant cloned in pARL over-expression vector [121]. The transfected parasites at all three intra- erythrocytic stages were treated with 0.002% and 0.005% MMS for 2 hrs and returned to grow for 48 hrs, after washing off MMS. Simultaneously,

Α.



В.



C.

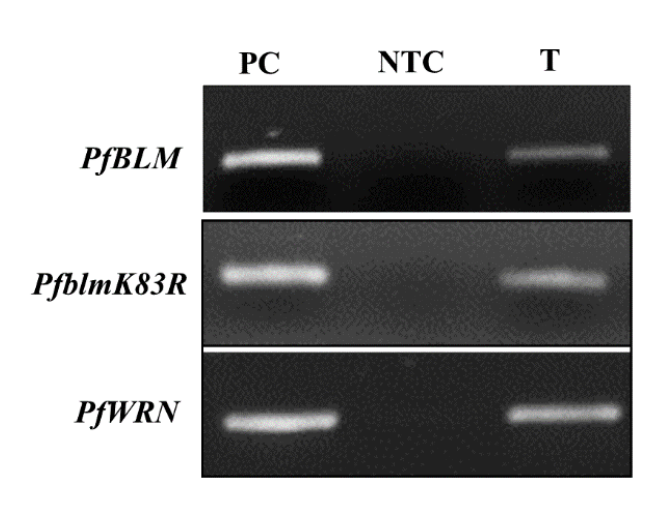
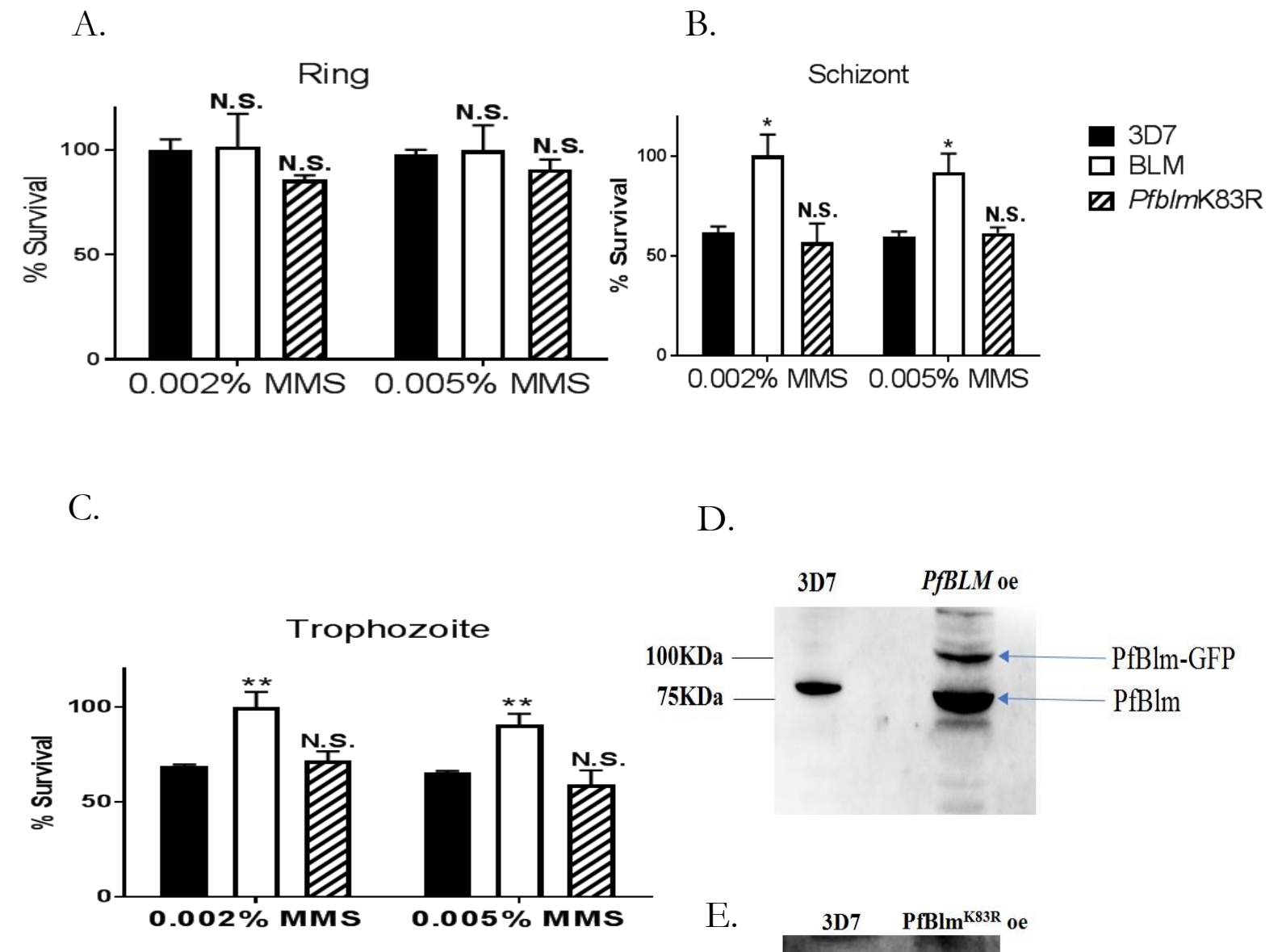


Fig. 11

FIG. 11: *PfBLM* functionally complements MMS sensitivity of Δ*sgs1* mutant of *S. cerevisiae*. (A) Spotting assay on SC-HIS plate without (control) or with 0.01% MMS. The genotypes of each strain were mentioned on the left. (B) Return to growth assay was performed where all the complementation strains were either untreated or treated with 0.03% MMS for 2 hrs. and allowed to grow on SC-HIS plate without MMS after washing. Percentage cell survival for each strain was obtained by taking ratio of number of colonies formed between treated and untreated cultures. Each bar represents mean number ±SD after normalizing with untreated controls from three independent experiments (n=3). Two tailed t-test was used to calculate the p value (\* indicates *P* value <0.05; N.S. indicates not significant). (C) Expression of *PfBLM*, *PfblmK83R* and *PfWRN* were confirmed by isolating RNA and performing semi-quantitative RT-PCR from complementation strains. PC: positive control (*Plasmodium* genomic DNA was used as template); NTC: non template control; T: test (cDNA from respective complementation strains used as template).

same experiment was performed with 3D7 culture which acted as control. In such experiments parasites capable of repairing the DSBs would only survive. The survivability of *PfBLM* over-expressing strain upon DNA damage was found to be significantly better than the wild type 3D7 strain. Interestingly, such survival advantages were observed only for the parasites where DNA damage was induced at the trophozoite or schizont stages, but not at the ring stage (Fig. 12A, 12B & 12C). No such survival advantage under DNA damaging condition was observed for parasites over-expressing the helicase dead mutant version of the gene *PfblmK83R* (Fig. 12A, 12B & 12C). Expression of GFP tagged PfBlm and Pfblm<sup>K83R</sup> were confirmed by performing western blotting (Fig. 12D & 12E). These findings provide a direct evidence for the participation of PfBlm in DSB repair pathway of *P. falciparum*.



100KDa

75KDa

Fig. 12

PfBlm<sup>K83R</sup>-GFP

PfBlm

FIG. 12: Over-expression of *PfBLM* provides survival advantage to the parasites under DNA damaging conditions. (A), (B) and (C) Plasmodium falciparum 3D7 cells harboring PfBLM-GFP and PfblmK83R-GFP were either untreated or treated with 0.002% and 0.005% MMS for 2 hrs. and subsequently allowed to grow for 48 hrs. after washing. The experiment was also performed with 3D7 cultures which acted as control. After 48 hrs. smears were prepared, and infected erythrocytes were counted to obtain parasitemia. Experiment was performed with three intra-erythrocytic stages of parasite. Stages are mentioned on the top. Percent survival was plotted by taking the ratio of percent parasitemia between treated and untreated cultures of respective strains. Each bar represents mean survival values  $\pm$  SD (n=3). Significance was calculated with respect to wild type strain (3D7). (D) Western blotting shows the expression of PfBlm protein. The strain name is written on the top. OE indicates over-expression. Expression of PfBlm (80 kDa) protein in 3D7 strain and the expression of GFP tagged PfBlm (107 kDa) protein (indicated by arrow) along with endogenous PfBlm (80kDa) are shown. (E) Left lane shows the expression of PfBlm (80 kDa) protein in 3D7 strain and the right lane shows the expression of GFP tagged Pfblm<sup>K83R</sup> (107 kDa) protein (indicated by arrow) along with endogenous PfBlm (80 kDa). The position of molecular markers is indicated on the left. Two tailed t-test was used to calculate the p value (\* indicates P value < 0.05; \*\* indicates P value < 0.01; N.S. indicates not significant).

### 3.2 Summary of the results:

In this chapter, we have shown that P/BLM was majorly expressed during the trophozoite and schizont stages compared to the ring stage. P/BLM was up-regulated upon DNA damage suggesting its role in DNA repair. PfBlm interacted with essential DNA repair proteins PfRad51 and PfalMre11. However, we failed to establish interaction points between PfBlm and PfRad51. Using yeast as a surrogate system, we have shown that P/BLM could complement the MMS sensitivity of  $\Delta sgs1$  strain, whereas helicase dead mutant P/BlMK83R and P/WRN failed to do the function. Finally, by carrying an overexpression study, we have shown that P/BLM can perform DNA repair function in parasite also. Altogether, our data suggest that the DNA repair activity of P/BLM is conserved in Plasmodium.

### **CHAPTER IV**

Studying the effect of small molecule inhibitor of RecQ helicase on *Plasmodium* growth

### 4. Introduction:

RecQ helicases regulate significant genome events by functioning at replication, recombination, and repair processes of the cell. In humans, germline mutations of BLM, WRN, and RECQL4 accounts for heritable genetic diseases. Previous studies have reported small molecule inhibitors for human BLM and WRN. These inhibitors are specific to their respective proteins and have a cytotoxic effect on human cell lines [122, 123]. Targeting RecQ helicases in *Plasmodium* is a viable approach since they share less homology with their human counterparts. Earlier studies have reported that knockout of RecQ helicases in Plasmodium significantly impacted replication and transcription of parasites. Complete loss of function of RecQ helicases might disturb parasites' genome stability, ultimately leading to death. In this study, we did chemical inhibition of RecQ helicase and studied its impact on parasite growth. As a proof of the concept, we used two commercially available chemical inhibitors: ML216 and MIRA-1 [122, 123]. Initially, we did in silico docking analysis to predict the binding affinities of human RecQ helicase inhibitors ML216 and MIRA-1 to PfBlm protein. Next, we investigated the impact of those inhibitors on in vivo and in vitro growth of Plasmodium. Finally, we evaluated the efficacy of the drug in the presence of external DNA damage.

#### 4.1 Results:

# 4.1.1 *In silico* analysis of the binding poses and binding affinity of inhibitors against PfBlm:

We investigated whether the chemical inhibitors of RecQ helicases, namely ML216 and MIRA-1 [122, 123], could potentially bind to PfBlm. To this end we have taken in silico approach. Since the crystal structure for PfBlm is not available, we have modeled the protein based on the crystal structure of Homo sapiens BLM (HsBlm), details of which are described in the Methods section. The inhibitor molecules were first docked on to the PfBlm structure. It was seen that ML216 can bind either at the ATP-binding site or the DNA-binding region, whereas MIRA-1 can bind only in the vicinity of the ATP-binding site (Fig. 13A). In order to evaluate the stability of the docking poses, molecular dynamics simulations of the docked complexes were performed. It was seen that ML216 interacts with two residues Gln111 and Arg407 in the ATP binding site of PfBlm (Fig. 13B), but when it is bound to the DNAbinding region of PfBlm it is seen to bind with two poses at the same binding site: one in which it interacts with Arg404, and the other in which it interacts with Trp191 (Fig. 13C). MIRA-1 interacts with the residues Gly80 and Arg282 in the vicinity of the ATP-binding site (Fig. 13D). An estimate of the binding affinity between PfBlm and the inhibitors was made by calculating the free energy of binding (Table 3). The values show that ML216 has greater affinity towards PfBlm, compared to MIRA-1. These results predicted that ML216 could be a potent inhibitor of PfBlm and hence a chemical inhibition strategy could be employed to elucidate the function of PfBlm during DSB repair in this parasite.

### 4.1.2 Compared to MIRA-1, ML216 is a more potent inhibitor of the intraerythrocytic growth of *P. falciparum*:

To study the effect of RecQ helicase inhibitors (ML216 and MIRA-1) on *Plasmodium* growth we performed growth inhibition assay in the presence of different

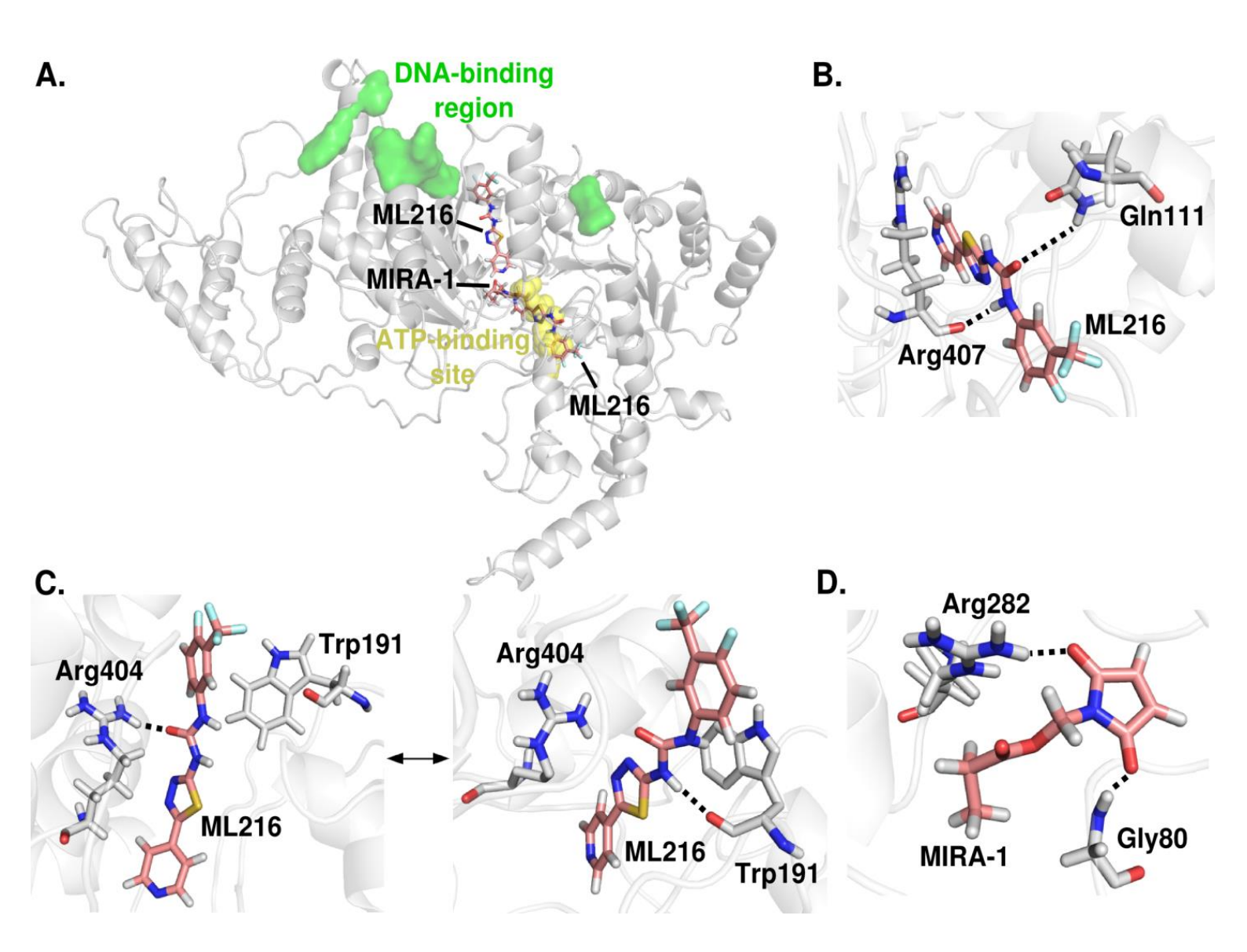


Fig. 13

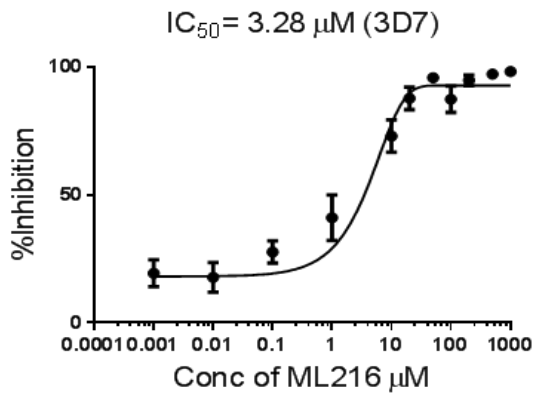
FIG. 13: *In silico* analysis of the binding poses and binding affinity of inhibitors against PfBlm. (A) Two binding poses for ML216 and single binding pose for MIRA-1 are shown here. ML216 can bind either at the ATP-binding site or the DNA-binding region whereas MIRA-1 binds only in the vicinity of the ATP-binding site. (B) ML216 interacts with Gln111 and Arg407 in the ATP-binding site. (C) ML216 bound near the DNA-binding region is seen to exist in two poses: one in which it interacts with Arg404, and one in which it interacts with Trp191. (D) MIRA-1 interacts with the residues Gly80 and Arg282 near the ATP-binding site. Hydrogen bonds between the protein and the inhibitor are shown as dotted lines. This work was done in collaboration with S. Padhi, G. Bulusu, and A. Roy from TCS, Hyderabad.

**Table 3.**Free energies of binding for inhibitors bound to PfBlm

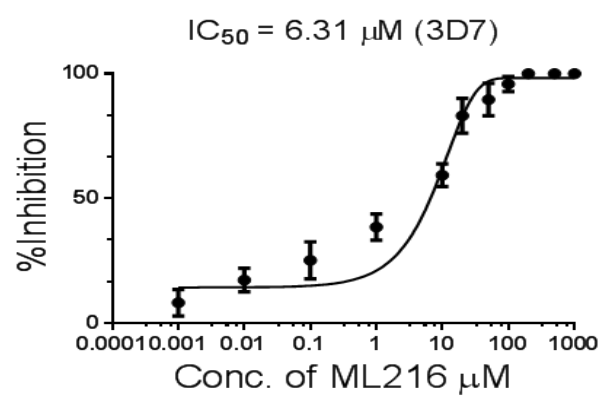
Inhibitor name and binding site	$\Delta E_{MM}$ (kcal/mol)	$\Delta G_{ m solv,polar}$ (kcal/mol)	$\Delta G_{ m solv,  non-polar}$ (kcal/mol)	$\Delta G_{ ext{binding}}$ (kcal/mol)
ML216 at ATP-binding site	-56.6	33.2	-4.5	-27.9
ML216 in DNA-binding region	-51.9	32.8	-3.7	-22.7
MIRA-1 at ATP-binding site	-36.7	27.0	-2.7	-12.4

concentrations of both the drugs. RecQ helicases are involved in replication and DSB repair in a variety of organisms. Malaria parasites undergo several rounds of replication during the erythrocytic schizogony and repair of endogenous DNA damage is a common occurrence in the life cycle of *Plasmodium*. We investigated whether any of the aforementioned RecQ inhibitors actually inhibit the blood stage development of the parasite. We treated trophozoite culture with ML216 or MIRA-1 at varying concentrations (1 nM to 1000 µM) for 48 hrs. and evaluated the parasitemia by staining the smears with Giemsa stain. Both ML216 and MIRA-1 were able to inhibit the intra-erythrocytic developmental cycle (IDC) of the parasites. However, ML216 was more potent when compared to MIRA-1. The IC<sub>50</sub> value obtained from the dose response curve was 3.28 µM and 67.6 µM for ML216 and MIRA-1 (giemsa staining), respectively (Fig. 14A & 14G). We also employed fluorescence based SYBR Green-I method to estimate the survivability. This method yielded an IC<sub>50</sub> value of 6.31 μM for ML216 and 55.2 μM for MIRA-1 (Fig. 14B & 14H). We further tested the effect of ML216 and MIRA-1 on drug resistant strains Dd2. We observed that the IC<sub>50</sub> values are in the similar range, albeit lower than what was observed for the drug sensitive 3D7 strain. For ML216 the observed IC<sub>50</sub> value was 1.01 μM and for MIRA-1 the value was 44 μM (Giemsa staining) (Fig. 14C & 14]). SYBR Green-I method yielded an IC<sub>50</sub> value of 3.24 µM for ML216 and 58 μM for MIRA-I (Fig. 14D & 14I). In addition, we also examined the inhibitory effect of ML216 on artemisinin resistant strain PfK13R539T [124]. Giemsa staining method yielded an IC<sub>50</sub> value of 1.26 μM (Fig. 14E) and in SYBR Green-I method IC<sub>50</sub> value was 2.19 μM (Fig. 14F). The IC<sub>50</sub> values obtained by both giemsa staining method and SYBR Green-I method are in similar range. Thus, ML216 was found to be more potent inhibitor of IDC than MIRA-1.

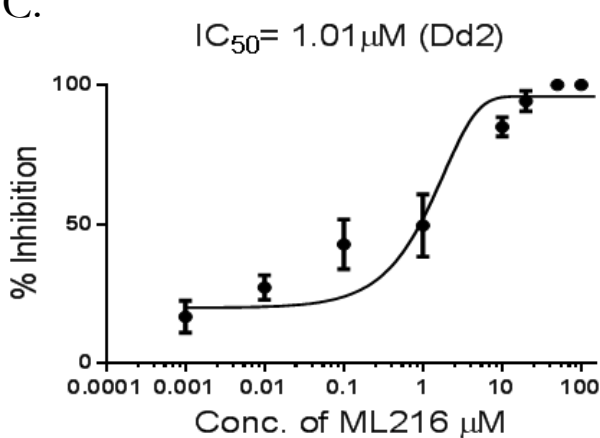




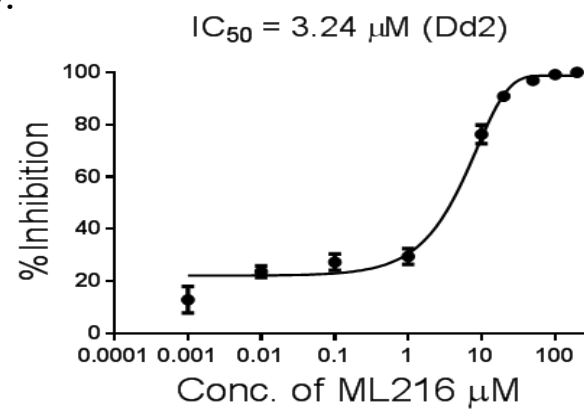




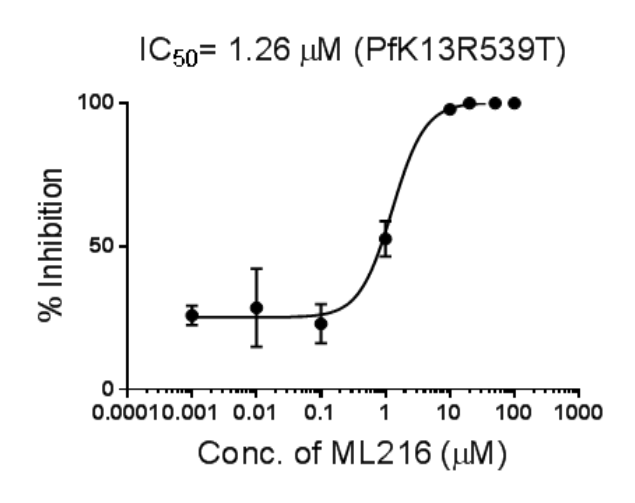
C.



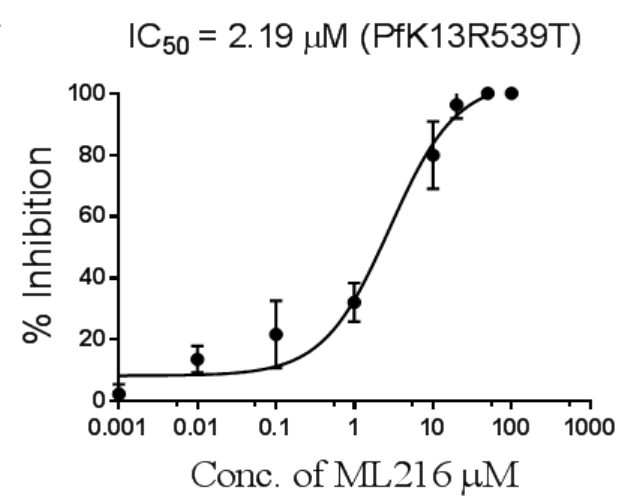
D.

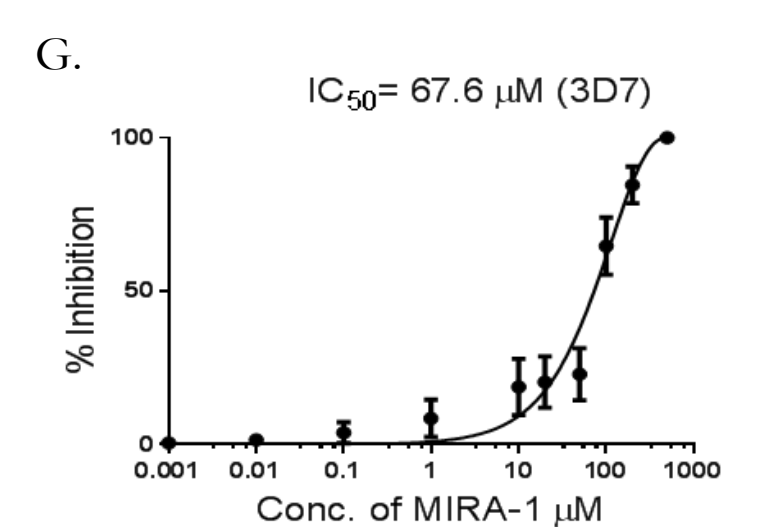


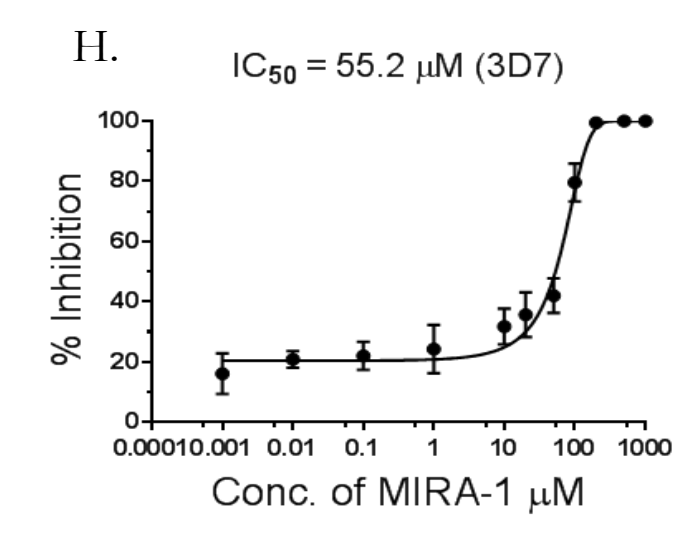
E.



F.

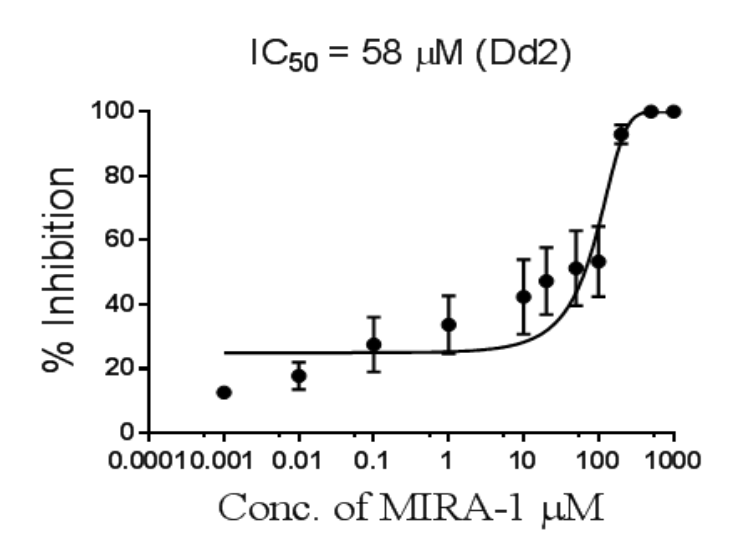


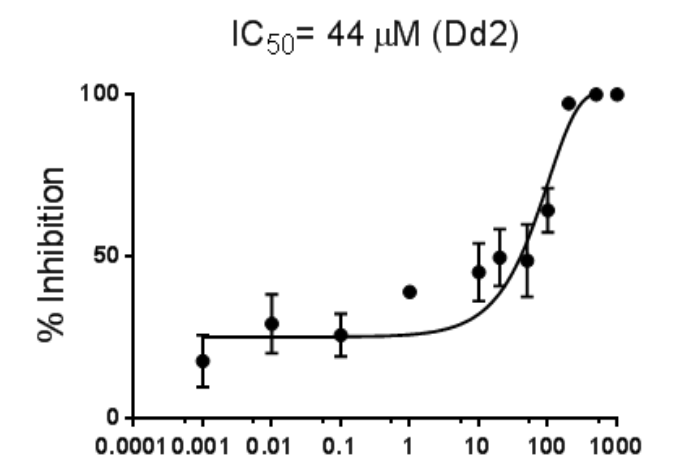




J.

I.





Conc. of MIRA-1  $\mu\!M$ 

Fig. 14

## FIG. 14: Compared to MIRA-1, ML216 is a more potent inhibitor of the intra erythrocytic growth of *P. falciparum*.

(A) & (B) Synchronous trophozoite stage parasites (3D7) were grown for 48hrs. in the presence of various concentrations of ML216 and parasitemia was assessed by Giemsa staining method and SYBR Green-I method. Parasite growth inhibition at various concentrations of drug was plotted to obtain IC<sub>50</sub> value. (C) & (D) Growth inhibition with ML216 evaluated by Giemsa staining method and SYBR Green-I method in Dd2 parasites was plotted to obtain IC<sub>50</sub> value. (E) & (F) The effect of ML216 was tested in artemisinin resistant strain PfK13R539T by Giemsa staining and SYBR Green-I method. Percentage inhibition was plotted against various concentrations of drug to obtain IC<sub>50</sub> value. (G) & (H) Growth inhibition with MIRA-1 in 3D7 parasites by Giemsa staining and SYBR Green-I method. Percentage inhibition was plotted against various concentrations of drug to obtain IC<sub>50</sub> value. (I) & (J) Growth inhibition with MIRA-1 in Dd2 parasites assessed by Giemsa staining and SYBR Green-I method. Percentage inhibition was plotted against various concentrations of drug to obtain IC<sub>50</sub> value. Each assay was repeated thrice for reproducibility (n=3).

### 4.1.3 ML216 inhibits in vivo growth of Plasmodium berghei:

We performed Peter's 4-day suppressive test to investigate the *in vivo* anti-malarial activity of ML216 on rodent malaria parasite *Plasmodium berghei*. To this end, two groups (4 mice in each group) of Swiss albino mice were taken and infected with an equal number of parasites. After that, to one group of mice, we injected ML216 (25mg/kg body weight) intraperitoneally for four consecutive days beginning from day 0 of infection. The second group of mice, we injected 0.1% DMSO, which acted as vehicle control since the drug was dissolved in DMSO. Blood smears were prepared from the tail of each mice and stained with Giemsa to count the parasitemia. Percentage parasitemia was plotted with days post-infection. We monitored the survivability of the host for a period of 40 days from the beginning of the infection. We found that, in contrast, to the control group, the parasitemia of drug-treated group reduced drastically, and the host survived for a long time (Fig. 15A & 15B). These results imply that ML216 has a profound effect on *in vivo* growth of parasites.

A. B.

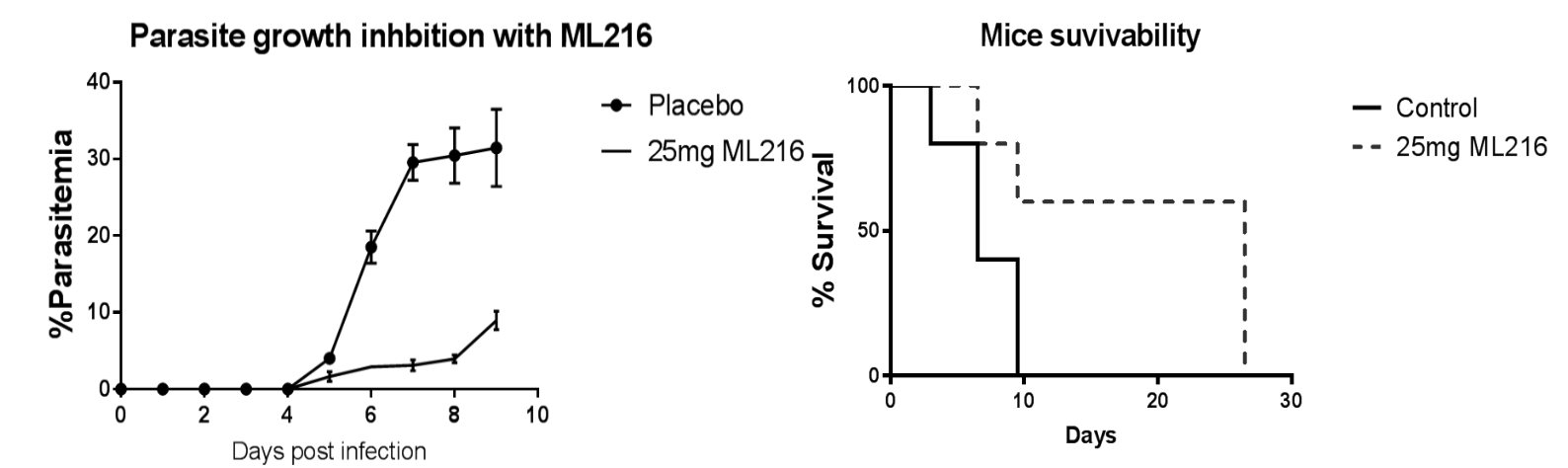


Fig. 15: ML216 inhibits *in vivo* growth of *Plasmodium berghei* (A) Graph depicts the parasitemia of mice at different days post infection for both placebo and ML216 treated group (25mg/kg). (B) The survival curve for mice in both placebo and ML216 treated group.

# 4.1.4 Parasites treated with ML216 become hypersensitive to DNA damaging agent MMS:

To investigate the effect of ML216 on DNA damaged cells, we performed growth inhibition assay with MMS treated cells. Previous studies have shown that MMS creates numerous double strand breaks and such breaks are repaired over the period [18]. However, if such breaks are not successfully repaired, cells bearing the unrepaired breaks succumb to death. Thus, MMS sensitivity assay is a good measure of the DSB repair capability of the cells. We reasoned that inhibition of PfBlm with ML216 would render parasites more sensitive to MMS treatment. To this end, we treated synchronized parasite cells of all the stages with varying concentrations of ML216 (1 nM to  $1000 \mu M$ ) in the presence or in the absence of MMS. The assay was performed in both drug sensitive (3D7) and drug resistant strains (Dd2). MMS treatment drastically lowered down the IC<sub>50</sub> value of ML216 for both 3D7 and Dd2 parasite strains (Table 4). The effect was most prominent when DSBs were induced at the trophozoite stage. The drop in the IC<sub>50</sub> values at trophozoite stage was 264fold and 218-fold for 3D7 and Dd2, respectively. Creation of DSBs at the schizont stage also has profound effect on the IC<sub>50</sub> value of ML216. There were about 185fold and 40-fold reduction in the IC<sub>50</sub> value for the 3D7 and Dd2 strains, respectively. The effect on the ring stage was very minimal: only 2 to 2.5-fold reduction. Such dramatic drop in the IC<sub>50</sub> values are not due to an additive effect of MMS toxicity, as the survival of the ring-, trophozoite-and schizont-stage parasites to MMS are 97%, 65% and 60%, respectively (Fig. 12A, 12B, & 12C). These results indicate that treating with external DNA damaging agents ML216 could be an effective inhibitor of parasite growth as it works at the nano-molar range.

**Table 4:** IC<sub>50</sub> values of ML216 with or without MMS treated cultures at different IDC stages in 3D7 and Dd2 strains

Stage	Treatment	$IC_{50}$ ( $\mu M$ )		
Ring				
3D7	ML216 (alone)	3.49		
	ML216 + MMS	1.42		
Dd2	ML216 (alone)	1.85		
	ML216 + MMS	0.96		
Trophozoite				
3D7	ML216 (alone)	2.8		
	ML216 + MMS	0.0106		
Dd2	ML216 (alone)	0.871		
	ML216 + MMS	0.004		
Schizont				
3D7	ML216 (alone)	3.21		
	ML216 + MMS	0.0174		
Dd2	ML216 (alone)	1.49		
	ML216 + MMS	0.0374		

### 4.2 Summary of the results:

In this chapter, through *in silico* analysis we have shown that out of two RecQ helicase inhibitors, ML216 and MIRA-1, ML216 binds to PfBlm with more affinity. ML216 has profound growth inhibitory effect on *Plasmodium* both *in vitro* and *in vivo* in contrast to MIRA-1. The IC<sub>50</sub> value of ML216 reduced drastically during trophozoite and schizont stages in the presence of external DNA damage.

### **CHAPTER V**

Studying the interaction of RecQ helicase inhibitor with current anti-malarial drugs

### 5. Introduction:

Combination therapies are known to be effective in the treatment of malaria. In artemisinin-based combination therapy (ACT), artemisinin combined with synergistically acting partner drugs increases the anti-parasitic effect rather than monotherapy. Previous reports have shown that chronic treatment with artesunate in cancer cells induces double-strand breaks [125]. Similarly, in *Plasmodium*, artesunate is known to create DSBs during its course of action [91]. Failure in the repair of such DSBs might be detrimental to the cells. Likewise, chloroquine inhibits polymerization of heme, resulting in free radicals, which might lead to the creation of DSBs [126]. In our study, we reasoned that DSB inducers DHA/CQ combined with DNA repair inhibitor (ML216) as a partner drug might intensify the parasite killing effect. Here, we determined the mode of interaction between ML216 and DHA/CQ by performing a fixed ratio isobologram method. We have also checked whether DHA/CQ can potentiate the action of ML216 and vice versa.

### 5.1 Results:

### 5.1.1 ML216 interacts synergistically with ART and CQ:

We studied the interaction of ML216 with the known anti-malarial drugs ART. Since ART creates DSBs [91] and in the presence of ML216 the repair of such breaks is inhibited, we hypothesized that ML216 and ART might potentiate each other's action. We have used a derivative of ART, name by dihydroartemisinin (DHA) in our study. To that end, we performed fixed ratio drug combination assay. Dose response curves were plotted for each combination and FIC values were calculated from the graphs. The  $\Sigma$ FIC values are tabulated in Table 5. Finally, isobologram was constructed based on the calculated  $\Sigma$ FIC values. As depicted in the isobologram the interaction between ML216 and DHA is synergistic in nature (Fig. 16A). A similar result of synergistic relationship was observed for the drug resistant strains Dd2 and PfK13R539T (Fig. 16B & 16C). As CQ treatment inhibits heme polymerization leading to generation of free radicals, it is speculated that treatment of parasites with CQ is also likely to create DSBs in the parasite [126]. As expected, we observed that ML216 also synergizes with CQ in both drug sensitive and drug resistant strains (Fig. 16D & 16E). We also tested the interaction of ML216 with atovaquone (ATQ) whose mode of action does not interfere with DNA metabolism. As expected, we did not observe any synergistic action between these two drugs (Fig. 16F & 16G). These results suggest that the action of both DHA and CQ can be potentiated by RecQ inhibitor ML216.

### 5.1.2 ML216 lowers the IC<sub>50</sub> of anti-malarial drugs and vice versa:

We have investigated the potentiation effect of ML216 on anti-malarial drugs DHA and CQ. To this end, we performed standard growth inhibition assays with DHA/CQ in two sets: one in the presence of IC<sub>50</sub> concentration of ML216 and the second set without any addition of ML216. We observed that in the presence of IC<sub>50</sub> concentration of ML216 (3.28 μM), the action of DHA was potentiated 5.5-folds, and CQ by 3.5- folds (Table 6). A similar experiment was performed with a fixed IC<sub>50</sub> concentration of ART/CQ and varying concentrations of ML216. In the

**Table. 5** FIC values of drug combinations

(n.d: not determined)

Strain	DHA:ML216	FICDHA	FICML216	∑FIC	CQ:ML216	FICcQ	FIC <sub>ML216</sub>	∑FIC	ATQ:ML216	FICATQ	FICML216	∑FIC
3D7	5:0	1	0	1	5:0	1	0	1	5:0	1	0	1
	4:1	0.64	0.22	0.86	4:1	0.56	0.31	0.87	4:1	0.73	0.27	1
	3:2	0.52	0.48	1.0	3:2	0.34	0.50	0.84	3:2	0.54	0.55	1.09
	2:1	0.27	0.64	0.91	2:1	0.17	0.60	0.77	2:1	0.37	0.87	1.24
	1:4	0.08	0.48	0.56	1:2	0.09	0.63	0.72	1:2	0.18	0.98	1.16
	0:5	0	1	1	0:5	0	1	1	0:5	0	1	1
Dd2	5:0	1.0	0	1	5:0	1.0	0	1	5:0	1	0	1
	4:1	0.23	0.13	0.36	4:1	0.28	0.12	0.40	4:1	0.85	0.17	1.02
	3:2	0.40	0.29	0.69	3:2	0.21	0.16	0.37	3:2	0.63	0.34	0.97
	2:1	0.25	0.42	0.67	2:1	0.20	0.34	0.54	2:1	0.52	0.54	1.06
	1:4	0.25	0.64	0.89	1:4	0.03	0.21	0.24	1:4	0.28	0.88	1.16
	0:5	0	1	1	0:5	0	1	1	0:5	0	1	1
PfK13R539T	5:0	1	0	1	n.d.	n.d.	n.d.	n.d.	n.d.	n.d.	n.d.	n.d.
	4:1	0.5	0.08	0.58	n.d.	n.d.	n.d.	n.d.	n.d.	n.d.	n.d.	n.d.
	3:2	0.55	0.25	0.8	n.d.	n.d.	n.d.	n.d.	n.d.	n.d.	n.d.	n.d.
	2:1	0.26	0.29	0.55	n.d.	n.d.	n.d.	n.d.	n.d.	n.d.	n.d.	n.d.
	1:4	0.11	0.32	0.43	n.d.	n.d.	n.d.	n.d.	n.d.	n.d.	n.d.	n.d.
	0:5	0	1	1	n.d.	n.d.	n.d.	n.d.	n.d.	n.d.	n.d.	n.d.

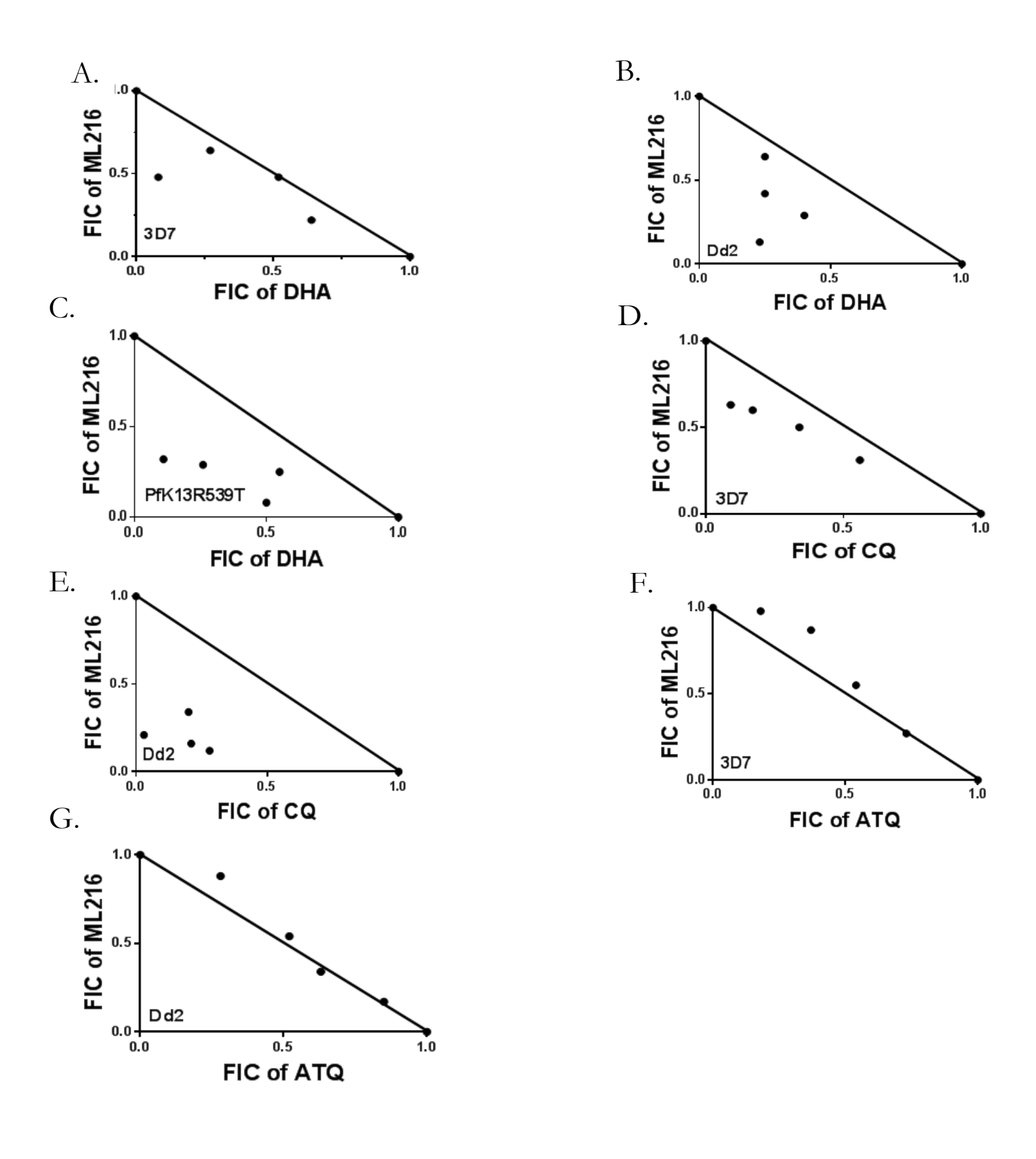


Fig. 16

Fig. 16: ML216 interacts synergistically with DHA and CQ. (A), (B) and (C) Isobologram of DHA-ML216 in 3D7, Dd2 and PfK13R539T strains, respectively. (D) and (E) Isobologram of CQ-ML216 in 3D7 and Dd2 strains, respectively. (F) and (G) Isobologram of ATQ-ML216 in 3D7 and Dd2 strains, respectively. Fixed-ratio drug combination assay was performed. FIC: Fraction inhibitory concentration. Each point represents the mean IC<sub>50</sub> of drug combination from three independent experiments. The solid line is plotted between the IC<sub>50</sub> values of each drug when used alone. DHA: Dihydroartemisinin, CQ: Chloroquine, ATQ: Atovaquone.

presence of IC<sub>50</sub> concentration of DHA (50nM), the anti-malarial action of ML216 was potentiated by 2.26-folds, whereas in the presence of 26nM CQ (IC<sub>50</sub> concentration), the activity of ML216 was potentiated by 1.3-folds (Table 4). These results indicate that ML216 boosts the anti-parasitic effect of current anti-malarial drugs.

**Table 6.**IC<sub>50</sub> of ML216 in combination with ART/CQ and vice versa

Strain	Combination of drugs	IC <sub>50</sub>	Potentiation factor
3D7	ML216 (Alone)	3.39μΜ	1
	ML216 (DHA)	1.5μΜ	2.26
	DHA (Alone)	36.5nM	1
	DHA (ML216)	6.59nM	5.5
	ML216 (Alone)	2.54μΜ	1
	ML216 (CQ)	1.83μΜ	1.38
	CQ (Alone)	20.1nM	1
	CQ (ML216)	5.65nM	3.55

### 5.2 Summary of the results:

In this chapter, we have shown that ML216 exhibited synergistic relation with artemisinin in both drug sensitive (3D7) and drug resistant strains (Dd2 and PfK13R539). The anti-malarial action of artemisinin was potentiated in the presence of ML216 and vice versa. A similar synergistic relation was observed between ML216 and chloroquine in drug sensitive (3D7) and chloroquine resistant strain (Dd2). The anti- parasitic effect of chloroquine was intensified in the presence of ML216 and vice versa.

## **CHAPTER VI**

**DISCUSSION** 

### 6. Discussion:

In this study, we established one of the RecQ helicases of *Plasmodium*, PfBlm as a DNA repair protein and we have shown that RecQ helicase inhibitor blocks the repair of ART generated DSB in *Plasmodium* genome. Firstly, the expression *PfBLM* was maximum during the schizont stage and over produced in response to DNA damage. Secondly, it was was able to complement the MMS sensitivity of  $\Delta sgs1$  mutant of *S. cerevisiae* and interacts with DNA repair proteins of *Plasmodium*. Thirdly, over-expression of this protein increased the survivability of parasites upon DNA damage. Finally, a chemical inhibition of this protein: ML216 impaired the growth of parasite and the inhibitor interacted synergistically with first line anti-malarial drugs.

The expression of PfBlm was at the peak during replicative stage (schizont) compared to the trophozoite and the ring stages. A possible interpretation of this result is that RecQ helicases play a critical role in rescuing the stalled replication forks [127] and in a recent study of *Plasmodium*, it has been shown that replication fork stalled at elevated rates in  $\Delta Pfblm$  strain [22] indicating the active role of PfBlm in replication and repair. The up-regulation of this protein in the presence of external DNA damaging agent implies its role in DNA repair and it is in congruence with earlier reports in which DNA repair proteins PfRad51 and PfalMre11 were also upregulated [14, 15]. We observed that PfBlm associates itself with PfRad51 and PfalMre11. The interaction with PfRad51 as scored by yeast-two-hybrid assay was found to be weaker in nature. It could be possible that within the parasites certain post-translation modifications may modulate the strength of such interaction, which is absent in the surrogate model. It is known from studies in other organisms that depending upon the post translation modification of HsBLM, the consequence of its interaction with Rad51 can be either pro or anti recombinogenic [78]. Earlier reports suggest that Mre11 helps in the recruitment of HsBLM to DNA ends thereby stimulating BLM-DNA2-RPA mediated resection of DSB [67]. PfRPA has been characterized [18] and from the genome information the putative ortholog of DNA2

has been annotated in *P. falciparum* (Gene ID:PF3D7\_1106700) [10]. Future experiments in *Plasmodium* may enlighten us about the importance of PfBLM-PfDNA2-PfRPA interaction.

In the current study, using yeast surrogate system we have shown that PfBLM rescued the MMS sensitivity phenotype of  $\Delta sgs1$  strain. However, helicase dead mutant of PfBLM (PfblmK83R) and PfWRN were unable to perform the function. In model organisms the DNA unwinding activity of BLM is required in two steps of HR: one during resectioning of DSB ends through DNA2 mediated pathway and other during dissolution of Holliday junction along with TopoIII. Although, the orthologs of all these genes are annotated in *Plasmodium* genome, whether PfBlm can engage itself with PfDNA2 or PfTopoIII and participates at these two distinct steps of HR needs to be experimentally tested. Nonetheless, our results suggest that the helicase activity of PfBLM is important in repairing the damaged DNA. Earlier reports have shown that human WRN failed to rescue MMS sensitivity of  $\Delta sgs1$ strain indicating its function is dispensable in DSB repair [128]. This holds true even for PfWRN which was also unable to complement MMS sensitivity phenotype in  $\Delta sgs1$  strain. In model organisms, it was found that the RecQ helicases possess both pro-recombination and anti-recombination functions [24, 111]. An earlier study has observed increased recombination frequency among the sub-telomeric var genes in a Pfwrn knockdown parasite line but not in a Pfblm knockout parasite line [22], emphasizing an anti-recombination activity of PfWrn protein. Our study provides an evidence of pro-recombination activity of PfBlm protein. Thus, it could be possible that the two RecQ paralogs of *Plasmodium* may have opposing roles in HR. It is also possible that as observed in the model organisms the pro-and antirecombination function of these two proteins may be regulated via post-translation modifications [78, 112, 129-131]. Such possibilities need to be explored in future. We observed that over-expression of PfBLM reduced the MMS sensitivity of parasites. This finding indicates the DNA repair activity of PfBLM in the parasite. A plausible explanation for increase in repair efficiency of PfBlm might be its

involvement in unwinding different substrates of HR pathway as over-expression of the helicase dead mutant did not provide any advantage. BLM also possesses helicase independent stimulatory function in Exo1 mediated resection step during HR. Although PfEXO1 has been annotated (PF3D7\_0725000), we currently do not know whether over-expression of PfBlm also stimulates such pathway in *Plasmodium*. Here, we reported binding affinities of known RecQ helicase inhibitors ML216 and MIRA-1 to PfBlm by performing docking and molecular dynamics simulations. Our results demonstrated that ML216 binds efficiently to PfBlm when compared with MIRA-1. This result is in accordance with IDC inhibition of parasites with both the drugs. The parasites are more sensitive to ML216 in contrast to MIRA-1. Interestingly, ML216 mediated inhibition seems to be more selective towards Plasmodium rather than human fibroblast cell lines where the half inhibitory concentration was more than 50 µM after 48 hr incubation [122]. Given the strong selectivity of ML216 towards *Plasmodium*, we believe that chemical modification of the lead compound may bring anti-parasitic activity to nanomolar range. Notably, Dd2 (multi-drug-resistant strain) was more sensitive to ML216 and similar effect was observed with PfRad51 inhibitor B02 [17]. The likely explanation for this result could be that the Dd2 strain might have a compromised DNA repair system and recent reports have shown that the Dd2 strain has failed to respond to DNA damage induced by MMS [132].

The failure in repair of DSB inflicted by various endogenous sources like metabolites, reactive oxygen species (ROS) and replication errors during schizogony lead to death of parasites. The possible mechanism for anti-parasitic activity of ML216 is to hinder the repair of such endogenous damage. Consistent with this interpretation, the effect of drug should intensify in the presence of external DNA damage. Our growth inhibition experiment with MMS treated cells confirmed this hypothesis, with the parasite being hypersensitive to lower concentrations of drug. The known anti-malarial drug, ART inhibits different cellular pathways of parasite and creating DSB is one such established mode of action among them. Our

laboratory has taken particular interest in blocking the repair of such ART generated DSB [91] with ML216. Indeed, ML216 was able to inhibit the repair of DSB offering a ray of hope for Artemisinin based combination therapy (ACT). Finally, our results demonstrated that ML216 interacts synergistically with first line anti-malarial drugs ART and CQ. The plausible explanation for CQ-ML216 synergistic action might be that CQ inhibits the heme polymerization resulting in generation of free radicals that potentially creates DSB. However, there is no experimental evidence for this hypothesis.

Altogether our data provide compelling evidence for PfBlm's participation in *Plasmodium* DNA repair. In addition, we have shown that RecQ helicase in *Plasmodium* can be targeted given their functions in different DNA metabolic pathways. This study raises the possibility of using RecQ helicase inhibitors in combination with first line anti-malarial drugs ART and CQ.

#### **References:**

- 1. WHO, world malaria report 2019.
- 2. Payne, D., Spread of chloroquine resistance in Plasmodium falciparum. Parasitol Today, 1987. **3**(8): p. 241-6.
- 3. Dondorp, A.M., et al., *Artemisinin resistance in Plasmodium falciparum malaria*. N Engl J Med, 2009. **361**(5): p. 455-67.
- 4. Pannunzio, N.R., G. Watanabe, and M.R. Lieber, *Nonhomologous DNA end-joining for repair of DNA double-strand breaks.* J Biol Chem, 2018. **293**(27): p. 10512-10523.
- 5. Chang, H.H.Y., et al., *Non-homologous DNA end joining and alternative pathways to double-strand break repair.* Nat Rev Mol Cell Biol, 2017. **18**(8): p. 495-506.
- 6. Scully, R., et al., *DNA double-strand break repair-pathway choice in somatic mammalian cells.* Nature Reviews Molecular Cell Biology, 2019. **20**(11): p. 698-714.
- 7. Krejci, L., et al., *Homologous recombination and its regulation*. Nucleic Acids Res, 2012. **40**(13): p. 5795-818.
- 8. Symington, L.S. and J. Gautier, *Double-strand break end resection and repair pathway choice*. Annu Rev Genet, 2011. **45**: p. 247-71.
- 9. Wright, W.D., S.S. Shah, and W.D. Heyer, *Homologous recombination and the repair of DNA double-strand breaks*. J Biol Chem, 2018. **293**(27): p. 10524-10535.
- 10. Gardner, M.J., et al., *Genome sequence of the human malaria parasite Plasmodium falciparum*. Nature, 2002. **419**(6906): p. 498-511.
- 11. Fox, B.A., et al., Efficient gene replacements in Toxoplasma gondii strains deficient for nonhomologous end joining. Eukaryot Cell, 2009. **8**(4): p. 520-9.
- 12. Kirkman, L.A., E.A. Lawrence, and K.W. Deitsch, *Malaria parasites utilize both homologous recombination and alternative end joining pathways to maintain genome integrity.* Nucleic Acids Res, 2014. **42**(1): p. 370-9.
- 13. Roy, N., et al., Dominant negative mutant of Plasmodium Rad51 causes reduced parasite burden in host by abrogating DNA double-strand break repair. Mol Microbiol, 2014. **94**(2): p. 353-66.
- 14. Badugu, S.B., et al., *Identification of Plasmodium falciparum DNA Repair Protein Mre11 with an Evolutionarily Conserved Nuclease Function.* PLoS One, 2015. **10**(5): p. e0125358.

- 15. Bhattacharyya, M.K. and N. Kumar, *Identification and molecular characterisation of DNA damaging agent induced expression of Plasmodium falciparum recombination protein PfRad51*. Int J Parasitol, 2003. **33**(12): p. 1385-92.
- 16. Bhattacharyya, M.K., et al., Characterization of kinetics of DNA strand-exchange and ATP hydrolysis activities of recombinant PfRad51, a Plasmodium falciparum recombinase. Mol Biochem Parasitol, 2005. **139**(1): p. 33-9.
- 17. Vydyam, P., et al., A small-molecule inhibitor of the DNA recombinase Rad51 from Plasmodium falciparum synergizes with the antimalarial drugs artemisinin and chloroquine. J Biol Chem, 2019. **294**(20): p. 8171-8183.
- 18. Gopalakrishnan, A.M. and N. Kumar, Opposing roles for two molecular forms of replication protein A in Rad51-Rad54-mediated DNA recombination in Plasmodium falciparum. mBio, 2013. 4(3): p. e00252-13.
- 19. Mlambo, G., I. Coppens, and N. Kumar, *Aberrant sporogonic development of Dmc1 (a meiotic recombinase) deficient Plasmodium berghei parasites.* PLoS One, 2012. **7**(12): p. e52480.
- 20. Rahman, F., M. Tarique, and R. Tuteja, *Plasmodium falciparum Bloom homologue, a nucleocytoplasmic protein, translocates in 3' to 5' direction and is essential for parasite growth.* Biochim Biophys Acta, 2016. **1864**(5): p. 594-608.
- 21. Rahman, F., et al., *Plasmodium falciparum Werner homologue is a nuclear protein and its biochemical activities reside in the N-terminal region*. Protoplasma, 2016. **253**(1): p. 45-60.
- 22. Claessens, A., et al., RecQ helicases in the malaria parasite Plasmodium falciparum affect genome stability, gene expression patterns and DNA replication dynamics. PLoS Genet, 2018. **14**(7): p. e1007490.
- 23. Li, Z., et al., DNA helicase RecQ1 regulates mutually exclusive expression of virulence genes in Plasmodium falciparum via heterochromatin alteration. Proc Natl Acad Sci U S A, 2019. **116**(8): p. 3177-3182.
- 24. Croteau, D.L., et al., *Human RecQ helicases in DNA repair, recombination, and replication.* Annu Rev Biochem, 2014. **83**: p. 519-52.
- 25. Oshima, J., et al., RECQ helicase disease and related progeroid syndromes: RECQ2018 meeting. Mech Ageing Dev, 2018. 173: p. 80-83.
- 26. Bachrati, C.Z. and I.D. Hickson, RecQ helicases: guardian angels of the DNA replication fork. Chromosoma, 2008. 117(3): p. 219-33.
- 27. Matsuno, K., et al., The N-terminal noncatalytic region of Xenopus RecQ4 is required for chromatin binding of DNA polymerase alpha in the initiation of DNA replication. Mol Cell Biol, 2006. **26**(13): p. 4843-52.

- 28. Selak, N., et al., The Bloom's syndrome helicase (BLM) interacts physically and functionally with p12, the smallest subunit of human DNA polymerase delta. Nucleic Acids Res, 2008. **36**(16): p. 5166-79.
- 29. Franchitto, A. and P. Pichierri, Werner syndrome protein and the MRE11 complex are involved in a common pathway of replication fork recovery. Cell Cycle, 2004. **3**(10): p. 1331-9.
- 30. Kamath-Loeb, A.S., et al., Interactions between the Werner syndrome helicase and DNA polymerase delta specifically facilitate copying of tetraplex and hairpin structures of the d(CGG)n trinucleotide repeat sequence. J Biol Chem, 2001. **276**(19): p. 16439-46.
- 31. Barefield, C. and J. Karlseder, *The BLM helicase contributes to telomere maintenance through processing of late-replicating intermediate structures.* Nucleic Acids Res, 2012. **40**(15): p. 7358-67.
- 32. Aygun, O., et al., *Direct inhibition of RNA polymerase II transcription by RECQL5*. J Biol Chem, 2009. **284**(35): p. 23197-203.
- 33. Islam, M.N., et al., RecQL5 promotes genome stabilization through two parallel mechanisms-interacting with RNA polymerase II and acting as a helicase. Mol Cell Biol, 2010. **30**(10): p. 2460-72.
- 34. Popuri, V., et al., Human RECQL5: guarding the crossroads of DNA replication and transcription and providing backup capability. Crit Rev Biochem Mol Biol, 2013. **48**(3): p. 289-99.
- 35. Grierson, P.M., S. Acharya, and J. Groden, *Collaborating functions of BLM and DNA topoisomerase I in regulating human rDNA transcription.* Mutat Res, 2013. **743-744**: p. 89-96.
- 36. Laine, J.P., et al., Werner protein stimulates topoisomerase I DNA relaxation activity. Cancer Res, 2003. **63**(21): p. 7136-46.
- 37. Nguyen, G.H., et al., Regulation of gene expression by the BLM helicase correlates with the presence of G-quadruplex DNA motifs. Proc Natl Acad Sci U S A, 2014. 111(27): p. 9905-10.
- 38. Johnson, J.E., et al., Altered gene expression in the Werner and Bloom syndromes is associated with sequences having G-quadruplex forming potential. Nucleic Acids Res, 2010. **38**(4): p. 1114-22.
- 39. Opresko, P.L., et al., The Werner syndrome helicase and exonuclease cooperate to resolve telomeric D loops in a manner regulated by TRF1 and TRF2. Mol Cell, 2004. **14**(6): p. 763-74.
- 40. Ghosh, A.K., et al., *RECQLA*, the protein mutated in Rothmund-Thomson syndrome, functions in telomere maintenance. J Biol Chem, 2012. **287**(1): p. 196-209.
- 41. Opresko, P.L., et al., *POT1 stimulates RecQ helicases WRN and BLM to unwind telomeric DNA substrates.* J Biol Chem, 2005. **280**(37): p. 32069-80.
- 42. Lillard-Wetherell, K., et al., Association and regulation of the BLM helicase by the telomere proteins TRF1 and TRF2. Hum Mol Genet, 2004. **13**(17): p. 1919-32.

- 43. Das, A., et al., The human Werner syndrome protein stimulates repair of oxidative DNA base damage by the DNA glycosylase NEIL1. J Biol Chem, 2007. **282**(36): p. 26591-602.
- 44. Schurman, S.H., et al., *Direct and indirect roles of RECQLA in modulating base excision repair capacity*. Hum Mol Genet, 2009. **18**(18): p. 3470-83.
- 45. Trego, K.S., et al., The DNA repair endonuclease XPG interacts directly and functionally with the WRN helicase defective in Werner syndrome. Cell Cycle, 2011. **10**(12): p. 1998-2007.
- 46. Huber, M.D., et al., A conserved G4 DNA binding domain in RecQ family helicases. J Mol Biol, 2006. **358**(4): p. 1071-80.
- 47. Chu, W.K. and I.D. Hickson, RecQ helicases: multifunctional genome caretakers. Nat Rev Cancer, 2009. **9**(9): p. 644-54.
- 48. Kocsis, Z.S., et al., A nucleotide-dependent and HRDC domain-dependent structural transition in DNA-bound RecQ helicase. J Biol Chem, 2014. **289**(9): p. 5938-49.
- 49. Mohaghegh, P., et al., *The Bloom's and Werner's syndrome proteins are DNA structure-specific helicases.* Nucleic Acids Res, 2001. **29**(13): p. 2843-9.
- 50. Bachrati, C.Z., R.H. Borts, and I.D. Hickson, *Mobile D-loops are a preferred substrate for the Bloom's syndrome helicase.* Nucleic Acids Res, 2006. **34**(8): p. 2269-79.
- 51. Sun, H., et al., *The Bloom's syndrome helicase unwinds G4 DNA*. J Biol Chem, 1998. **273**(42): p. 27587-92.
- 52. Orren, D.K., S. Theodore, and A. Machwe, *The Werner syndrome helicase/exonuclease (WRN) disrupts and degrades D-loops in vitro.* Biochemistry, 2002. **41**(46): p. 13483-8.
- 53. Popuri, V., et al., *The Human RecQ helicases, BLM and RECQ1, display distinct DNA substrate specificities.* J Biol Chem, 2008. **283**(26): p. 17766-76.
- 54. Umezu, K., K. Nakayama, and H. Nakayama, *Escherichia coli RecQ protein is a DNA helicase*. Proc Natl Acad Sci U S A, 1990. **87**(14): p. 5363-7.
- 55. Harmon, F.G. and S.C. Kowalczykowski, RecQ helicase, in concert with RecA and SSB proteins, initiates and disrupts DNA recombination. Genes Dev, 1998. **12**(8): p. 1134-44.
- 56. Bachrati, C.Z. and I.D. Hickson, RecQ helicases: suppressors of tumorigenesis and premature aging. Biochem J, 2003. **374**(Pt 3): p. 577-606.
- 57. Cooper, M.P., et al., *Ku complex interacts with and stimulates the Werner protein.* Genes Dev, 2000. **14**(8): p. 907-12.
- 58. Kusumoto, R., et al., Werner protein cooperates with the XRCC4-DNA ligase IV complex in end-processing. Biochemistry, 2008. 47(28): p. 7548-56.

- 59. Kusumoto-Matsuo, R., et al., Cooperation of DNA-PKcs and WRN helicase in the maintenance of telomeric D-loops. Aging (Albany NY), 2010. **2**(5): p. 274-84.
- 60. Parvathaneni, S., et al., Human RECQ1 interacts with Ku70/80 and modulates DNA endjoining of double-strand breaks. PLoS One, 2013. **8**(5): p. e62481.
- 61. Sallmyr, A., A.E. Tomkinson, and F.V. Rassool, *Up-regulation of WRN and DNA ligase IIIa* in chronic myeloid leukemia: consequences for the repair of DNA double-strand breaks. Blood, 2008. **112**(4): p. 1413-1423.
- 62. Lisby, M., et al., Choreography of the DNA damage response: spatiotemporal relationships among checkpoint and repair proteins. Cell, 2004. **118**(6): p. 699-713.
- 63. Sartori, A.A., et al., *Human CtIP promotes DNA end resection*. Nature, 2007. **450**(7169): p. 509-14.
- 64. Nicolette, M.L., et al., Mre11-Rad50-Xrs2 and Sae2 promote 5' strand resection of DNA double-strand breaks. Nat Struct Mol Biol, 2010. 17(12): p. 1478-85.
- 65. Shibata, A., et al., *DNA double-strand break repair pathway choice is directed by distinct MRE11 nuclease activities.* Mol Cell, 2014. **53**(1): p. 7-18.
- 66. Anand, R., et al., *Phosphorylated CtIP Functions as a Co-factor of the MRE11-RAD50-NBS1 Endonuclease in DNA End Resection.* Mol Cell, 2016. **64**(5): p. 940-950.
- 67. Nimonkar, A.V., et al., BLM-DNA2-RPA-MRN and EXO1-BLM-RPA-MRN constitute two DNA end resection machineries for human DNA break repair. Genes Dev, 2011. **25**(4): p. 350-62.
- 68. Tran, P.T., et al., Characterization of nuclease-dependent functions of Exo1p in Saccharomyces cerevisiae. DNA Repair (Amst), 2002. **1**(11): p. 895-912.
- 69. Sturzenegger, A., et al., DNA2 cooperates with the WRN and BLM RecQ helicases to mediate long-range DNA end resection in human cells. J Biol Chem, 2014. **289**(39): p. 27314-26.
- 70. Niu, H., et al., Mechanism of the ATP-dependent DNA end-resection machinery from Saccharomyces cerevisiae. Nature, 2010. **467**(7311): p. 108-11.
- 71. Cejka, P., et al., *DNA end resection by Dna2-Sgs1-RPA and its stimulation by Top3-Rmi1 and Mre11-Rad50-Xrs2*. Nature, 2010. **467**(7311): p. 112-6.
- 72. Daley, J.M., et al., Multifaceted role of the Topo IIIa-RMI1-RMI2 complex and DNA2 in the BLM-dependent pathway of DNA break end resection. Nucleic Acids Res, 2014. **42**(17): p. 11083-91.
- 73. Nimonkar, A.V., et al., *Human exonuclease 1 and BLM helicase interact to resect DNA and initiate DNA repair.* Proc Natl Acad Sci U S A, 2008. **105**(44): p. 16906-11.

- 74. Cannavo, E., P. Cejka, and S.C. Kowalczykowski, Relationship of DNA degradation by Saccharomyces cerevisiae exonuclease 1 and its stimulation by RPA and Mre11-Rad50-Xrs2 to DNA end resection. Proc Natl Acad Sci U S A, 2013. **110**(18): p. E1661-8.
- 75. Chen, H., M. Lisby, and L.S. Symington, *RPA coordinates DNA end resection and prevents formation of DNA hairpins*. Mol Cell, 2013. **50**(4): p. 589-600.
- 76. Bugreev, D.V., et al., *Novel pro- and anti-recombination activities of the Bloom's syndrome helicase.* Genes Dev, 2007. **21**(23): p. 3085-94.
- 77. Hu, Y., et al., RECQL5/Recql5 helicase regulates homologous recombination and suppresses tumor formation via disruption of Rad51 presynaptic filaments. Genes Dev, 2007. **21**(23): p. 3073-84.
- 78. Ouyang, K.J., et al., SUMO modification regulates BLM and RAD51 interaction at damaged replication forks. PLoS Biol, 2009. **7**(12): p. e1000252.
- 79. Bugreev, D.V., O.M. Mazina, and A.V. Mazin, *Bloom syndrome helicase stimulates RAD51* DNA strand exchange activity through a novel mechanism. J Biol Chem, 2009. **284**(39): p. 26349-59.
- 80. Raynard, S., W. Bussen, and P. Sung, *A double Holliday junction dissolvasome comprising BLM, topoisomerase IIIalpha, and BLAP75.* J Biol Chem, 2006. **281**(20): p. 13861-4.
- 81. Ip, S.C., et al., *Identification of Holliday junction resolvases from humans and yeast.* Nature, 2008. **456**(7220): p. 357-61.
- 82. Wyatt, H.D. and S.C. West, *Holliday junction resolvases*. Cold Spring Harb Perspect Biol, 2014. **6**(9): p. a023192.
- 83. Constantinou, A., et al., Werner's syndrome protein (WRN) migrates Holliday junctions and colocalizes with RPA upon replication arrest. EMBO Rep, 2000. 1(1): p. 80-4.
- 84. LeRoy, G., et al., *Identification of RecQL1 as a Holliday junction processing enzyme in human cell lines.* Nucleic Acids Res, 2005. **33**(19): p. 6251-7.
- 85. Kikuchi, K., et al., Bloom DNA helicase facilitates homologous recombination between diverged homologous sequences. J Biol Chem, 2009. **284**(39): p. 26360-7.
- 86. Yang, Y.Z., W. Asawamahasakda, and S.R. Meshnick, *Alkylation of human albumin by the antimalarial artemisinin*. Biochem Pharmacol, 1993. **46**(2): p. 336-9.
- 87. Asawamahasakda, W., et al., Reaction of antimalarial endoperoxides with specific parasite proteins. Antimicrob Agents Chemother, 1994. **38**(8): p. 1854-8.
- 88. Berman, P.A. and P.A. Adams, *Artemisinin enhances heme-catalysed oxidation of lipid membranes*. Free Radic Biol Med, 1997. **22**(7): p. 1283-8.

- 89. Eckstein-Ludwig, U., et al., *Artemisinins target the SERCA of Plasmodium falciparum*. Nature, 2003. **424**(6951): p. 957-61.
- 90. Wang, J., et al., Artemisinin directly targets malarial mitochondria through its specific mitochondrial activation. PLoS One, 2010. 5(3): p. e9582.
- 91. Gopalakrishnan, A.M. and N. Kumar, *Antimalarial action of artesunate involves DNA damage mediated by reactive oxygen species.* Antimicrob Agents Chemother, 2015. **59**(1): p. 317-25.
- 92. Phyo, A.P., et al., Emergence of artemisinin-resistant malaria on the western border of Thailand: a longitudinal study. Lancet, 2012. **379**(9830): p. 1960-6.
- 93. Sinclair, D., et al., Artemisinin-based combination therapy for treating uncomplicated Plasmodium vivax malaria. Cochrane Database Syst Rev, 2011(7): p. CD008492.
- 94. Guidelines for the Treatment of Malaria. 2015: World Health Organization.
- 95. Price, R.N., et al., Effects of artemisinin derivatives on malaria transmissibility. Lancet, 1996. **347**(9016): p. 1654-8.
- 96. Targett, G., et al., Artesunate reduces but does not prevent posttreatment transmission of Plasmodium falciparum to Anopheles gambiae. J Infect Dis, 2001. **183**(8): p. 1254-9.
- 97. Nsanzabana, C., Resistance to Artemisinin Combination Therapies (ACTs): Do Not Forget the Partner Drug! Trop Med Infect Dis, 2019. 4(1).
- 98. Chalapareddy, S., et al., Radicicol confers mid-schizont arrest by inhibiting mitochondrial replication in Plasmodium falciparum. Antimicrob Agents Chemother, 2014. **58**(8): p. 4341-52.
- 99. Dana, S., et al., *Potent antimalarial activity of acriflavine in vitro and in vivo*. ACS Chem Biol, 2014. **9**(10): p. 2366-73.
- 100. Roy, A., A. Kucukural, and Y. Zhang, *I-TASSER: a unified platform for automated protein structure and function prediction.* Nat Protoc, 2010. **5**(4): p. 725-38.
- 101. Yang, J. and Y. Zhang, *I-TASSER server: new development for protein structure and function predictions.* Nucleic Acids Res, 2015. **43**(W1): p. W174-81.
- 102. Laskowski, R.A., et al., PROCHECK: a program to check the stereochemical quality of protein structures. Journal of Applied Crystallography, 1993. **26**(2): p. 283-291.
- 103. Newman, J.A., et al., Crystal structure of the Bloom's syndrome helicase indicates a role for the HRDC domain in conformational changes. Nucleic Acids Res, 2015. **43**(10): p. 5221-35.
- 104. Abraham, M.J., et al., GROMACS: High performance molecular simulations through multi-level parallelism from laptops to supercomputers. SoftwareX, 2015. 1-2: p. 19-25.

- 105. Best, R.B., et al., Optimization of the Additive CHARMM All-Atom Protein Force Field Targeting Improved Sampling of the Backbone φ, ψ and Side-Chain χ1 and χ2 Dihedral Angles. Journal of Chemical Theory and Computation, 2012. **8**(9): p. 3257-3273.
- 106. Trott, O. and A.J. Olson, AutoDock Vina: improving the speed and accuracy of docking with a new scoring function, efficient optimization, and multithreading. J Comput Chem, 2010. **31**(2): p. 455-61.
- 107. Vanommeslaeghe, K. and A.D. MacKerell, Jr., *Automation of the CHARMM General Force Field (CGenFF) I: bond perception and atom typing.* J Chem Inf Model, 2012. **52**(12): p. 3144-54.
- 108. Vanommeslaeghe, K., E.P. Raman, and A.D. MacKerell, Jr., *Automation of the CHARMM General Force Field (CGenFF) II: assignment of bonded parameters and partial atomic charges.* J Chem Inf Model, 2012. **52**(12): p. 3155-68.
- 109. Kumari, R., R. Kumar, and A. Lynn, *g\_mmpbsa--a GROMACS tool for high-throughput MM-PBSA calculations.* J Chem Inf Model, 2014. **54**(7): p. 1951-62.
- 110. Baker, N.A., et al., *Electrostatics of nanosystems: application to microtubules and the ribosome.* Proc Natl Acad Sci U S A, 2001. **98**(18): p. 10037-41.
- 111. Bernstein, K.A., S. Gangloff, and R. Rothstein, *The RecQ DNA helicases in DNA repair*. Annu Rev Genet, 2010. **44**: p. 393-417.
- 112. Böhm, S. and K.A. Bernstein, *The role of post-translational modifications in fine-tuning BLM helicase function during DNA repair*. DNA Repair (Amst), 2014. **22**: p. 123-32.
- 113. Frei, C. and S.M. Gasser, *The yeast Sgs1p helicase acts upstream of Rad53p in the DNA replication checkpoint and colocalizes with Rad53p in S-phase-specific foci.* Genes Dev, 2000. **14**(1): p. 81-96.
- 114. Dutertre, S., et al., Cell cycle regulation of the endogenous wild type Bloom's syndrome DNA helicase. Oncogene, 2000. **19**(23): p. 2731-8.
- 115. Bártfai, R., et al., H2A.Z demarcates intergenic regions of the plasmodium falciparum epigenome that are dynamically marked by H3K9ac and H3K4me3. PLoS Pathog, 2010. **6**(12): p. e1001223.
- 116. Hoeijmakers, W., R. Bartfai, and P.R. Kensche, *Transcriptome of the P. falciparum 3D7 intraerythrocytic cycle assayed by RNA-Seq*, PlasmoDB, Editor. 2015.
- 117. Wu, L., et al., Potential role for the BLM helicase in recombinational repair via a conserved interaction with RAD51. J Biol Chem, 2001. **276**(22): p. 19375-81.
- 118. Tripathi, V., et al., MRN complex-dependent recruitment of ubiquitylated BLM helicase to DSBs negatively regulates DNA repair pathways. Nat Commun, 2018. 9(1): p. 1016.

- 119. Ui, A., et al., The N-terminal region of Sgs1, which interacts with Top3, is required for complementation of MMS sensitivity and suppression of hyper-recombination in sgs1 disruptants. Mol Genet Genomics, 2001. **265**(5): p. 837-50.
- 120. Mirzaei, H. and K.H. Schmidt, *Non-Bloom syndrome-associated partial and total loss-of-function variants of BLM helicase.* Proc Natl Acad Sci U S A, 2012. **109**(47): p. 19357-62.
- 121. Mitra, P., et al., Functional dissection of proliferating-cell nuclear antigens (1 and 2) in human malarial parasite Plasmodium falciparum: possible involvement in DNA replication and DNA damage response. Biochem J, 2015. **470**(1): p. 115-29.
- 122. Nguyen, G.H., et al., A small molecule inhibitor of the BLM helicase modulates chromosome stability in human cells. Chem Biol, 2013. **20**(1): p. 55-62.
- 123. Aggarwal, M., et al., Inhibition of helicase activity by a small molecule impairs Werner syndrome helicase (WRN) function in the cellular response to DNA damage or replication stress. Proc Natl Acad Sci U S A, 2011. **108**(4): p. 1525-30.
- 124. Mbengue, A., et al., *A molecular mechanism of artemisinin resistance in Plasmodium falciparum malaria.* Nature, 2015. **520**(7549): p. 683-7.
- 125. Berdelle, N., et al., Artesunate induces oxidative DNA damage, sustained DNA double-strand breaks, and the ATM/ATR damage response in cancer cells. Mol Cancer Ther, 2011. **10**(12): p. 2224-33.
- 126. Sullivan, D.J., Jr., et al., *A common mechanism for blockade of heme polymerization by antimalarial quinolines.* J Biol Chem, 1998. **273**(47): p. 31103-7.
- 127. Davies, S.L., P.S. North, and I.D. Hickson, *Role for BLM in replication-fork restart and suppression of origin firing after replicative stress.* Nat Struct Mol Biol, 2007. **14**(7): p. 677-9.
- 128. Aggarwal, M. and R.M. Brosh, WRN helicase defective in the premature aging disorder Werner syndrome genetically interacts with topoisomerase 3 and restores the top3 slow growth phenotype of sgs1 top3. Aging (Albany NY), 2009. 1(2): p. 219-33.
- 129. Kusumoto, R., M. Muftuoglu, and V.A. Bohr, *The role of WRN in DNA repair is affected by post-translational modifications.* Mech Ageing Dev, 2007. **128**(1): p. 50-7.
- 130. Mukherjee, S., et al., *Werner Syndrome Protein and DNA Replication*. Int J Mol Sci, 2018. **19**(11).
- 131. Ammazzalorso, F., et al., ATR and ATM differently regulate WRN to prevent DSBs at stalled replication forks and promote replication fork recovery. Embo j, 2010. **29**(18): p. 3156-69.
- 132. Gupta, D.K., et al., *DNA damage regulation and its role in drug-related phenotypes in the malaria parasites.* Sci Rep, 2016. **6**: p. 23603.

# **APPENDIX**

# **Synopsis**

The expanding severity of malaria disease is mainly because of unsuccessful vaccine development efforts and emerging resistance to available drugs. Complete eradication of malaria became a difficult process. Artemisinin-based combination therapies (ACTs) introduced in the year 1994 are still in use to treat malaria. There are five types of WHO adopted ACTs, namely: artesunate-amodiaquine (ASAQ), artesunate-sulfadoxine-pyrimethamine (ASSP), artemether-lumefantrine (AL), dihydro-artemisinin-piperaquine (DP), and artesunate-mefloquine (ASMQ) [1]. Recent reports suggest that resistance has emerged to all the five types of ACTs, and hence there is an immediate need to develop a partner drug for artemisinin [2].

In a cellular environment, DNA double-strand breaks (DSB) occur from multiple sources throughout the cell cycle [3]. Each of that double-strand break needs to be appropriately repaired to maintain genome stability. There are two main pathways to repair such DSBs: "error-free" homologous recombination (HR) and "errorprone" non-homologous end joining (NHEJ). In addition to these pathways, there are two other minor pathways called Rad51 independent single-strand annealing (SSA) and alternative non-homologous end joining (Alt-NHEJ) [4]. HR pathway requires a homologous template to repair the break, whereas NHEJ does not require any homologous sequence; instead, it ligates the broken ends. In mammalian cells, NHEJ is the primary pathway to repair DSBs compared to lower organisms, where HR pathway is frequent. In the NHEJ pathway, DSB is recognized by MRN (Mre11-Rad51-Nbs1) complex which recruits Ku70-Ku80 heterodimer protecting DNA ends from degradation. Ku complex further recruit's DNA-PKcs which exists in a tight complex with nuclease, artemis. The endonuclease, artemis chops the broken ends. Poly X family polymerases (Pol  $\mu$  and Pol  $\lambda$ ) add nucleotides to broken ends. Finally, ligation of the DSB end is carried out by DNA ligase IV complex along with XRCC4, XLF and PAXX protein [5].

HR pathway utilizes an undamaged template to repair DSBs, which restores lost sequence information. HR pathway starts with the resection of broken ends to generate 3' single-stranded DNA. Resection takes place in two steps: short-range resection and long-range resection. Short-range resection is carried out by MRN (Mre11-Rad50-Nbs1) complex together with CtIP [6-8]. Long-range resection is mediated by either the Dna2-Blm-Rpa complex or Exo1 mediated pathway [9]. After resection, the overhanging 3' single-stranded DNA is bound by Rad51, forming a Rad51-ssDNA complex capable of homologous pairing. Rad51 nucleofilament complex invades into a donor template to yield a DNA joint known as a displacement loop or D-loop. Further, D-loop captures the second end of the break to form double Holliday junctions (HJs). The HJs are resolved by either dissolvosome complex (Blm-Topo3-Rmi1) to form exclusively non-crossover products or by resolvases (Gen1, Mus81-Eme1) to generate both crossover and non-crossover product [10-12].

In *Plasmodium*, genome sequence analysis revealed that genes for c-NHEJ are absent [13]. However, Alt-NHEJ is functional, but it is a rare event [14]. The primary pathway to repair DSBs in *Plasmodium* is HR [14, 15] and the essential proteins of this pathway PfRad51, PfalMre11 have been identified and characterized [15-19].

RecQ helicases are the genome gatekeepers considering their functions in different DNA metabolic pathways [20]. There are five types of RecQ helicases in humans, whereas in yeast (\$G\$\$1\$) and bacteria (\$RecQ\$), there is only one type of RecQ helicase. RecQ helicases' functions are prominent during the DNA repair pathway since most of their substrates resemble DNA repair intermediates. Apart from helicase-dependent DNA repair activities, they also have helicase independent regulatory functions during the HR pathway. Out of five RecQ helicases in humans, the functions of RECQL2 (BLM) are well known in the HR pathway. To begin with, the long-range resection during HR can happen in two independent ways involving Exo1 and Dna2-Blm-Rpa complexes [9]. In the Dna2-Blm-Rpa complex-mediated pathway, Dna2 relies on helicase activity of Blm for DNA unwinding, whereas in

Exo1 mediated pathway, Blm, Rpa, Blm, and MRN complex has stimulatory function [21-23]. Out of five RecQ helicases in humans, this stimulatory function is exclusive to BLM [21]. During the strand invasion step of HR, Blm exhibits anti-recombinogenic activity by disrupting Rad51 nucleofilament [24]. However, in two cases this effect is reversed. When Blm gets SUMOylated, it facilitates the recruitment of Rad51 at the site of DSB [25]. Second, Blm stimulates strand exchange activity when Rad51 is in ATP-bound form in place of ADP-bound form [26]. After strand invasion, D-loop captures the second end of the break to form double Holliday junctions (dHJ). The dHJ can be resolved by either resolvases GEN1, MUS81/EME1 (YEN1, Mus81-Mms4 in yeast) to generate crossover and non-crossover products or by dissolvosome complex (Blm-TopoIII-Rmi1/Blap75) to generate exclusively non-crossover products [10-12]. RECQL1 and WRN are also able to perform processing of Holliday junctions [27, 28].

Two RecQ helicases have been identified in *Plasmodium*, namely *PfBLM* and *PfWRN*. Previous reports have shown that the helicase activity of PfBlm and PfWrn is conserved in *Plasmodium* [29, 30]. Both the helicases are required for normal transcription and replication [31]. Also, it has been shown that *PfWRN* knockout increased the recombination rates underscoring its anti-recombination activity. However, there are no reports highlighting the DNA repair functions of *PfBLM* or *PfWRN*. Since in model organisms, it is reported that BLM has significant HR pathway functions compared to WRN, here we focused on studying the DNA repair functions of *PfBLM*.

In this work, we have addressed three questions. Firstly, whether DNA repair functions of BLM are conserved in *Plasmodium*? Secondly, how the inhibitors of RecQ helicase affect the *in vitro* and *in vivo* growth of *Plasmodium*? Finally, how the inhibitor of RecQ helicase interacts with current anti-malarial drugs artemisinin and chloroquine?

In the first part, we investigated the DNA repair activity of *PfBLM*. For this purpose, we tried to express full-length PfBlm protein to raise an antibody against it. The protein expression was too low; as a result, we could not proceed with purification. We raised a peptide antibody against the unique C-terminal region of PfBlm protein and checked whether it could detect it. The peptide antibody could detect PfBlm protein at the appropriate size, and the pre-immune serum was clean. We used this peptide antibody for our protein expression studies. Firstly, we investigated the expression of PfBLM in all the intra-erythrocytic stages at both RNA and protein levels. At the RNA level, the expression of PfBLM was high during the trophozoite and schizont stages compared to the ring stage. A similar result was obtained at the protein level as well. Next, we studied the expression of *PfBLM* upon DNA damage. For this purpose, we treated ring, trophozoite, and schizont stage parasites with DNA damaging agent methyl methane sulfonate (MMS) and examined RNA/protein level expression. Here, we found that the expression of PfBLM was up regulated upon DNA damage during ring and trophozoite stages, whereas its expression was unchanged during the schizont stage. The expression of PfBLM during the schizont stage was high in control; any further up-regulation upon DNA damage was not quantifiable. A similar pattern of up-regulation was observed at the protein level, suggesting the likely implications of PfBLM in the DNA repair pathway. In model organisms, it has been shown that to function in HR pathway, Blm interacts with Rad51 and Mre11 during resection and strand invasion steps [32, 33]. Here, we checked the interaction of PfBlm with PfRad51/PfalMre11. For this purpose, we did a yeast two-hybrid assay in which we cloned PfBLM in prey vector (pGADC1) and PfRAD51/ PfalMRE11 in bait vector (pGBDUC1). We observed weak interaction between PfBLM and PfRAD51 as the growth was seen only on the SC-Lue-Ura-His plate, whereas strong interaction was observed between PfBLM and PfalMRE11 as growth was seen on both SC-Lue-Ura-His and SC-Lue-Ura-Ade plates. The co-purification assay further confirmed the interaction between PfBlm and PfRad51. We planned to disrupt the interaction between PfBlm and PfRad51

with a small molecule inhibitor. For this purpose, an in silico analysis was done that predicted two contact points on PfRad51 through which it is supposed to interact with PfBlm. We have generated both single and double mutants in those regions. We expressed these mutants and performed a co-purification assay to check their interaction with PfBlm protein. To our surprise, both single and double mutants interacted with PfBlm protein, so we did not proceed further with this project. Next, we examined the DNA repair activity of PfBLM using yeast as a surrogate system. We generated helicase dead mutant of PfBLM (PfblmK83R) and used this mutant as a negative control for the complementation assay. To perform complementation assay, we knocked out the only RecQ helicase of yeast (SGS1) and generated  $\Delta sgs1$ strain, which was sensitive to MMS. We transformed PfBLM, PfblmK83R, and another RecQ helicase PfWRN into \(\Delta sgs1\) strain. MMS sensitivity assay was performed with the generated strains, where we observed that PfBLM was able to complement the MMS sensitivity of  $\Delta sgs1$  strain partially. However, PfblmK83R and PfWRN failed to do the function. Finally, to inspect the DNA repair activity of *PfBLM* in the parasite, we did overexpression studies. To this end, we cloned *PfBLM* and PfblmK83R in overexpression vector pARL and transfected these clones into Plasmodium falciparum 3D7 to generate overexpression strains. MMS sensitivity assay was performed with these strains at three intra-erythrocytic stages of the parasite. Here, we observed an increase in survivability of PfBLM overexpression strain compared to wild type 3D7 during trophozoite and schizont stages but not during the ring stage. However, we did not notice such a type of survival advantage with PfblmK83R overexpression strain. This data suggests that the DNA repair function of *PfBLM* is conserved in *Plasmodium*.

In the second part, we tested the effect of RecQ helicase inhibitors on *Plasmodium* growth. Initially, we did an *in silico* docking study to predict the binding affinities of two known human RecQ helicase inhibitors ML216 and MIRA-1 [34, 35] to PfBlm protein. Our bioinformatics study predicted that ML216 is like to bind with more

affinity to PfBlm protein compared to MIRA-1. Next, we tested the effect of this inhibitor on *Plasmodium* growth for which we have done standard growth inhibition assay with these two inhibitors ML216 and MIRA-1. To this end, we treated the trophozoite stage parasites with varying concentrations of ML216 and MIRA-1 (0.1nM to 1000µM) for 48 hrs. We evaluated the survivability of parasites by the Giemsa staining method and the fluorescence-based SYBR Green-I method. Here, we found that the IC<sub>50</sub> value of ML216 was ten times lesser than MIRA-1, indicating it to be a more potent inhibitor of *Plasmodium* growth. A similar result was obtained with multidrug-resistant strain Dd2 and artemisinin-resistant strain PfK13R539T. Likewise, we tested the effect of ML216 on in vivo growth of mouse malarial parasite Plasmodium berghei. To this end, we performed Peter's 4-day suppressive test with a single dose of ML216 (25mg/kg body weight). Here, we observed gradual decrement in percentage parasitemia and increased survivability of host in the drug-treated mice group compared to the untreated group. Finally, we studied the effect of ML216 on DNA damaged cells. To this end, we performed a growth inhibition assay with cells treated with MMS. In the presence of external DNA damage, the IC<sub>50</sub> value of ML216 was reduced drastically to the nanomolar range during the trophozoite and schizont stages. However, such decrement in IC<sub>50</sub> value was not observed with ringstage parasites. This data suggests the growth inhibitory as well as the DNA repair inhibitory effect of ML216.

In the final part, we investigated whether a RecQ helicase inhibitor can be used as a partner drug in combination therapies. Previous reports have shown that artemisinin and chloroquine create double-strand breaks during their course of action [36, 37]. Here, we combined DNA repair inhibitor (ML216) with DSB inducers (artemisinin and chloroquine) and checked their mode of interaction. To this end, we performed a fixed ratio method with drugs ML216 and DHA (dihydroartemisinin) in 3D7, Dd2, and PfK13R539T strains. We found that ML216 interacts synergistically with artemisinin in both 3D7 and drug-resistant strains. Similar synergistic relation was observed between ML216 and chloroquine in 3D7 and chloroquine resistant Dd2

strain. Atovaquone was used as a negative control for drug interaction studies because of its non-interference with DNA metabolic pathways during its course of action. We did not observe any such synergistic relation between ML216 and atovaquone. Also, we have performed a potentiation assay where we found that the anti-malarial activity of ML216 was potentiated in the presence of IC<sub>50</sub> concentrations of DHA/CQ and vice versa. This data suggests that the RecQ helicase inhibitor can be a potent partner drug for combination therapies.

Altogether our data suggest that the DNA repair activity of *PfBLM* is conserved in *Plasmodium*. The RecQ helicase inhibitor ML216 can inhibit *in vitro* and *in vivo* growth of *Plasmodium*. The growth inhibitory effect of ML216 intensified in DNA damaged cells. Finally, ML216 exhibited a synergistic relation with well-known anti-malarial drugs, artemisinin, and chloroquine, encouraging its use in combination therapies.

## **References:**

- 1. *Guidelines for the Treatment of Malaria*. 2015: World Health Organization.
- 2. Nsanzabana, C., Resistance to Artemisinin Combination Therapies (ACTs): Do Not Forget the Partner Drug! Trop Med Infect Dis, 2019. **4**(1).
- 3. Mehta, A. and J.E. Haber, *Sources of DNA double-strand breaks and models of recombinational DNA repair.* Cold Spring Harb Perspect Biol, 2014. **6**(9): p. a016428.
- 4. Scully, R., et al., *DNA double-strand break repair-pathway choice in somatic mammalian cells.* Nature Reviews Molecular Cell Biology, 2019. **20**(11): p. 698-714.
- 5. Pannunzio, N.R., G. Watanabe, and M.R. Lieber, *Nonhomologous DNA end-joining for repair of DNA double-strand breaks.* J Biol Chem, 2018. **293**(27): p. 10512-10523.
- 6. Lisby, M., et al., *Choreography of the DNA damage response: spatiotemporal relationships among checkpoint and repair proteins*. Cell, 2004. **118**(6): p. 699-713.
- 7. Sartori, A.A., et al., *Human CtIP promotes DNA end resection.* Nature, 2007. **450**(7169): p. 509-14.
- 8. Nicolette, M.L., et al., *Mre11-Rad50-Xrs2 and Sae2 promote 5' strand resection of DNA double-strand breaks*. Nat Struct Mol Biol, 2010. **17**(12): p. 1478-85.
- 9. Nimonkar, A.V., et al., *BLM-DNA2-RPA-MRN* and *EXO1-BLM-RPA-MRN* constitute two *DNA* end resection machineries for human *DNA* break repair. Genes Dev, 2011. **25**(4): p. 350-62.
- 10. Raynard, S., W. Bussen, and P. Sung, *A double Holliday junction dissolvasome comprising BLM, topoisomerase Illalpha, and BLAP75.* J Biol Chem, 2006. **281**(20): p. 13861-4.
- 11. Ip, S.C., et al., *Identification of Holliday junction resolvases from humans and yeast.* Nature, 2008. **456**(7220): p. 357-61.
- 12. Wyatt, H.D. and S.C. West, *Holliday junction resolvases*. Cold Spring Harb Perspect Biol, 2014. **6**(9): p. a023192.
- 13. Gardner, M.J., et al., *Genome sequence of the human malaria parasite Plasmodium falciparum.* Nature, 2002. **419**(6906): p. 498-511.
- 14. Kirkman, L.A., E.A. Lawrence, and K.W. Deitsch, *Malaria parasites utilize both homologous recombination and alternative end joining pathways to maintain genome integrity.* Nucleic Acids Res, 2014. **42**(1): p. 370-9.
- 15. Roy, N., et al., *Dominant negative mutant of Plasmodium Rad51 causes reduced parasite* burden in host by abrogating DNA double-strand break repair. Mol Microbiol, 2014. **94**(2): p. 353-66.
- 16. Bhattacharyya, M.K. and N. Kumar, *Identification and molecular characterisation of DNA damaging agent induced expression of Plasmodium falciparum recombination protein PfRad51*. Int J Parasitol, 2003. **33**(12): p. 1385-92.
- 17. Bhattacharyya, M.K., et al., *Characterization of kinetics of DNA strand-exchange and ATP hydrolysis activities of recombinant PfRad51, a Plasmodium falciparum recombinase*. Mol Biochem Parasitol, 2005. **139**(1): p. 33-9.
- 18. Badugu, S.B., et al., *Identification of Plasmodium falciparum DNA Repair Protein Mre11 with an Evolutionarily Conserved Nuclease Function*. PLoS One, 2015. **10**(5): p. e0125358.

- 19. Vydyam, P., et al., *A small-molecule inhibitor of the DNA recombinase Rad51 from Plasmodium falciparum synergizes with the antimalarial drugs artemisinin and chloroquine.* J Biol Chem, 2019. **294**(20): p. 8171-8183.
- 20. Croteau, D.L., et al., *Human RecQ helicases in DNA repair, recombination, and replication.*Annu Rev Biochem, 2014. **83**: p. 519-52.
- 21. Nimonkar, A.V., et al., *Human exonuclease 1 and BLM helicase interact to resect DNA and initiate DNA repair*. Proc Natl Acad Sci U S A, 2008. **105**(44): p. 16906-11.
- 22. Cannavo, E., P. Cejka, and S.C. Kowalczykowski, *Relationship of DNA degradation by Saccharomyces cerevisiae exonuclease 1 and its stimulation by RPA and Mre11-Rad50-Xrs2 to DNA end resection.* Proc Natl Acad Sci U S A, 2013. **110**(18): p. E1661-8.
- 23. Chen, H., M. Lisby, and L.S. Symington, *RPA coordinates DNA end resection and prevents formation of DNA hairpins*. Mol Cell, 2013. **50**(4): p. 589-600.
- 24. Bugreev, D.V., et al., *Novel pro- and anti-recombination activities of the Bloom's syndrome helicase*. Genes Dev, 2007. **21**(23): p. 3085-94.
- 25. Ouyang, K.J., et al., *SUMO modification regulates BLM and RAD51 interaction at damaged replication forks.* PLoS Biol, 2009. **7**(12): p. e1000252.
- 26. Bugreev, D.V., O.M. Mazina, and A.V. Mazin, *Bloom syndrome helicase stimulates RAD51 DNA strand exchange activity through a novel mechanism.* J Biol Chem, 2009. **284**(39): p. 26349-59.
- 27. Constantinou, A., et al., *Werner's syndrome protein (WRN) migrates Holliday junctions and co-localizes with RPA upon replication arrest.* EMBO Rep, 2000. **1**(1): p. 80-4.
- 28. LeRoy, G., et al., *Identification of RecQL1 as a Holliday junction processing enzyme in human cell lines.* Nucleic Acids Res, 2005. **33**(19): p. 6251-7.
- 29. Rahman, F., et al., *Plasmodium falciparum Werner homologue is a nuclear protein and its biochemical activities reside in the N-terminal region.* Protoplasma, 2016. **253**(1): p. 45-60.
- 30. Rahman, F., M. Tarique, and R. Tuteja, *Plasmodium falciparum Bloom homologue, a nucleocytoplasmic protein, translocates in 3' to 5' direction and is essential for parasite growth.* Biochim Biophys Acta, 2016. **1864**(5): p. 594-608.
- 31. Claessens, A., et al., *RecQ helicases in the malaria parasite Plasmodium falciparum affect genome stability, gene expression patterns and DNA replication dynamics.* PLoS Genet, 2018. **14**(7): p. e1007490.
- 32. Wu, L., et al., *Potential role for the BLM helicase in recombinational repair via a conserved interaction with RAD51*. J Biol Chem, 2001. **276**(22): p. 19375-81.
- 33. Tripathi, V., et al., MRN complex-dependent recruitment of ubiquitylated BLM helicase to DSBs negatively regulates DNA repair pathways. Nat Commun, 2018. **9**(1): p. 1016.
- 34. Nguyen, G.H., et al., *A small molecule inhibitor of the BLM helicase modulates chromosome stability in human cells*. Chem Biol, 2013. **20**(1): p. 55-62.
- 35. Aggarwal, M., et al., Inhibition of helicase activity by a small molecule impairs Werner syndrome helicase (WRN) function in the cellular response to DNA damage or replication stress. Proc Natl Acad Sci U S A, 2011. **108**(4): p. 1525-30.
- 36. Gopalakrishnan, A.M. and N. Kumar, *Antimalarial action of artesunate involves DNA damage mediated by reactive oxygen species.* Antimicrob Agents Chemother, 2015. **59**(1): p. 317-25.
- 37. Sullivan, D.J., Jr., et al., *A common mechanism for blockade of heme polymerization by antimalarial quinolines*. J Biol Chem, 1998. **273**(47): p. 31103-7.

# **PUBLICATIONS**





# Elucidation of DNA Repair Function of PfBlm and Potentiation of Artemisinin Action by a Small-Molecule Inhibitor of RecQ Helicase

Niranjan Suthram, a Siladitya Padhi, b Payal Jha, a Sunanda Bhattacharyya, c Gopalakrishnan Bulusu, b Arijit Roy, b Mrinal Kanti Bhattacharyya

<sup>a</sup>Department of Biochemistry, School of Life Sciences, University of Hyderabad, Hyderabad, India

ABSTRACT Artemisinin (ART)-based combination therapies are recommended as first- and second-line treatments for Plasmodium falciparum malaria. Here, we investigated the impact of the RecQ inhibitor ML216 on the repair of ART-mediated damage in the genome of P. falciparum. PfBLM and PfWRN were identified as members of the RecQ helicase family in P. falciparum. However, the role of these RecQ helicases in DNA double-strand break (DSB) repair in this parasite has not been explored. Here, we provide several lines of evidence to establish the involvement of PfBlm in DSB repair in P. falciparum. First, we demonstrate that PfBlm interacts with two well-characterized DSB repair proteins of this parasite, namely, PfRad51 and PfalMre11. Second, we found that PfBLM expression was upregulated in response to DNA-damaging agents. Third, through yeast complementation studies, we demonstrated that *PfBLM* could complement the DNA damage sensitivity of a  $\Delta sqs1$  mutant of Saccharomyces cerevisiae, in contrast to the helicase-dead mutant PfblmK83R. Finally, we observe that the overexpression of PfBLM induces resistance to DNA-damaging agents and offers a survival advantage to the parasites. Most importantly, we found that the RecQ inhibitor ML216 inhibits the repair of DSBs and thereby renders parasites more sensitive to ART. Such synergism between ART and ML216 actions was observed for both drug-sensitive and multidrug-resistant strains of *P. falciparum*. Taken together, these findings establish the implications of PfBlm in the Plasmodium DSB repair pathway and provide insights into the antiparasitic activity of the ART-ML216 combination.

**IMPORTANCE** Malaria continues to be a serious threat to humankind not only because of the morbidity and mortality associated with the disease but also due to the huge economic burden that it imparts. Resistance to all available drugs and the unavailability of an effective vaccine cry for an urgent discovery of newer drug targets. Here, we uncovered a role of the PfBlm helicase in Plasmodium DNA doublestrand break repair and established that the parasitic DNA repair mechanism can be targeted to curb malaria. The small-molecule inhibitor of PfBlm tested in this study acts synergistically with two first-line malaria drugs, artemisinin (ART) and chloroquine, in both drug-sensitive and multidrug-resistant strains of P. falciparum, thus qualifying this chemical as a potential partner in ART-based combination therapy. Additionally, the identification of this new specific inhibitor of the Plasmodium homologous recombination (HR) mechanism will now allow us to investigate the role of HR in *Plasmodium* biology.

KEYWORDS PfBlm, PfWrn, DNA repair, homologous recombination, Plasmodium falciparum, yeast complementation, molecular docking

Citation Suthram N, Padhi S, Jha P, Bhattacharyya S, Bulusu G, Roy A, Bhattacharyya MK. 2020. Elucidation of DNA repair function of PfBlm and potentiation of artemisinin action by a small-molecule inhibitor of RecQ helicase. mSphere 5:e00956-20. https://doi.org/10.1128/mSphere.00956-20.

Editor Ron Dzikowski, The Hebrew University of Jerusalem

Copyright © 2020 Suthram et al. This is an open-access article distributed under the terms of the Creative Commons Attribution 4.0 International license.

Address correspondence to Mrinal Kanti Bhattacharyya, mkbsl@uohyd.ernet.in.

Received 21 September 2020 Accepted 28 October 2020 Published 25 November 2020



<sup>&</sup>lt;sup>b</sup>TCS Innovation Labs-Hyderabad (Life Sciences Division), Tata Consultancy Services Limited, Hyderabad, India

Department of Biotechnology and Bioinformatics, School of Life Sciences, University of Hyderabad, Hyderabad, India



alaria is a deadly disease that accounts for major deaths across the world. Plasmodium falciparum is the most virulent among the five species of Plasmodium known to cause malarial pathology. Moreover, complete eradication of malaria has been difficult because of the continuous emergence of resistance to available drugs (1) and unsuccessful vaccine development efforts. Consequently, there is a pressing need to explore the pathways implicated in pathogenicity to ensure better understanding and targeted drug discovery.

The DNA double-strand break (DSB) repair pathway is one such reliable pathway in unicellular organisms since a single unrepaired DSB leads to the death of the organism (2). P. falciparum, being a unicellular organism, becomes vulnerable if not repaired. Previous reports have shown homologous recombination (HR) to be one of the primary pathways for DSB repair in Plasmodium (3). Although there is a possibility of an alternative end-joining pathway, it is a rare event (4). Key proteins of the HR pathway, such as PfRad51 and PfalMre1, have been identified and characterized (5, 6). Since these genes share high homology with their human counterparts, it is reasonable that we explore less-conserved genes.

RecQ family DNA helicases are considered the gatekeepers of the genome owing to their predominant roles in various DNA metabolic processes (7). In humans, five RecQ helicases have been characterized; however, in yeast (SGS1) and bacteria (RecQ), only one RecQ helicase has been identified. Bloom's syndrome helicase (BLM) is one such RecQ helicase among five RecQ helicases in humans, known for its pro- and antirecombinogenic activities to maintain genome stability (8). BLM helicase exhibits its prorecombinogenic activity at various steps of the HR pathway. The first step in HR involves the resectioning of the 5' terminus of the DSB to produce 3'-single-stranded DNA (ssDNA) overhangs, mediated by either DNA2 or EXO1. The helicase activity of BLM is essential for the DNA2-mediated resectioning pathway (9), where it serves a helicaseindependent stimulatory function in the Exo1-mediated pathway (10). Among all other RecQ helicases, the ability to stimulate resection is specific for BLM (9, 10). Previous research has shown that the SUMOylation of BLM facilitates the enrichment of the key HR protein Rad51 at the site of DNA damage (11). BLM stimulates the strand exchange activity of Rad51 when it is in the active ATP-bound form instead of the inactive ADPbound form (12). BLM, along with TopollI and Rmil, forms the dissolvasome complex to resolve double Holliday junctions, which results in the formation of noncrossover products, and this process is critical in somatic cells (13).

In Plasmodium, only two RecQ helicases, PfBLM and PfWRN, have been identified (14-16). Apart from the limited sequence similarity of their helicase domains, PfBlm and PfWrn are very divergent from their human orthologs (22.5% and 23.7% sequence similarity, respectively). Nonetheless, it was shown with purified PfBlm and PfWrn proteins that their helicase activities are conserved. Both proteins are found to be expressed during all intraerythrocytic stages of Plasmodium (15, 16). Recent studies have shown that PfBIm is essential for maintaining the clonal expression of var genes, and the rate of recombination at the *var* locus was unchanged in a  $\Delta Pfblm$  strain (17, 18). Owing to the fact that *Plasmodium* solely relies on HR to repair DSBs, it is of the utmost importance to explore the functional roles of these RecQ proteins of the parasite during DSB repair. In this study, we implicate PfBIm in Plasmodium DSB repair. We demonstrate that a RecQ helicase inhibitor abrogates the repair of DNA damage. Finally, we provide compelling evidence that the synergistic interaction between the RecQ inhibitor and the DNA-damaging agent artemisinin (ART) holds true in both drug-sensitive and multidrug-resistant parasites.

### **RESULTS**

PfBLM expression is maximal at the mitotically active schizont stage. To check the expression of PfBLM during blood stages of P. falciparum, we performed real-time reverse transcription-PCR (RT-PCR) and Western blotting. Previous reports have shown that HsBLM and ScSGS1 expression levels are at their peak during the S phase of the



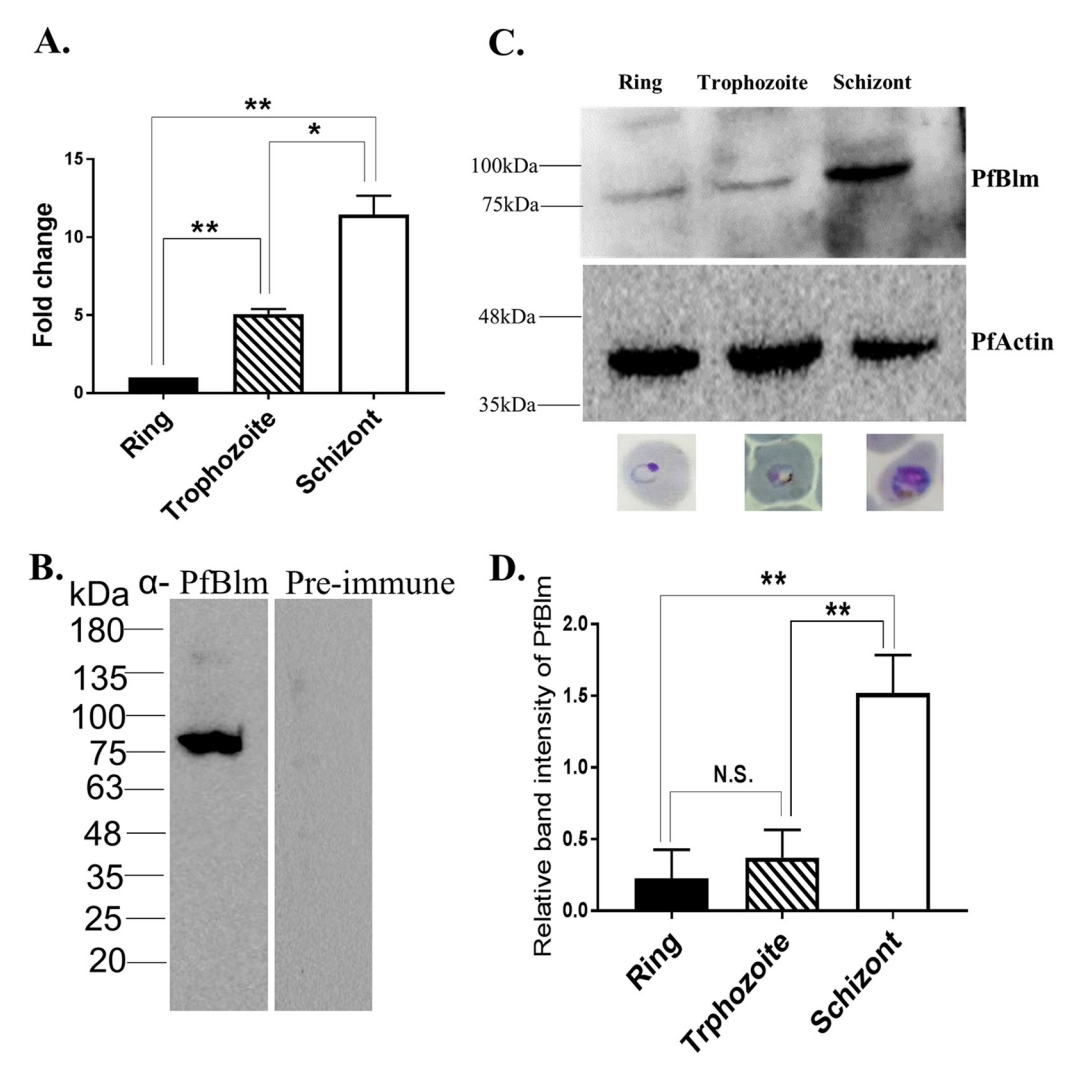


FIG 1 PfBLM expression is maximal at the mitotically active schizont stage. (A) Relative abundances of PfBLM transcripts during the ring (12 h postinvasion [hpi]), trophozoite (24 hpi), and schizont (38 hpi) stages quantified by real-time RT-PCR analysis. Data were normalized against PfARP. The mean values ± standard deviations (SD) from three independent experiments are plotted. (B) Specificity of anti-PfBIm antibody versus the preimmune sera. (C) Stage-specific expression of the PfBIm protein. PfActin was used as the loading control. The position of molecular markers is indicated on the left. Representative microscopic images of different blood stages are shown below the blot. (D) Quantification of Western blot data from three independent experiments. Data were normalized against loading control PfActin. Each bar represents mean density  $\pm$  SD (n=3). The P value was calculated using the twotailed t test (\* means a P value of <0.05, \*\* means a P value of <0.01, and N.S. means not significant).

cell cycle (19, 20). Since intraerythrocytic developmental stages of Plasmodium follow the pattern of the regular cell cycle, we sought to investigate its expression level during different blood stages. To this end, we isolated RNA and protein from synchronous parasites at the ring, trophozoite, and schizont stages to perform real-time RT-PCR and Western blotting. At the RNA level, the expression of PfBLM was found to be high during the schizont and trophozoite stages compared to the ring stage. PfARP (asparagine-rich protein) was used as a loading control. By real-time RT-PCR, we observed 5and 11-fold upregulations of PfBLM in the trophozoite and schizont stages compared to the ring stage (Fig. 1A). These findings are in good agreement with several highthroughput transcriptome data sets available in the PlasmoDB database (21, 22). For Western blot experiments, we used an antipeptide antibody that recognized a specific band of 80 kDa corresponding to PfBIm (Fig. 1B). The schizont-stage-specific abundant expression of the PfBIm protein corroborated well with the mRNA expression data (Fig. 1C and D). PfActin was used as a loading control for the Western blot experiments.



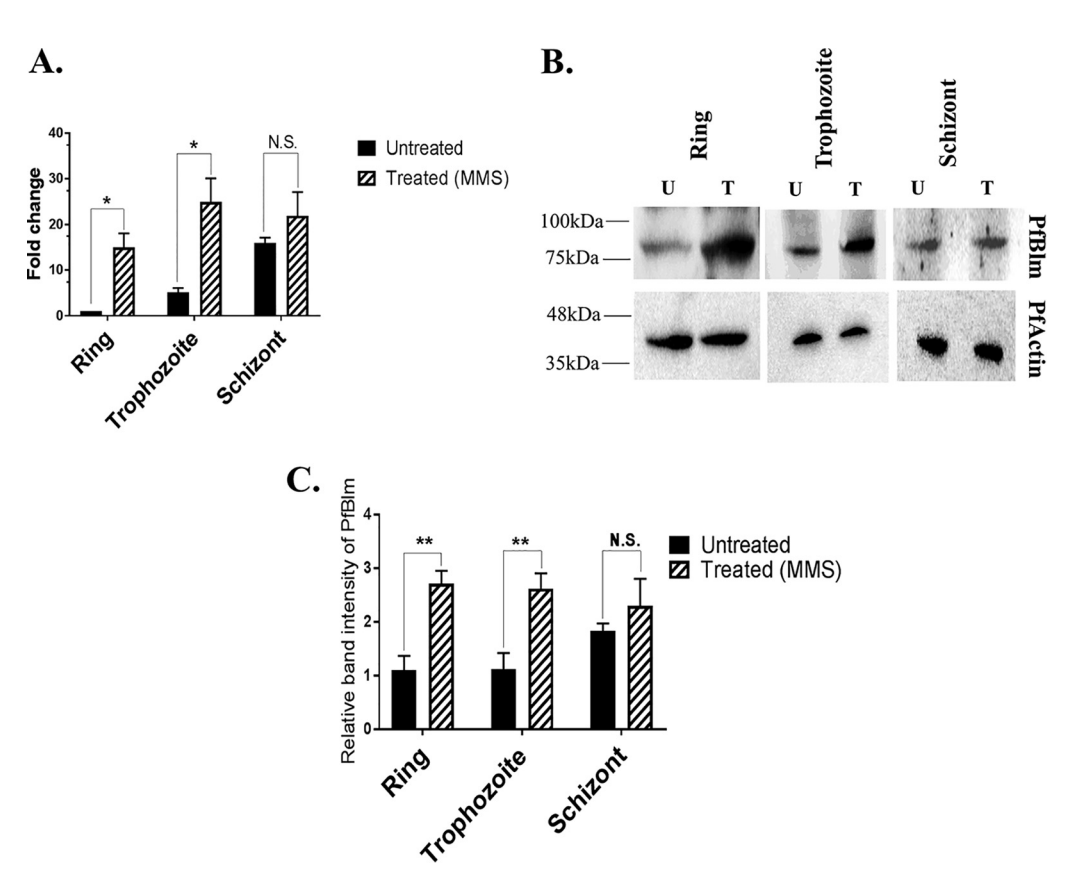


FIG 2 DNA damage-induced upregulation of PfBLM during intraerythrocytic developmental stages. (A) Synchronized P. falciparum in vitro cultures at the ring, trophozoite, and schizont stages were either untreated (U) or treated (T) with 0.05% MMS for 6 h. Real-time RT-PCR on extracted RNA revealed the upregulation of PfBLM mRNA during the ring and trophozoite stages upon DNA damage, but its level was not changed during the schizont stage. PfARP transcripts were used as a loading control. Each bar represents the mean value  $\pm$  SD (n=3). (B) Western blots show that MMS induced the expression of the PfBIm protein at the ring and trophozoite stages, but in the case of the schizont stage, it remained unchanged. PfActin acted as a loading control. The position of molecular markers is indicated on the left. (C) Quantification of Western blot data from three independent experiments. Data were normalized against PfActin. Each bar represents the mean band intensity  $\pm$  SD (n=3). The P value was calculated using the two-tailed t test (\* means a P value of <0.05, \*\* means a P value of <0.01, and N.S. means not significant).

As the schizont stage is associated with replication and HR activities, our results suggest the likely involvement of PfBIm in these two conserved processes.

DNA damage-induced upregulation of PfBLM during intraerythrocytic developmental stages. We investigated whether PfBLM is overexpressed in response to DNA damage. Previous reports have shown that *Plasmodium* proteins involved in DSB repair are overproduced upon DNA damage (5, 6). Hence, we sought to investigate the stage-specific induction of PfBLM under DNA-damaging conditions. To this end, we took tightly synchronous parasites of the ring, trophozoite, and schizont stages and treated them with the known DNA-damaging agent methyl methanesulfonate (MMS) for 6 h. Following this, total RNAs/proteins were isolated from both untreated and treated cultures. We performed real-time RT-PCR to check the expression of PfBLM in both treated and untreated cultures. PfARP was used as a loading control. We observed a 14-fold upregulation of PfBLM under DNA-damaging conditions at the ring stage and a 5-fold upregulation at the trophozoite stage, but its level remained unchanged during the schizont stage (Fig. 2A). We examined the induction of the PfBlm protein by Western blotting in the three blood stages of the parasite. The expression of PfBIm was increased almost 3-fold under DNA-damaging conditions in the ring and the trophozoite stages, whereas no significant induction was observed at the schizont stage (Fig. 2B and C), which correlates with the transcript level. It could be possible that the steady-state level of PfBLM mRNA or protein is already so high at the schizont stage that any further induction was



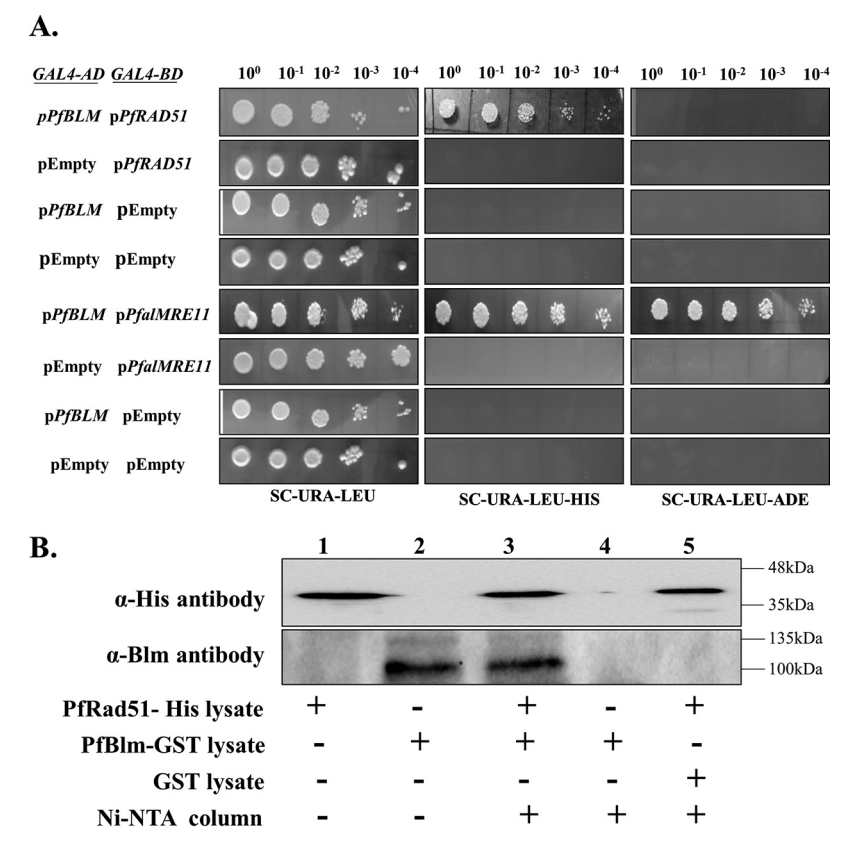


FIG 3 PfBIm interacts with the key DNA repair proteins PfRad51 and PfalMre11. (A) Full-length PfBLM was fused to the GAL4 activation domain (GAL4-AD) of pGADC1. Similarly, full-length PfalMRE11 and PfRAD51 were fused to the GAL4 binding domain (GAL4-BD) of pGBDUC1. The interaction was tested in yeast strain PJ69-4A, which bears ADE2 and HIS as reporter genes. Starting with the same OD (1 OD/ml), 10-fold serially diluted cells were spotted onto plates lacking leucine and uracil to check for the presence of bait and prey plasmids. Simultaneously, cells were spotted onto plates lacking histidine and adenine to check the interaction. (B) Western blotting shows the interaction between PfRad51 and PfBIm in the Ni-NTA pulldown (lane 3). The cell lysate of histidine-tagged PfRad51 mixed with the empty GST cell lysate (lane 5) did not show a signal with anti-Blm antibody. The description of each lane is shown at the bottom. The position of molecular markers is indicated on the right.

not quantifiable. Nonetheless, the upregulation of PfBLM in response to DNA damage suggests its likely involvement in DSB repair.

PfBlm interacts with the key DNA repair proteins PfRad51 and PfalMre11. We investigated whether PfBIm physically interacts with other bona fide DSB repair proteins of P. falciparum. In order to function in the DSB repair pathway, PfBlm must interact with proteins of the HR pathway. Previous studies have shown that HsBLM interacts with both HsRad51 and HsMre11 (23, 24). We investigated whether PfBIm interacts with PfRad51 and PfalMre11, which were previously implicated as DNA repair proteins in Plasmodium (5, 6). To this end, we performed a yeast two-hybrid analysis. PfBLM was cloned into the prey vector harboring the GAL4 activation domain and the LEU2 selectable marker. PfRAD51 or PfalMRE11 was cloned into the bait vector having the GAL4 DNA binding domain and URA3 as a selectable marker. Doubly transformed yeast cells were scored for HIS3 or ADE2 reporter gene expression. We observed an interaction between PfBIm and PfRad51 as growth was seen on SC-Leu-Ura-His (synthetic complete medium minus leucine, minus uracil, minus histidine) triple-dropout plates. The interaction with PfalMre11 was found to be much stronger as growth was observed not only on SC-Leu-Ura-His plates but also on SC-Ura-Leu-Ade (synthetic complete medium minus leucine, minus uracil, minus adenine) triple-dropout plates (Fig. 3A). To further confirm the interaction between PfBlm and PfRad51, a copurification assay was



performed. To this end, we expressed recombinant PfRad51 with a histidine tag and PfBlm with a glutathione S-transferase (GST) tag in Escherichia coli. Both cell lysates were mixed, passed through a Ni-nitrilotriacetic acid (NTA) column, and eluted. We detected both PfBlm and PfRad51 signals in Western blots of the eluates, suggesting their interaction, whereas no signal was detected when only the PfBlm-GST lysate was passed through a Ni-NTA column or the empty GST tag lysate was mixed with histidine-tagged PfRad51 and passed through a Ni-NTA column (Fig. 3B). As full-length PfalMRE11 could not be expressed in bacterial systems (6), such copurification experiments could not be performed for these pairs of proteins. These observations that PfBlm associates with two well-established DSB repair proteins of P. falciparum strongly suggest a role of PfBlm in the DSB repair pathway in this parasite.

PfBLM functionally complements the MMS sensitivity of an  $\Delta sgs1$  mutant of S. cerevisiae. We investigated whether PfBLM can functionally rescue the DNA repair defect of the RecQ mutant of budding yeast. Saccharomyces cerevisiae possesses a single RecQ gene, namely, SGS1. The DSB repair properties of Sgs1 are well established. Previous studies have shown that an  $\Delta sgs1$  mutant strain is sensitive to the genotoxic agent MMS (25), and full-length HsBLM was able to complement the MMS sensitivity (26). Complementation was dependent on the helicase activity of the HsBLM protein since the helicase-dead mutant HsblmK695R was not able to perform the DNA repair function (26). In our study, we investigated whether full-length PfBLM and a helicasedead mutant of PfBLM (PfblmK83R) can complement the DNA damage sensitivity of the Δsqs1 mutant strain. Along with PfBLM, another identified RecQ helicase of Plasmodium, PfWRN, was also tested. To this end, we knocked out the SGS1 gene from S. cerevisiae to generate the SNY1 strain. PfBLM, PfblmK83R, and PfWRN cloned into the pBFM vector were transformed into SNY1 to generate SNY3, SNY4, and SNY5. We also transformed ScSGS1 cloned into the pBFM vector and the empty pBFM vector to generate SNY2 and SNY6, which acted as the positive and negative controls, respectively. Complementation studies were done using a return-to-growth assay and by growing strains on plates containing MMS. In both assays, we observed that PfBLM could partially complement the DNA damage sensitivity of the  $\Delta sas1$  mutant, whereas PfblmK83R or PfWRN was inefficient to overcome the sensitivity (Fig. 4A and B). In the return-to-growth assay, the helicase-dead mutant behaved similarly to the negative control, indicating the importance of the helicase activity of the PfBIm protein in performing the DNA repair function. The expression levels of PfBLM, PfblmK83R, and PfWRN were determined by a semiquantitative RT-PCR method, and the expression levels were found to be comparable to that of ScSGS1 (Fig. 4C). We used the pBFM plasmid as it would enable us to detect the protein expression of the cloned genes using anti-Myc antibody. However, we failed to detect the expression of any Myc-tagged proteins. These results strongly suggest that the DSB repair function of RecQ helicase is also conserved in PfBlm.

Overexpression of PfBLM provides a survival advantage to the parasites under DNA-damaging conditions. In order to amplify the function of PfBlm in HR-mediated DSB repair (if any), we performed overexpression studies. The idea behind such experiments was that if PfBIm is involved in the repair of DSBs, the overexpression of PfBLM would confer a better repair efficiency than the normal level of the protein. To this end, P. falciparum 3D7 cells were transfected separately with both wild-type PfBLM and the PfblmK83R mutant cloned into the pARL overexpression vector (27). The transfected parasites at all three intraerythrocytic stages were treated with 0.002% and 0.005% MMS for 2 h and returned to growth for 48 h, after washing off MMS. Simultaneously, the same experiment was performed with a 3D7 culture, which acted as a control. In such experiments, only parasites capable of repairing the DSBs would survive. The survival of the PfBLM-overexpressing strain upon DNA damage was found to be significantly better than that of the wild-type 3D7 strain. Interestingly, such survival advantages were observed only for the parasites where DNA damage was induced at the trophozoite or schizont stage but not at the ring stage (Fig. 5A to C). No such survival advantage under DNA-damaging conditions was observed for parasites overexpressing the helicase-dead mutant version of the gene PfblmK83R (Fig. 5A to C).



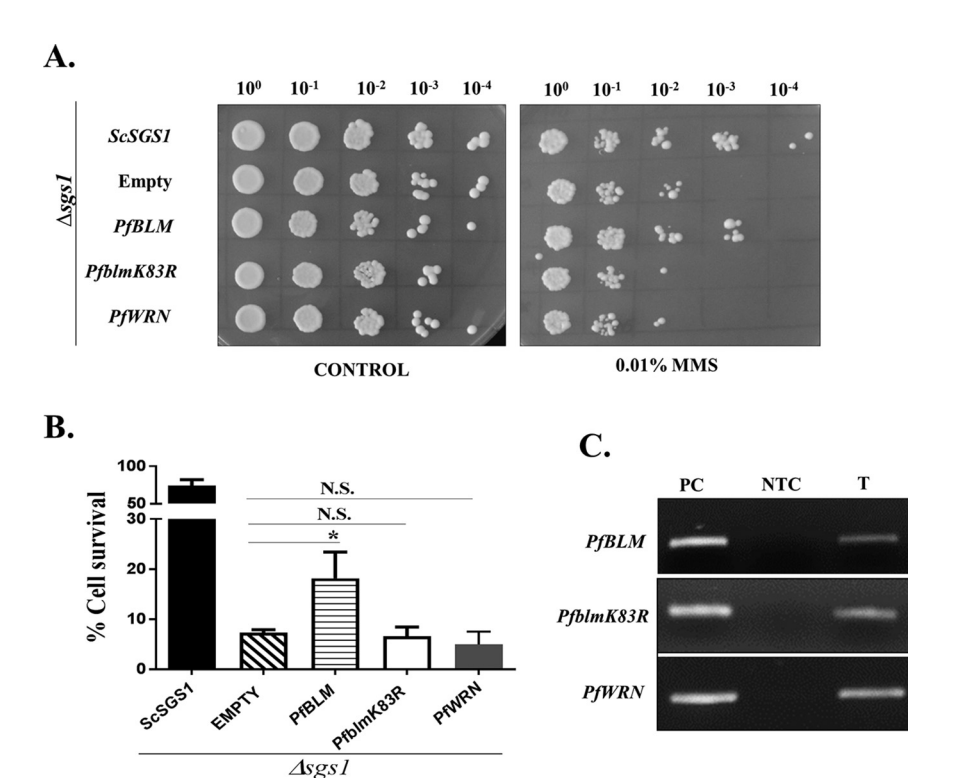


FIG 4 PfBLM functionally complements the MMS sensitivity of the Δsgs1 mutant of S. cerevisiae. (A) Spotting assay on SC-His plates without (control) or with 0.01% MMS. The genotype of each strain is shown on the left. (B) A return-to-growth assay was performed, where all the complementation strains were either untreated or treated with 0.03% MMS for 2 h and allowed to grow on SC-His plates without MMS after washing. The percentage of cell survival for each strain was obtained by taking the ratio of the numbers of colonies formed between treated and untreated cultures. Each bar represents the mean number  $\pm$  SD after normalization with untreated controls from three independent experiments (n=3). The P value was calculated using the two-tailed t test (\* means a P value of <0.05, and N.S. means not significant). (C) The expression of PfBLM, PfblmK83R, and PfWRN was confirmed by isolating RNA and performing semiquantitative RT-PCR from complementation strains. PC, positive control (Plasmodium genomic DNA used as the template); NTC, nontemplate control; T, test (cDNA from the respective complementation strains used as the template).

The expression of green fluorescent protein (GFP)-tagged PfBIm and PfbImK83R was confirmed by performing Western blotting (Fig. 5D and E). These experiments provide direct evidence for the involvement of PfBIm in the DSB repair pathway of P. falciparum.

In silico analysis of the binding poses and binding affinity of inhibitors against PfBlm. We investigated whether chemical inhibitors of RecQ helicases, namely, ML216 and MIRA-1 (28, 29), could potentially bind to PfBlm. To this end, we have taken an in silico approach. Since the crystal structure of PfBlm is not available, we have modeled the protein based on the crystal structure of Homo sapiens BLM (HsBlm), the details of which are described in Materials and Methods (see also Fig. S1 in the supplemental material). The inhibitor molecules were first docked onto the PfBIm structure. It was seen that ML216 can bind at either the ATP binding site or the DNA binding region, whereas MIRA-1 can bind only in the vicinity of the ATP binding site (Fig. 6A). In order to evaluate the stability of the docking poses, molecular dynamics simulations of the docked complexes were performed. It was seen that ML216 interacts with two residues, Gln111 and Arg407, in the ATP binding site of PfBlm (Fig. 6B), but when it is bound to the DNA binding region of PfBlm, it is seen to bind with two poses at the same binding site: one in which it interacts with Arg404 and the other in which it interacts with Trp191 (Fig. 6C). MIRA-1 interacts with the residues Gly80 and Arg282 in the vicinity of the ATP binding site (Fig. 6D). An estimate of the binding affinity between PfBIm and the inhibitors was made by calculating the free energy of binding



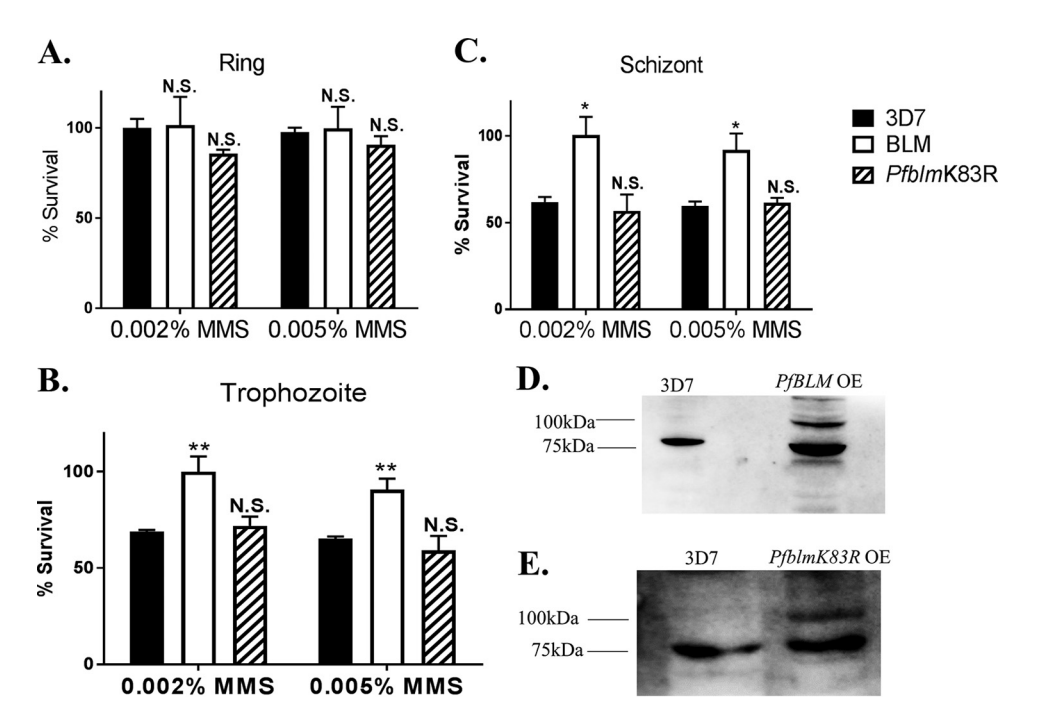


FIG 5 Overexpression of PfBLM provides a survival advantage to the parasites under DNA-damaging conditions. (A to C) Plasmodium falciparum 3D7 cells harboring PfBLM-GFP and PfblmK83R-GFP were either untreated or treated with 0.002% and 0.005% MMS for 2h and subsequently allowed to grow for 48h after washing. The experiment was also performed with 3D7 cultures, which acted as a control. After 48 h, smears were prepared, and infected erythrocytes were counted to obtain parasitemia data. The experiment was performed with three intraerythrocytic stages of parasites. Stages are indicated at the top. Percent survival was plotted by taking the ratio of the percentages of parasitemia between the treated and untreated cultures of the respective strains. Each bar represents the mean survival value  $\pm$  SD (n=3). Significance was calculated with respect to the wildtype strain (3D7). (D) Western blotting shows the expression of the PfBIm protein. The strains are indicated at the top. The expression of the PfBlm (80 kDa) protein in the 3D7 strain and the expression of GFP-tagged PfBlm (107 kDa) protein along with endogenous PfBlm (80 kDa) are shown. OE, overexpression. (E) Expression of the PfBIm (80 kDa) protein in the 3D7 strain (left) and expression of the GFP-tagged PfbImK83R (107 kDa) protein along with endogenous PfBIm (80 kDa) (right). The positions of molecular markers are indicated on the left. The P value was calculated using the two-tailed t test (\* means a P value of <0.05, \*\* means a P value of <0.01, and N.S. means not significant).

(Table S1). The values show that ML216 has a high affinity for PfBlm, compared to MIRA-1. These results predicted that ML216 could be a potent inhibitor of PfBIm, and hence, a chemical inhibition strategy could be employed to elucidate the function of PfBlm during DSB repair in this parasite.

Compared to MIRA-1, ML216 is a potent inhibitor of the intraerythrocytic growth of P. falciparum. To study the effect of RecQ helicase inhibitors (ML216 and MIRA-1) on Plasmodium growth, we performed a growth inhibition assay in the presence of different concentrations of both drugs. RecQ helicases are involved in replication and DSB repair in a variety of organisms. Malaria parasites undergo several rounds of replication during erythrocytic schizogony, and repair of endogenous DNA damage is a common occurrence in the life cycle of *Plasmodium*. We investigated whether any of the above-mentioned RecQ inhibitors actually inhibit the blood-stage development of the parasite. We treated trophozoite cultures with ML216 or MIRA-1 at various concentrations (1 nM to 1,000  $\mu$ M) for 48 h and assessed parasitemia by staining the smears with Giemsa stain. Both ML216 and MIRA-1 were able to inhibit the intraerythrocytic developmental cycle (IDC) of the parasites. However, ML216 was more potent than MIRA-1. The dose-response curve yielded 50% inhibitory concentration (IC<sub>50</sub>) values of  $3.28 \,\mu\text{M}$  and  $67.6 \,\mu\text{M}$  for ML216 and MIRA-1 (Giemsa staining), respectively (Fig. 7A and D). We also employed a fluorescence-based SYBR green I method to estimate survival. This method yielded IC<sub>50</sub> values of 6.31  $\mu$ M for ML216 and 55.2  $\mu$ M for MIRA-1 (Fig. S2A and D). We further tested the effects of ML216 and MIRA-1 on the



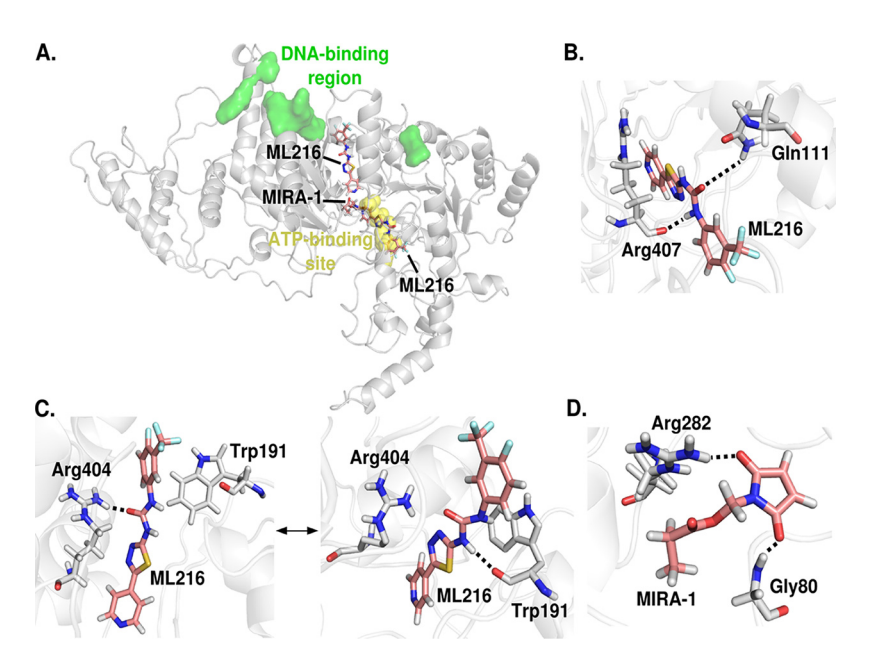


FIG 6 In silico analysis of the binding poses and binding affinities of inhibitors against PfBIm. (A) Two binding poses for ML216 and a single binding pose for MIRA-1. ML216 can bind at either the ATP binding site or the DNA binding region, whereas MIRA-1 binds only in the vicinity of the ATP binding site. (B) ML216 interacts with Gln111 and Arg407 in the ATP binding site. (C) ML216 bound near the DNA binding region is seen to exist in two poses: one in which it interacts with Arg404 and one in which it interacts with Trp191. (D) MIRA-1 interacts with the residues Gly80 and Arg282 near the ATP binding site. Hydrogen bonds between the protein and the inhibitor are shown as dotted lines.

drug-resistant strain Dd2. We observed that the IC<sub>so</sub> values are in similar ranges albeit lower than what was observed for the drug-sensitive 3D7 strain. For ML216, the observed IC<sub>50</sub> value was 1.01  $\mu$ M, and for MIRA-1, the value was 44  $\mu$ M (Giemsa staining) (Fig. 7B and E). The SYBR green I method yielded IC so values of 3.24  $\mu$ M for ML216 and 58  $\mu$ M for MIRA-I (Fig. S2B and E). In addition, we also examined the inhibitory effect of ML216 on the artemisinin-resistant strain PfK13R539T (30). The Giemsa staining method yielded an IC<sub>50</sub> value of 1.26  $\mu$ M (Fig. 7C), and with the SYBR green I method, the IC $_{50}$  value was 2.19  $\mu M$  (Fig. S2C). The IC $_{50}$  values obtained by both the Giemsa staining method and the SYBR green I method are in similar ranges. Thus, ML216 was found to be a more potent inhibitor of the IDC than MIRA-1.

Parasites treated with ML216 become hypersensitive to the DNA-damaging agent MMS. To investigate the effect of ML216 on DNA-damaged cells, we performed a growth inhibition assay with MMS-treated cells. Previous studies have shown that MMS creates numerous double-strand breaks and that such breaks are repaired over the period (31). However, if such breaks are not successfully repaired, cells bearing the unrepaired breaks succumb to death. Thus, the MMS sensitivity assay is a good measure of the DSB repair capability of the cells. We reasoned that inhibition of PfBlm with ML216 would render parasites more sensitive to MMS treatment. To this end, we treated synchronized parasite cells of all stages with various concentrations of ML216  $(1 \text{ nM to } 1,000 \,\mu\text{M})$  in the presence or absence of MMS. The assay was performed in both drug-sensitive (3D7) and drug-resistant (Dd2) strains. MMS treatment drastically lowered the  $IC_{50}$  value of ML216 for both the 3D7 and Dd2 parasite strains (Table 1). The effect was most prominent when DSBs were induced at the trophozoite stage. The drops in the  $IC_{50}$  values at the trophozoite stage were 264-fold and 218-fold for 3D7 and Dd2, respectively. The creation of DSBs at the schizont stage also had a profound effect on the IC<sub>50</sub> value of ML216. There were about 185-fold and 40-fold reductions in the IC<sub>50</sub> values for the 3D7 and Dd2 strains, respectively. The effect on the ring stage was very minimal, with only a 2- to 2.5-fold reduction. Such dramatic drops in the IC<sub>50</sub> values are not due to an additive effect of MMS toxicity as the survival rates of the



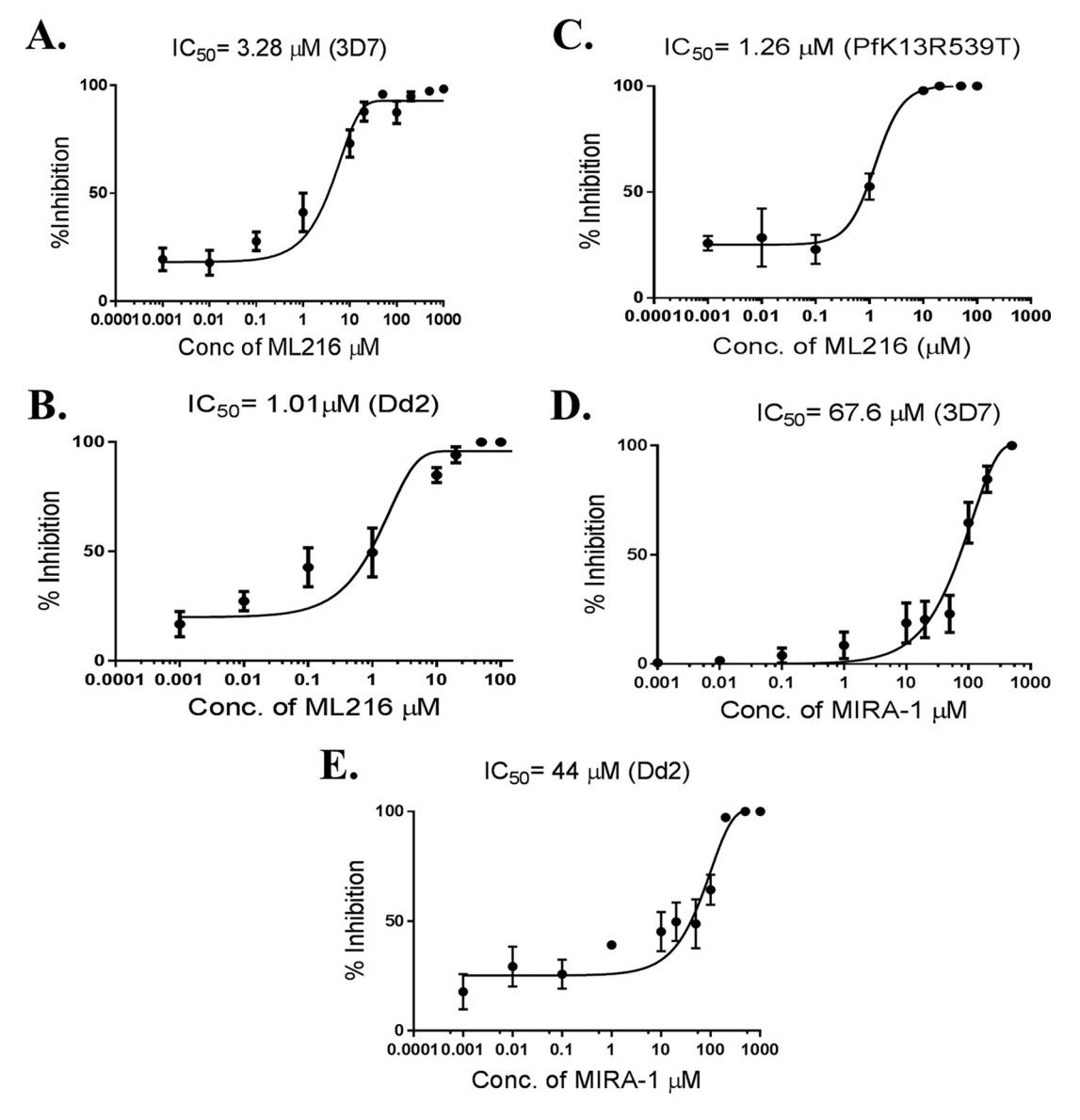


FIG 7 Compared to MIRA-1, ML216 is a potent inhibitor of the intraerythrocytic growth of P. falciparum. We employed a Giemsa staining method to evaluate percent parasitemia and deduced percent inhibition from the obtained parasitemia values. (A) Synchronous trophozoite-stage parasites (3D7) were grown for 48 h in the presence of various concentrations of ML216. Parasite growth inhibition at various concentrations of the drug was plotted to obtain the IC<sub>50</sub> values. (B) Growth inhibition with ML216 in Dd2 parasites was plotted to obtain  $IC_{50}$  values. (C) Growth inhibition with ML216 in PfK13R539T parasites was plotted to obtain IC<sub>so</sub> values. (D) The effect of MIRA-1 on 3D7 parasites was tested according to the same protocol as the one for ML216 treatment. Percent inhibition was plotted against various concentrations of the drug to obtain the IC<sub>50</sub> values. (E) Growth inhibition with MIRA-1 in Dd2 parasites was plotted to obtain the IC<sub>50</sub> values. Each assay was repeated three times for reproducibility (n = 3).

ring-, trophozoite-, and schizont-stage parasites against MMS are 97%, 65%, and 60%, respectively (Fig. 5A to C). These results imply that in the presence of external DNAdamaging agents, ML216 could be an effective inhibitor of parasite growth as it works at the nanomolar range.

ML216 blocks the repair of UV-induced DNA damage in the nuclear genome of the parasite. Next, we investigated the effect of ML216 on the repair of DNA breaks in the parasite genome. To this end, we employed a PCR-based technique to estimate the amount of UV-induced damage at a particular region of the parasite genome as defined by the position of PCR primers (32). This method relies on the fact that a longer stretch of genomic DNA is more likely to experience UV-induced damage, and for a very short stretch of the genome, such a probability is negligible. Thus, a decrease in



TABLE 1 IC<sub>50</sub> values of ML216 with or without MMS in treated cultures at different IDC stages in the 3D7 and Dd2 strains

Stage and strain	Treatment	IC <sub>50</sub> (μΜ)
Ring		
3D7	ML216 (alone)	3.49
	ML216 + MMS	1.42
Dd2	ML216 (alone)	1.85
	ML216 + MMS	0.96
Trophozoite		
3D7	ML216 (alone)	2.8
	ML216 + MMS	0.0106
Dd2	ML216 (alone)	0.871
	ML216 + MMS	0.004
Schizont		
3D7	ML216 (alone)	3.21
	ML216 + MMS	0.0174
Dd2	ML216 (alone)	1.49
	ML216 + MMS	0.0374

the long-range PCR product would indicate the accumulation of DNA damage in the template DNA. As the amount of the short-range PCR product is expected to remain unchanged before and after DNA damage, this can be used to normalize the data. We treated the cultures with a sublethal concentration of ML216, monitored the repair kinetic of UV-induced DNA damage, and compared it with the repair kinetic of the untreated parasites. As a positive control, we used B02, a known small-molecule inhibitor of the Plasmodium DSB repair pathway. B02 is a potent inhibitor of PfRad51, and hence, it blocks the repair of DSBs in the Plasmodium genome (33). As a negative control, we included atovaquone (ATQ) in our study, as this chemical is not related to DSB damage or repair. We observed that in the untreated parasites, DNA damage is repaired by 24 h, but in the parasites treated with ML216, the damage remained unrepaired even after 48 h (Fig. 8). Similar kinetics were observed with parasites treated with B02. Atovaquone treatment did not have any inhibitory effect on the repair of UVinduced DNA damage. Thus, these results strongly suggest that the Blm inhibitor ML216 is also a potent inhibitor of *Plasmodium* DSB repair.

ML216 interacts synergistically with ART and CQ. We studied the interaction of ML216 with the known antimalarial drug ART. Since ART creates DSBs (34), and in the presence of ML216, the repair of such breaks is inhibited, we hypothesized that ML216

#### Repair kinetics of UV-damaged genome

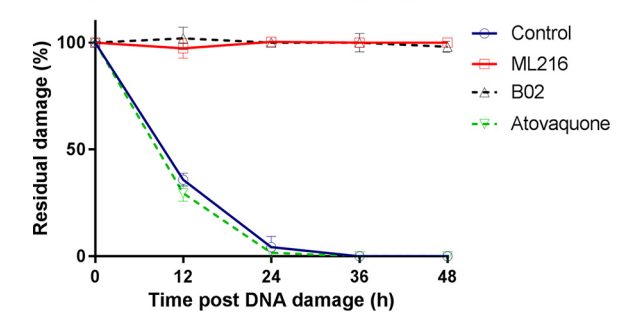


FIG 8 ML216 blocks the repair of UV-induced DNA damage in the nuclear genome of the parasite. ML216-, BO2-, and atoyaguone-pretreated and mock-treated cultures were UV irradiated at 100 J/m<sup>2</sup> at the trophozoite stage. After UV treatment, cells were grown in the presence of sublethal doses of the respective drugs (ML216, B02, or atovaquone) for 48 h. The mock-treated culture was also grown in parallel in normal complete medium, which acted as the control. Genomic DNA was isolated before and after treatment (untreated and 0 h posttreatment) and at 12-h intervals until 48 h. The percentage of unrepaired damage was plotted at the indicated time points using GraphPad Prism software.



and ART might potentiate each other's action. To that end, we performed a fixed-ratio drug combination assay. Dose-response curves were plotted for each combination, and fractional inhibitory concentration (FIC) values were calculated from the graphs. The  $\Sigma$ FIC values are tabulated in Table S2. Finally, an isobologram was constructed based on the calculated  $\Sigma$ FIC values. As depicted in the isobologram, the interaction between ML216 and ART is synergistic in nature (Fig. 9A). A similar result of a synergistic relationship was observed for the drug-resistant strains Dd2 and PfK13R539T (Fig. 9B and C). As chloroquine (CQ) treatment inhibits heme polymerization leading to the generation of free radicals, it is speculated that the treatment of parasites with CQ is also likely to create DSBs in the parasite (35). As expected, we observed that ML216 also synergizes with CQ in both drug-sensitive and drug-resistant strains (Fig. 9D and E). We also tested the interaction of ML216 with ATQ, whose mode of action does not interfere with DNA metabolism. As expected, we did not observe any synergistic action between these two drugs (Fig. 9F and G). These results suggest that the action of both ART and CQ can be potentiated by the RecQ inhibitor ML216.

#### **DISCUSSION**

In this study, we established one of the RecQ helicases of Plasmodium, PfBlm, as a DNA repair protein, and we have shown that a RecQ helicase inhibitor blocks the repair of ART-generated DSBs in the Plasmodium genome. First, the expression level of PfBLM was high during the schizont stage and upregulated in response to DNA damage. Second, this protein is able to complement the MMS sensitivity of an  $\Delta sqs1$  mutant of S. cerevisiae and interacts with DNA repair proteins of Plasmodium. Third, the overexpression of this protein increased the survival of parasites upon DNA damage. Finally, a chemical inhibitor of this protein, ML216, impaired the growth of parasites, and the inhibitor interacted synergistically with first-line antimalarial drugs.

The expression of PfBlm was at its peak during the replicative stage (schizont) compared to the trophozoite and ring stages. A possible interpretation of this result is that RecQ helicases play a crucial role in rescuing stalled replication forks (36), and in a recent study of Plasmodium, it has been shown that replication forks stalled at elevated rates in a  $\Delta Pfblm$  strain (18), indicating the active role of PfBlm in replication and repair. The upregulation of this protein in the presence of an external DNA-damaging agent implies its role in DNA repair, and it is in congruence with previous reports in which the DNA repair proteins PfRad51 and PfalMre11 were also upregulated (5, 6). We observed that PfBlm associates with PfRad51 and PfalMre11. The interaction with PfRad51 as scored by yeast twohybrid assays was found to be weak. It could be possible that within the parasites, certain posttranslational modifications may modulate the strength of such an interaction, which is absent in yeast. It is known from studies in other organisms that depending upon the posttranslational modification of HsBLM, the consequence of its interaction with Rad51 can be either pro- or antirecombinogenic (11). Previous reports suggest that Mre11 helps in the recruitment of HsBLM to DNA ends, thereby stimulating BLM-DNA2-RPA-mediated resection of DSBs (9). PfRPA has been characterized (31), and from the genome information, the putative ortholog of DNA2 has been annotated in P. falciparum (gene identifier PF3D7 1106700) (37). Future experiments in Plasmodium may enlighten us about the importance of the PfBLM-PfDNA2-PfRPA interaction.

In the current study, using a yeast surrogate system, we have shown that PfBLM rescued the MMS sensitivity phenotype of the  $\Delta sqs1$  strain. However, the helicase-dead mutants of PfBLM (PfbImK83R) and PfWRN were unable to perform this function. In model organisms, the helicase activity of BLM is required for two steps of HR: one during the resectioning of DSB ends through the DNA2-mediated pathway and the other during the dissolution of Holliday junctions along with Topolll. Although the orthologs of all these genes are annotated in the Plasmodium genome, whether PfBlm can engage with PfDNA2 or PfTopolII and participates at these two distinct steps of HR needs to be experimentally tested. Nonetheless, our results indicate that the helicase activity of PfBLM is important in repairing damaged DNA. Previous reports have shown that human WRN failed to rescue



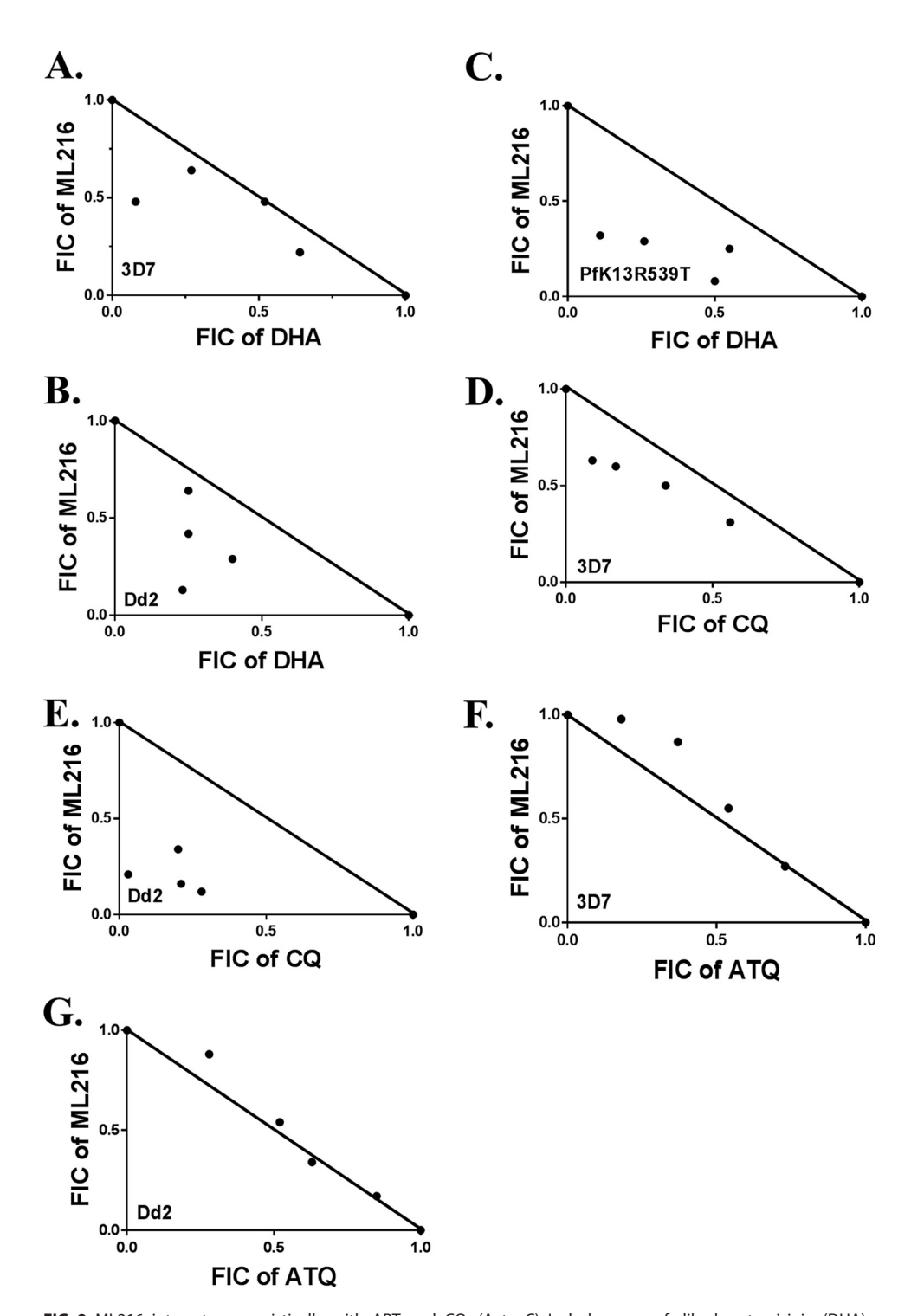


FIG 9 ML216 interacts synergistically with ART and CQ. (A to C) Isobolograms of dihydroartemisinin (DHA)-ML216 in the 3D7 (A), Dd2 (B), and PfK13R539T (C) strains. (D and E) Isobolograms of chloroquine (CQ)-ML216 in the 3D7 (D) and Dd2 (E) strains. (F and G) Isobolograms of atovaquone (ATQ)-ML216 in the 3D7 (F) and Dd2 (G) strains. Fixed-ratio drug combination assay. Each point represents the mean  $IC_{50}$  of the drug combination from three independent experiments. A solid line is plotted between the  $IC_{50}$  values of each drug when used alone. FIC, fractional inhibitory concentration.

the MMS sensitivity of the  $\Delta sqs1$  strain, indicating that its function is dispensable for DSB repair (38). This holds true even for PfWRN, which was also unable to complement the MMS sensitivity phenotype of the  $\Delta sgs1$  strain. In model organisms, it was found that the RecQ helicases possess both prorecombination and antirecombination functions (7, 8). A



previous study observed increased recombination frequencies among the subtelomeric var genes in a Pfwrn knockdown parasite line but not in a Pfblm knockout parasite line (18), emphasizing the antirecombination activity of the PfWrn protein. Our study provides evidence of the prorecombination activity of the PfBlm protein. Thus, it is possible that the two RecQ paralogs of Plasmodium may have opposing roles in HR. It is also possible that as observed in model organisms, the pro- and antirecombination functions of these two proteins may be regulated via posttranslational modifications (11, 39-42). Such possibilities need to be explored in the future.

We observed that the overexpression of PfBLM reduced the MMS sensitivity of parasites. This finding indicates the DNA repair activity of PfBLM in the parasite. A plausible explanation for the increase in the repair efficiency of PfBIm might be its involvement in the unwinding of different substrates of the HR pathway as the overexpression of the helicase-dead mutant did not provide any advantage. BLM also possesses a helicase-independent stimulatory function in the Exo1-mediated resection step during HR. Although PfEXO1 has been annotated (PF3D7\_0725000), we currently do not know whether the overexpression of PfBlm also stimulates such a pathway in *Plasmodium*.

Here, we report the binding affinities of the known RecQ helicase inhibitors ML216 and MIRA-1 for PfBIm by performing docking and molecular dynamics simulations. Our results demonstrated that ML216 binds efficiently to PfBIm compared with MIRA-1. This result is in accordance with the IDC inhibition of parasites with both drugs. The parasites are more sensitive to ML216 than to MIRA-1. Interestingly, ML216-mediated inhibition seems to be more selective toward Plasmodium than human fibroblast cell lines, where the half-maximal inhibitory concentration was more than 50  $\mu$ M after 48 h of incubation (28). Given the strong selectivity of ML216 toward Plasmodium, we believe that chemical modification of the lead compound may bring antiparasitic activity in the nanomolar range. Notably, multidrug-resistant strain Dd2 was more sensitive to ML216, and a similar effect was observed with the PfRad51 inhibitor B02 (33). The likely explanation for this result could be that the Dd2 strain might have a compromised DNA repair system, and recent reports have shown that the Dd2 strain failed to respond to DNA damage induced by MMS (43).

Failure in the repair of DSBs inflicted by various endogenous sources such as metabolites and reactive oxygen species (ROS) and replication errors during schizogony lead to the death of parasites. The possible mechanism for the antiparasitic activity of ML216 is to hinder the repair of such endogenous damage. Consistent with this interpretation, the effect of the drug should intensify in the presence of external DNA damage. Our growth inhibition experiment with MMS-treated cells confirmed this hypothesis, with the parasite being hypersensitive to lower concentrations of the drug. The known antimalarial drug ART inhibits different cellular pathways of parasites, and creating DSBs is one such established mode of action among them. Our laboratory has taken a particular interest in blocking the repair of such ART-generated DSBs (34) with ML216. Indeed, ML216 was able to inhibit the repair of DSBs, offering a ray of hope for artemisinin-based combination therapy (ACT). Finally, our results demonstrated that ML216 interacts synergistically with the first-line antimalarial drugs ART and CQ. The plausible explanation for the CQ-ML216 synergistic action might be that CQ inhibits heme polymerization resulting in the generation of free radicals, which potentially creates DSBs. However, there is no experimental evidence for this hypothesis.

Altogether, our data provide compelling evidence for PfBlm's participation in Plasmodium DNA repair. In addition, we have shown that RecQ helicases in Plasmodium can be targeted given their functions in different DNA metabolic pathways. This study raises the possibility of using RecQ helicase inhibitors in combination with the first-line antimalarial drugs ART and CQ.

## **MATERIALS AND METHODS**

Dihydroartemisinin (DHA) was used as an artemisinin (ART) derivative. DHA, CQ, ML216, and MIRA-1 were purchased from Sigma-Aldrich. DHA, ML216, and MIRA-1 were dissolved in dimethyl sulfoxide (DMSO). CQ was dissolved in MilliQ water.



Plasmodium culture. The 3D7 or Dd2 strain of P. falciparum was grown in human erythrocytes (RBCs) in RPMI 1640 medium supplemented with 0.005% hypoxanthine and 1% Albumax. The hematocrit of RBCs was maintained at 5%.

Plasmids. For complementation assays, PfBLM, PfblmK83R, and PfWRN were cloned into the yeast expression vector pBFM, pBFM is a  $2\mu$  yeast expression vector prepared by fusing the promoter region of the pTA vector (44) and the vector backbone from the pESC-HIS plasmid (Agilent Technologies). P. falciparum 3D7 genomic DNA was used as the template for the amplification of Plasmodium genes. The PfblmK83R mutant was generated by splicing by overlap extension PCR. A list of primers used in this study is given in Table S3 in the supplemental material.

For yeast two-hybrid analyses, pGBDU-C1 was used as the bait vector, and pGAD-C1 was used as the prey vector, which are  $2\mu$  plasmids having URA3 and LEU2 markers, respectively (3). PfRAD51 and PfalMRE11 were cloned into the bait vector containing the N-terminal GAL4 DNA binding domain, generating the PfRAD51-BD and PfalMRE11-BD fusions, respectively. PfBLM and PfWRN were cloned into the prey vector containing the N-terminal GAL4 activation domain, generating the PfBLM-AD and PfWRN-AD fusions, respectively.

For copurification assays, PfBLM was cloned into the pGEX-6P2 vector (GE Healthcare Life Sciences), and PfRAD51 was cloned into the pET101D vector (45).

For overexpression studies in Plasmodium, PfBLM and PfbImK83R were cloned into the pARL-GFP vec-

Yeast strains. Vector pBFM harboring ScSGS1, PfBLM, PfWRN, or PfblmK83R was transformed into the Δsgs1 strain SNY1 to generate the SNY2, SNY3, SNY4, and SNY5 strains. The empty pBFM vector was transformed into SNY1 to generate SNY6. Yeast two-hybrid analysis was performed using the PJ69-4A strain. Bait and prey plasmids were transformed into this strain to check the interaction of proteins. A list of yeast strains with genotypes is given in Table S4.

RNA isolation and RT-PCR. Synchronous P. falciparum cultures were harvested at the ring, trophozoite, or schizont stage when parasitemia was between 8 and 10%. For stage-specific DNA damage experiments, cells were harvested from untreated and MMS-treated cultures. RNA isolation was done as mentioned previously (6). Similarly, total RNA was isolated from yeast strains SNY3 to SNY5 after incubation at 30°C using an acid-phenol method as described previously (44). Equal amounts of RNA were taken after estimating the concentration by spectroscopic analysis (EMC-709 spectrophotometer; JASCO) and subjected to DNase I (Fermentas) treatment to eliminate genomic DNA contamination. PCR was performed to confirm the absence of genomic DNA. The synthesis of cDNA was performed as described previously (44). Briefly,  $10 \mu g$  of total RNA was reverse transcribed using reverse transcriptase (Qiagen), and the cDNA product was then subjected to real-time RT-PCR. cDNA was diluted 1:10 and subjected to real-time PCR using SYBR Premix ExTag (TaKaRa) and the Applied Biosystems 7500 Fast real-time PCR system. The threshold cycle ( $C_T$ ) value of PfARP for each sample was normalized to the corresponding  $C_T$  value of *PfBLM* transcripts. After normalization,  $C_T$  values of *PfBLM* for different samples were compared to obtain  $\Delta C_{\tau}$  values. The  $2^{\Delta CT}$  formula was used to determine the relative levels of PfBLM mRNA. Each experiment was repeated three times (n = 3), and the P value was calculated using the two-tailed t test (\* means a P value of <0.05, \*\* means a P value of <0.01, \*\*\* means a P value of < 0.001, and N.S. means not significant).

Antibodies and Western blotting. The anti-PfBlm antibody was generated by selecting a unique peptide at the C terminus of the PfBIm protein (KELEKREEELNEKTKNDQE), and antibody was raised against the peptide in rabbit. Anti-PfBIm antibody, anti-hAct1 antibody (Abcam), and anti-His tag antibody (Invitrogen) were used at a 1:5,000 dilution. Horseradish peroxidase (HRP)-conjugated anti-rabbit secondary antibody (Calbiochem) was used at a 1:10,000 dilution. HRP-conjugated anti-mouse secondary antibody (Calbiochem) was used at a 1:10,000 dilution for actin and His-tagged proteins. Western blotting was performed as previously described (3). The Western blots were developed using a chemiluminescence system (Thermo Scientific), and the band intensities were quantified using ImageJ software. Each experiment was repeated three times (n=3), and the P value was calculated using the two-tailed t test (\* means a P value of <0.05, \*\* means a P value of <0.01, \*\*\* means a P value of <0.001, and N.S. means not significant).

DNA damage experiments in yeast. Spotting assays with yeast strains SNY2 to SN6 were performed according to a previously mentioned protocol (6). Briefly, complementation strains were grown in medium lacking histidine at 30°C to an optical density at 600 nm  $(OD_{600})$  of 0.5. After normalization and serial dilution of the cells, spotting was done on an SC-His plate containing 0.01% MMS and an SC-His plate without MMS, which acted as the untreated control. The plates were incubated at 30°C, and their growth was compared. A return-to-growth assay with yeast strains SNY2 to SNY6 was performed as previously described (3). Briefly, yeast strains SNY2 to SNY6 were grown until the logarithmic phase and then divided into two equal parts. One part was exposed to 0.03% MMS for 2 h, whereas the other part was incubated without any treatment. The MMS was then washed off, and equal numbers of cells from both parts for each strain were spread on an SC-His plate and incubated for 48 h at 30°C. Percent survival was determined by taking the ratio of the numbers of colonies formed in treated versus untreated cultures. Each experiment was repeated three times (n = 3), and a graph was plotted using GraphPad Prism software. The P value was calculated using the two-tailed t test (\* means a P value of <0.05, \*\* means a P value of <0.01, \*\*\* means a P value of <0.001, and N.S. means not significant).

Yeast two-hybrid analyses. A yeast two-hybrid analysis was performed as described previously (3). Briefly, the interaction between bait and prey fusion constructs was analyzed by assessing the growth of the SNY8, SNY11, SNY9, SNY12, SNY13, and SNY15 strains on SC-Ura-Leu-His and SC-Ura-Leu-Ade triple-dropout plates. The plates were incubated at 30°C for 5 days.



**Copurification assay.** For performing copurification assays, Rosetta(DE3) cells harboring pGEX6P2: *PfBLM* were induced with 1 mM isopropyl-thiogalactosidase (IPTG) at 16°C overnight, whereas the same cells harboring pET101D:*PfRAD51* were induced with 1 mM IPTG at 37°C for 4 h. Lysis and Ni-NTA purification were performed as described previously (46). Similarly, extracts of cells expressing recombinant PfRad51 and an empty GST tag were also processed in the same manner, which acted as controls. The eluted samples were further analyzed by Western blot techniques.

**Transfection in P. falciparum.** Tightly synchronized ring-stage *Plasmodium* parasites having a parasitemia of around 6% were transfected with  $100\,\mu g$  of the *PfBLM-pARL* and *PfblmK83R-pARL* constructs according to a protocol described previously (47). Briefly, 1 day before transfection, both plasmids were resuspended in  $50\,\mu l$  of a Cytomix solution ( $10\,m M$  K<sub>2</sub>HPO<sub>4</sub> [pH 7.6],  $120\,m M$  KCl,  $0.15\,m M$  CaCl<sub>2</sub>,  $25\,m M$  HEPES [pH 7.6], 2 mM EGTA [pH 7.6], and 5 mM MgCl<sub>2</sub>) and kept at 4°C overnight. Electroporation was done using a Bio-Rad gene pulser. After transfection, cells were allowed to grow in the absence of the drug until parasitemia reached 4%. Later, cells were maintained in drug medium until transfectants appeared. Pyrimethamine was used as a selectable drug.

**DNA damage experiments in parasites.** DNA damage-specific expression of *PfBLM* was done by treating cells with 0.05% MMS for 6 h, and untreated cells were grown simultaneously. RNA/protein was isolated from both groups of cells for real-time RT-PCR and Western blotting.

For survival assays with the overexpression of *PfBLM* and *PfbImK83R*, parasites were synchronized, and parasites having a parasitemia of around 1% were taken for treatment with 0.002% or 0.005% MMS for 2 h. After 2 h of treatment with MMS, cells were washed twice and allowed to grow for 48 h in complete medium. Wild-type parasites (3D7) were also given MMS treatment in a similar manner, which served as controls. The ratio of the percentages of survival between the transfectant and the wild type was taken to plot the fold survival advantage. Each experiment was repeated three times, and the graph was plotted using GraphPad Prism software. The *P* value was calculated using the two-tailed *t* test (\* means a *P* value of <0.05, \*\* means a *P* value of <0.001, and N.S. means not significant).

Docking and molecular dynamics simulations. The PfBIm protein was modeled using the I-TASSER server (48, 49). A quality check of the predicted structural models was performed using the PROCHECK program (50). The model closest to the HsBLM structure (PDB accession number 4CGZ) (51) in terms of the root mean square deviation (RMSD) was chosen for further studies. A 10-ns equilibration of the model was carried out using the GROMACS program with the CHARMM36 force field (52, 53). In order to choose a representative structure from the simulation trajectory, clustering of structures from the last 5 ns of the trajectory was performed using the GROMACS program. The structure at the center of the largest cluster was chosen as a representative structure for docking studies. The inhibitors ML216 and MIRA-1 were docked onto the PfBIm model using the AutoDock Vina program (54). Two independent docking runs were performed for both inhibitors: one with the ATP binding site as the docking search space and one with the DNA binding region as the docking search space. For each run, the docking pose with the highest number of protein-inhibitor hydrogen bonds was selected for molecular dynamics simulations. The protein-inhibitor complex was simulated for 50 ns using the GROMACS program with the CHARMM36 force field (52, 53). Force field parameters for the inhibitor molecules were obtained using the Paramchem server (55, 56). The binding free energy for the protein-inhibitor complex was calculated using the molecular mechanics Poisson-Boltzmann surface area (MM-PBSA) method (57, 58).

**Inhibition of** *Plasmodium* **growth by ML216 and MIRA-1.** Drug inhibition assays with ML216 and MIRA-1 were performed as previously described (33). Both Giemsa staining and SYBR green I-based evaluation of parasite survival were done as previously described (59). The semilog graph was plotted for the concentration of the drug versus the percent inhibition to determine the 50% inhibitory concentrations ( $IC_{50}$ s) of ML216 and MIRA-1 using GraphPad Prism software. Each assay was repeated three times for reproducibility (n = 3).

Effect of ML216 on DNA-damaged cells. To check the effect of ML216 on DNA-damaged cells, the cultures were divided into two equal parts. One part was treated with 0.005% MMS for 2 h, and MMS was washed off after treatment. The cells were allowed to grow in complete medium containing various concentrations of ML216 (0.1 nM to 1,000  $\mu$ M) for one generation (48 h). The second aliquot of the culture was maintained in the presence of ML216 without MMS treatment. In the positive control, MMS and ML216 were not added. Each assay was repeated three times for reproducibility (n = 3).

PCR-based method to quantify DNA damage. An amplification-based technique was performed to measure nuclear DNA damage as previously described, with modifications (32). Briefly, ring-stage parasites were pretreated with sublethal doses of the drug atovaquone (0.3 nM), ML216 (1  $\mu$ M), or B02  $(1 \mu M)$ , followed by exposure to UV light  $(100 \text{ J/m}^2)$  at the trophozoite stage to induce DNA damage. After treatment, the mock-treated or the drug-treated cultures were grown in the presence of the respective drug-containing media for 48 h. Genomic DNA was collected before (untreated sample) and immediately after (0-h sample) UV treatment and every 12 h until 48 h. The isolated genomic DNA was quantified using a SYBR green I dye-based standard plot method. An equal amount of genomic DNA was taken to set up PCR for amplifying long- and short-range fragments (7,200 bp and 269 bp). Primer sets OMKB463 and -464 and OSB94 and -95 were used to amplify the long-range PCR and short-range PCR products, respectively. The PCR products were quantified using SYBR green I dye, and the fluorescence readings of the long-range PCR product were normalized using the readings of the short-range product. The amount of damaged DNA at any given time point was deduced from the following equation: damaged DNA = 1 - (fluorescence intensity of the long PCR product/fluorescence intensity of the short PCR product  $\times$  26.76), where the factor 26.76 represents the ratio of the long-range PCR amplicon size to the short-range PCR amplicon size. The amounts of damaged DNA from the untreated sample



and the 0-h sample were considered 0 and 100%, respectively. The amount of residual damage at each time point was plotted using GraphPad Prism software. The P value was calculated using the two-tailed t test (\* means a P value of <0.05, \*\* means a P value of <0.01, \*\*\* means a P value of <0.001, and N.S. means not significant).

Fixed-ratio method to determine the interaction between ML216 and DHA/CQ. Synchronous P. falciparum cultures of the trophozoite stage were used to determine the interactions between ML216 and DHA/CQ/ATQ. A fixed-ratio method was performed as previously mentioned (33). A Giemsa stainbased evaluation of parasitemia was done to estimate percent inhibition. A semilog graph was plotted for each combination to determine the  $IC_{50}$  value using GraphPad Prism software. The fractional inhibitory concentration (FIC) for each drug was determined by using the equation FIC =  $IC_{50}$  of the drug in the mixture/IC<sub>50</sub> of the drug alone. The FIC values of both drugs were used to determine the interaction between ML216 and DHA by using the following equation:  $\Sigma FIC = (IC_{50} \text{ of DHA in the mixture/IC}_{50} \text{ of DHA})$ DHA alone) + ( $IC_{50}$  of ML216 in the mixture/ $IC_{50}$  of ML216 alone). An isobologram was plotted by using GraphPad Prism software. An  $\Sigma$ FIC of <1 represents synergism,  $\Sigma$ FICs of  $\ge$ 1 and 2 represent an additive interaction, and an ΣFIC of ≥2 represents antagonism. A similar equation was used for the CQ/ATQ and ML216 combination.

#### SUPPLEMENTAL MATERIAL

Supplemental material is available online only.

FIG S1, PDF file, 0.2 MB.

FIG S2, PDF file, 0.1 MB.

TABLE \$1, PDF file, 0.1 MB.

TABLE S2, PDF file, 0.1 MB.

TABLE S3, PDF file, 0.03 MB.

TABLE S4, PDF file, 0.1 MB.

#### **ACKNOWLEDGMENTS**

This work is supported by grants from the DBT, Government of India (BT/PR25858/ GET/119/169/2017), to M.K.B. We acknowledge support from DST-FIST and UGC-SAP to the Department of Biochemistry. N.S. and P.J. are supported by senior research fellowships from the University Grants Commission, Government of India, and the Council for Scientific and Industrial Research, Government of India, respectively.

We thank Souvik Bhattacharjee (JNU, India) for the kind gift of P. falciparum isolate PfK13R539T.

### **REFERENCES**

- 1. Wongsrichanalai C, Sibley CH. 2013. Fighting drug-resistant Plasmodium falciparum: the challenge of artemisinin resistance. Clin Microbiol Infect 19:908-916. https://doi.org/10.1111/1469-0691.12316.
- 2. Frankenberg-Schwager M, Frankenberg D. 1990. DNA double-strand breaks: their repair and relationship to cell killing in yeast. Int J Radiat Biol 58:569-575. https://doi.org/10.1080/09553009014551931.
- 3. Roy N, Bhattacharyya S, Chakrabarty S, Laskar S, Babu SM, Bhattacharyya MK. 2014. Dominant negative mutant of Plasmodium Rad51 causes reduced parasite burden in host by abrogating DNA double-strand break repair. Mol Microbiol 94:353-366. https://doi.org/10.1111/mmi.12762.
- 4. Kirkman LA, Lawrence EA, Deitsch KW. 2014. Malaria parasites utilize both homologous recombination and alternative end joining pathways to maintain genome integrity. Nucleic Acids Res 42:370-379. https://doi .org/10.1093/nar/gkt881.
- 5. Bhattacharyya MK, Kumar N. 2003. Identification and molecular characterisation of DNA damaging agent induced expression of Plasmodium falciparum recombination protein PfRad51. Int J Parasitol 33:1385-1392. https://doi.org/10.1016/s0020-7519(03)00212-1.
- 6. Badugu SB, Nabi SA, Vaidyam P, Laskar S, Bhattacharyya S, Bhattacharyya MK. 2015. Identification of Plasmodium falciparum DNA repair protein Mre11 with an evolutionarily conserved nuclease function. PLoS One 10: e0125358. https://doi.org/10.1371/journal.pone.0125358.
- 7. Croteau DL, Popuri V, Opresko PL, Bohr VA. 2014. Human RecQ helicases in DNA repair, recombination, and replication. Annu Rev Biochem 83:519-552. https://doi.org/10.1146/annurev-biochem-060713-035428.
- 8. Bernstein KA, Gangloff S, Rothstein R. 2010. The RecQ DNA helicases in DNA repair. Annu Rev Genet 44:393-417. https://doi.org/10.1146/annurev -genet-102209-163602.
- Nimonkar AV, Genschel J, Kinoshita E, Polaczek P, Campbell JL, Wyman C, Modrich P, Kowalczykowski SC. 2011. BLM-DNA2-RPA-MRN and EXO1-

- BLM-RPA-MRN constitute two DNA end resection machineries for human DNA break repair. Genes Dev 25:350-362. https://doi.org/10.1101/gad 2003811.
- 10. Nimonkar AV, Ozsoy AZ, Genschel J, Modrich P, Kowalczykowski SC. 2008. Human exonuclease 1 and BLM helicase interact to resect DNA and initiate DNA repair. Proc Natl Acad Sci U S A 105:16906-16911. https://doi .org/10.1073/pnas.0809380105.
- 11. Ouyang KJ, Woo LL, Zhu J, Huo D, Matunis MJ, Ellis NA. 2009. SUMO modification regulates BLM and RAD51 interaction at damaged replication forks. PLoS Biol 7:e1000252, https://doi.org/10.1371/journal.pbio.1000252.
- 12. Bugreev DV, Mazina OM, Mazin AV. 2009. Bloom syndrome helicase stimulates RAD51 DNA strand exchange activity through a novel mechanism. J Biol Chem 284:26349–26359. https://doi.org/10.1074/jbc.M109.029371.
- 13. Manthei KA, Keck JL. 2013. The BLM dissolvasome in DNA replication and repair. Cell Mol Life Sci 70:4067-4084. https://doi.org/10.1007/s00018 -013-1325-1.
- 14. Suntornthiticharoen P, Srila W, Chavalitshewinkoon-Petmitr P, Limudomporn P, Yamabhai M. 2014. Characterization of recombinant malarial RecQ DNA helicase. Mol Biochem Parasitol 196:41-44. https://doi.org/10.1016/j .molbiopara.2014.07.013.
- 15. Rahman F, Tarique M, Tuteja R. 2016. Plasmodium falciparum Bloom homologue, a nucleocytoplasmic protein, translocates in 3' to 5' direction and is essential for parasite growth. Biochim Biophys Acta 1864:594–608. https:// doi.org/10.1016/j.bbapap.2016.02.016.
- 16. Rahman F, Tarique M, Ahmad M, Tuteja R. 2016. Plasmodium falciparum Werner homologue is a nuclear protein and its biochemical activities reside in the N-terminal region. Protoplasma 253:45–60. https://doi.org/10 .1007/s00709-015-0785-6.
- 17. Li Z, Yin S, Sun M, Cheng X, Wei J, Gilbert N, Miao J, Cui L, Huang Z, Dai X, Jiang L. 2019. DNA helicase RecQ1 regulates mutually exclusive



- expression of virulence genes in Plasmodium falciparum via heterochromatin alteration. Proc Natl Acad Sci U S A 116:3177–3182. https://doi.org/10.1073/pnas.1811766116.
- Claessens A, Harris LM, Stanojcic S, Chappell L, Stanton A, Kuk N, Veneziano-Broccia P, Sterkers Y, Rayner JC, Merrick CJ. 2018. RecQ helicases in the malaria parasite Plasmodium falciparum affect genome stability, gene expression patterns and DNA replication dynamics. PLoS Genet 14:e1007490. https://doi.org/10.1371/journal.pgen.1007490.
- Dutertre S, Ababou M, Onclercq R, Delic J, Chatton B, Jaulin C, Amor-Gueret M. 2000. Cell cycle regulation of the endogenous wild type Bloom's syndrome DNA helicase. Oncogene 19:2731–2738. https://doi .org/10.1038/sj.onc.1203595.
- Frei C, Gasser SM. 2000. The yeast Sgs1p helicase acts upstream of Rad53p in the DNA replication checkpoint and colocalizes with Rad53p in S-phase-specific foci. Genes Dev 14:81–96.
- Bártfai R, Hoeijmakers WA, Salcedo-Amaya AM, Smits AH, Janssen-Megens E, Kaan A, Treeck M, Gilberger TW, Françoijs KJ, Stunnenberg HG. 2010.
   H2A.Z demarcates intergenic regions of the Plasmodium falciparum epigenome that are dynamically marked by H3K9ac and H3K4me3. PLoS Pathog 6:e1001223. https://doi.org/10.1371/journal.ppat.1001223.
- Hoeijmakers W, Bartfai R, Kensche PR. 2015. Data from "Transcriptome of the P. falciparum 3D7 intraerythrocytic cycle assayed by RNA-Seq." PlasmoDB. https://plasmodb.org/plasmo/app/record/dataset/DS\_715bf2deda.
- Wu L, Davies SL, Levitt NC, Hickson ID. 2001. Potential role for the BLM helicase in recombinational repair via a conserved interaction with RAD51. J Biol Chem 276:19375–19381. https://doi.org/10.1074/jbc.M009471200.
- Tripathi V, Agarwal H, Priya S, Batra H, Modi P, Pandey M, Saha D, Raghavan SC, Sengupta S. 2018. MRN complex-dependent recruitment of ubiquitylated BLM helicase to DSBs negatively regulates DNA repair pathways. Nat Commun 9:1016. https://doi.org/10.1038/s41467-018-03393-8.
- Ui A, Satoh Y, Onoda F, Miyajima A, Seki M, Enomoto T. 2001. The N-terminal region of Sgs1, which interacts with Top3, is required for complementation of MMS sensitivity and suppression of hyper-recombination in sgs1 disruptants. Mol Genet Genomics 265:837–850. https://doi.org/10.1007/s004380100479.
- Mirzaei H, Schmidt KH. 2012. Non-Bloom syndrome-associated partial and total loss-of-function variants of BLM helicase. Proc Natl Acad Sci U S A 109:19357–19362. https://doi.org/10.1073/pnas.1210304109.
- Mitra P, Banu K, Deshmukh AS, Subbarao N, Dhar SK. 2015. Functional dissection of proliferating-cell nuclear antigens (1 and 2) in human malarial parasite Plasmodium falciparum: possible involvement in DNA replication and DNA damage response. Biochem J 470:115–129. https://doi.org/10.1042/BJ20150452.
- Nguyen GH, Dexheimer TS, Rosenthal AS, Chu WK, Singh DK, Mosedale G, Bachrati CZ, Schultz L, Sakurai M, Savitsky P, Abu M, McHugh PJ, Bohr VA, Harris CC, Jadhav A, Gileadi O, Maloney DJ, Simeonov A, Hickson ID. 2013.
   A small molecule inhibitor of the BLM helicase modulates chromosome stability in human cells. Chem Biol 20:55–62. https://doi.org/10.1016/j .chembiol.2012.10.016.
- Aggarwal M, Sommers JA, Shoemaker RH, Brosh RM, Jr. 2011. Inhibition of helicase activity by a small molecule impairs Werner syndrome helicase (WRN) function in the cellular response to DNA damage or replication stress. Proc Natl Acad Sci U S A 108:1525–1530. https://doi.org/10.1073/ pnas.1006423108.
- Mbengue A, Bhattacharjee S, Pandharkar T, Liu H, Estiu G, Stahelin RV, Rizk SS, Njimoh DL, Ryan Y, Chotivanich K, Nguon C, Ghorbal M, Lopez-Rubio JJ, Pfrender M, Emrich S, Mohandas N, Dondorp AM, Wiest O, Haldar K. 2015. A molecular mechanism of artemisinin resistance in Plasmodium falciparum malaria. Nature 520:683–687. https://doi.org/10 .1038/nature14412.
- 31. Gopalakrishnan AM, Kumar N. 2013. Opposing roles for two molecular forms of replication protein A in Rad51-Rad54-mediated DNA recombination in Plasmodium falciparum. mBio 4:e00252-13. https://doi.org/10.1128/mBio.00252-13.
- Furda A, Santos JH, Meyer JN, Van Houten B. 2014. Quantitative PCR-based measurement of nuclear and mitochondrial DNA damage and repair in mammalian cells. Methods Mol Biol 1105:419–437. https://doi.org/10.1007/978-1-62703-739-6\_31.
- Vydyam P, Dutta D, Sutram N, Bhattacharyya S, Bhattacharyya MK. 2019.
   A small-molecule inhibitor of the DNA recombinase Rad51 from Plasmodium falciparum synergizes with the antimalarial drugs artemisinin and chloroquine. J Biol Chem 294:8171–8183. https://doi.org/10.1074/jbc.RA118.005009.
- 34. Gopalakrishnan AM, Kumar N. 2015. Antimalarial action of artesunate

- involves DNA damage mediated by reactive oxygen species. Antimicrob Agents Chemother 59:317–325. https://doi.org/10.1128/AAC.03663-14.
- Sullivan DJ, Jr, Matile H, Ridley RG, Goldberg DE. 1998. A common mechanism for blockade of heme polymerization by antimalarial quinolines. J Biol Chem 273:31103–31107. https://doi.org/10.1074/jbc.273.47.31103.
- Davies SL, North PS, Hickson ID. 2007. Role for BLM in replication-fork restart and suppression of origin firing after replicative stress. Nat Struct Mol Biol 14:677–679. https://doi.org/10.1038/nsmb1267.
- 37. Gardner MJ, Hall N, Fung E, White O, Berriman M, Hyman RW, Carlton JM, Pain A, Nelson KE, Bowman S, Paulsen IT, James K, Eisen JA, Rutherford K, Salzberg SL, Craig A, Kyes S, Chan MS, Nene V, Shallom SJ, Suh B, Peterson J, Angiuoli S, Pertea M, Allen J, Selengut J, Haft D, Mather MW, Vaidya AB, Martin DM, Fairlamb AH, Fraunholz MJ, Roos DS, Ralph SA, McFadden GI, Cummings LM, Subramanian GM, Mungall C, Venter JC, Carucci DJ, Hoffman SL, Newbold C, Davis RW, Fraser CM, Barrell B. 2002. Genome sequence of the human malaria parasite Plasmodium falciparum. Nature 419:498–511. https://doi.org/10.1038/nature01097.
- 38. Aggarwal M, Brosh RM. 2009. WRN helicase defective in the premature aging disorder Werner syndrome genetically interacts with topoisomerase 3 and restores the top3 slow growth phenotype of sgs1 top3. Aging (Albany NY) 1:219–233. https://doi.org/10.18632/aging.100020.
- Böhm S, Bernstein KA. 2014. The role of post-translational modifications in fine-tuning BLM helicase function during DNA repair. DNA Repair (Amst) 22:123–132. https://doi.org/10.1016/j.dnarep.2014.07.007.
- Kusumoto R, Muftuoglu M, Bohr VA. 2007. The role of WRN in DNA repair is affected by post-translational modifications. Mech Ageing Dev 128:50–57. https://doi.org/10.1016/j.mad.2006.11.010.
- 41. Mukherjee S, Sinha D, Bhattacharya S, Srinivasan K, Abdisalaam S, Asaithamby A. 2018. Werner syndrome protein and DNA replication. Int J Mol Sci 19:3442. https://doi.org/10.3390/ijms19113442.
- 42. Ammazzalorso F, Pirzio LM, Bignami M, Franchitto A, Pichierri P. 2010. ATR and ATM differently regulate WRN to prevent DSBs at stalled replication forks and promote replication fork recovery. EMBO J 29:3156–3169. https://doi.org/10.1038/emboj.2010.205.
- 43. Gupta DK, Patra AT, Zhu L, Gupta AP, Bozdech Z. 2016. DNA damage regulation and its role in drug-related phenotypes in the malaria parasites. Sci Rep 6:23603. https://doi.org/10.1038/srep23603.
- 44. Laskar S, Bhattacharyya MK, Shankar R, Bhattacharyya S. 2011. HSP90 controls SIR2 mediated gene silencing. PLoS One 6:e23406. https://doi.org/10.1371/journal.pone.0023406.
- Bhattacharyya MK, Bhattacharyya nee Deb S, Jayabalasingham B, Kumar N. 2005. Characterization of kinetics of DNA strand-exchange and ATP hydrolysis activities of recombinant PfRad51, a Plasmodium falciparum recombinase. Mol Biochem Parasitol 139:33–39. https://doi.org/10.1016/j .molbiopara.2004.09.007.
- Jha P, Laskar S, Dubey S, Bhattacharyya MK, Bhattacharyya S. 2017. Plasmodium Hsp40 and human Hsp70: a potential cochaperone-chaperone complex. Mol Biochem Parasitol 214:10–13. https://doi.org/10.1016/j.molbiopara .2017.03.003.
- Wu Y, Sifri CD, Lei HH, Su XZ, Wellems TE. 1995. Transfection of Plasmodium falciparum within human red blood cells. Proc Natl Acad Sci U S A 92:973–977. https://doi.org/10.1073/pnas.92.4.973.
- Roy A, Kucukural A, Zhang Y. 2010. I-TASSER: a unified platform for automated protein structure and function prediction. Nat Protoc 5:725–738. https://doi.org/10.1038/nprot.2010.5.
- Yang J, Zhang Y. 2015. I-TASSER server: new development for protein structure and function predictions. Nucleic Acids Res 43:W174–W181. https://doi.org/10.1093/nar/gkv342.
- Laskowski RA, MacArthur MW, Moss DS, Thornton JM. 1993. PROCHECK: a program to check the stereochemical quality of protein structures. J Appl Crystallogr 26:283–291. https://doi.org/10.1107/S0021889892009944.
- Newman JA, Savitsky P, Allerston CK, Bizard AH, Özer Ö, Sarlós K, Liu Y, Pardon E, Steyaert J, Hickson ID, Gileadi O. 2015. Crystal structure of the Bloom's syndrome helicase indicates a role for the HRDC domain in conformational changes. Nucleic Acids Res 43:5221–5235. https://doi.org/10 .1093/nar/gkv373.
- Abraham MJ, Murtola T, Schulz R, Páll S, Smith JC, Hess B, Lindahl E. 2015. GROMACS: high performance molecular simulations through multi-level parallelism from laptops to supercomputers. SoftwareX 1–2:19–25. https:// doi.org/10.1016/j.softx.2015.06.001.
- 53. Best RB, Zhu X, Shim J, Lopes PEM, Mittal J, Feig M, MacKerell AD. 2012. Optimization of the additive CHARMM all-atom protein force field targeting improved sampling of the backbone  $\phi$ ,  $\psi$  and side-chain  $\chi 1$  and  $\chi 2$



- dihedral angles. J Chem Theory Comput 8:3257–3273. https://doi.org/10.1021/ct300400x.
- 54. Trott O, Olson AJ. 2010. AutoDock Vina: improving the speed and accuracy of docking with a new scoring function, efficient optimization, and multithreading. J Comput Chem 31:455–461. https://doi.org/10.1002/jcc.21334.
- Vanommeslaeghe K, MacKerell AD, Jr. 2012. Automation of the CHARMM general force field (CGenFF) I: bond perception and atom typing. J Chem Inf Model 52:3144–3154. https://doi.org/10.1021/ci300363c.
- 56. Vanommeslaeghe K, Raman EP, MacKerell AD, Jr. 2012. Automation of the CHARMM general force field (CGenFF) II: assignment of bonded
- parameters and partial atomic charges. J Chem Inf Model 52:3155–3168. https://doi.org/10.1021/ci3003649.
- Kumari R, Kumar R, Open Source Drug Discovery Consortium, Lynn A. 2014.
   g\_mmpbsa—a GROMACS tool for high-throughput MM-PBSA calculations. J
   Chem Inf Model 54:1951–1962. https://doi.org/10.1021/ci500020m.
- Baker NA, Sept D, Joseph S, Holst MJ, McCammon JA. 2001. Electrostatics of nanosystems: application to microtubules and the ribosome. Proc Natl Acad Sci U S A 98:10037–10041. https://doi.org/10.1073/pnas.181342398.
- Chalapareddy S, Bhattacharyya MK, Mishra S, Bhattacharyya S. 2014. Radicicol confers mid-schizont arrest by inhibiting mitochondrial replication in Plasmodium falciparum. Antimicrob Agents Chemother 58:4341–4352. https://doi.org/10.1128/AAC.02519-13.



## A small-molecule inhibitor of the DNA recombinase Rad51 from Plasmodium falciparum synergizes with the antimalarial drugs artemisinin and chloroquine

Received for publication, July 22, 2018, and in revised form, March 27, 2019 Published, Papers in Press, April 1, 2019, DOI 10.1074/jbc.RA118.005009

Pratap Vydyam<sup>‡1</sup>, Dibyendu Dutta<sup>‡</sup>, Niranjan Sutram<sup>‡1</sup>, Sunanda Bhattacharyya<sup>§</sup>, and Mrinal Kanti Bhattacharyya<sup>‡2</sup> From the Departments of  $^{\dagger}$ Biochemistry and  $^{\S}$ Biotechnology and Bioinformatics, School of Life Sciences, University of Hyderabad, Gachibowli, Hyderabad 500046, TS, India

Edited by Patrick Sung

Malaria parasites repair DNA double-strand breaks (DSBs) primarily through homologous recombination (HR). Here, because the unrepaired DSBs lead to the death of the unicellular parasite Plasmodium falciparum, we investigated its recombinase, PfRad51, as a potential drug target. Undertaking an in silico screening approach, we identified a compound, B02, that docks to the predicted tertiary structure of PfRad51 with high affinity. B02 inhibited a drug-sensitive P. falciparum strain (3D7) and multidrug-resistant parasite (Dd2) in culture, with  $IC_{50}$  values of 8 and 3  $\mu$ M, respectively. We found that B02 is more potent against these P. falciparum strains than against mammalian cell lines. Our findings also revealed that the antimalarial activity of B02 synergizes with those of two first-line malaria drugs, artemisinin (ART) and chloroquine (CQ), lowering the IC<sub>50</sub> values of ART and CQ by 15- and 8-fold, respectively. Our results also provide mechanistic insights into the anti-parasitic activity of B02, indicating that it blocks the ATPase and strand-exchange activities of PfRad51 and abrogates the formation of PfRad51 foci on damaged DNA at chromosomal sites, probably by blocking homomeric interactions of PfRad51 proteins. The B02-mediated PfRad51 disruption led to the accumulation of unrepaired parasitic DNA and rendered parasites more sensitive to DNA-damaging agents, including ART. Our findings provide a rationale for targeting the Plasmodium DSB repair pathway in combination with ART. We propose that identification of a specific inhibitor of HR in Plasmodium may enable investigations of HR's role in Plasmodium biology, including generation of antigenic diversity.

Malaria continues to be one of the biggest public health problems in this era. Up to 303 million new malaria cases are reported each year with almost a half-million of them resulting in death (1). Although artemisinin (ART)<sup>3</sup>-based combination

This work was supported by grants from DST-SERB, Government of India Grant DST-SERB/2015/000999 (to M. K. B.), and UPE-II (University of Hyderabad) (to M. K. B.). The authors declare that they have no conflicts of interest with the contents of this article.

This article contains Figs. S1–S5.

therapies have helped reduce the World's malaria burden, the parasite's ability to develop resistance has overcome our efforts to curb this disease. Thus, there is an urgent need to come up with new anti-malaria drugs. To that end, one of the approaches could be the identification of novel drug targets. Here, we propose that targeting the DNA double-strand break (DSB) repair pathway of the malaria parasites could be a viable approach.

DSBs are inevitable in the life cycle of Plasmodium falciparum. Their sources could be endogenous, exogenous, or even physiologic. Whatever the source of DSBs, each DSB needs to be mended to ensure viability of a unicellular organism (2). In *Plasmodium,* DSBs are repaired primarily by the HR pathway. Parasites lacking functional HR machinery fail to repair DSBs and succumb to death (3), suggesting that the HR pathway cannot be compensated by any other DSB repair mechanisms in these parasites. Mice infected with parasites with defective HR live longer with significantly lower parasite burden (3).

In eukaryotes, Rad51 protein plays a central role during HR. Rad51 coats the ssDNA and forms nucleoprotein filament during strand invasion (4). Its ATP hydrolysis activity is required for product release during the synapsis step (5). The two Walker motifs (A and B) are responsible for its ATP-binding and hydrolysis activities (6). The ortholog of Rad51 from P. falciparum has been identified (7). PfRad51 shows ssDNA-dependent ATP hydrolysis activity and strand-exchange activity (8). A mutation in the Walker-A motif (PfRad51K143R) not only abrogates its ATPase activity but also exhorts a dominant-negative effect by inhibiting the ATPase activity of WT PfRad51 proteins (3). Yeast two-hybrid data indicate that PfRad51 interacts with itself (3), suggesting that PfRad51 also forms multimeric complexes like other eukaryotic Rad51 proteins. Using yeast as a surrogate model, it has been demonstrated that PfRad51 can repair DSBs, perform gene conversions, and facilitate gene targeting at the correct genomic locus (3).

A large-scale screening of the NCBI chemical library using a high-throughput fluorescence resonance energy transfer (FRET) assay, for identification of inhibitors of human Rad51 (hRad51)-mediated DNA strand exchange, has identified 17

ine; PDB, Protein Data Bank; FIC, fractional inhibitory concentration; ssDNA, single-strand DNA; MMS, methyl methanesulfonate; IFA, immunofluorescence assay; DAPI, 4,6-diamidino-2-phenylindole; RBC, red blood cell; MEF, mouse embryonic fibroblast; IDC, intra-erythrocytic developmental cycle; Y2H, yeast two-hybrid; DHA, dihydroartemisinin.



<sup>&</sup>lt;sup>1</sup> Supported by a Senior Research Fellowship from the University Grants Commission, Government of India.

<sup>&</sup>lt;sup>2</sup> To whom correspondence should be addressed. Tel.: 91-23134528; Fax: 91-23010120; E-mail: mkbsl@uohyd.ernet.in.

<sup>&</sup>lt;sup>3</sup> The abbreviations used are: ART, artemisinin; DSB, DNA double-strand break; HR, homologous recombination; CQ, chloroquine; PY, pyrimetham-

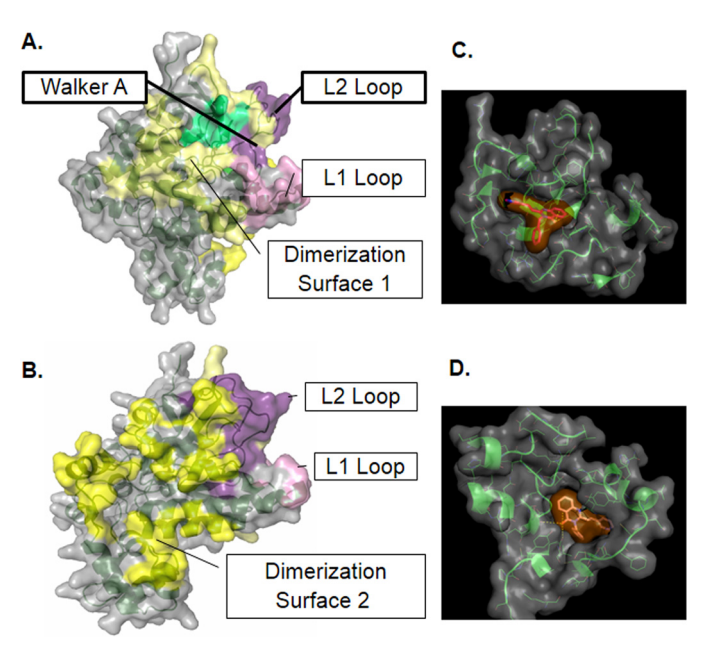


**Figure 1. Docking of B02 onto the predicted tertiary structure of PfRad51.** Front view (*A*) and rear view (*B*) of the homology model of PfRad51. *C*, docked conformation of B02 at the Walker site. *D*, docked conformation of B02 at the dimerization site.

compounds (9). Few of them were very specific to hRad51 as they did not inhibit the bacterial RecA, which is the structural and functional ortholog of Rad51 (9). Separate studies have identified additional inhibitors of hRad51 (10, 11), and some of them were further chemically modified to increase their specificity (12). Here, we report the in silico screening of small molecules for docking onto the predicted three-dimensional structure of PfRad51. One of the top-scoring ligands (B02) inhibits the ATPase activity of purified recombinant PfRad51 protein and its self-interaction. We further provide mechanistic insights for the anti-parasitic activity of B02 that it abrogates the formation of PfRad51 foci on the damaged DNA at chromosomal sites, probably by blocking the self-interaction of the PfRad51 proteins. This leads to the failure to repair damaged parasitic DNA and renders the parasites more sensitive toward DNA-damaging agents. B02 inhibits parasite growth more selectively than that of mammalian cell lines. We found out that the anti-parasitic activity of B02 can be potentiated by antimalarial drugs chloroquine (CQ) and ART. Furthermore, we report that the anti-parasitic activity of B02 synergizes with ART and CQ but not with pyrimethamine (PY).

### Results

# Homology modeling of PfRad51 and in silico screening of small-molecule inhibitors

Because the X-ray crystal structure of PfRad51 is unavailable, we wished to develop an *in silico* 3D structure of PfRad51 by homology modeling. To achieve this, we have used the available crystal structure of the yeast Rad51 (ScRad51) as a template. The modeled structure of PfRad51 revealed the presence of all the characteristic features of the ScRad51 structure, namely the Walker motifs, the L1 site, the L2 site, and the dimerization surfaces 1 and 2 (Fig. 1, *A* and *B*). This is in corroboration with the sequence identity observed between PfRad51 and ScRad51

(Fig. S1). To predict the chemical compounds that might have anti-PfRad51 activity, we have prepared a virtual ligand library of small molecules that have previously established anti-Rad51/ RecA activity (9-11). Seventeen ligands were chosen (Fig. S2) that inhibit the activity of eukaryotic Rad51 or Escherichia coli RecA proteins. With each of the 17 ligands, we performed blindfold docking, by setting the entire protein as the search space. This allowed us to identify the most preferred sites for binding, namely the Walker site and the dimerization site. The binding affinities of each ligand as predicted by different models are listed in Table 1. The docking scores from each of the models were totaled for each docking site to represent a measure of total affinity of ligand binding. A cutoff value of -30kcal/mol was set because the binding affinity of ATP, which is the natural ligand of PfRad51, was found to be near this value. At the Walker site five ligands showed maximum affinity. These ligands are as follows: A04, A08, A07, A05, and B02. Similarly, at the dimerization site eight ligands showed maximum affinity. These ligands are as follows: A04, A08, A07, A05, B02, A10, A03, and RI-2. Interestingly, two well-characterized inhibitors of human Rad51, RI-1 and RI-2, exhibited weak docking at the Walker site of PfRad51. The binding affinity of RI-1 to the dimerization site of PfRad51 was also found to be below the cutoff value. Such differential binding affinity of RI-1 can be explained by the fact that the sequence of the ATP-binding site of PfRad51 and hRad51 are similar but not identical (Fig. S1) (13). Overall, A04, A08, A07, A05, and B02 showed high affinity toward docking at both the sites. Of these five ligands, B02 is commercially available, and hence it was used for the experimental validation of our bioinformatics prediction. The docking of B02 on PfRad51 is depicted in Fig. 1, C and D. The docking of the other top-scoring ligands (A04, A07, and A08) at the Walker A site is shown in Fig. S3A. The docking of the three top-scoring ligands (A04, A08, and A10) at the dimerization face is shown in Fig. S3B.

# B02 binds to PfRad51 and inhibits its ATP hydrolysis and three-strand exchange activities

To study the effect of B02 on PfRad51's activity, we measured the inhibition of ssDNA-dependent ATPase activity and strand-exchange activity of PfRad51 in the presence of B02. Our docking study has predicted that B02 binds at the Walker A motif of Rad51, a site for ATP binding (Fig. S3A). To test this prediction, we have done binding assays using a fluorescence quenching experiment. PfRad51 has a single tryptophan residue (Trp-170) that, when excited at 295 nm, emits fluorescence with an emission wavelength maximum at 332 nm (Fig. S3C). In the presence of increasing concentrations of B02, a dose-dependent quenching of the intrinsic fluorescence was observed (Fig. S3C). From the Stern-Volmer plot, the association constant  $(K_a)$  value was calculated as 0.8  $\mu$ M<sup>-1</sup> (Fig. 2A). As ATP is the natural substrate that binds to the Rad51 protein, we have also calculated the  $K_a$  value of ATP binding, which was determined as 0.22  $\mu$ M<sup>-1</sup>. Thus, the association of B02 with PfRad51 is greater than the association of ATP and PfRad51. We have used radicicol as a negative control in our experiment as it did not show any quenching of the intrinsic fluorescence of the PfRad51 protein.



Table 1 Binding affinities of docked ligands (in -kcal/mol) A = 3LDA,  $B = 3LDA_MIN$ , C = 1SZP, and  $D = ITASSER_AUTO$ .

	Walker A site				Walker adjacent site			Dimerization site				Dimerization adjacent site						
Ligand	A	В	С	D	SUM	Α	В	С	SUM	A	В	С	D	SUM	Α	В	С	SUM
A03	-6.6	-6.6	-7.1	-7.3	-27.6	-6.6	-7.1	-6.4	-20.1	-7.8	-7.8	-8	-8.8	-32.4	-6.6	-7.1	-7.6	-21.3
A04	-8.9	-7.8	-8.8	-8.6	-34.1	-8.9	-7.2	-7.6	-23.7	-8.8	-9.4	-10.1	-9.4	-37.7	-8.9	-8.6	-8.7	-26.2
A05	-7.3	-6.8	-8.7	-7.3	-30.1	-7.3	-7.3	-7.3	-21.9	-8.6	-8.4	-8.4	-8.8	-34.2	-7.3	-6.6	-7.5	-21.4
A06	-6.5	-6.7	-7.3	-7.5	-28	-6.5	-6.3	-6.7	-19.5	-7.5	-7	-7	-8.4	-29.9	-6.5	-6.7	-7.1	-20.3
A07	-8.7	-7.3	-9.2	-7	-32.2	-8.7	-7.6	-9	-25.3	-9.7	-8.7	-8.5	-9.4	-36.3	-8.7	-8.1	-8.5	-25.3
A08	-8.3	-7.7	-9.3	-7.9	-33.2	-8.3	-7.6	-7.6	-23.5	-7.9	-11	-8.2	-10.9	-38	-8.3	-8.1	-8.7	-25.1
A09	-5.9	-6.2	-7.7	-5.7	-25.5	-5.9	-6.2	-6.1	-18.2	-7.1	-6.8	-6.4	-7.1	-27.4	-5.9	-6.9	-7	-19.8
A10	-6.8	-6.8	-7.7	-6.9	-28.2	-6.8	-7	-7.2	-21	-7.6	-8.3	-7.8	-8.8	-32.5	-6.8	-7.6	-8.1	-22.5
A11	-6.5	-6.2	-6.9	-7.2	-26.8	-6.5	-6.3	-6.2	-19	-7.4	-7.2	-7.5	-8.2	-30.3	-6.5	-6.8	-7.5	-20.8
A12	-6.7	-6.3	-7.8	-6.8	-27.6	-6.7	-6.6	-6.6	-19.9	-7.6	-7.1	-7.8	-7.1	-29.6	-6.7	-6.7	-7.7	-21.1
A13	-7.4	-6.4	-8.1	-6.2	-28.1	-7.4	-7	-7.1	-21.5	-7.3	-7.5	-7.2	-8.5	-30.5	-7.4	-6.4	-7	-20.8
A14	-6.7	-6.1	-8.7	-6.4	-27.9	-6.7	-7.3	-6.8	-20.8	-7	-7.6	-6.9	-8.9	-30.4	-6.7	-6.5	-6.7	-19.9
A15	-6.7	-5.4	-8.3	-6.4	-26.8	-6.7	-7.2	-6.8	-20.7	-6.7	-7.3	-7.1	-8.8	-29.9	-6.7	-6.4	-6.7	-19.8
ATP	-7.2	-7.1	-8.6	-8.4	-31.3	-6.7	-6.8	-6.5	-20	-7.3	-7.4	-7.5	-7.7	-29.9	-6.7	-6.5	-6.8	-20
B01	-8.6	-7.7	-7.9	-6.7	-30.9	-6.8	-6.7	-6.2	-19.7	-7	-6.7	-6.9	-7.4	-28	-6.8	-7.1	-6.9	-20.8
B02	-7.7	-7.2	-8.8	-7.5	-31.2	-7.7	-5.8	-6.9	-20.4	-7.8	-8.1	-7.8	-8.6	-32.3	-7.7	-7.4	-7.5	-22.6
B04	-6.4	-6.4	-8.2	-5.5	-26.5	-6.4	-6.2	-6.4	-19	-7.4	-7.1	-7	-7.4	-28.9	-6.4	-7.3	-6.9	-20.6
B05	-6.1	-7.1	-7.1	-7.2	-27.5	-6.1	-5.8	-6.1	-18	-6.6	-6.9	-6.9	-7.3	-27.7	-6.1	-6	-6.9	-19
RI-1	-6.3	-5.7	-7.4	-5.7	-25.1	-6.3	-6.3	-5.9	-18.5	-7	-6.8	-6.9	-7.7	-28.4	-6.3	-7.1	-6.7	-20.1
RI-2	-6.6	-6.8	-8.4	-6.7	-28.5	-6.6	-6.1	-6.6	-19.3	-7.9	-7.2	-7.4	-8.9	-31.4	-6.6	-7.2	-7	-20.8

Because ATP binding is a prerequisite for the ATP hydrolysis activity of Rad51, we hypothesized that B02 might inhibit the ATPase activity of PfRad51. We performed the ATPase assay with purified PfRad51 proteins in the presence of varying concentrations (0.01–40  $\mu$ M) of B02, and we measured the percent activity by taking the activity of PfRad51 in the absence of any inhibitor as 100%. We observed a sharp decline in the ATPase activity of the protein with an increasing concentration of B02 (Fig. 2A). To ascertain whether such an inhibitory effect is specific to B02, we included two more chemical compounds, namely RI-1 and radicicol, and we investigated their effect on the ATPase activity of PfRad51. RI-1 has previously been found to inhibit the strand-exchange activity of hRad51 (10). However, radicicol has been reported to bind to the Bergerat fold and inhibit the ATPase activity of Hsp90 and TopoVIB proteins (14). In our experiments, RI-1 exhibited moderate inhibition to the ATPase activity of PfRad51 (Fig. 2A). This finding is consistent with our docking study, which predicted a weaker binding affinity of RI-1 with PfRad51. However, radicicol did not show any inhibitory effect to the ATPase activity of PfRad51 (Fig. 2B). This corroborates well with the prediction that radicicol does not bind to PfRad51 (data not shown). Thus, radicicol has acted as a negative control in our experiment. To obtain the IC<sub>50</sub> value of B02 inhibition on the ATPase activity of PfRad51, we have plotted the percent inhibition of the ATPase activity in the presence of various concentrations of B02. The IC<sub>50</sub> of PfRad51 inhibition by B02 was determined to be 8.48  $\mu$ M (Fig. 2C). We further investigated the effect of B02 on the three-strand

exchange activity of PfRad51 using circular single-stranded  $\varphi$ X174 DNA and linear double-stranded  $\varphi$ X174 DNA as substrates. As observed earlier (8), PfRad51 generated the intermediate joint molecules at the end of 30 min and the product nicked circular DNA at the end of 90 min (Fig. S3D). However, in the presence of B02, a dramatic inhibition of the product formation was observed in the presence of 20  $\mu$ M B02 (Fig. S3E). The IC<sub>50</sub> of such inhibition was determined to be 7.96  $\mu$ M (Fig. 2D). In a previous study, the IC<sub>50</sub> of B02 against hRad51-mediated strand-exchange reaction was found to be 27.4  $\mu$ M (9). Thus, it seems that B02 has a higher specificity toward PfRad51.

### B02 inhibits the repair of damaged Plasmodium DNA

Because HR is the primary DSB repair mechanism of Plasmodium, we hypothesized that B02 could block the repair of damaged Plasmodium DNA, thereby impairing parasite growth. To this end, we performed an MMS sensitivity assay. MMS creates numerous single-stranded and dsDNA breaks (DSB) in the *Plasmodium* genome (15). Each of the DSBs need to be repaired to ensure parasite survival. Thus, a decrease in parasite survival upon MMS treatment reflects a lack of DSB repair. We observed that parasites that are not exposed to B02 do not show MMS hypersensitivity, suggesting that these parasites are able to repair MMS-induced DSBs. This result is consistent with previous reports (7, 15, 16). Parasites, if treated with lower concentrations of B02 (10 nm), also do not show any significant hypersensitivity to MMS. However, treatment of para-



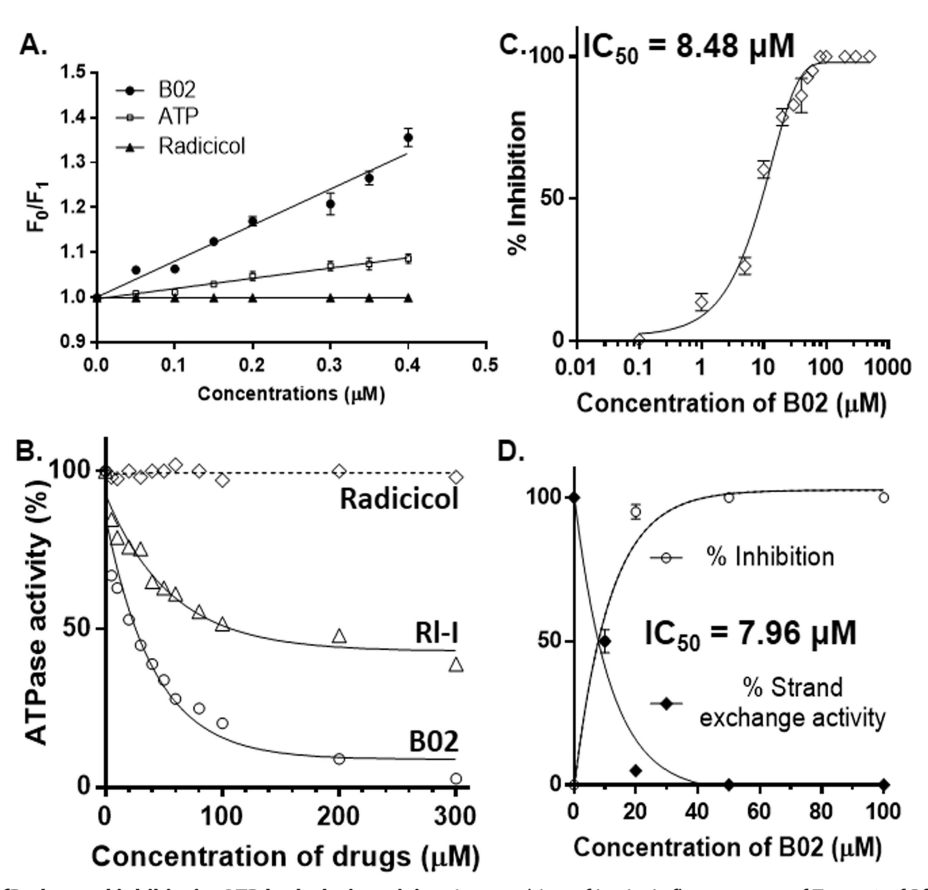


Figure 2. B02 binds to PfRad51 and inhibits its ATP hydrolysis activity. A, quenching of intrinsic fluorescence of Trp-170 of PfRad51 upon B02 binding. Stern-Volmer plots showing the ratio of intrinsic fluorescence ( $F_0$ ) and quenched fluorescence ( $F_1$ ) at different concentrations of ligand binding are shown. The excitation was at 295 nm, and the emission was recorded at 332 nm. Data are the mean  $\pm$  S.D. from three experiments. B, ssDNA-dependent ATPase activity of PfRad51 in the presence of various concentrations of drugs (as indicated on the x axis) as indicated. C, at 200  $\mu$ M ATP concentration and 60  $\mu$ M ssDNA, the activity of 1  $\mu$ M PfRad51 is inhibited by B02 with an IC<sub>50</sub> value of 8.48  $\mu$ M. Mean and standard errors from three independent experiments are plotted. D, three-strand exchange activity of PfRad51 is inhibited by B02 with an IC<sub>50</sub> value of 7.96  $\mu$ M. Mean and standard errors from three independent experiments are plotted. DD, linear dsDNA (substrate); DDC, nicked circular DNA (product).

sites with higher concentrations of B02 (100 nm to 10  $\mu$ M) results in significant hyper-sensitivity toward MMS (Fig. 3*A*). Such effects cannot be scored at a much higher B02 concentration (20 or 50  $\mu$ M) due to excessive toxicity.

To visualize and quantify the persistence of damaged parasitic DNA in the presence of B02, we performed the comet assay. Treatment with MMS creates DSBs, and the extent of damaged DNA can be quantified as a function of the tail length in a comet assay. Under normal circumstances, P. falciparum DNA repair machinery takes between 10 and 20 h to repair DSBs, and as a result, the tail length decreases (15). We treated P. falciparum in vitro culture with 0.05% MMS for 6 h to generate damaged DNA. Because such treatment was not lethal for the parasites (Fig. S4), the parasites were allowed to recover for 40 h in the presence or absence of B02 (10 µM). The extent of damaged DNA was measured at different time intervals (10, 20, and 40 h post-MMS treatment). Comets with long tails were observed upon MMS treatment. Such comets were absent in the control samples. In the absence of B02, the tail length of the comets was found to decrease with time. An initial rapid recovery was observed (at the end of 10 h) followed by a slower recovery. At the end of 40 h, the tail length of the comets was comparable with the untreated control samples (Fig. 3B, upper panel). In the presence of B02, an initial rapid recovery (10 h) was observed, albeit to a lesser extent. Interestingly, no further recovery was observed even until the last time point (40 h) (Fig. 3*B*, *lower panel*). Our data indicate an inefficient repair of damaged parasitic DNA in the presence of B02. Fig. 3*C* illustrates the graphical representation of the mean value of tail length (displacement of the tail's center of mass relative to the center of the head) with a recovery period in the presence and absence of B02. Taken together, our results suggest that B02 inhibits the repair of MMS-induced DSB repair in the parasite genome by inhibiting the activity of PfRad51.

### B02 inhibits the formation of PfRad51 foci upon DNA damage

To gain further mechanistic insights into the mode of action of B02, we investigated whether PfRad51 foci formation is affected in the presence of B02. The cytoplasmic Rad51 proteins enter the nucleus upon DNA damage and oligomerize to form a nucleoprotein filament on ssDNA, which is generated due to the nucleolytic processing of a DSB. Such oligomerization of Rad51 onto the ssDNA represents the accumulation of numerous Rad51 proteins at the broken junctions that appear as foci under a fluorescent microscope (17). These foci are known as Rad51 foci and are crucial for the repair of DSB by the HR mechanism. It should be noted that other DSB repair pro-



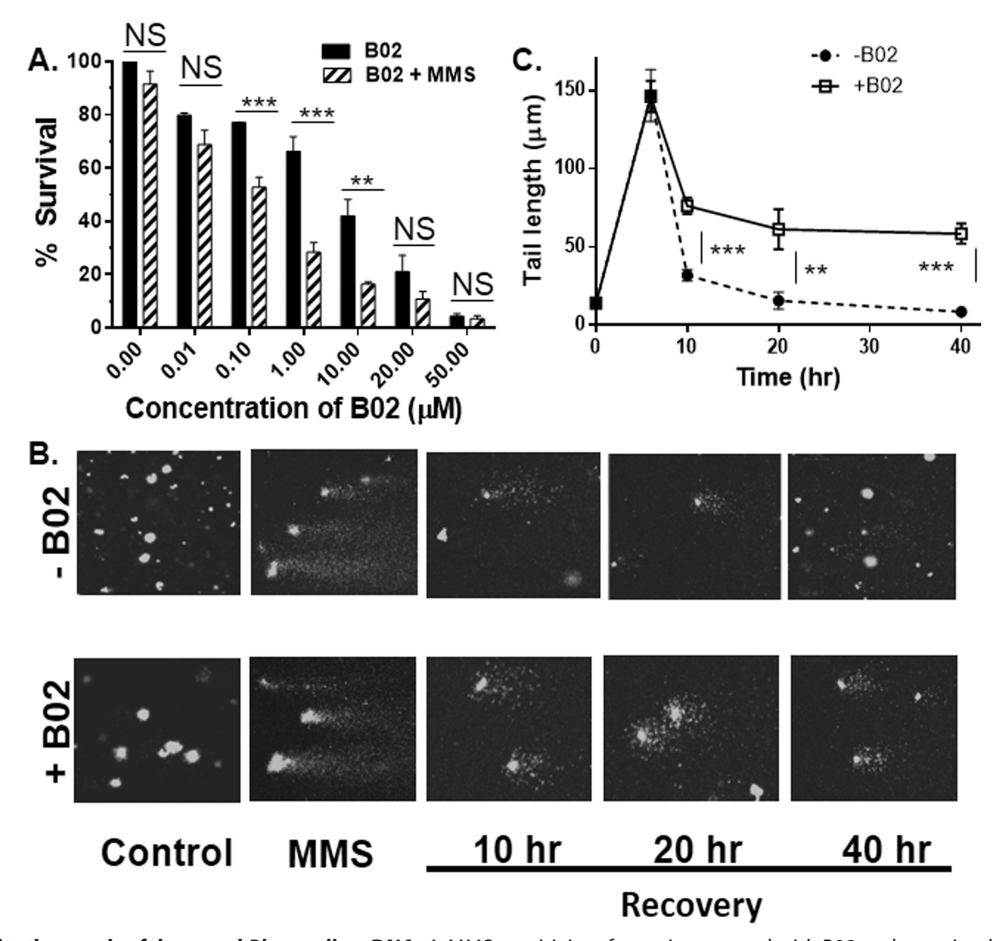


Figure 3. B02 inhibits the repair of damaged Plasmodium DNA. A, MMS sensitivity of parasites treated with B02 as determined by return-to-growth assay. Growth of parasites that are neither treated with B02 nor with MMS represents 100% survival. Error bars indicate S.D. (n = 3 experiments); asterisks indicate values significantly different from the control, as follows: \*\*, p < 0.01; NS, not significant. B, comet assay visualization of the persistence of damaged DNA upon MMS treatment in the presence or absence of B02 (8  $\mu$ M). Control represents undamaged DNA. Shortening of the comet length indicates the repair of damaged DNA during recovery time. C, quantitative measurement of comet tail length at different time points ranging from pre-DNA damage to post-DNA damage. The average tail length of comets at each time point (n > 50) was calculated. The mean of the averages from six independent experiments is plotted. Asterisks indicate values significantly different from the control, as follows: \*\*\*, p < 0.001; \*\*\*, p < 0.01; \*\*, p < 0.01; \*\*NS, not significant.

teins are also recruited at these DNA damaged sites. Formation of such a DNA damage-induced foci has been reported in P. falciparum as well (18). We performed an indirect immunofluorescence assay (IFA) to detect nuclear foci formation of PfRad51. When in vitro cultures of P. falciparum were treated with 0.05% MMS, distinct nuclear foci of PfRad51 were observed (Fig. 4A). No such nuclear focus was observed for the control (untreated) parasites. In the presence of B02, a marked reduction in the number of foci formation was observed upon MMS treatment. Quantification of the data revealed that there is almost an 80% reduction in the number of foci in the presence of B02 (Fig. 4B). As a control, we treated parasites with B02 alone, and as expected, PfRad51 foci were not observed.

Homodimerization of Rad51 is a prerequisite for Rad51 foci formation. The dimerization of Rad51 takes place in a frontto-rear fashion, where the ATP-binding site (the front side) of one monomer lies in close proximity to the dimerization face (the rear side) of the other monomer, also the adenine ring of ATP mediates dimer interactions (19). Because our docking studies also predicted that B02 might inhibit PfRad51 dimerization by blocking the dimerization site, as it competes for the

ATP-binding site, we wanted to explore whether PfRad51 could form homodimers in the presence of B02. To this end, we have employed yeast two-hybrid analysis (Y2H). Earlier, it was observed that PfRad51 was able to interact with itself, and such self-interaction could be detected by Y2H (3). Similar Y2H experiments were performed with both bait and prey vectors having PfRAD51, and a positive interaction was observed as robust growth on triple dropout plates (Sc-Leu-Ura-Ade). Lack of growth on triple dropout plates indicated the lack of interaction. We found out that PfRad51 is able to interact with itself (Fig. 4C) in the absence of B02. However, in the presence of B02 no such interaction was observed. To ascertain that the lack of growth on the triple dropout plates containing B02 is due to the lack of interaction between the bait-protein and the prey-protein (in this case both are PfRad51) and not due to any toxic effect of B02, yeast cells harboring the bait-plasmid and the prey-plasmid were grown in double-dropout plates (Sc-Leu-Ura) in the presence of B02. Robust growth was observed. These results demonstrate that B02 inhibits the homodimerization of PfRad51 proteins. This could be one of the reasons behind the dramatic reduction in the formation of PfRad51 foci in the presence of B02.



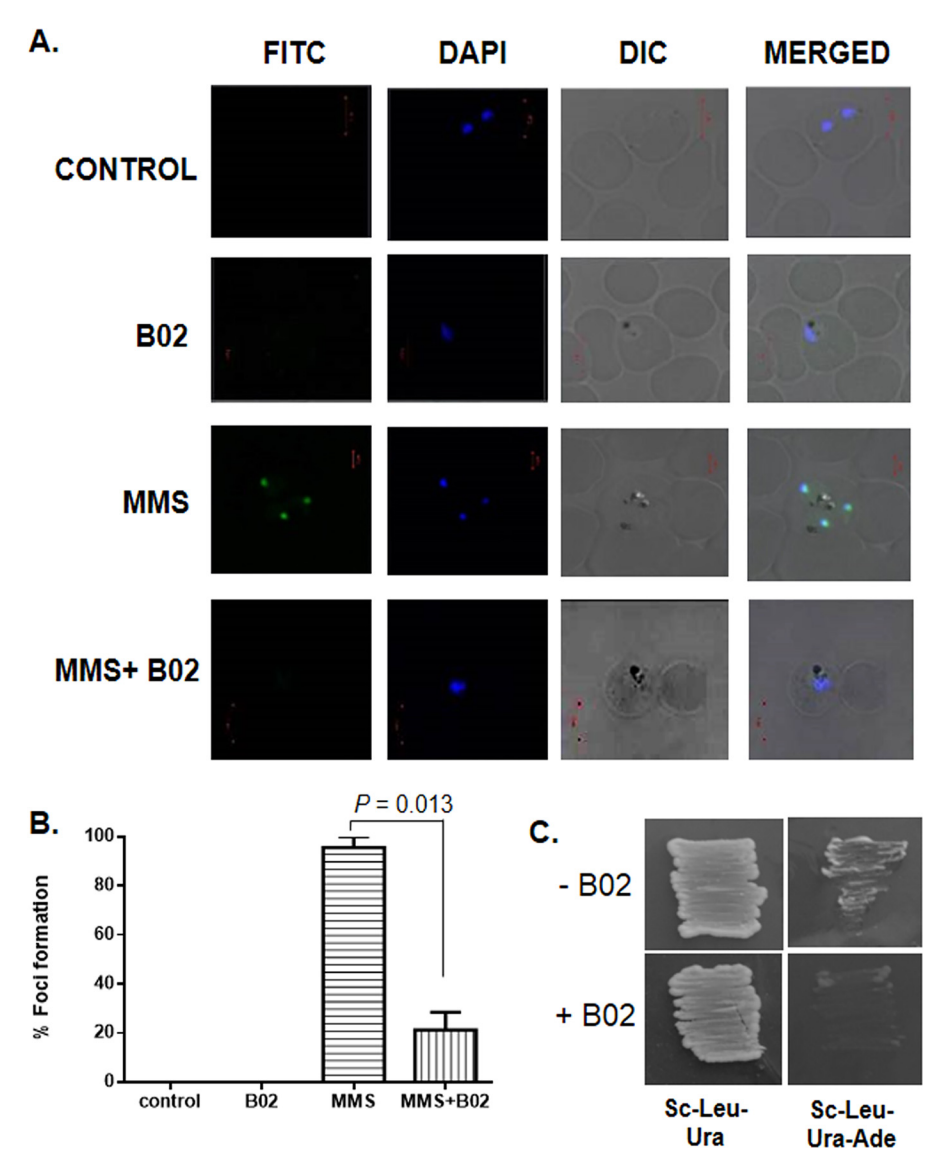


**Figure 4. B02** inhibits the formation of PfRad51 foci upon DNA damage. *A*, IFA displays PfRad51 foci (FITC) upon treatment with the DNA-damaging agent MMS (3rd row). Such foci are not visible in the control cells (untreated with MMS) neither in the presence (2nd row) nor in the absence of 8 μM B02 (1st row). MMS-induced PfRad51 foci formation are inhibited in the presence of 8 μM B02 (4th row). DAPI staining indicates the location of the parasite nucleus. *B*, quantitative analysis of PfRad51 foci formation. Percent of focus formation is defined as the number of infected RBC having PfRad51 foci (FITC-stained) of 100 infected RBC (DAPI-stained). The mean and the standard deviations from three independent experiments are plotted. Two-tailed *t* test was performed to obtain the statistical significance. The *p* value is indicated at the *top. C*, self-interaction of PfRad51 is inhibited in the presence of 8 μM B02. pGADC1 and PGBDUC1 are the parent plasmids encoding the *GAL4* activation domain and DNA-binding domain, respectively. DNA fragments corresponding to the full-length WT *PfRAD51* ORF were fused to the *GAL4* activation domain in pGADC1 and fused to the DNA-binding domain in pGBDUC1. Two-hybrid interactions were tested with yeast strain PJ694A, which bears the *ADE2* gene as one of the reporters. Yeast cells harboring both plasmids were patched on control plates (*SC-Ura-Leu*) as well as experimental plates (*SC-Ura-Leu-Ade*) to test for protein–protein interactions in the absence or in the presence of 8 μM B02 (as indicated at the *bottom*).

# B02 inhibits the intra-erythrocytic developmental cycle (IDC) of P. falciparum

To investigate the effects of B02 on the growth of *P. falciparum*, we monitored the intra-erythrocytic development of the *in vitro* culture of *P. falciparum* 3D7 in the presence of different concentrations of B02. Previous studies have demonstrated that malarial parasites lacking a functional HR mechanism exhibit lower parasitemia during long-term propagation *in vivo*. This finding is suggestive of a failure of the parasite to repair naturally occurring DSBs in its genome, which results in the elimination of such parasites from the parasite population (3). We reasoned that *Plasmodium* recombinase inhibitor B02

should also have a similar effect on the parasite's survival. To test this hypothesis, we treated synchronous trophozoite–stage parasites with different concentrations of B02 and monitored their growth after 48 h by counting the parasitemia from thin smears stained with Giemsa. B02 treatment resulted in a dose-dependent inhibition of parasite growth (Fig. 5A). The dose-response curve yielded an IC $_{50}$  value of 8.25  $\mu\rm M$  (Fig. 5B). To validate this finding, we employed a second method of parasite counting, namely the SYBR Green method. In this method, the fluorescent dye SYBR Green I intercalates between the base stacks of parasite DNA, hence the measured fluorescent intensity is directly proportional to the number of parasites. First, we

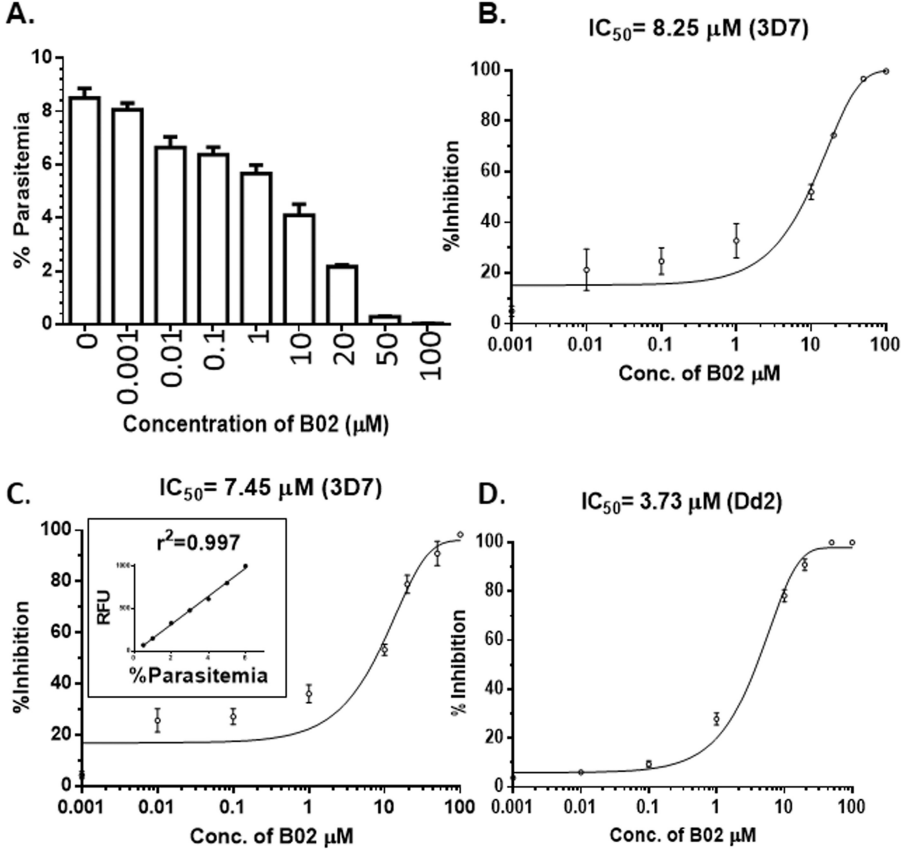


Figure 5. B02 inhibits intra-erythrocytic development of P. falciparum. A, synchronous trophozoite stage 3D7 cultures were grown for 48 h in the presence of various concentrations of B02 (as marked on the x axis). After 48 h, percent of parasitemia of different cultures was counted. The mean and standard deviations from three parallel experiments are plotted. B, inhibition of parasite growth at various concentrations of B02 is plotted to obtain the IC<sub>50</sub> value. Growth of P. falciparum 3D7 strain was monitored by the Giemsa staining method. Parasite growth in the absence of B02 is considered as zero inhibition. Mean and standard deviations from three independent experiments are plotted. C and D, inhibition of growth of P. falciparum 3D7 and Dd2 as measured by SYBR Green I method. C, inset, depicts the standard curve of parasitemia versus SYBR Green I fluorescence intensity.

plotted the relative fluorescence intensity versus the parasitemia to obtain a standard curve. The correlation coefficient was found to be very high ( $r^2 = 0.997$ ). We observed a similar dosedependent inhibition of the parasite growth. The IC<sub>50</sub> value was determined to be 7.45  $\mu$ M (Fig. 5C). To investigate whether B02 could inhibit the growth of other strains of P. falciparum, we tested the effect of B02 on the in vitro culture of one of the drug-resistant strains of P. falciparum, namely Dd2. We found out that B02 inhibits the IDC of Dd2 as well (IC $_{50}$  = 3.73  $\mu$ M) (Fig. 5D). We also investigated the toxic effects of B02 in two mammalian cell lines: mouse cell line MEF and human cell line HepG2, and we observed that B02 has a killing effect against these cell lines with an IC $_{50}$  value of 18.2 and 11.93  $\mu$ M, respectively (Fig. S5). Thus, the selectivity of B02 action toward P. falciparum is found to be much higher when compared with the mammalian cell lines (Table 2). The selectivity indexes for different parasite strains are found to vary between 2 and 5.

### Inhibitory effect of B02 on IDC of P. falciparum can be potentiated by DHA and CQ

To further investigate the anti-parasitic effects of B02, we used three well-established anti-malarial drugs, namely ART, CQ, and PY. Because ART causes DSBs in the *Plasmodium* genome (20), we predicted that the inhibitory effect of B02 could be potentiated in the presence of ART. We have used

Table 2 IC<sub>50</sub> of B02 in different P. falciparum strains as compared with mammalian cell lines

Strain/cell line	$IC_{50}$ (mean $\pm$ S.D.)	Selectivity index
	$\mu$ M	
3D7	$7.45 \pm 0.89$	2.44
Dd2	$3.73 \pm 0.35$	4.88
HepG2	$11.93 \pm 0.23$	1.52
MÊF	$18.2 \pm 0.7$	1

DHA as an ART derivative throughout our experiments. We observed that in the presence of 60 nm DHA (the IC<sub>50</sub> concentration against 3D7 strain), the action of B02 is potentiated by 2.86-fold (Table 3). Similar potentiation (2.85-fold) was observed in Dd2 strain in the presence of 65 nm DHA (the  $IC_{50}$ concentration against Dd2 strain). A more dramatic potentiation was observed in the presence of CQ. In the presence of 26 nm CQ in 3D7 strain and 72 nm CQ in Dd2 strain, 9- and 5.2fold potentiation of B02 was observed. Interestingly, the presence of PY did not result in any potentiation of B02 in either strain. This observation underscores the specificity of DHA and CQ in the potentiation of B02 action.

We wanted to investigate whether the potentiation of B02 activity by DHA could alter the selectivity of the drug toward the parasite strains. We have treated the mammalian cell lines (MEF and HepG2) with varying concentrations of B02 in the



Table 3
IC<sub>50</sub> of B02 in combination with other anti-malarial drugs

Strain	Combination of drugs	$IC_{50}$ (mean $\pm$ S.D.)	Potentiation factor
		μм	
3D7	B02 (alone)	$7.45 \pm 0.89$	1
	B02 (DHA) <sup>a</sup>	$2.6 \pm 0.2$	2.86
	B02 (CQ) <sup>b</sup>	$0.82 \pm 0.04$	9
	B02 (PY) <sup>c</sup>	$7.59 \pm 0.38$	0.98
Dd2	B02 (alone)	$3.73 \pm 0.35$	1
	B02 (DHA) <sup>d</sup>	$1.31 \pm 0.05$	2.85
	B02 (CQ) <sup>e</sup>	$0.72 \pm 0.07$	5.2
	B02 (PY) <sup>f</sup>	$3.85 \pm 0.4$	0.97

<sup>&</sup>lt;sup>a</sup> IC<sub>50</sub> concentration of DHA in 3D7 strain was used.

**Table 4**IC<sub>50</sub> of B02 in combination with DHA in different *P. falciparum* strains as compared with mammalian cell lines

Strain/cell line	IC <sub>50</sub> (mean ± S.D.)	Selectivity index
	$\mu$ M	
3D7	$2.6 \pm 0.2$	3.12
Dd2	$1.31 \pm 0.05$	6.19
HepG2	$7.6 \pm 0.43$	1.06
MÊF	$8.12 \pm 0.6$	1

presence of 60 nm DHA and determined the IC $_{50}$  value of B02 in such combination assays. We observed that B02 has greater selectivity for the parasite strains when combined with DHA than when administered alone. For the 3D7 strain, the selectivity of B02 in combination with DHA was found to be 3.12 (Table 4) as opposed to 2.44 when B02 was administered alone. For the multidrug-resistant strain Dd2, the selectivity index was found to be 6.19 in combination therapy (Table 4)  $\it versus$  4.88 for B02 alone.

### B02 lowers the IC<sub>50</sub> value of DHA and CQ in synergistic ways

We wanted to investigate the interactions between DHA and B02. Because DHA causes DSBs in the Plasmodium genome, and HR is the main mechanism to repair such breaks in malarial parasites, we predicted that inhibition of HR mechanism by B02 would render the parasites more sensitive toward DHA action. We have determined the IC<sub>50</sub> of DHA in our experimental setup. To this end, we have treated synchronous trophozoite stage parasites with different concentrations of DHA for 48 h followed by parasite quantification by the SYBR Green method. We observed dos-dependent inhibition of parasite growth, and the IC<sub>50</sub> value was determined to be 59.7 nm. When similar experiments were performed in the presence of IC<sub>50</sub> concentrations of B02 (8  $\mu$ M), a dramatic decrease of 15.34-fold in the  $IC_{50}$  value was observed (3.89 nm) (Table 5). Similarly, B02 also potentiated the anti-malarial activities of CQ by 8.33-fold (Table 5). We sought to investigate whether such interactions of DHA or CQ with B02 are synergistic or additive in nature. For that we performed a fixed-ratio drug combination assay. The mean FIC values derived from the dose-response curve for each combination are compiled in Table 6. The sum of FICs is plotted in isobolograms (Fig. 6). The isobologram demonstrates that the profound effect of B02 on the anti-malarial action of DHA is synergistic (Fig. 6, A and B). Similarly, the interaction

**Table 5**IC<sub>50</sub> of DHA and CQ in combination with B02

Strain	Combination of drugs	IC <sub>50</sub> (mean ± S.D.)	Potentiation factor
		пм	
3D7	DHA (alone)	$59.7 \pm 3.27$	1
	DHA (B02) <sup>a</sup>	$3.89 \pm 2.04$	15.34
	CQ (alone)	$26.4 \pm 1.98$	1
	CQ (B02) <sup>a</sup>	$3.17 \pm 0.47$	8.33
Dd2	DHA (alone)	$64.8 \pm 3.56$	1
	DHA $(B02)^b$	$14.1 \pm 3.06$	4.6
	CQ (alone)	$63.5 \pm 2.33$	1
	$CQ$ $(B02)^b$	$9.8 \pm 0.71$	6.48

 $<sup>^</sup>a$  IC  $_{50}$  concentration of B02 in 3D7 strain was used.  $^b$  IC  $_{50}$  concentration of B02 in Dd2 strain was used.

between B02 and CQ is also found to be synergistic (Fig. 6, C and D).

### Discussion

The data presented in this article provide compelling evidence that B02 inhibits DSB repair in P. falciparum. First, it inhibits the ATPase activity of PfRad51, which is important for the product release during HR. Second, by binding at the dimerization site, B02 blocks the dimerization of PfRad51, which is the first step for the formation of the higher-order nucleoprotein filament. Finally, B02 inhibits the formation of the PfRad51 foci at the damaged DNA ends, leading to the persistence of an unrepaired broken DNA. Our findings provide the first "proof of the concept" that parasitic HR pathways can be inhibited to attenuate parasitic growth, and such attenuation works in a synergistic way with two of the very potent malaria drugs: artemisinin and chloroquine. Our data also demonstrate that the native B02 on its own has a higher selectivity toward PfRad51 compared with hRad51 and is also more potent for inhibiting the growth of malaria parasite compared with the mammalian host. Lead compound optimization might lead to an even better selectivity against PfRad51 compared with hRad51. It could also be possible that certain chemical modifications of B02 might have anti-malarial action at lower nanomolar concentrations. Additionally, it is not necessary to inhibit PfRad51 per se; other key proteins of Plasmodium HR pathway that are less conserved in humans could serve as better targets. For example, the DNA repair nucleases (such as PfalMre11, PfExo1, etc.), or the RecQ helicases (PfBLM and PfWRN) have minimal sequence conservation with their human counterparts. Future experiments might explore the suitability of these DNA repair proteins as potential anti-malarial targets.

B02 and ART potentiate each other's action. This can be explained by the fact that ART creates numerous DSBs in the *Plasmodium* genome (20), and such DSBs can only be repaired by the HR pathways in this parasite. B02 is a potent inhibitor of the *Plasmodium* HR pathway, and it blocks the repair of ART-induced DSBs and thus potentiates the action of ART. B02 and CQ also potentiate each other's action. Currently, we do not have any mechanistic explanations to this. However, two plausible explanations could be as follows. First, CQ inhibits heme polymerization in malarial parasites, thereby generating free radicals that can potentially create DSBs in the parasitic genome. This way CQ may potentiate the action of B02.



 $<sup>^{</sup>b}$  IC<sub>50</sub> concentration of CQ in 3D7 strain was used.

<sup>&</sup>lt;sup>c</sup> IC<sub>50</sub> concentration of PY in 3D7 strain was used.

 $<sup>^</sup>d$  IC $_{50}$  concentration of DHA in Dd2 strain was used.

 $<sup>^</sup>e$  IC $_{50}$  concentration of CQ in Dd2 strain was used.

<sup>&</sup>lt;sup>f</sup>IC<sub>50</sub> concentration of PY in Dd2 strain was used.

Table 6 Mean FIC values of drug combinations

Strain	DHA: B02	FIC <sub>DHA</sub>	FIC <sub>B02</sub>	ΣFIC	CQ: B02	$FIC_{CQ}$	FIC <sub>B02</sub>	ΣFIC
3D7	5:0	1	0	1	5:0	1	0	1
	4:1	0.41	0.12	0.53	4:1	0.57	0.14	0.71
	3:2	0.35	0.27	0.62	3:2	0.39	0.27	0.66
	2:3	0.25	0.50	0.75	2:3	0.21	0.34	0.55
	1:4	0.13	0.67	0.80	1:4	0.14	0.63	0.77
	0:5	0	1	1	0:5	0	1	1
Dd2	5:0	1	0	1	5:0	1	0	1
	4:1	0.74	0.10	0.84	4:1	0.84	0.08	0.92
	3:2	0.63	0.20	0.83	3:2	0.65	0.18	0.83
	2:3	0.46	0.32	0.78	2:3	0.54	0.24	0.78
	1:4	0.34	0.49	0.83	1:4	0.38	0.51	0.89
	0:5	0	1	1	0:5	0	1	1

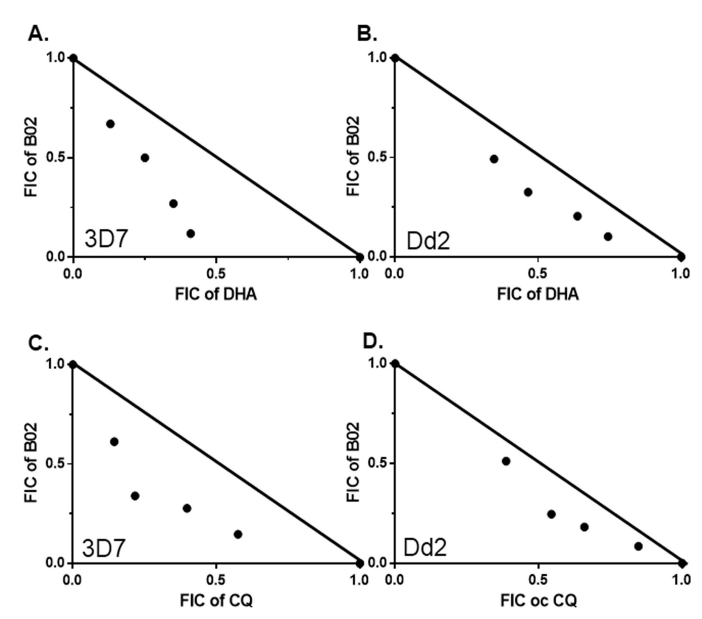


Figure 6. Synergy of DHA and CQ with recombinase inhibitor B02. A and B, isobologram of DHA-B02 combination in 3D7 and Dd2 strains, respectively. C and D, isobologram of CQ-B02 combination in 3D7 and Dd2 strains, respectively. Fixed-ratio drug combination assays were performed. FIC, fraction inhibitory concentration. Each point represents the mean IC<sub>50</sub> of drug combination from three independent experiments. The solid line is plotted between the IC<sub>50</sub> values of each drug when used alone to emphasize the concave nature of the isobolograms.

Although this is a plausible explanation, currently it is not established whether CQ treatment leads to creation of DSBs in parasite genome or not. Future experiments may shed important light into this possibility. A second possibility is that CQ is a well-established inhibitor of the human DNA repair kinase, Chk1. If CQ also inhibits the *Plasmodium* DNA repair kinase, it might lead to an unrepaired DSB, thereby potentiating the action of B02. As of now, the DNA repair kinases remain unidentified in *Plasmodium*. So, it is not known whether CQ also inhibits the Plasmodium DNA damage-response signaling pathway or not. PY, however, inhibits *Plasmodium* dihydrofolate reductase and thereby blocks purine and pyrimidine biosynthesis. Thus it is unlikely to create DSBs in a parasite genome. Probably for that reason we did not observe any synergism between PY and B02.

Our results demonstrated that B02 synergizes ART action. However, the asymmetric concave nature of the isobologram is very interesting, and this can be explained in the following way. By definition, when the combined effect of two drugs is greater than the additive effect of the two, it is known as synergism. In such a case, both drugs must have their individual effects. In contrast, if one of the drugs does not have any effect on its own, but becomes a potent drug only in the presence of the second drug, it is called potentiation (21). As discussed earlier, Plasmodium parasites encounter numerous DSBs that are generated spontaneously during their normal course of propagation, and such breaks are usually repaired by the HR. Parasites lacking a functional HR mechanism fail to mend such DSBs thereby succumbing to death (22). Similarly, if selected parasites are treated with B02, then such parasites cannot repair DSBs, and they also meet the same fate. Moreover, ARTs have multiple targets: DNA, proteins, membrane lipids, and possibly several other uncharacterized cellular targets. As mentioned earlier, activated ARTs create DSBs, and in most cases such DSBs are repaired by the efficient HR pathway of the parasite (unless the number of DSBs is too overwhelming for the parasite to repair). Thus, it is unlikely that ART-mediated parasite deaths are primarily due to the generation of DSBs. It is probably due to other cellular damages caused by ART. As our model suggests (Fig. 7) in the case of B02 and ART interactions, the DSBs created by the ARTs remain unrepaired as the PfRad51-mediated HR mechanism is inhibited by B02, and such unrepaired DSBs lead to parasite death. Thus, B02 potentiates the action of ART as far as the unrepaired DSB-mediated parasite killing is concerned. Therefore, in the absence of B02, ARTs kill parasites by damaging other cellular targets, and in the presence of B02, ARTs kill parasites by damaging the DNA as well. Thus, of the many types of cellular damages that ARTs create, only one of them (namely DSB) can be synergized by B02, explaining the asymmetric nature of the concave isobologram.

Whole-genome sequencing of ART-resistant mutant strains reveals that there are sequence polymorphisms in 38 Plasmodium genes between ART-sensitive strains and ART-resistant strains. Interestingly, no such polymorphism has been found in genes that are predicted to be involved in the HR pathway (23, 24). Thus, it is reasonable to propose that the HR pathways of ART-sensitive parasites and ART-resistant parasites are not likely to be different. In other words, B02 might synergize with ART's activity and lower the IC50 value of ART even in the ART-resistant parasite strains. This hypothesis can be experimentally tested in the future. We have noticed that the multidrug-resistant strain Dd2 is more sensitive to B02 than that of the sensitive strain 3D7. Currently, we do not have any mechanistic insights into this finding. However, one likely



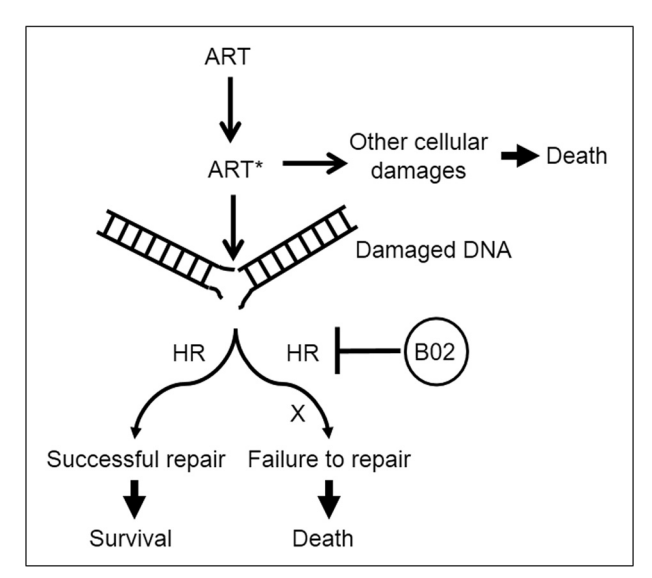


**Figure 7. Model of parasite killing by the combination of ART and B02.** ART is activated by Fe<sup>2+</sup> source within the parasite to generate activated ART\*, which creates DNA double-strand breaks and several other cellular damages (protein alkylations, membrane lipid peroxidation, etc.). DSBs are repaired by PfRad51-mediated HR pathway leading to survival of parasites. In the presence of B02, the parasitic HR mechanism is blocked resulting in unrepaired DSBs that eventually lead to parasite death. Similarly, the other kinds of cellular damages if remaining unrepaired also lead to parasite death. However, this second process of parasite killing is independent of B02 action.

explanation could be that the strain Dd2 carries mutations in 12 DNA repair genes (25); thus, it may have a less efficient DNA repair mechanism.

In addition to serving as a potential anti-malarial chemical compound, B02 can also be used as a chemical knockout strategy to explore the role of PfRad51 in *Plasmodium* biology. For example, it will now be possible to investigate whether or not PfRad51 is involved in the diversification of *var* gene sequences by carrying out recombination between closely related, yet non-identical *var* genes. Such studies will throw important lights into our understanding of antigenic variation, a potent immune evasion strategy of the parasite.

### **Experimental procedures**

### Materials

We have used dihydroartemisinin (DHA) as an artemisinin derivative (ART). DHA, B02, RI-1, and radicicol were purchased from Sigma. DHA, B02, and RI-1 were dissolved in DMSO. Radicicol was dissolved in ethanol.

### Parasite culture

*P. falciparum* 3D7 or Dd2 cultures were maintained in RPMI 1640 medium supplemented with 1% albumax and 0.005% hypoxanthine in human erythrocytes with 5% hematocrit at 37 °C as described earlier (2).

### ATP hydrolysis assay and three-strand exchange assay for PfRad51

Recombinant PfRad51 protein was expressed and purified as described earlier (3). We measured the ATPase activity of PfRad51 in the presence of BO2, RI-1, and radiciol by using EnzChek phosphate assay kit (Molecular Probe) as described

earlier (26). Briefly, the enzyme (2 μM PfRad51 protein) was incubated with a fixed concentration of the substrate (200  $\mu$ M ATP) and  $\varphi$ X174 ssDNA (60  $\mu$ M) in the presence or absence of varying concentrations of individual inhibitors, and the formation of the product (P<sub>i</sub>) was measured. The following concentrations of the inhibitors were used in our assay: B02 (3, 6, 13, 15, 18, 20, 24, 27, 35, 40, 50, 100, 200, and 300  $\mu$ M); RI-1 (5, 10, 20, 30, 40, 50, 60, 80, 100, 200, and 300 μM); radicicol (0.1, 10, 100, and 300  $\mu$ M). ATPase activity of PfRad51 determined in the absence of any inhibitor was taken as 100%, and accordingly, the percent inhibition values were calculated for various concentrations of the inhibitors. For determination of the IC<sub>50</sub> value, the ATPase activity of PfRad51 1 μM enzyme was incubated with various concentrations of B02 (ranging from 0.1 to 1000  $\mu$ M). The data were plotted in a semi-log graph to determine the IC<sub>50</sub> value with the help of the GraphPad Prism software. Three-strand exchange assays were performed as described earlier (8). Briefly,  $\varphi X174$  ssDNA (5  $\mu$ M) and linear double-stranded  $\varphi$ X174 DNA (15  $\mu$ M) were incubated with 1  $\mu$ M PfRad51 in the presence of B02 (10, 20, 50, and 100  $\mu$ M) or DMSO. Formation of nicked circular dsDNA product at 90 min was measured from the band intensity using ImageJ software. The product formation in the absence of B02 was taken as 100%, and accordingly, the percent inhibition values were calculated for various B02 concentrations. The date obtained from three independent experiments was plotted to determine the IC<sub>50</sub> value.

### Fluorescence quenching assay for ligand binding to PfRad51

To study the selective binding of B02 with PfRad51 protein, an intrinsic fluorescence spectra of the protein was recorded using the Jasco FP-8500 spectrofluorometer. Briefly, 1 µM PfRad51 protein in phosphate buffer was taken in a quartz cuvette with a 1-cm path length, and the excitation wavelength of 295 nm was used. The emission spectra of PfRad51 protein was recorded in both the absence and presence of B02. The maximum fluorescence emission at 332 nm wavelength was recorded for PfRad51 ( $F_0$ ) and in the presence of varying B02 concentrations (0.05 to 0.4  $\mu$ M) ( $F_1$ ). A blank run (0.1 M phosphate buffer with vehicle) was subtracted from each spectral reading. The ratio of fluorescence intensities  $(F_1/F_0)$  was calculated at every drug concentration. A Stern-Volmer plot was plotted taking the mean value from three independent experiments, and the association constant  $(K_a)$ , which is the slope of the graph, was determined.

### Inhibition of P. falciparum in vitro culture by B02

Highly synchronous P. falciparum cultures of the trophozoite stage were treated with various concentrations of B02 (1 nm to 100  $\mu$ m) for 48 h. The percent of parasitemia was measured by two independent methods, Giemsa staining method and SYBR Green-I—based assay. For the Giemsa staining method, thin smear slides were prepared, fixed with methanol, and stained with Giemsa solution and for counting the number of parasitized erythrocytes in random, adjacent microscopic fields equivalent to about 12,000 erythrocytes under oil immersion. The slides were counted by two independent scientists. The SYBR Green-I—based parasite quantification was performed as



described previously (27). Briefly, 100  $\mu$ l of *in vitro* culture was taken in 96-well plates containing an equal volume of lysis buffer having a SYBR Green reagent (20 mm Tris-HCl (pH 7.5), 5 mм EDTA, 0.008% saponin, and 0.08% Triton X-100) and was incubated at room temperature in the dark for 1 h. Fluorescence intensities were measured with the multimode reader (Spectramax m2e) at excitation and emission wavelengths of 485 and 530 nm, respectively. Each assay was repeated three times for reproducibility. Corrected fluorescent readings were obtained by subtracting the background readings of the culture without parasites. The 50% inhibitory concentration (IC<sub>50</sub>) of B02 was determined by plotting the concentration of the drug versus the percent inhibition on a semi-log graph by using GraphPad Prism.

The MEF cell line and human liver cell line (HepG2) were cultured in a culture medium of Dulbecco's modified Eagle's medium (Gibco), supplemented with 10% fetal bovine serum (Gibco), 0.5 mg/ml gentamicin (Sigma), and incubated at 37 °C in a humidified atmosphere of 5% CO<sub>2</sub>. Following treatments with various concentrations of B02 for the stipulated times, the cells were collected by trypsinization and enumerated the number of viable and dead cells by trypan blue (Sigma) dye exclusion method using a hemocytometer under microscope.

### Interaction of B02 with DHA or CQ by fixed-ratio isobologram method

To determine the interactions between different drug combinations, synchronous P. falciparum cultures of the trophozoite stage were used. For the determination of the IC<sub>50</sub> of DHA, parasite cultures were incubated in the presence of various concentrations of DHA (0.1 nm to 1  $\mu$ m) for 48 h followed by parasite quantification by SYBR Green-I based method. The  $IC_{50}$ value was taken from a semi-log plot of percent inhibition versus concentrations of DHA using GraphPad Prism. Similarly, the IC<sub>50</sub> of CQ was also determined. Fixed ratio of drug combination was performed as mentioned (28, 29). Briefly, in combination assay DHA/CQ and B02 were combined in four fixed ratios (4:1, 3:2, 2:3, and 1:4). Approximately 8-fold  $IC_{50}$  concentrations of each compound were taken as 100% so that the IC<sub>50</sub> of the individual compound falls in between the third and fourth of a 2-fold serial dilution. The effect of each of the drug combinations (along with their 2-fold serial dilutions) on the intra-erythrocytic development of the parasite was assayed in triplicate in a flat-bottom 96-well plate. Each experimental well contained a total volume of 200  $\mu$ l of medium with or without drug and 1% parasitemia with 5% hematocrit. After seeding the wells, plates were incubated at 37 °C for a 48-h asexual cycle, followed by estimation of a parasite count by the SYBR Green I-based method. The IC<sub>50</sub> value for each combination of drugs was identified by plotting the semi-log graph by using GraphPad Prism software. The FIC for each drug was determined by using the equation FIC =  $IC_{50}$  of drug in mixture/ $IC_{50}$ of drug alone. The interaction between B02 and DHA was identified by using the FIC values of both drugs using Equation 1.

 $\Sigma$ FIC = (IC<sub>50</sub> of DHA in mixture/IC<sub>50</sub> of DHA alone)

+ (IC<sub>50</sub> of B02 in mixture/IC<sub>50</sub> of B02 alone)

The isobologram was prepared by using GraphPad Prism software.  $\sum$ FIC <1 represents synergism;  $\sum$ FIC  $\ge$ 1 and <2 represent additive interaction; and  $\sum FIC \ge 2$  represents antagonism. Similar equation was used for CQ and B02 combination.

### Inhibition of the repair of damaged DNA in the presence B02

For determining the IC<sub>50</sub> of B02 upon treatment with DNAdamaging agent MMS, the cultures were divided into two equal parts. One part was treated with 0.005% MMS for 6 h followed by washing off MMS and returned to growth in complete medium containing various concentrations of B02 (as mentioned earlier) for one generation (48 h). The second aliquot of the culture was maintained in the presence of B02 without prior treatment with MMS. The culture without MMS and B02 treatment acted as the positive control.

### Comet assay

The extent and recovery of DNA damage were assessed by alkaline comet assay. Briefly, synchronous trophozoite parasites were treated with 0.05% MMS for 6 h. Higher concentration of MMS was used in this assay to create numerous DSBs in the parasite genome so that they can be easily visualized on the gel. For measuring the viability of the parasites due to the MMS treatment, an aliquot of the culture was returned to growth in fresh culture medium without MMS, and the parasitemia were determined after 48 h as described elsewhere (7). For performing comet assay, after the treatment the washed parasites were returned to growth for 40 h in the presence or absence of B02 (8  $\mu$ M). Parasites were harvested at different time points (at 0 h and after 10, 20, and 40 h). Alkaline comet assays were performed with saponin-lysed parasites as described earlier (20). The comets were visualized using a laser scanning confocal Microscope (Carl Zeiss). From each sample the extent of DNA damage and tail migration (horizontal distance from the end of the head to the end of the tail) was calculated using Comet Assay IV software. Quantification of data were done by using GraphPad Prism software.

### **IFA**

IFA of parasites were performed according to the protocol described elsewhere (18). Briefly, parasite cultures pre-treated with B02 (8  $\mu$ M) for 12 h were divided into two parts. One part was treated with 0.05% MMS for 6 h, and the other part remained untreated. Similarly, parasite cultures that were not pre-treated with B02 were also treated with MMS. As a control, parasites that were neither treated with B02 nor with MMS were also analyzed. Cold methanol-fixed slides were treated with anti-PfRad51 antibody (1:100 dilution) followed by incubation with anti-rabbit IgG (FITC-conjugated) (1:200 dilution). Parasite nuclei were stained with DAPI (10 µg/ml) and visualized using a laser-scanning confocal microscope (Carl Zeiss). Parasite samples not treated with MMS acted as the "no DNA damage control." Parasite samples treated with B02 but not with MMS were also used as a control to demonstrate that B02 treatment per se does not induce DNA damage.

### Yeast two-hybrid analysis

Yeast two-hybrid analysis was performed as described earlier (3). Briefly, the strain NRY13 (3) was grown in Sc-Leu-Ura



medium with or without B02 (8  $\mu$ M) up to mid-log phase. To ensure the presence of the bait and the prey plasmid, cells were patched on an Sc–Leu–Ura plate with or without B02. To score for protein–protein interaction, cells were also patched on an Sc–Leu–Ura–Ade plate with or without B02 and allowed to grow for 72 h.

### **Bioinformatics analysis**

Homology model of PfRad51 protein was generated by using offline tool MODELLER (30), as well as the most widely used on-line server I-TASSER (31). Homology models of Rad51 were developed from the X-ray crystal structures of yeast Rad51 (PDB (32) codes 1SZP (33), 3LDA (34), 1XU4 (35), 1PZN (36), and Rad A (PDB code 2ZUC (37). Best models were selected based on the C-Scores in I-TASSER and DOPE Score in MODELLER. However, for further analysis only I-TASSER models were selected because the large gaps in the template X-ray structures of Rad51 could not be modeled efficiently in MODELLER. Models were viewed in PyMOL (38). Models were analyzed using MolProbity (39). To rectify finer issues, a short partially constrained molecular dynamics simulationbased energy minimization was run using the YASARA Minimization Server (http://www.yasara.org/minimizationserver. htm)4 (40). This analysis allowed us to obtain the final relaxed structures which are ready for docking studies.

Most of the ligands were obtained from the ZINC Database (41), as ready to dock 3D models with different bond types at different pH environments. Ligands, A04 and B01, were obtained as 2D models from NCBI PubChem and converted to 3D structures on the PRODRG server (42).

The docking search grid box was defined to encompass residues in and around the ATPase domain of the Rad51 protein models to obtain the most effective binding sites. For docking with Autodock Vina (43), we converted the obtained ligands from mol2 files into respective PDBQT files using MGLTools suite (44). For rigid receptor docking, we converted the protein models into single PDBQT files. For docking flexible residues, we also converted the protein models into a flexible-residue PDBQT file. (Residues set as flexible were the residues of the Walker domain that are well-conserved across different organisms and species.) Because the architecture of AutoDock Vina is such that it allows for variability of results from run to run, we ran the docking calculations a total of three times for both rigid and flexible docking to obtain a more concordant set of results.

In DOCK 6.6 (45), ligand models were fed directly as mol2 files. The protein models, however, needed to be processed. First, a receptor surface is created after removal of all hydrogen atoms from the model. It is then used to identify ligand-binding cavities by generating spheres that fit onto the surface and then by clustering the intersecting spheres. Cluster 3 in the case of PfRad51 was selected for docking as it is present in the ATPase domain of the protein model. The PfRad51 cluster 3 had to be manually trimmed as it encompassed more than the ATPase domain. A box of sufficient size (5 Å in PfRad51) encompassing the cluster was then defined as a docking grid and was pre-

calculated to minimize calculations while docking. Thereafter, docking calculations were run, and the top docked poses for each ligand were generated. The generated poses were then rescored using the AMBER score (46) (GBSA score) function of DOCK 6. This was used to perform short molecular dynamics simulations of the ligand as well as the proximal residues of the protein model to obtain an induced fit of the ligand to the protein (47). The docking protocol was verified by docking ATP, the native ligand of the ATPase domain of PfRad51 protein. We observed binding modes similar to that present in the X-ray structures of yeast Rad51 in the top five docked poses.

*Author contributions*—P. V., D. D., N. S., S. B., and M. K. B. investigation; S. B. and M. K. B. supervision; M. K. B. conceptualization; M. K. B. resources; M. K. B. formal analysis; M. K. B. funding acquisition; M. K. B. writing-original draft.

Acknowledgments—Support from Department of Science and Technology-FIST and University Grant Commission-SAP to the Department of Biochemistry is acknowledged. Computational work incorporated in the paper was carried out at the Department of Biotechnology and funded the Bioinformatics Infrastructure Facility, University of Hyderabad. We thank Mrinnanda Bhattacharya for line editing of the manuscript.

#### References

- World Health Organization. (2015) World Malaria Report 2015. World Health Organization, Geneva, Switzerland.
- Frankenberg-Schwager, M., and Frankenberg, D. (1990) DNA doublestrand breaks: their repair and relationship to cell killing in yeast. *Int. J. Radiat. Biol.* 58, 569–575 CrossRef Medline
- 3. Roy, N., Bhattacharyya, S., Chakrabarty, S., Laskar, S., Babu, S. M., and Bhattacharyya, M. K. (2014) Dominant negative mutant of *Plasmodium* Rad51 causes reduced parasite burden in host by abrogating DNA double-strand break repair. *Mol. Microbiol.* **94**, 353–366 CrossRef Medline
- Stark, J. M., Hu, P., Pierce, A. J., Moynahan, M. E., Ellis, N., and Jasin, M. (2002) ATP hydrolysis by mammalian RAD51 has a key role during homology-directed DNA repair. *J. Biol. Chem.* 277, 20185–20194 CrossRef Medline
- Chi, P., Van Komen, S., Sehorn, M. G., Sigurdsson, S., and Sung, P. (2006) Roles of ATP binding and ATP hydrolysis in human Rad51 recombinase function. DNA Repair 5, 381–391 CrossRef Medline
- Symington, L. (2002) Role of RAD52 epistasis group genes in homologous recombination and double-strand break repair. *Microbiol. Mol. Biol. Rev.* 66, 630 – 670 CrossRef Medline
- Bhattacharyya, M. K., and Kumar, N. (2003) Identification and molecular characterisation of DNA damaging agent induced expression of *Plasmo-dium falciparum* recombination protein PfRad51. *Int. J. Parasitol.* 33, 1385–1392 CrossRef Medline
- 8. Bhattacharyya, M. K., Bhattacharyya nee Deb, S., Jayabalasingham, B., and Kumar, N. (2005) Characterization of kinetics of DNA strand-exchange and ATP hydrolysis activities of recombinant PfRad51, a Plasmodium falciparum recombinase. *Mol. Biochem. Parasitol.* **139**, 33–39 CrossRef Medline
- Huang, F., Motlekar, N. A., Burgwin, C. M., Napper, A. D., Diamond, S. L., and Mazin, A. V. (2011) Identification of specific inhibitors of human RAD51 recombinase using high-throughput screening. ACS Chem. Biol. 6, 628 – 635 CrossRef Medline
- Budke, B., Logan, H. L., Kalin, J. H., Zelivianskaia, A. S., Cameron McGuire, W., Miller, L. L., Stark, J. M., Kozikowski, A. P., Bishop, D. K., and Connell, P. P. (2012) RI-1: a chemical inhibitor of RAD51 that disrupts homologous recombination in human cells. *Nucleic Acids Res.* 40, 7347–7357 CrossRef Medline



<sup>&</sup>lt;sup>4</sup> Please note that the JBC is not responsible for the long-term archiving and maintenance of this site or any other third party hosted site.

- 11. Normand, A., Rivière, E., and Renodon-Cornière, A. (2014) Identification and characterization of human Rad51 inhibitors by screening of an existing drug library. Biochem. Pharmacol. 91, 293–300 CrossRef Medline
- 12. Budke, B., Kalin, J. H., Pawlowski, M., Zelivianskaia, A. S., Wu, M., Kozikowski, A. P., and Connell, P. P. (2013) An optimized Rad51 inhibitor that disrupts homologous recombination without requiring Michael acceptor reactivity. J. Med. Chem. 56, 254-263 CrossRef Medline
- 13. Bhattacharyya, M. K., Norris, D. E., and Kumar, N. (2004) Molecular players of homologous recombination in protozoan parasites: implications for generating antigenic variation. Infect. Genet. Evol. 4, 91-98 CrossRef
- 14. Chalapareddy, S., Chakrabarty, S., Bhattacharyya, M. K., and Bhattacharyya, S. (2016) radicicol-mediated inhibition of topoisomerase VIB-VIA activity of the human malaria parasite Plasmodium falciparum. mSphere **1,** e00025-15 Medline
- 15. Gopalakrishnan, A. M., and Kumar, N. (2013) Opposing roles for two molecular forms of replication protein A in Rad51-Rad54-mediated DNA recombination in *Plasmodium falciparum*. MBio 4, e00252-13 Medline
- 16. Badugu, S. B., Nabi, S. A., Vaidyam, P., Laskar, S., Bhattacharyya, S., and Bhattacharyya, M. K. (2015) Identification of Plasmodium falciparum DNA repair protein Mre11 with an evolutionarily conserved nuclease function. PLoS ONE 10, e0125358 CrossRef Medline
- 17. Haaf, T., Golub, E. I., Reddy, G., Radding, C. M., and Ward, D. C. (1995) Nuclear foci of mammalian Rad51 recombination protein in somatic cells after DNA damage and its localization in synaptonemal complexes. Proc. Natl. Acad. Sci. U.S.A. 92, 2298-2302 CrossRef Medline
- 18. Mitra, P., Banu, K., Deshmukh, A. S., Subbarao, N., and Dhar, S. K. (2015) Functional dissection of proliferating-cell nuclear antigens (1 and 2) in human malarial parasite *Plasmodium falciparum*: possible involvement in DNA replication and DNA damage response. Biochem. J. 470, 115-129 CrossRef Medline
- 19. Kokabu, Y., and Ikeguchi, M. (2013) Molecular modeling and molecular dynamics simulations of recombinase Rad51. Biophys. J. 104, 1556-1565 CrossRef Medline
- 20. Gopalakrishnan, A. M., and Kumar, N. (2015) Antimalarial action of artesunate involves DNA damage mediated by reactive oxygen species. Antimicrob. Agents Chemother. 59, 317-325 CrossRef Medline
- 21. Breitinger, H.-G., and Acree, B. (eds) (2012) Drug Synergy-Mechanisms and Methods of Analysis, Toxicity and Drug Testing. InTech. CrossRef
- 22. Klonis, N., Creek, D. J., and Tilley, L. (2013) Iron and heme metabolism in Plasmodium falciparum and the mechanism of action of artemisinins. Curr. Opin. Microbiol. 16, 722-727 CrossRef Medline
- 23. Ariey, F., Witkowski, B., Amaratunga, C., Beghain, J., Langlois, A. C., Khim, N., Kim, S., Duru, V., Bouchier, C., Ma, L., Lim, P., Leang, R., Duong, S., Sreng, S., Suon, S., et al. (2014) A molecular marker of artemisinin resistant Plasmodium falciparum malaria. Nature 505, 50-55 CrossRef Medline
- 24. Miotto, O., Amato, R., Ashley, E. A., MacInnis, B., Almagro-Garcia, J., Amaratunga, C., Lim, P., Mead, D., Oyola, S. O., Dhorda, M., Imwong, M., Woodrow, C., Manske, M., Stalker, J., Drury, E., et al. (2015) Genetic architecture of artemisinin-resistant Plasmodium falciparum. Nat. Genet. 47, 226–234 CrossRef Medline
- 25. Gupta, D. K., Patra, A. T., Zhu, L., Gupta, A. P., and Bozdech, Z. (2016) DNA damage regulation and its role in drug-related phenotypes in the malaria parasites. Sci. Rep. 6, 23603 CrossRef Medline
- 26. Achanta, S. S., Varunan, S. M., Bhattacharyya, S., and Bhattacharyya, M. K. (2012) Characterization of Rad51 from apicomplexan parasite Toxoplasma gondii: an implication for inefficient gene targeting. PLoS ONE 7, e41925 Medline
- 27. Chalapareddy, S., Bhattacharyya, M. K., Mishra, S., and Bhattacharyya, S. (2014) radicicol confers mid-schizont arrest by inhibiting mitochondrial replication in Plasmodium falciparum. Antimicrob. Agents Chemother. 58, 4341-4352 CrossRef Medline
- 28. Fivelman, Q. L., Adagu, I. S., and Warhurst, D. C. (2004) Modified fixedratio isobologram method for studying in vitro interactions between atovaquone and proguanil or dihydroartemisinin against drug-resistant strains of Plasmodium falciparum. Antimicrob. Agents Chemother. 48, 4097-4102 CrossRef Medline

- 29. Tallarida, R. J. (2006) An overview of drug combination analysis with isobolograms. J. Pharmacol. Exp. Ther. 319, 1-7 CrossRef Medline
- 30. Webb, B., and Sali, A. (2014) Comparative protein structure modeling using MODELLER. Curr. Protoc. Bioinformatics 47, 5.6.1-32 CrossRef Medline
- 31. Yang, J., Yan, R., Roy, A., Xu, D., Poisson, J., and Zhang, Y. (2015) The I-TASSER Suite: protein structure and function prediction. Nat. Methods 12, 7-8 Medline
- 32. Berman, H. M., Westbrook, J., Feng, Z., Gilliland, G., Bhat, T. N., Weissig, H., Shindyalov, I. N., and Bourne, P. E. (2000) The Protein Data Bank. Nucleic Acids Res. 28, 235-242 CrossRef Medline
- 33. Conway, A. B., Lynch, T. W., Zhang, Y., Fortin, G. S., Fung, C. W., Symington, L. S., and Rice, P. A. (2004) Crystal structure of a Rad51 filament. Nat. Struct. Mol. Biol. 11, 791-796 CrossRef Medline
- 34. Chen, J., Villanueva, N., Rould, M. A., and Morrical, S. W. (2010) Insights into the mechanism of Rad51 recombinase from the structure and properties of a filament interface mutant. Nucleic Acids Res. 38, 4889 - 4906 CrossRef Medline
- 35. Wu, Y., Qian, X., He, Y., Moya, I. A., and Luo, Y. (2005) Crystal structure of an ATPase-active form of Rad51 homolog from Methanococcus voltae: insights into potassium dependence. J. Biol. Chem. 280, 722-728 CrossRef Medline
- 36. Shin, D. S., Pellegrini, L., Daniels, D. S., Yelent, B., Craig, L., Bates, D., Yu, D. S., Shivji, M. K., Hitomi, C., Arvai, A. S., Volkmann, N., Tsuruta, H., Blundell, T. L., Venkitaraman, A. R., and Tainer, J. A. (2003) Full-length archaeal Rad51 structure and mutants: mechanisms for RAD51 assembly and control by BRCA2. EMBO J. 22, 4566-4576 CrossRef Medline
- 37. Chang, Y. W., Ko, T. P., Lee, C. D., Chang, Y. C., Lin, K. A., Chang, C. S., Wang, A. H., and Wang, T. F. (2009) Three new structures of left-handed RADA helical filaments: structural flexibility of N-terminal domain is critical for recombinase activity. PLoS ONE 4, e4890 CrossRef Medline
- 38. Schrödinger, LLC (2015) The PyMOL Molecular Graphics System, Version 1.7.1.0, Schrödinger, LLC, New York
- Chen, V. B., Arendall, W. B., 3rd., Headd, J. J., Keedy, D. A., Immormino, R. M., Kapral, G. J., Murray, L. W., Richardson, J. S., and Richardson, D. C. (2010) MolProbity: all-atom structure validation for macromolecular crystallography. Acta Crystallogr. D Biol. Crystallogr. 66, 12-21 CrossRef Medline
- Krieger, E., Joo, K., Lee, J., Lee, J., Raman, S., Thompson, J., Tyka, M., Baker, D., and Karplus, K. (2009) Improving physical realism, stereochemistry, and side-chain accuracy in homology modeling: four approaches that performed well in CASP8. Proteins 77, Suppl. 9, 114-122 CrossRef Medline
- 41. Irwin, J. J., Sterling, T., Mysinger, M. M., Bolstad, E. S., and Coleman, R. G. (2012) ZINC: a free tool to discover chemistry for biology. J. Chem. Inf. Model. 52, 1757-1768 CrossRef Medline
- 42. Schüttelkopf, A. W., and van Aalten, D. M. (2004) PRODRG: a tool for high-throughput crystallography of protein-ligand complexes. Acta Crystallogr. D Biol. Crystallogr. 60, 1355-1363 CrossRef Medline
- 43. Trott, O., and Olson, A. J. (2010) AutoDock Vina: improving the speed and accuracy of docking with a new scoring function, efficient optimization, and multithreading. J. Comput. Chem. 31, 455-461 Medline
- 44. Morris, G. M., Huey, R., Lindstrom, W., Sanner, M. F., Belew, R. K., Goodsell, D. S., and Olson, A. J. (2009) AutoDock4 and AutoDockTools4: automated docking with selective receptor flexibility. J. Comput. Chem. 30, 2785-2791 CrossRef Medline
- 45. Lang, P. T., Brozell, S. R., Mukherjee, S., Pettersen, E. F., Meng, E. C., Thomas, V., Rizzo, R. C., Case, D. A., James, T. L., and Kuntz, I. D. (2009) Dock 6: combining techniques to model RNA-small molecule complexes. RNA 15, 1219-1230 CrossRef Medline
- 46. Wang, J., Wolf, R. M., Caldwell, J. W., Kollman, P. A., and Case, D. A. (2004) Development and testing of a general Amber force field. J. Comput. Chem. 25, 1157-1174 CrossRef Medline
- 47. Graves, A. P., Shivakumar, D. M., Boyce, S. E., Jacobson, M. P., Case, D. A., and Shoichet, B. K. (2008) Rescoring docking hit lists for model cavity sites: predictions and experimental testing. J. Mol. Biol. 377, 914-934 CrossRef Medline



A small-molecule inhibitor of the DNA recombinase Rad51 from *Plasmodium* falciparum synergizes with the antimalarial drugs artemisinin and chloroquine Pratap Vydyam, Dibyendu Dutta, Niranjan Sutram, Sunanda Bhattacharyya and Mrinal Kanti Bhattacharyya

J. Biol. Chem. 2019, 294:8171-8183. doi: 10.1074/jbc.RA118.005009 originally published online April 1, 2019

Access the most updated version of this article at doi: 10.1074/jbc.RA118.005009

### Alerts:

- · When this article is cited
- When a correction for this article is posted

Click here to choose from all of JBC's e-mail alerts

This article cites 45 references, 11 of which can be accessed free at http://www.jbc.org/content/294/20/8171.full.html#ref-list-1

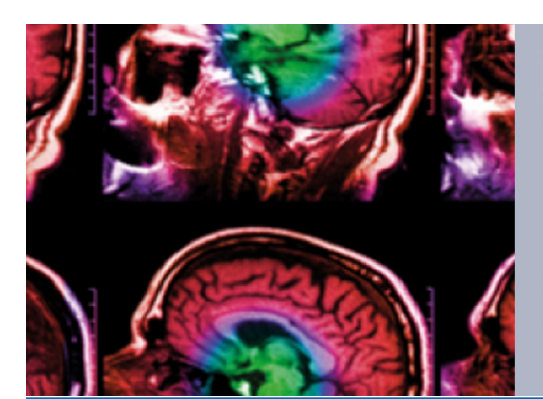


### **PAPER**

### Hollow mesoporous polymer capsules with Dihydroartemisinin and Chloroquine diphosphate for knocking down Plasmodium falciparum infection

To cite this article: Himadri Medhi et al 2018 Biomed. Phys. Eng. Express 4 035006

View the <u>article online</u> for updates and enhancements.



IPEM IOP

Series in Physics and Engineering in Medicine and Biology

Your publishing choice in medical physics, biomedical engineering and related subjects.

Start exploring the collection-download the first chapter of every title for free.

### Biomedical Physics & Engineering Express



RECEIVED 12 December 2017

REVISED

29 January 2018

ACCEPTED FOR PUBLICATION 8 February 2018

PUBLISHED
7 March 2018

### **PAPER**

# Hollow mesoporous polymer capsules with Dihydroartemisinin and Chloroquine diphosphate for knocking down Plasmodium falciparum infection

Himadri Medhi<sup>2</sup>, Somedutta Maity<sup>2</sup>, Niranjan Suthram<sup>3</sup>, Suresh Kumar Chalapareddy<sup>4</sup>, Mrinal K Bhattacharyya<sup>3</sup> and Pradip Paik<sup>1,2</sup>

- School of Biomedical Engineering, Indian Institute of Technology (BHU), Varanasi 220 051, India
- School of Engineering Sciences and Technology, University of Hyderabad, 500 046, India
- <sup>3</sup> Department of Biochemistry, School of Life Sciences, University of Hyderabad, 500 046, India
- Department of Biotechnology and Bio-informatics, School of Life Sciences, University of Hyderabad, 500 046, India

E-mail: paik.bme@iitbhu.ac.in, ppse@uohyd.ernet.in, pradip.paik@gmail.com and paik@uohyd.ac.in

**Keywords:** porous polymer capsules, nanoformulation, antimalarial drugs, *P. falciparum*, temperature clock Supplementary material for this article is available online

### **Abstract**

Plasmodium falciparum is resistant to all antimalarial drugs and a challenge for treatment. With this respect, formulations of antimalarial drugs with polymeric capsules with nanostructure carry a significant signature to suppress the resistance and to kill the Plasmodium falciparum. In this work, idiosyncratic hollow mesoporous polycaprolactone (ihmPCL) capsules were designed through ultrasonic-template synthesis approach with hollow core of dia. ca.  $\sim 450$  nm and shell thickness of ca.  $\sim 30$  nm and pore size of ca.  $\sim 8-9$  nm. Then two formulations of ihmPCL capsules with Dihydroartemisinin (DHA) and Chloroquine diphosphate (CQDP) have been developed. ihmPCL capsules are capable to load 200.0  $\mu$ g of DHA and 18.6  $\mu$ g of CQDP per mg of capsules. With this formulation we can empowered to tune the doses of DHA and CQDP with time and temperature (30 °C–43 °C). It is observed that up to 143.20  $\mu$ g (~71.6%) of DHA and 17.71  $\mu$ g (~95.2%) of CQDP release can be controlled at different essential conditions which further can be sustained for longer period of time. Further, the half-maximum inhibitory concentration ( $IC_{50}$ ) have been investigated with these formulations and calculated to be 66.60 nM and 25.14 nM for DHA and CQDP, respectively in P. falciparum inhibition in vitro. Based on the unique release behaviour of these antimalarial drugs a 'temperature clock' module have been proposed for further accelerate the inhibition rate of P. falciparum infection. In conclusion, the PCL-DHA and PCL-CQDP formulations developed in this work could be effective in knocking down the *P. falciparum* infection and is paramount for treatment of malaria.

### 1. Introduction

Malaria is one of the most life threatening ailment in human which causes annually about 212 million cases and 429 000 deaths across the globe according to WHO [1]. Among the four parasite species i.e., Plasmodium falciparum (*P. falciparum*), Plasmodium vivax, Plasmodium malariae and Plasmodium ovale, responsible for causing malaria in humans, *P. falciparum* is the most deadly one. Many treatment appoaches have come to eradicate *P. falciparum*. Among them the artemisinin-based combination

therapy (ACT), chloroquine (CQDP) undermining malaria control efforts and reversing gains in child survival and vector control are the potent interventions that can reduce malaria. *P. falciparum* genomewide scans suggested that it is more resistant to drugs. Moreover drug resistivity differs from continent to continents [2]. It is also noticed that antimalarial drugs enforce strong selective pressure on *P. falciparum* parasite and leave signature of selection in the parasitic genome [2–4]. It is more concerned that drug resistance in *P. falciparum* spread rapidly. It shows resistance for drug like CQDP, which is used as first-line

drug for treatment in most of the epidemic areas [5]. The presence of Artemisinin resistance has found ≥5 h of parasitic half-life during artesunate monotherapy in Surinam [6]. To the best of our knowledge none of the remarkable vaccination is known till date. Only one research vaccine against *P. falciparum* is known as RTS, S/AS01 and which is in a clinical trial in 7 countries in Africa and has been submitted to the European Medicines Agency under art 58 for regulatory review [1].

New treatment approach of malaria via antimalarial drugs are urgently required due to the increased resistance of P. falciparum against the available treatments. Moreover, extensively used antimalarial drugs like Dihydroartemisinin (DHA) has short life time, low stability and also has low bioavailability [7] in its free therapeutic form. Therefore, acuity of controlling the P. falciparum infection using biodegradable porous polymeric nanocapsules based nanomedicinal approach encapsulating antimalarial drugs has been established in this work. The concept of polymer based nanomedicine and drug delivery vehicles are a recognized approach in the clinic [8, 9] since drugs confined in polymeric nanocapsules increase the stability, bioavailability as well as the effectiveness of the treatment [10, 11]. To date, polyester based poly(D,L-lactic-co-glycolic acid) (PLGA) capsules are used in controlled delivery of malaria drugs due to their biocompatibility and biodegradability [12]. However, PLGA can degrade under hydrolytic conditions due to hydrolysis of its ester group [13]. A polymer with moderate degradation rate could advance the sustained delivery of antimalarial drugs in physiological conditions under periodic enhancement of body temperature. Additionally, encapsulation of antimalarial drugs has become urgency since overdose of these free drugs are very risky as they have numerous side effects e.g., gastrointestinal problems, stomach ache, itch, headache, postural hypertension, nightmares, blurred vision etc. These serious concerns motivate us to design polymer based nanoformulations of essential antimalarial drugs such as DHA (PCL-DHA) and CQDP (PCL-CQDP) with PCL capsules with hollow core and mesoporous shell which can help to circumvent these side effects caused by the inappropriate dosages of the free DHA and CQDP. Recently, rigid block copolymer (PCL-b-MPEG) with artemisinin has been used for cerebral malaria treatment, where, (i) the polymer used was not hollow and mesoporous in structure and (ii) temperature dependent monitoring of doses were not confirmed [14].

In this work, idiosyncratic hollow and mesoporous PCL nanocapsules (ihmPCL) have been synthesized and used for the formulation with DHA and CQDP. Formulated ihmPCL-DHA and ihmPCL-CQDP have been used to prevent the intra erythrocyte *in vitro* growth of *P. falciparum* with monitoring the doses of DHA and CQDP precisely. ihmPCL capsules

have been synthesized through ultra-sonication induced template synthesis approach. Two different sizes of SiO<sub>2</sub> templates have been used to generate the hollow core and porous shell structure. Loading capacities of DHA and CQDP in ihmPCL capsules have been investigated through LASER confocal microscopy and the extent of releases have been investigated through the UV-Vis spectroscopy and time dependent release behaviour and mechanism have been find out through the kinetic study. Temperature dependent release efficiencies have also been studied for the both drugs to tune the release based doses for treatment. Biocompatibility of hollow mesoporous PCL capsules have been checked through the cytotoxicity assay. Finally, nanoformulations are used for the treatment of the P. falciparum infected RBCs in vitro and the inhibition efficiencies have been evaluated through the calculation of  $IC_{50}$  values.

### 2. Materials and methods

### 2.1. Materials

Tetraethyl orthosilicate (TEOS) (98%), ammonium hydroxide (NH<sub>4</sub>OH) (30%), PCL (C<sub>6</sub>H<sub>10</sub>O<sub>2</sub>)n, Dihydroartemisinin (DHA) (99%), chloroquine diphosphate salt (CQDP) (98%), Rhodamine 6 G (95%), RPMI 1640 and Igepal CO-520 were purchased from Sigma Aldrich. Ethanol (98%), acetone (99.5%), isopropanol (99.5%) were purchased from SRL and hydrofluoric acid (HF) (5%) was purchased from Fisher Scientific. RPMI 1640 from Lonza, SyBr green from Invitrogen, Giemsa stain from Sigma, RBC collected from human blood, Parasitemia 3D7 has been cultured in laboratory. All the chemicals were used as received.

### 2.2. Synthesis of SiO<sub>2</sub> NPs

SiO<sub>2</sub> NPs were synthesized followed by Stöber method [15]. In brief, 2 ml of TEOS was added to 30 ml of ethanol and stirred at room temperature (25 °C). Then 1 ml of H<sub>2</sub>O was added to the mixture and left for half an hour under stirring (600 RPM). Then NH<sub>4</sub>OH was added drop wise to the mixture and the whole mixture was kept under vigorous stirring for overnight. The resulting white colloidal solution was centrifuged at 5000 RPM for 10 min and SiO2 NPs were separated and washed thoroughly using dH2O and Isopropyl alcohol mixture to remove the unreacted reactants. Then, SiO<sub>2</sub> NPs were dried at 120 °C. SiO<sub>2</sub> NPs of two different sizes such as, (i) average size of ~10 nm named as SiO<sub>2</sub> NPs-1 (ii) average size of ~450 nm named as SiO<sub>2</sub> NPs-2 were prepared. Sample SiO<sub>2</sub> NPs-2 was prepared taking high concentration of TEOS (5 ml), keeping all other reaction parameters same. It is worth mentioning here that the larger sizes of SiO<sub>2</sub> (SiO<sub>2</sub> NPs-2) have been used to create the hollow core and the smaller sizes particles (SiO<sub>2</sub> NPs1) have been used to create pores on the shell of the polymeric capsules.

### 2.3. Synthesis of solid core-shell polymer NPs

In brief, 50 mg of synthesized SiO<sub>2</sub> NPs-1 was thoroughly dispersed in acetone through ultra-sonication. Then 50 mg PCL (average M<sub>n</sub> 45 000) was also dissolved in acetone at 45 °C. Thereafter, dispersed SiO<sub>2</sub> NPs-1 and dissolved PCL were mixed together. Then, 50 mg SiO<sub>2</sub> NPs-2 was dispersed in 20 ml acetone separately through ultra-sonication and the homogeneous dispersion of SiO<sub>2</sub> NPs-2 was added to the mixture of SiO<sub>2</sub> NPs-1 and PCL under constant stirring at 45 °C. Then the resultant mixture of SiO<sub>2</sub> NPs-1, PCL and SiO<sub>2</sub> NPs-2 was added continuously to a 150 ml (water/surfactant, Igepal CO 50) emulsion under sonication at the feeding rate of 150  $\mu$ l.min<sup>-1</sup>. Finally, the mixture was kept under stirring for 24 h (1000 RPM). The resultant product is core-shell NPs of SiO2 and PCL (PCL-SiO2 NPs) which were collected after repeated washing and centrifugation (at 5000 RPM) followed by drying through lyophilisation. In the core–shell structure SiO<sub>2</sub> is in the core and shell is PCL.

# 2.4. Formation of hollow porous PCL capsules (ihmPCL)

Above synthesized core–shell NPs were treated with HF (1 M solution) for 12 h to etch out the  $SiO_2$  NPs-1 and NPs-2. After 12 h of incubation, the etched core–shell polymeric NPs were centrifuged (at RPM 10 000) to separate the particles from the solution followed by repeated dispersion and washing. Finally the product was collected after freeze drying.

# 2.5. Characterization of SiO<sub>2</sub> NPs, core–shell NPs and mesoporous PCL capsules (ihmPCL)

Solid state crystal structures SiO<sub>2</sub> NPs, core–shell NPs and mesoporous PCL capsules (ihmPCL) were investigated through the XRD (Bruker AXS Model D8 with a Cu K $\alpha$  source,  $\lambda = 1.54$  Å). Particle size and morphology have been confirmed through Scanning Electron Microscopy (SEM) (HITACHI S-3400 N) and high resolution transmission electron microscopy (HRTEM, FEI TECHNAI G2 200 kV S-twin). Surface chemical structure has been investigated through Fourier transform Infrared spectroscopy (FTIR) (Nicolet model Impact-410). Brunauer-Emmett-Teller (BET) method (Micromeritics, TriStar II-3020™ Surface Area and Pore Analyser) was used to calculate surface area and pore size distribution of mesoporous ihmPCL capsules. Thermal stability has been investigated through Thermogravimetric analysis (TGA) (Thermo ONIX Gas lab 300 TGA) and Differential Scanning Calorimetry (DSC) analysis (TA Instrument, DSC Q2000V24.4).

# 2.6. Loading of Rh6G, DHA and CQDP in ihmPCL capsules

The dried ihmPCL capsules were collected and used for loading dye and anti-malaria drugs. The ihmPCL capsules were incubated with Rh6G and DHA, CQDP separately, with a concentration of dye/ drugs to ihmPCL capsules of 1:1 mg.ml<sup>-1</sup> in PBS (pH 7.4). The suspensions were stirred for 1 h and then kept for another 24 h in dark place without stirring. The Rh6G and DHA/CQDP loaded ihmPCL capsules were separated from PBS solution through centrifugation (at 8000 RPM). These loaded particles were then washed three times with PBS to remove the free dye/ drug molecules from the surface of the capsules followed by air drying in dark for further experiments. Fluorescence microscopy images of the samples were acquired with Laser scanning confocal microscopy (Carl Zeiss, Germany, 710 NLO) to check the loading of Rh6G.

# 2.7. Study the DHA and CQDP release kinetics from nanoformulations

PCL-DHA and PCL-CODP formulations were suspended in medium and the release behaviour has been studied. Maintaining a fixed time interval the absorbance of the released drugs in medium was recorded at different temperatures such as 30, 37, 40 and 43 °C using UV-Vis spectrometer and the extent of release of DHA and CQDP were calculated. The extent of release were calculated for 6 h with a fixed time interval and then investigated the kinetics for the release. To study the release kinetics, 0.6 mg of ihmPCL-DHA and ihmPCL-CQDP formulation for each were taken with 5 ml of medium in a cuvette. To calculate the extent of drug release the absorption band at 263 nm for DHA were considered. Following the similar procedure the release kinetics for CQDP were studied by considering absorption band at 260 nm. The release behaviours of the DHA and CQDP from ihmPCL capsules were studied in medium used for cell culture UV-Vis-NIR spectrometer (Perkin-Elmer LAMBDA 750).

# 2.8. Study the release kinetics and diffusion coefficients of ihmPCL-DHA and ihmPCL-CQDP

The release kinetics of DHA and CQDP have been studied using the zero and 1st order model kinetic equations as shown below (equation (1)) and (equation (2)) [16].

Zero order release kinetic equation (equation (1)),

$$Q_t/Q_0 = K_0 \cdot t \tag{1}$$

Where,  $Q_t$  is cumulative amount of drug released at time t,  $Q_0$  is initial amount of drug,  $K_0$  is zero order release constant, t is time in min.

First order release kinetic equation,

$$Q_t/Q_0 = 1 - e^{-kt} (2)$$

where,  $Q_t$  is cumulative amount of drug released at time t,  $Q_0$  is initial amount of drug, k is first order release constant, t is time in min.

The diffusion coefficients  $D_T$  for both DHA and CQDP released from the formulations with four different temperatures have been calculated by using the model equation (equation (3)) [17],

$$Y = \frac{M_t}{M_{\alpha}} = 6 \left( \frac{D_T \cdot t}{\pi \cdot R^2} \right) \tag{3}$$

Where,  $Y = \left(\frac{M_t}{M_{\alpha}}\right)$  is function of the extent of drug released at time t,  $D_T$  is the diffusion coefficient of drug molecules from the hollow-porous polymer capsules at temperature (T) and at time 't', R is the diameter of the pores of hollow-porous polymer capsules.

Where, the diffusion coefficient is defined by the equation (4) below,

$$D_T = \frac{Y^2 \pi \ R^2}{36t} \tag{4}$$

# 2.9. Cell viability analysis of bare ihmPCL capsules in *P. falciparum* culture medium

The *in vitro* cytotoxicity assays of the ihmPCL capsules were carried out in culture medium by taking the different concentrations of unloaded capsules such as 25, 50, 100, 150 and 200  $\mu$ g.ml<sup>-1</sup>. First 500  $\mu$ l of the master solution containing fresh media, RBC and Parasitemia was centrifuged (at 500 RPM for 3 min at RT) and the pellet was used for the study. Working solution of different ihmPCL concentrations were added to the pellet and mixed thoroughly. This step was repeated three times for all concentrations as mentioned above. The master solution without drugs (DHA/CQDP) was taken as control. Finally, all the solutions with different concentrations of ihmPCL capsules, control media and RBC were pipetted into the 96 well plate. The 96 well plate with sample was then incubated in CO<sub>2</sub> incubator for 48 h. After 48 h of incubation, 100  $\mu$ l of lysis buffer containing SYBR green I (Invitrogen) dye was added to each well and further incubated for 1 h at RT in dark. Then absorbance of the cells were recorded using multimode reader. Cytotoxicity of the ihmPCL-DHA and ihmPCL-CQDP nanoformulations with P. falciparum cell line in 96 well plate was studied at 37 °C using a Multimode Reader (SYNERGY H4 HYBRID MULTI-DETECTION MICROPLATE READER).

# 2.10. *P. falciparum* Inhibition study using ihmPCL-DHA and ihmPCL-CQDP formulations

Initially, the effect of ihmPCL-DHA formulation on the *P. falciparum* infected RBC was studied systematically with regulating temperatures and concentration of formulation *in vitro* by taking 2, 5, 10, 20, 50, 100, 200, 500 and 1000 nM concentrations of DHA loaded in ihmPCL capsules. The assays were conducted with the pellet obtained from 1 ml culture

having initial Parasitemia concentration of 1% and haematocrit of 5%. Then 1 ml medium containing different concentrations of ihmPCL-DHA formulations each were added to the pellet. The parasites were allowed to culture for 48 h at 37 °C and finally harvested to make blood smears. Total 1000 number of RBC were taken for each slide to estimate the Parasitemia. Similar experiments were performed by taking ihmPCL-CQDP formulation to study the inhibition of *P. falciparum*. Optical microscope (Zeiss M60-2-0007) has been used to calculate the inhibition.

### 3. Results

# 3.1. Designing ihmPCL capsules: size, morphology and porous structure of nanocapsules

ihmPCL capsules have been synthesized through template synthesis approach as it has been explained in the experimental section using two different SiO<sub>2</sub> templates i.e., SiO<sub>2</sub> NPs-1 (10–15 nm) and SiO<sub>2</sub> NPs-2 (~450 nm) (figures 1(a) and (b)). Initially core-shell structure of PCL- SiO<sub>2</sub> has been designed where the PCL network has been formed surrounding to the SiO<sub>2</sub> NPs-2 core thus formed shell and the smaller SiO<sub>2</sub> NPs-1 particles were entrapped in the network of the shell of PCL (figures 1(c)-(e)). Thus, the larger SiO<sub>2</sub> NPs-2 help to create hollow core at the centre, whereas the smaller particles (SiO2 NPs-1) help to create the mesopores on the polymeric shell of PCL. The average size of the core–shell PCL nanoparticles is found as 470-510 nm in diameter (figures 1(c) and (d)) with the shell thickness of ca. 30-35 nm (figure 1(e)). In figure 1(e) (HRTEM), the entrapped SiO<sub>2</sub> NPs-1 are clearly visible which helps to create the mesopores on the PCL shell. The FESEM micrograph in figures 2(a) and (b) clearly showed the pores on the shell of PCL capsules. The porous nature of the PCL capsules have further been confirmed through BET experiments (figure 3). Further to confirm the porous shell structure and to check the loading capability of small molecules confocal microscopy study was performed and the results have been shown in figures 2(c) and (d). For this study Rhodamine 6 G molecules were loaded. The high intense red emission from the capsules is the evidence for the hollow and porous shell structure of the PCL (figures 2(c) and (d)). Further, the FESEM image (figure 2(e)) is the clear evidence for the hollow nature of the capsules.

Further to check the porous structure, the BJH N2-adsorption-desorption isotherm for the capsules has obtained from the BET experiment and exhibited a type-IV isotherm with a clear hysteresis (figure 3(a)). The nature of the isotherm is the evidence for the porous structure of the PCL capsules. BET surface area for the ihmPCL capsules has also been calculated and found to be 50 m<sup>2</sup>.g<sup>-1</sup>. The hollow core has been created on removal of the bigger SiO<sub>2</sub> NPs-2 templates

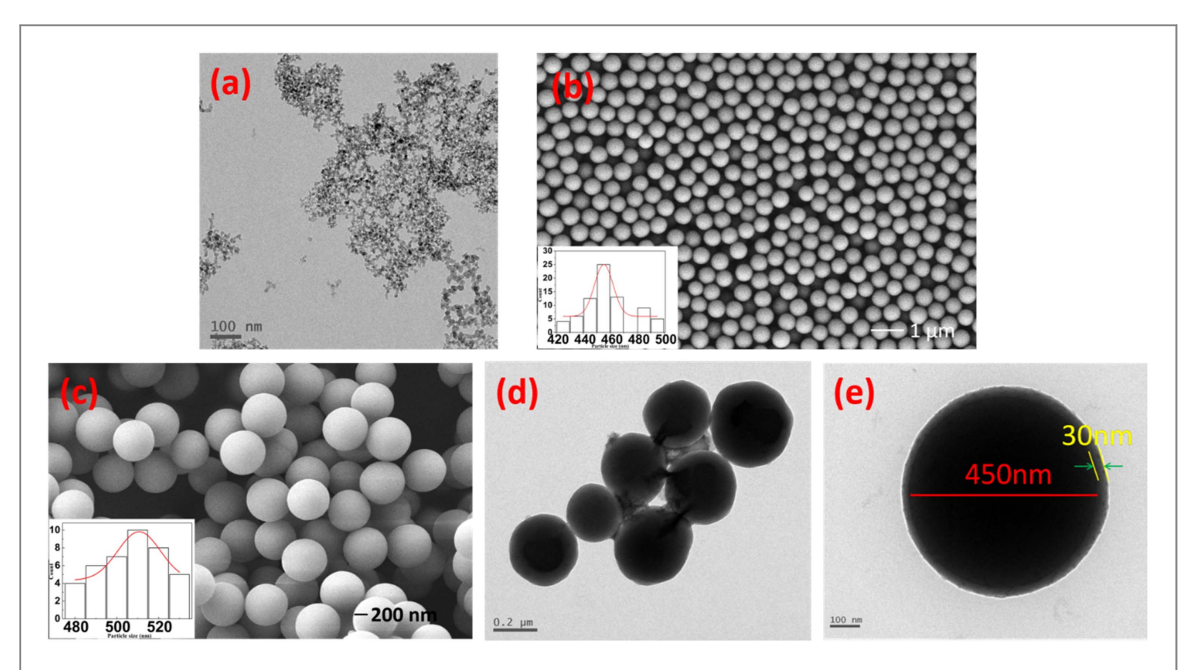


Figure 1. TEM micrograph of (a) SiO<sub>2</sub> NPs-1 (10–15 nm), FESEM micrograph of (b) SiO<sub>2</sub> NPs-2 (450 nm) and (c) core–shell PCL-SiO<sub>2</sub> NPs and TEM micrograph of (d) & (e) core-shell PCL-SiO<sub>2</sub> NPs.

from the core and the porous shell structure created by removing smaller SiO<sub>2</sub> NPs-1 from the core-shell structure of PCL-SiO<sub>2</sub> NPs. From BET, the average pore size is obtained to be in between 4.5 nm to 14.9 nm with different sizes of the pores such as 4.5, 8.7 and 14.9 nm in diameter as it is shown in figure 3(b). The pore size ca. 4.5 nm has been formed due to the micelles size of the surfactant (Igepal CO 50) and the sizes of the pores 8.7 and 14.9 nm have been formed due to the SiO<sub>2</sub>-1 nanoparticles which were entrapped in the shell of the PCL. It is worth to mention that, the shrinkage of the pore size in mesoporous polymeric shell compared to the size of SiO<sub>2</sub> NPs-1 has occurred due to the relaxation of the strain of the PCL chains (viscoelastic nature), once the SiO<sub>2</sub> (NPs-1) particles have been extracted from the shell. On loading of DHA in ihmPCL, the surface area is reduced to 32.2 m<sup>2</sup>.g<sup>-1</sup> since the pores are filled with DHA. Figures 3(c) and (d) are showing the BJH isotherm and pore size distribution profile for the DHA loaded in PCL capsules, respectively. The diminution of area of hysteresis in figure 3(c) compared to the figure 3(a)and the nonappearance of peaks for the pore size distribution (figure 3(d)) are the clear evidences for the loading of DHA in the pores of ihmPCL capsules. Thus it is confirmed that the DHA are loaded in porous and hollow PCL capsules. It can be assumed that the hollow core of the capsule acts as reservoir and the surface mesopores act as the channel for the loading drugs molecules into the core and releasing out from the core ihmPCL capsules.

# 3.2. Surface chemical structure of ihmPCL capsules

From the FTIR results, we have identified the functional groups present on the surface of the SiO<sub>2</sub> NPs, core-shell PCL-SiO2 NPs, ihmPCL (figure 4) and for pure PCL (figure S1 is available online at stacks.iop. org/BPEX/4/035006/mmedia). In mesoporous PCL the absorption band at 2936 cm<sup>-1</sup> arises for C-H (-CH<sub>2</sub>) group of PCL and band arises at 1720 cm<sup>-1</sup> is due to the C=O group of PCL [18]. At 1720 cm<sup>-1</sup> a sharp intense band is appeared due to the presence of – C=O group. It is worth mentioning that chemical structure of PCL before and after formation of capsules remained unaltered (figure S1 and figures 4(b), (c)). For SiO<sub>2</sub> (figure 4(a)), the band appeared at 1112 cm<sup>-1</sup> is for asymmetric vibration of Si-O, at 947 cm<sup>-1</sup> for asymmetric vibration of Si-OH and at 805 cm<sup>-1</sup> for symmetric vibration of Si-O. An intense absorption band at 3375 cm<sup>-1</sup> is appeared due to the stretching of O-H bond of water. Also this band has also cross checked through the 1635 cm<sup>-1</sup> band appeared due to scissor bending vibration of molecular water. None of the characteristic bands which could be for SiO<sub>2</sub> (figure 4(a)) [19-21] have been identified in ihmPCL capsules (figure 4(c)), meant SiO<sub>2</sub> templates have been removed completely from the core-shell structure (i.e. from PCL-SiO<sub>2</sub> NPs) and formed the ihmPCL capsules as it has been shown in the FESEM, and TEM images.

### 3.3. Thermal stability, solid state crystal structure and zeta potential analysis

The complete removal of SiO<sub>2</sub> NPs have further been confirmed through TGA (figure 5) and powder XRD analysis (figure S2). For TGA, all samples SiO2 NPs, pure PCL, core-shell PCL-SiO2 NPs and ihmPCL capsules were heated in the range of 40 °C-1000 °C with heating rate 10 °C min<sup>-1</sup>. TGA thermograms (figure 5) show 15% weight loss occurred in between

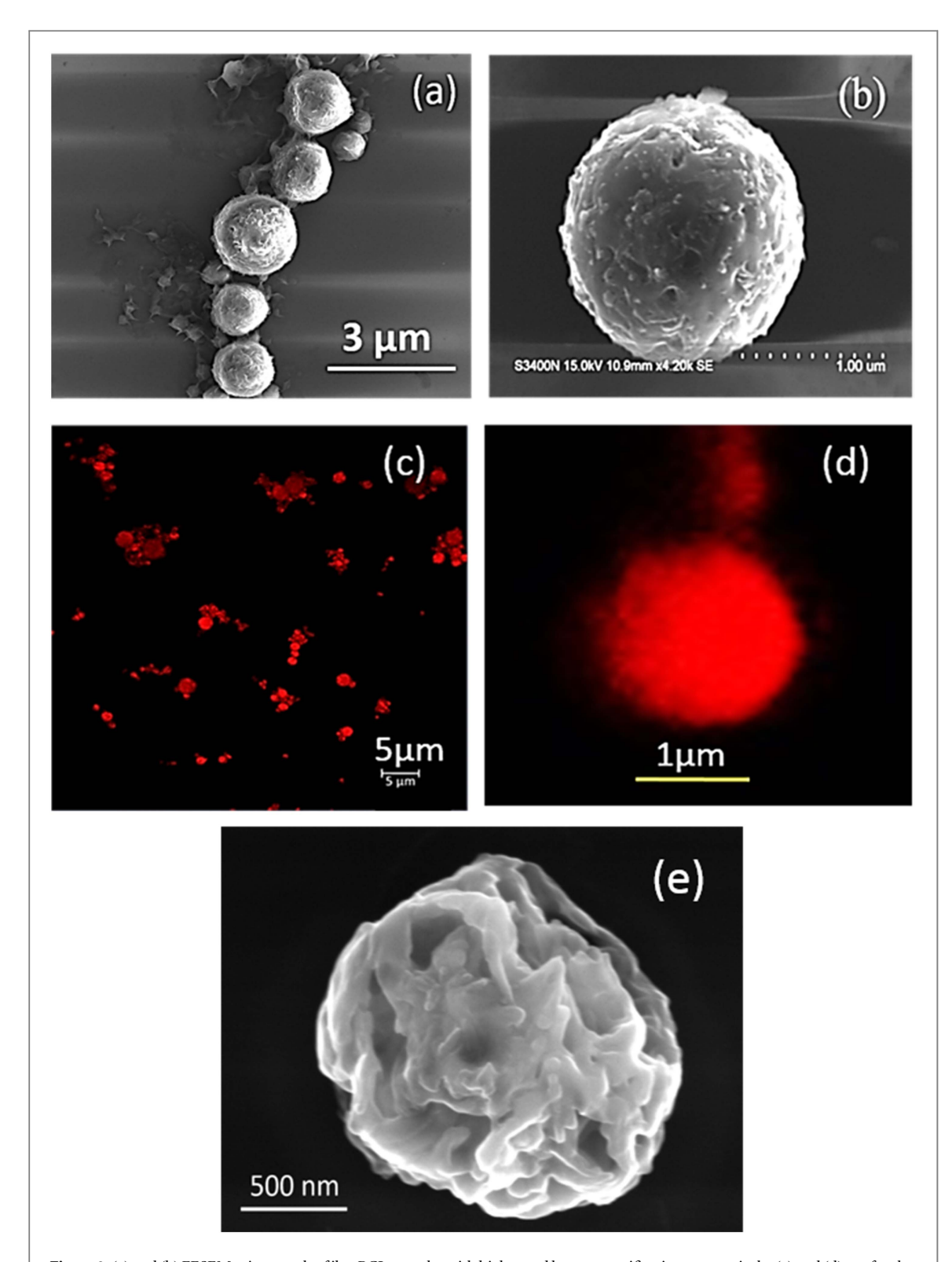
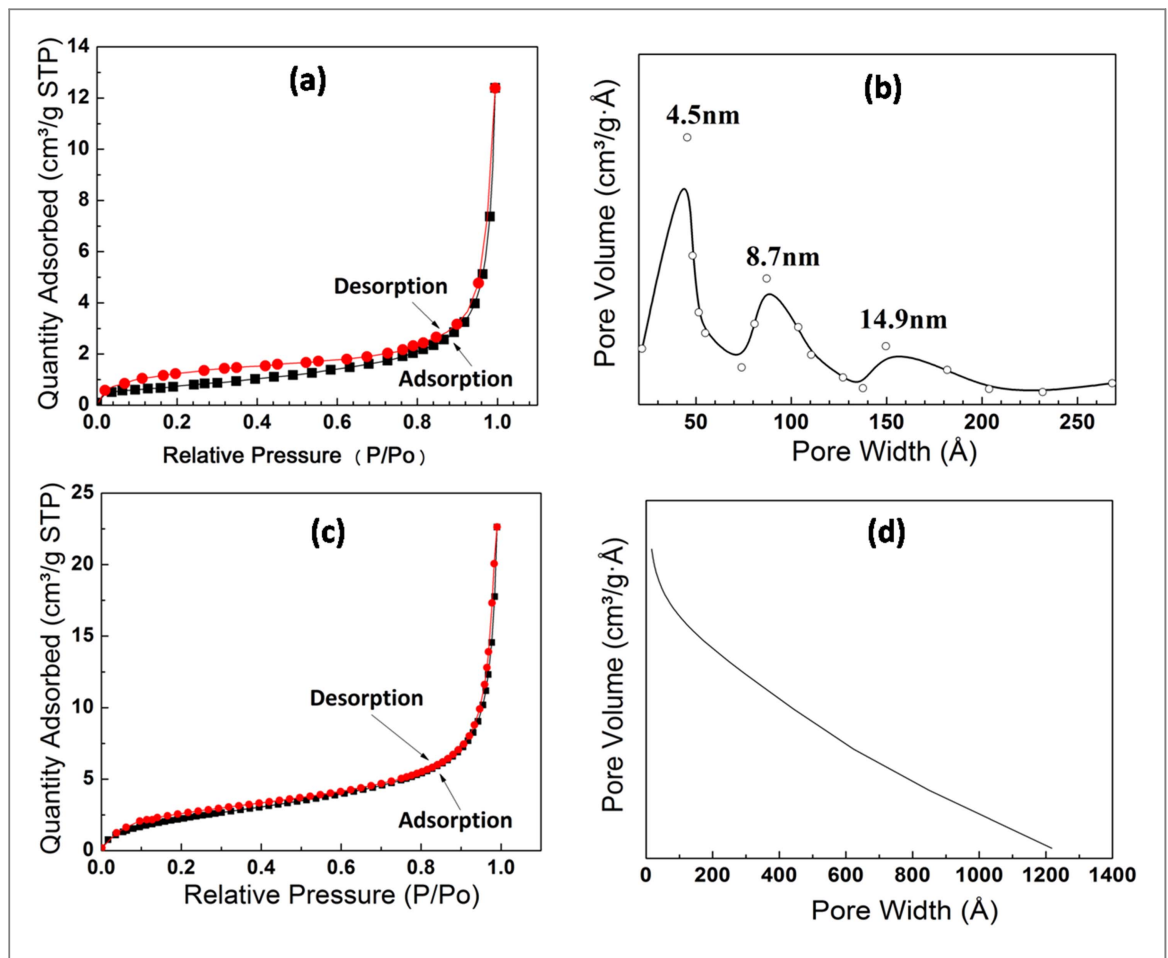


**Figure 2.** (a) and (b) FESEM micrograph of ihmPCL capsules with higher and lower magnifications respectively, (c) and (d) confocal microscopy images of ihmPCL loaded with Rhodamine 6 G at lower and higher magnification, respectively.

50 °C–450 °C due to the loss of free water molecules/moisture from the surface of template SiO<sub>2</sub> and after that region weight remained constant. However, for core–shell PCL-SiO<sub>2</sub> NPs weight loss occurred around 350 °C due to the weight loss of polymer PCL (pure PCL polymer has showed a firm weight loss after 350 °C and continued till 560 °C), after ~450 °C weight became constant due to the presence of SiO<sub>2</sub> in

the core. After removal of  $SiO_2$  the weight loss for ihmPCL capsules started at ~340 °C and continued up to 450 °C due to the complete degradation of PCL. Therefore, the ihmPCL capsules are thermally stable up to 340 °C. From the XRD results (figure S2), it is confirmed that the prepared ihmPCL capsules are semicrystalline in nature. XRD pattern of PCL-  $SiO_2$  NPs and ihmPCL capsules show diffraction peaks at



 $\textbf{Figure 3.} \ \ BET\ results\ (a)\ BJH\ adsorption\ - desorption\ isotherm\ for\ and\ (b)\ pore\ size\ distribution\ of\ ihmPCL\ capsules,\ respectively.\ (c)\ and\ (d)\ BJH\ adsorption\ - desorption\ isotherm\ and\ pore\ size\ distribution\ of\ DHA\ loaded\ capsules,\ respectively.$ 

 $2\theta=21.4^\circ$  and  $23.0^\circ$ , corresponding to the orthorhombic planes (110) and (200) of PCL, respectively [22, 23]. Further, the FTIR and DSC results (figure S3) confirmed that there was no modification on the chemical structure of PCL chain, in PCL-SiO<sub>2</sub> NPs and ihmPCL capsules, rather Tm (melting temperature) shifted little from PCL-SiO<sub>2</sub> nanoparticles (Tm  $\sim$  61 °C) to PCL capsules (Tm  $\sim$  63 °C) due to the rearrangement of the polymer chains during processing. The zeta potential value of hollow porous PCL capsules have been found as  $-30.6\,\mathrm{mV}$  and standard deviation  $\pm 5.93$  (single peak) (figure S4).

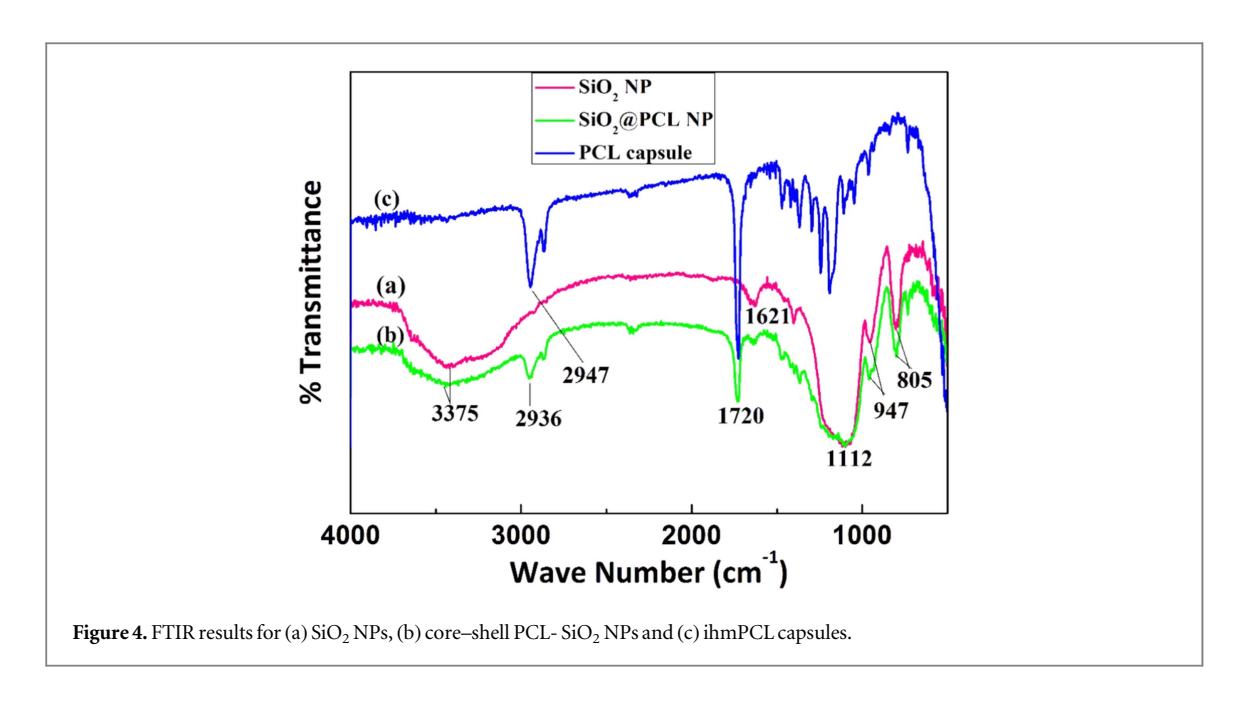
### 3.4. Cytotoxicity study of ihmPCL capsules

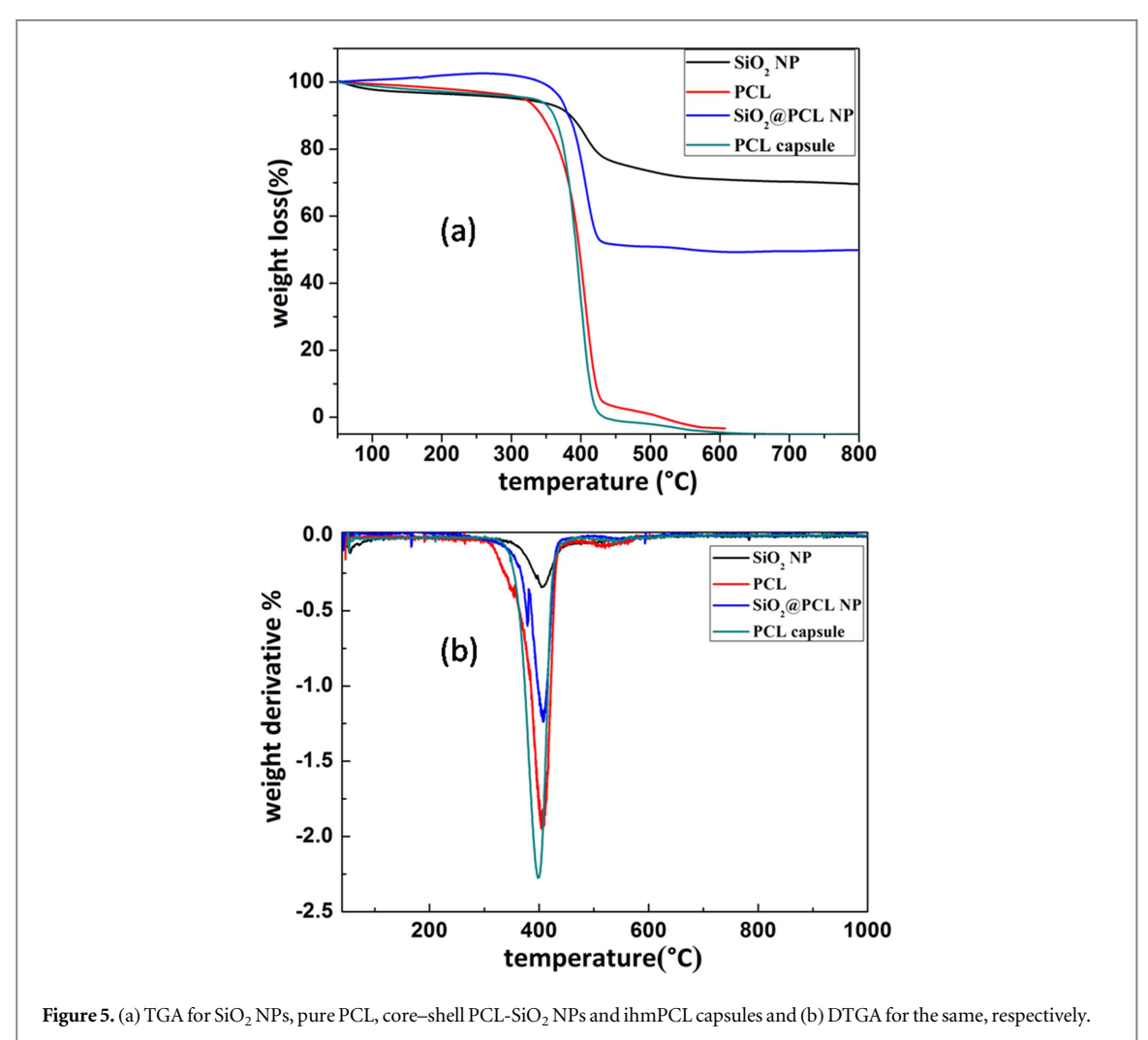
To evaluate the cytotoxicity of the synthesized ihmPCL capsules, it has been treated with parasitic cell line (P. falciparum) (figure 6) for 48 h. A series concentrations of the ihmPCL capsules (25, 50, 100, 150 and 200  $\mu$ g.ml<sup>-1</sup>) have been taken and viability in parasite culture in absence of ihmPCL capsules (taken as control) has also been studied. From the results it is confirmed that drug free ihmPCL capsules are biocompatible in nature, not toxic and they do not have any role in killing the parasites.

# 3.5. ihmPCL capsules facilitate loading and releasing of DHA and CQDP: study the kinetics and diffusion coefficients

It is worth mentioning that, the loading of the DHA/CQDP and dye molecules in ihmPCL capsules is occurred through the diffusion process. The pores present on the polymeric shell act as channel to diffuse the drugs/dye into the hollow core. Effective loading of Rhodamine 6 G dye has been confirmed through the confocal microscopy (figures 2(c) and (d)). A deep red light emission is detected from the Rhodamine 6 G loaded ihmPCL capsules.

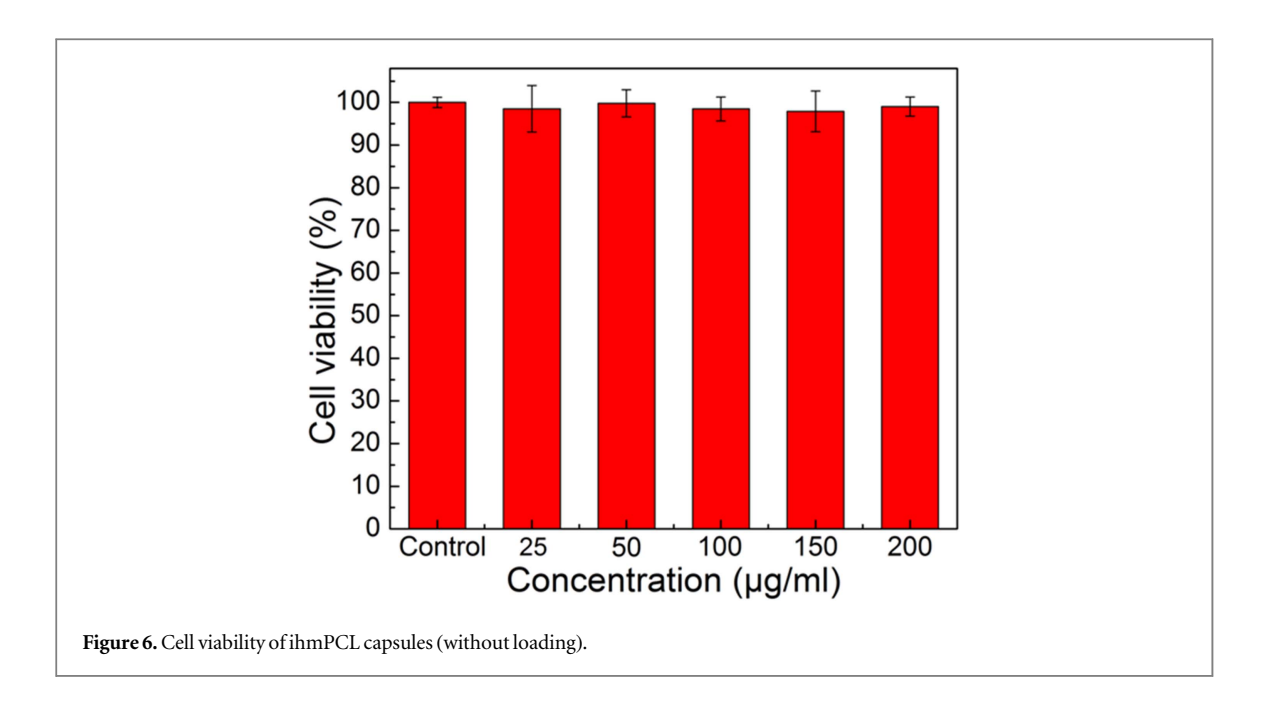
The release profiles of DHA and CQDP and their kinetics have studied with time and temperatures (figures 7(a) and (b)) to correlate with the body temperature. The temperature dependent release of DHA and CQDPA are studied at different temperatures such as 30, 37, 40 and 43 °C, since parasitic infection caused enhancement of body temperature periodically. The results obtained are very interesting as shown in figures 7(a) and (b). It is revealed from these release profiles that with increase in the temperature with time the extent of release of DHA and CQDP also increased. Within 1 h of incubation the percentage of release of DHA from ihmPCL-DHA formulation (200  $\mu$ g per mg of ihmPCL capsule) is found to be

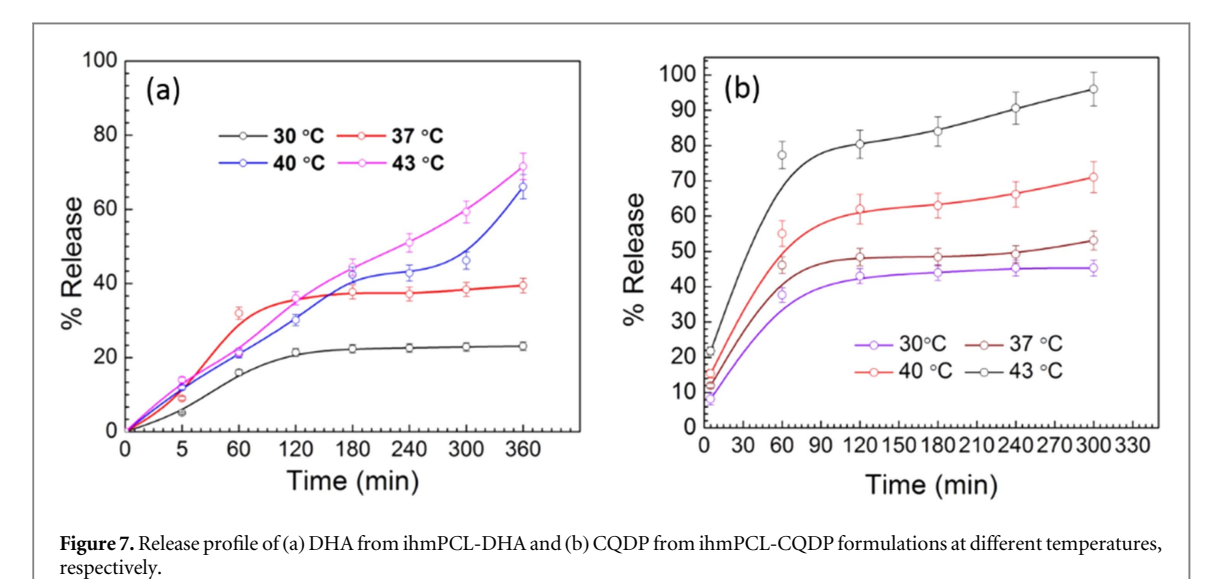




 $16 \pm 0.8$  (%),  $32 \pm 1.6$  (%),  $21 \pm 1.05$  (%),  $21.5 \pm 1.07$  (%) and after 5 h of incubation the percentage of release obtained to be  $23.1 \pm 1.5$  (%),  $39.4 \pm 1.8$  (%),  $66.1 \pm 3.3$  (%),  $71.6 \pm 3.5$  (%) at temperatures 30, 37, 40 and 43 °C, respectively.

Similarly, from ihmPCL-CQDP formulation, within 1 h the percentage of CQDP released,  $41.4\pm2.0$  (%),  $46.1\pm2.3$  (%),  $55.1\pm3.7$  (%) and  $77.3\pm3.8$  (%) for the temperature 30, 37, 40 and 43 °C, respectively, whereas after 5 h the amount of CQDP released for



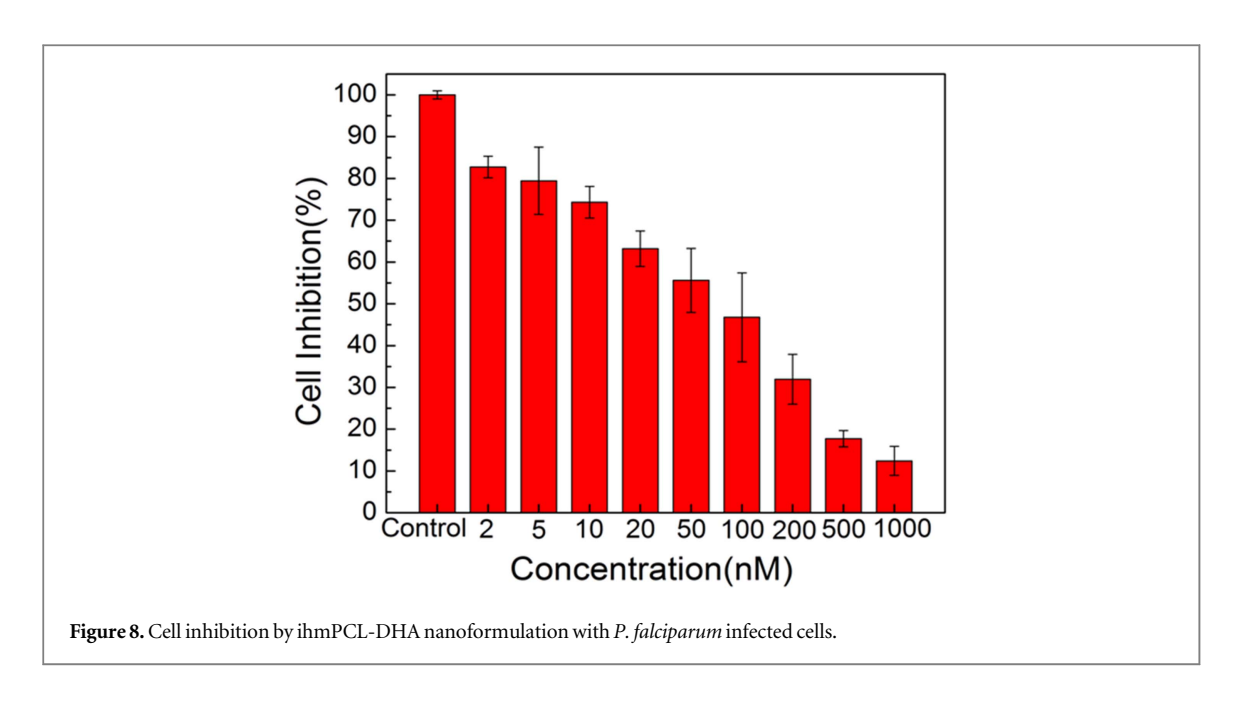


these temperatures obtained to be  $45.3 \pm 2.2$  (%),  $53.1 \pm 2.4$  (%),  $71.4 \pm 4.4$  (%) and  $95.2 \pm 3.8$  (%) of the total loaded CQDP (18.6  $\mu$ g per mg of capsules), respectively.

At lower temperatures, such as at 30 °C and 37 °C, the amount of DHA released from ihmPCL-DHA formulations exhibited a characteristic of first order release kinetics (figure S6) and at higher temperatures such as at 40 °C and 43 °C, drug releases behaviour followed a characteristic of zero order release kinetics (figure S7) in culture medium. To analyses the release kinetics, the experimental data were fitted in both first order and zero order release kinetic equations (equations (1) and (2)) which are shown in supporting file. Whereas, the release of CQDP followed a characteristic of first order release kinetic behaviour (figure S8).

It is observed that the releases of DHA and CQDP are controlled by the temperature dependent

diffusion. Therefore, diffusion coefficients for both DHA and CQDP released from the ihmPCL-DHA and ihmPCL-CQDP formulation, with different temperatures have been calculated and results are shown in tables S1 and S2 at different time interval considering different pore sizes. From the results (tables S1 and S2) we can conclude that the diffusion coefficient values of drug release depend on the time, temperature and pore size of ihmPCL capsules. Further, from the tables S1 and S2 it is obvious that the diffusion coefficient values are increased with the gradual increase in the pore size (from 4.5 nm to 14.9 nm) and temperatures (30 °C to 43 °C). For example (from table S1), as pore size increases from 4.5 nm to 14.9 nm, the diffusion coefficient value for DHA release increases from  $5.02 \times 10^{-19}$  to  $31.68 \times 10^{-19}$  at a fixed temperature (37 °C after 5 min). Similarly, with increase in temperature from 30 °C to 43 °C the diffusion coefficient increases from  $1.26 \times 10^{-19}$  to  $4.77 \times 10^{-19}$  (after



1 h, for 4.5 nm pore). Whereas with increase in time, from 5 min to 5 h, the diffusion coefficient decreases for all cases. As example, for 37 °C the diffusion coefficient after 5 min of release was  $5.02 \times 10^{-19}$ , whereas after 5 h of release the value obtained to be  $1.45 \times 10^{-19}$  (say 4.5 nm pores). Similar trend was observed for the release of CQDP (table S2).

# 3.6. ihmPCL-DHA and ihmPCL-CQDP formulation efficiently inhibit *P. falciparum*

Cell inhibition with DHA, CQDP and loaded formulations (ihmPCL-DHA and ihmPCL-CQDP) have been studied and the results have been shown in figure 8 and found that unloaded samples do not have any toxicity effects on P. falciparum, i.e., it is viable in nature. It revealed that free DHA and CQDP exhibited minimum inhibition effects on P. falciparum infection in RBC's compared to the ihmPCL-DHA and ihmPCL-CQDP formulations. Such as ihmPCL-DHA formulation with extent of DHA loading e.g., 2, 5, 10, 20, 50, 100, 200, 500 and 1000 nM were taken to evaluate the efficiency for suppression of P. falciparum infection (results in figure 8). Cell inhibition study of CQDP loaded formulation have been shown in figure S5. Parasites have a complex cell cycle of growth (48 h), which consists of three typical stages such as ring, trophozoite and schizoint stages (figure 9(a)). After reaching to the schizoint stage, merozoites emerge out of the erythrocytic vesicle and once again these merozoites invade erythrocytic cell and a new life cycle of the parasite repeats again for multiple times ihmPCL-DHA and ihmPCL-CQDP were added to the P. falciparum infected RBC's at the early trophozoite stage as the ring formed (at the stage, see figure 9(b)). On adding the formulation at this stage (figure 9(b)), either DHA or CQDP started to release from the polymer formulations and release sustained for a longer time and subsequently starts inhibit the growth

of the parasites. This process can be continued for a longer period of time due to the sustained release of DHA or CQDP and subsequently maintained the killing process as it is shown in the schematic figure 9(c).

Finally, we have investigated the bio-availability and inhibition of P. falciparum 3D7 using ihmPCL-DHA and ihmPCL-CQDP formulations separately through *in vitro* susceptibility assay. Three different *P*. falciparum 3D7 in vitro cultures set-ups have been taken in the similar condition. Set-1 is supplemented with free drugs DHA/CQDP, Set-2 is supplemented with ihmPCL capsules containing DHA/CQDP (formulations), and the set-3 is mock-treated (control). From the experimental results it is observed that the bear mesoporous PCL capsules do not have any antiparasitic effects up to 200  $\mu$ g.ml<sup>-1</sup> concentration (see figure 6), whereas individual ihmPCL-DHA and ihmPCL-CQDP formulations exhibited a major role in inhibition of parasite growth even at lower amount of drug concentrations. Based on the treatment module established in this work, the IC<sub>50</sub> value was calculated and found to be 66.6 nM, which is almost closed to the IC<sub>50</sub> value obtained for free DHA (65.4 nM). These results imply that formulation of hollow porous PCL nanocapsules with DHA is effective in inhibition of parasitic growth and killing of them in a sustained manner (figure 10(a)).

Additionally, the inhibitory effects of ihmPCL-CQDP were also investigated by performing *in vitro* viability assay in *P. falciparum* 3D7 strain following the similar procedure used for ihmPCL-DHA. Figure 10(b) shows the anti-parasite growth activities of ihmPCL-CQDP formulation in a dose dependent manner. The IC<sub>50</sub> value has been calculated for ihmPCL-CQDP formulation and found to be 25.14 nM, which is more compared to the value obtained for free CQDP (15.06 nM). The IC<sub>50</sub> value is

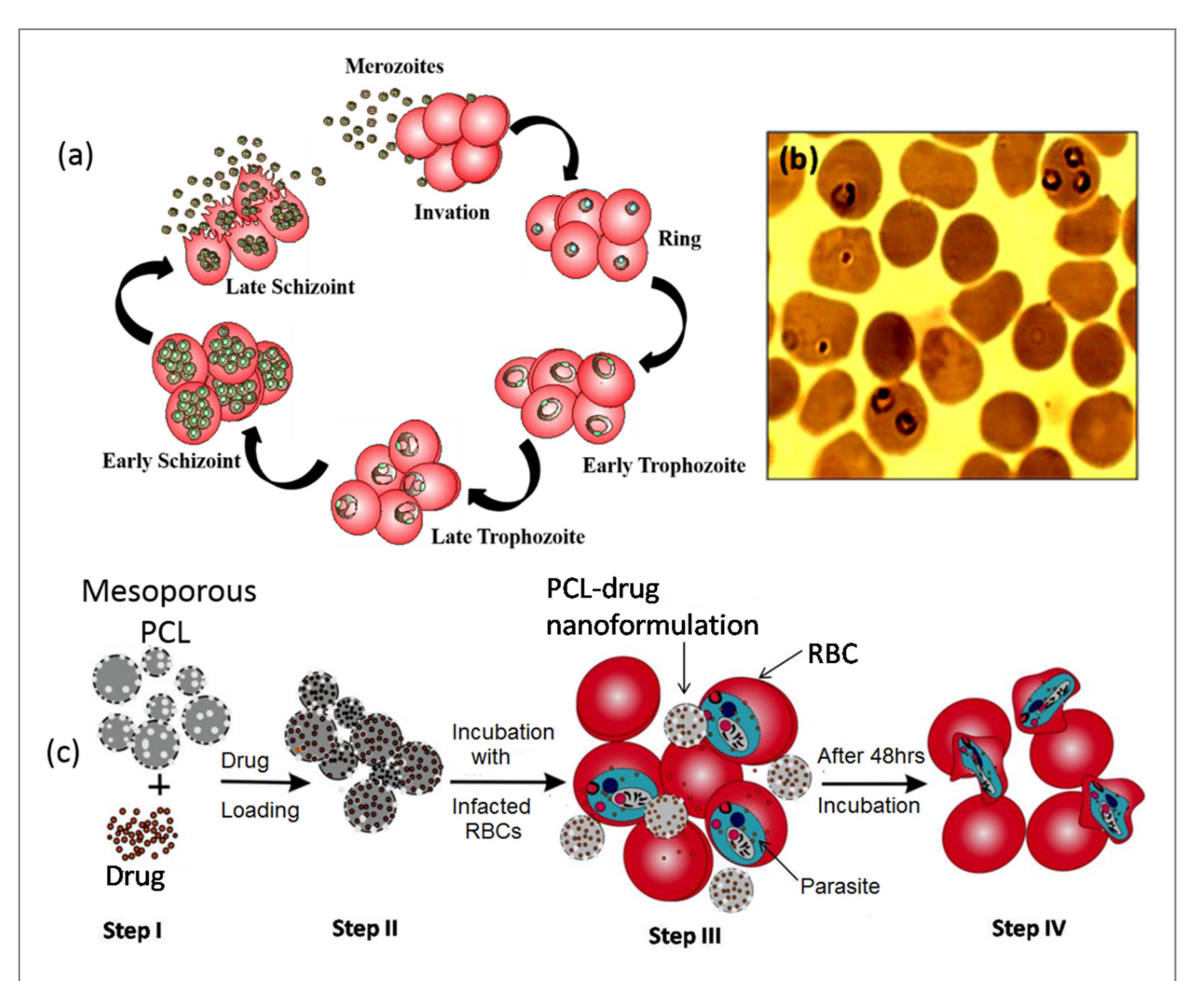


**Figure 9.** (a) Life-cycle of *P. falciparum*, (b) early Trophozoite stage of *P. falciparum* at which stage ihmPCL-DHA/ihmPCL-CQDP nanoformulations added for treatment and (c) schematic of different steps of making nanoformulations and treatment.

in good agreement with the previously reported IC<sub>50</sub> values for the free CQDP and six other available antimalarial drugs reported [2]. The results evident that the release of CQDP from the ihmPCL capsules is very effective and the marginal shift in the IC<sub>50</sub> value and the rightward shift of the curve indicates that the ihmPCL capsules still retained in CQDP for longer period of time and thus a sustained delivery is maintained and suppress the growth of parasites. It is further can be noted that treatment efficiencies with ihmPCL-DHA and ihmPCL-CQDP are quite excellent with respect to the other nanoparticles used for the same purposes.

### 4. Discussion

To date many nanoparticle based research works for antimalarial activities have been reported such as, phosphorothionate antisense oligodeoxyribo-nucleotide and chitosan based nanoparticles for silencing of malaria but those nanoparticles found are very unstable in physiological condition [24]. β-arteether lipid based nanoparticle formulation of curcumin is also reported and used for anti-malaria [25] but due to the poor solubility and bio-availability of curcumin this formulation found inefficient. Liposomes based

nanoparticles [26, 27] and PEG-coated liposomes nanocapsules [28, 29] have also been used against parasites, however their short-life in physiological conditions has become a major concern. Liposome based nanoformulations of halofantrine has also been studied for malaria treatment and found that due to the uncontrolled doses of halofantrine it caused the cardiac side effects (cardiac arrhythmias) [30] and it required the correct administration [31]. Metal oxide nanoparticles e.g. Al<sub>2</sub>O<sub>3</sub>, ZrO<sub>2</sub>, Fe<sub>3</sub>O<sub>4</sub>, MgO etc are found not suitable for abrogating P. falciparum, since they are not biodegradable [32]. Further, antimalarial activity using the nanoemulsion droplets of lipid molecules were found not possible, since without using surfactants the emulsion cannot be formed and it is toxic in nature [33]. Thus extensive efforts have been made to find out a suitable nanocarrier for antimalarial drugs to facilitate the treatment and for killing the P. falciparum where each having individual drawbacks. In this work, ihmPCL capsules that have been used is a quite stable biopolymer and slow degradable in biological fluid which helps in sustained release of antimalarial drugs such as DHA and CQDP. The ihmPCL nanocapsules designed biocompatible.

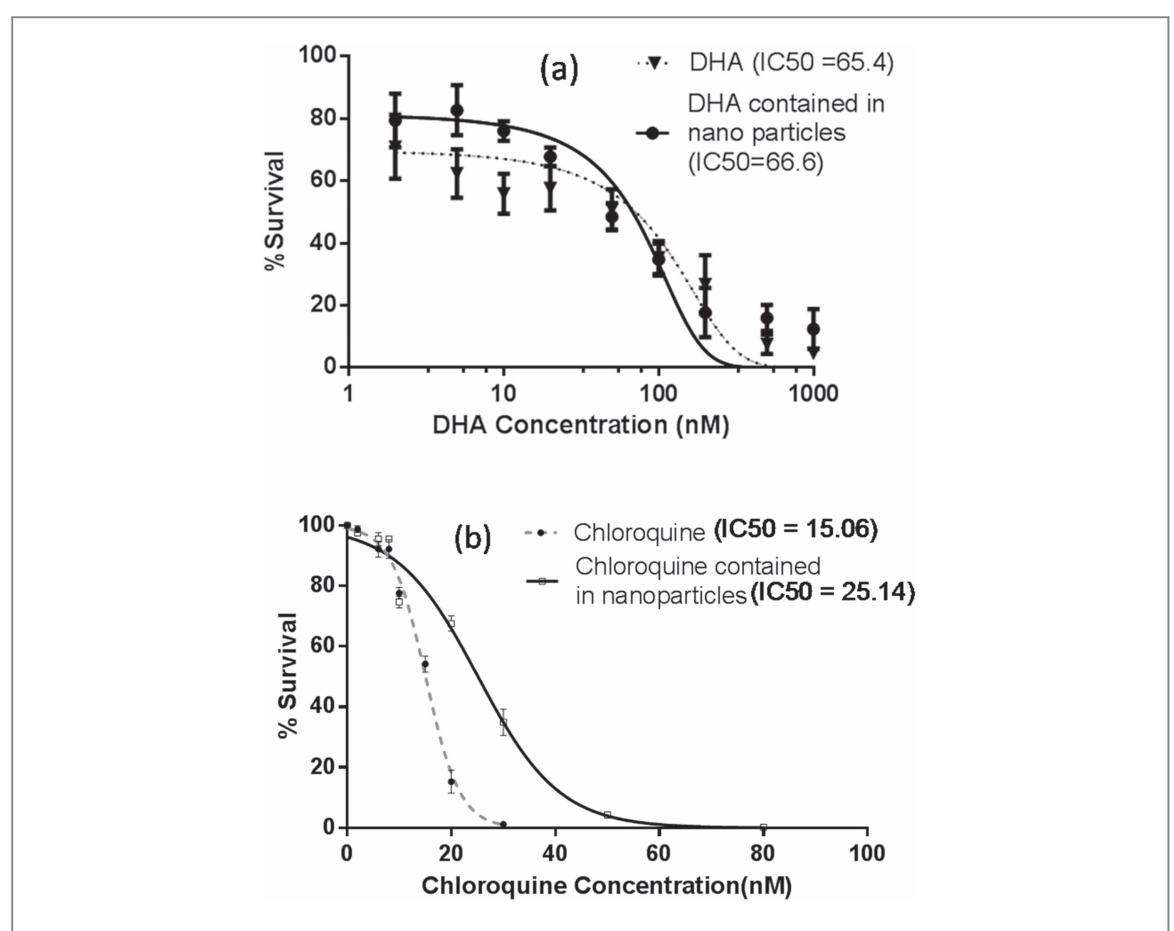
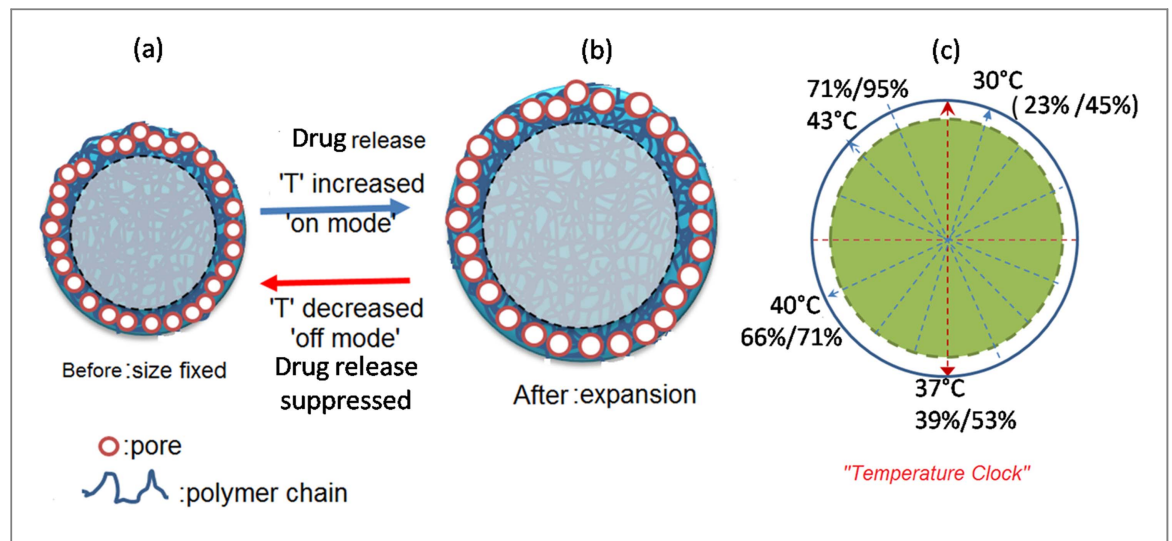


Figure 10. Antimalarial activity of (a) ihmPCL-DHA nanoformulation and (b) ihmPCL-CQDP nanoformulation in a dose dependent manner.

Furthermore, from our detail study it is evident that the novel formulation of DHA and CQDP ihmPCL capsules are successfully challenging P. falciparum growth with respect to the other six reported antimalarial drugs used lonely without any carriers [2] and our formulation could be a promising choice in the treatment of malaria. Additionally, the temperature dependent extents of DHA and CQDP release are very interesting (figures 7(a) and (b)) and have tremendous physiological significance in the light of periodic change in body temperature due to P. falciparum infection. As soon as the body temperature increases due to P. falciparum infection of RBCs, which could lead to the minor thermal expansion of the capsules as well as hollow core size and surface pore size which leads to the release of drugs DHA/CQDP from the formulations immediately to suppress the activity of P. falciparum and once the body temperature will be decreased then there will be contraction of the capsule's size, its pore size as well as the rate of diffusion of drugs also will be decreased. Thus reported formulations show temperature dependent release of DHA and CQDP. That is with increase in the temperature the release rate of drug molecules increase like a function of switching 'on-mode' and once the temperature decreases the release rate suppressed like a function of switching 'off-mode' as it is mechanized schematically

in figures 11(a) and (b). Thus, the release process can be represented as like as a 'temperature clock' and control by temperature dependent diffusion as it is shown in figure 11(c). Further the rate of diffusion of DHA and CQPD from hollow mesoporous PCL depends on the pore size as tabulated in tables S1 and S2. Similar phenomenon is observed for the other materials [34]. It is worth mentioning that, to date only the poly(N-Isopropylacrylamide) based copolymers were reported which control the temperature dependent release of drugs [35] but not for the hollow core-shell and mesoporous PCL capsules, where we observed the sustained release of DHA and CQDP at body temperature (37 °C-40 °C). The disadvantages of poly(N-Isopropylacrylamide) for treatment of malaria is that the critical transition temperature (Tc) of drug release for this polymer is 32 °C, which is very low compared to the normal body temperature (37.4 °C) and hence poly(N-Isopropylacrylamide) may not useful for control release of DHA/CQDP for treatment of the P. falciparum, because most of the drug released below the body temperature. Further, the excess release of drugs from poly(N-Isopropylacrylamide) at low temperature (33 °C) caused side effects and increased the resistance of drugs to the *P. falciparum* [1]. Therefore, our formulations of DHA and CQDP with ihmPCL are of special kinds and are paramount for knockdown



**Figure 11.** (a) and (b) representative schematic showing with change in body temperature how the DHA/CQDP release happened with 'on' and 'off' mode from the ihmPCL-DHA and ihmPCL-CQDP nanoformulations, and (c) a proposed 'temperature clock' showing different extent of release with temperature.

the *P. falciparum* infection in RBCs and the doses can be tuned by controlling the temperature very easily.

### 5. Conclusions

In this work, new formulations of ihmPCL capsules with antimalarial drugs such as DHA and CODP have been designed to suppress the growth of *P. falciparum*. Porous-PCL capsules designed are biocompatible. For P. falciparum suppression, the temperature dependent release and regulation of sustained release are found very important. The dose dependent suppression of P. falciparum has been studied and found that our formulations have similar IC<sub>50</sub> value for both encapsulated and free DHA and exhibited more IC50 compared to the IC<sub>50</sub> obtained for free antimalarial drugs and is quite efficient in killing the P. falciparum infection in RBCs and the efficiency is very high compared to previous reports using other nanopaticles. Therefore, formulations developed here in this work demonstrated their excellent efficiencies as a carrier in an in vitro anti-malaria drug delivery system and successfully abrogating P. falciparum growth and is well monitored by changing temperatures. Thus, our formulations act as a 'temperature clock' to suppress the normal activities of P. falciparum which is very unique and pioneering and can be used in treatment of malaria more efficiently to the existing approaches.

### Acknowledgments

Authors acknowledge DST Fast-Track Grant for Young Scientist (Ref: SR/FTP/ETA-0079/2011) and UPE-II project (Ref: UH/UPE-II/28/2015/5669), DST PUSE-II, for financial support, Nanoscience Centre, University of Hyderabad for TEM facilities

and School of Engineering Sciences and Technology for characterization facilities. P Paik is presently associate professor at Indian Institute of Technology (IIT), BHU, Varanasi, India.

### **ORCID iDs**

Pradip Paik https://orcid.org/0000-0001-7033-0636

### References

- [1] WHO World Malar. Rep. December 2016 (http://who.int/features/factfiles/malaria/en/)
- [2] Mu J et al 2010 Plasmodium falciparum genome-wide scans for positive selection, recombination hot spots and resistance to antimalarial drugs Nat. Genet. 42 268–71
- [3] John C W, Xiaorong Feng M T F, Roland A C, Jianbing M, Dror I Baruch A J M and Su X 2002 Genetic diversity and chloroquine selective sweeps in Plasmodium falciparum Nature 418 320–3
- [4] Roper C, Pearce R, Nair S, Sharp B, Nosten F and Anderson T 2004 Intercontinental spread of pyrimethamine-resistant malaria Science 305 1124
- [5] Zalis M G, Pang L, Silveira M S, Milhous W K and Wirth D F 1998 Characterization of Plasmodium falciparum isolated from the Amazon Region of Brazil: evidence for quinine resistance Am. J. Trop. Med. Hyg. 58 630–7
- [6] Vreden S G, Bansie R D, Jitan J K and Adhin M R 2016 Assessing parasite clearance during uncomplicated Plasmodium falciparum infection treated with artesunate monotherapy in Suriname Infect *Drug Resist.* 9 261–7
- [7] Wanta M Y, Islamuddin M, Chouhan G, Ozbak H A, Hemegb H A, Dasgupta A K, Chattopadhyay A P and Afrin F 2015 Therapeutic efficacy of artemisinin-loaded nanoparticles in experimental visceral leishmaniasis *Colloids Surfaces B Biointerfaces* 130 215–21
- [8] Jeong SY and Kim SW 1986 Biodegradable polymeric drug delivery systems Arch. Pharm. 9 63–73
- [9] Venkataraman S, Hedrick J L, Ong Z Y, Yang C, Ee P L R, Hammond P T and Yang Y Y 2011 The effects of polymeric nanostructure shape on drug delivery Adv. Drug. Deliv. Rev. 63 1228–46

- [10] Kumari A, Yadav S K and Yadav S C 2010 Colloids and surfaces B: biointerfaces biodegradable polymeric nanoparticles based drug delivery systems Colloids Surfaces B Biointerfaces 75 1–18
- [11] Mora-Huertas C E, Fessi H and Elaissari A 2010 Polymerbased nanocapsules for drug delivery *Int. J. Pharm.* 385 113–42
- [12] Fredenberg S, Wahlgren M, Reslow M and Axelsson A 2011 The mechanisms of drug release in poly(lactic-co-glycolic acid)-based drug delivery systems—a review *Int. J. Pharm.* 415 34–52
- [13] Makadia H K and Siegel S J 2011 Poly lactic-co-glycolic acid (PLGA) as biodegradable controlled drug delivery carrier Polymers (Basel) 3 1377–97
- [14] Golenser J, Buchholz V, Bagheri A, Nasereddin A, Dzikowski R, Guo J, Hunt N H, Eyal S, Vakruk N and Greiner A 2017 Controlled release of artemisone for the treatment of experimental cerebral malaria *Parasit. Vectors* 10 :117 1–10
- [15] Werner Stober A F 1968 Controlled growth of monodisperse silica spheres in the micron size range 1 J. Colloid Interface Sci. 26 62-9
- [16] Kumar V B, Medhi H, Yong Z and Paik P 2016 Designing idiosyncratic hmPCL-siRNA nanoformulated capsules for silencing and cancer therapy *Nanomedicine Nanotechnology*, *Biol. Med.* 12 579–88
- [17] Romero-cano M S and Vincent B 2002 Controlled release of 4-nitroanisole from poly (lactic acid) nanoparticles J. Control. Release 82 127–35
- [18] Bassi A K, Gough J E, Zakikhani M and Downes S 2011 The chemical and physical properties of poly(ε-caprolactone) scaffolds functionalised with poly(vinyl phosphonic acid-coacrylic acid) J. Tissue Eng. 2011 1–9
- [19] Paik P, Gedanken A and Mastai Y 2009 Mesoporous spherical silica prepared by templating of chiral block copolymers ACS Appl. Mater. Interfaces 1 1834–42
- [20] Hu H, Zhou H, Liang J, An L, Dai A, Li X, Yang H, Yang S and Wu H 2011 Facile synthesis of amino-functionalized hollow silica microspheres and their potential application for ultrasound imaging J. Colloid Interface Sci. 358 392–8
- [21] Sirutkaitis V, Urtinaitiene M, Nas R J É and Kareiva A 2004 FTIR, TEM and NMR iinvestigations of stöber silica nanoparticles Mater. Sci. 10 287–90
- [22] Agarwal S and Speyerer C 2010 Degradable blends of semicrystalline and amorphous branched poly(caprolactone): effect of microstructure on blend properties *Polymer (Guildf)* 51 1024–32
- [23] She H, Xiao X and Liu R 2007 Preparation and characterization of polycaprolactone-chitosan composites for tissue engineering applications J. Mater. Sci. 42 8113–9

- [24] Föger F, Noonpakdee W, Loretz B, Joojuntr S, Salvenmoser W, Thaler M and Bernkop-Schnürch A 2006 Corrigendum to 'inhibition of malarial topoisomerase II in Plasmodium falciparum by antisense nanoparticles' *Int. J. Pharm.* 319 139–46
- [25] Memvanga P B, Coco R and Préat V 2013 An oral malaria therapy: curcumin-loaded lipid-based drug delivery systems combined with  $\beta$ -arteether *J. Control. Release* 172 904–13
- [26] Owais M, Varshney G C, Choudhury A, Chandra S and Gupta C M 1995 Chloroquine encapsulated in malariainfected erythrocyte-specific antibody-bearing liposomes effectively controls chloroquine-resistant Plasmodium berghei infections in mice Antimicrob. Agents Chemother. 39 180–4
- [27] Urbán P, Estelrich J, Adeva A, Cortés A and Fernàndez-Busquets X 2011 Study of the efficacy of antimalarial drugs delivered inside targeted immunoliposomal nanovectors Nanoscale Res. Lett. 6:620 1–9
- [28] Mosqueira V C F, Loiseau P M, Bories C, Legrand P, Devissaguet J P and Barratt G 2004 Efficacy and pharmacokinetics of intravenous nanocapsule formulations of halofantrine in Plasmodium berghei-infected mice Antimicrob. Agents Chemother. 48 1222–8
- [29] Bakker-Woudenberg I A J M 2002 Long-circulating sterically stabilized liposomes as carriers of agents for treatment of infection or for imaging infectious foci *International Journal of Antimicrobial Agents* 19 299–311
- [30] Wesche D L, Schuster B G, Wang W-X and Woosley R L 2000 Mechanism of cardiotoxicity of halofantrine Clin. Pharmacol. Ther. 67 521–9
- [31] Bouchaud O, Imbert P, Touze J E, Dodoo A N O, Danis M and Legros F 2009 Fatal cardiotoxicity related to halofantrine: a review based on a worldwide safety data base *Malar. J.* 8:289 1–8
- [32] Jacob Inbaneson S and Ravikumar S 2013 In vitro antiplasmodial activity of PDDS-coated metal oxide nanoparticles against Plasmodium falciparum Appl. Nanosci. 3 197–201
- [33] Singh K K and Vingkar S K 2008 Formulation, antimalarial activity and biodistribution of oral lipid nanoemulsion of primaquine Int. J. Pharm. 347 136–43
- [34] Balas F, Manzano M, Horcajada P and Vallet-Regi M 2006 Confinement and controlled release of bisphosphonates on ordered mesoporous silica-based materials J. Am. Chem. Soc. 128 8116–7
- [35] Chung J E, Yokoyama M, Yamato M, Aoyagi T, Sakurai Y and Okano T 1999 Thermo-responsive drug delivery from polymeric micelles constructed using block copolymers of poly (N-isopropylacrylamide) and poly (butylmethacrylate) J. Control. Release 62 115–27

# Elucidation of DNA repair activity of PfBLM and potentiation of artemisinin action by small molecule inhibitor of RecQ helicase

by S Niranjan

**Submission date:** 18-Nov-2020 11:25AM (UTC+0530)

**Submission ID:** 1449781913

File name: Thesis for plagiarism checking.pdf (379.7K)

Word count: 14195 Character count: 74589

# Elucidation of DNA repair activity of PfBLM and potentiation of artemisinin action by small molecule inhibitor of RecQ helicase

**ORIGINALITY REPORT** 

13%

6%

4%

10%

SIMILARITY INDEX

INTERNET SOURCES

**PUBLICATIONS** 

STUDENT PAPERS

### **PRIMARY SOURCES**



Submitted to University of Hyderabad, Hyderabad

8%

Student Paper

2

Sugith Babu Badugu, Shaik Abdul Nabi, Pratap Vaidyam, Shyamasree Laskar, Sunanda Bhattacharyya, Mrinal Kanti Bhattacharyya. "Identification of Plasmodium falciparum DNA Repair Protein Mre11 with an Evolutionarily Conserved Nuclease Function", PLOS ONE, 2015

1%

Publication

3

www.jbc.org

Internet Source

<1%

4

Croteau, Deborah L., Venkateswarlu Popuri, Patricia L. Opresko, and Vilhelm A. Bohr. "Human RecQ Helicases in DNA Repair, Recombination, and Replication", Annual Review of Biochemistry, 2013.

<1%

Publication

20	tel.archives-ouvertes.fr Internet Source	<1%
21	www.frontiersin.org Internet Source	<1%
22	Submitted to Asia Pacific University College of Technology and Innovation (UCTI) Student Paper	<1%
23	Submitted to University of Surrey Student Paper	<1%
24	digitalcommons.wpi.edu Internet Source	<1%

Exclude quotes

On

Exclude matches

< 14 words

Exclude bibliography

On

It is to certify that the primary source I contains the method section of several thesis from our laboratory. Certain phrases under the method section cannot be modified and need to be written as is theree this can be eleminated from the total similarity score.

Dr. MRINAL KANTI BHATTACHARYYA PhD

DEPARTMENT OF BIOCHEMISTRY SCHOOL OF LIFE SCIENCES UNIVERSITY OF HYDERABAD HYDERABAD-500046, INDIA.